Check for updates

Fluorescent chemosensors facilitate the visualization of plant health and their living environment in sustainable agriculture

Yang-Yang Gao,[†][a] Jie He,[†][a] Xiao-Hong Li,[†][a] Jian-Hong Li,[a] Hong Wu,[a] Ting Wen,[a] Jun Li,*[b] Ge-Fei Hao [ID] *[a] and Juyoung Yoon [ID] *[c]

Globally, 91% of plant production encounters diverse environmental stresses that adversely affect their growth, leading to severe yield losses of 50–60%. In this case, monitoring the connection between the environment and plant health can balance population demands with environmental protection and resource distribution. Fluorescent chemosensors have shown great progress in monitoring the health and environment of plants due to their high sensitivity and biocompatibility. However, to date, no comprehensive analysis and systematic summary of fluorescent chemosensors used in monitoring the correlation between plant health and their environment have been reported. Thus, herein, we summarize the current fluorescent chemosensors ranging from their design strategies to applications in monitoring plant-environment interaction processes. First, we highlight the types of fluorescent chemosensors with design strategies to resolve the bottlenecks encountered in monitoring the health and living environment of plants. In addition, the applications of fluorescent small-molecule, nano and supramolecular chemosensors in the visualization of the health and living environment of plants are discussed. Finally, the major challenges and perspectives in this field are presented. This work will provide guidance for the design of efficient fluorescent chemosensors to monitor plant health, and then promote sustainable agricultural development.

1. Introduction

Exploring and understanding plant-environment interactions are essential components of sustainable agriculture, which is crucial for ensuring crop production and food security. Reportedly, global food production has increased by over threefold due to the advancement in sustainable agricultural practices regarding the connection between plant health and their environment during the past 50 years.[1] Balancing the relationship between plants and their environment to regulate plant health can increase grain production by 33 million tons and decrease nitrogen fertilizer utilization (1.2 million tons), which is equivalent to an enhanced net worth of $12.2 billion.[2] Plant health is directly associated with biodiversity, plant productivity, soil conditions, water quality, and climate change, thereby facilitating amplified ecosystem services and mitigating the dependence on extrinsic resources.[3] For example, soil serves as the primary medium for plants, and consequently the presence of certain pollutants such as heavy metals in the soil may negatively impact both plant growth and human dietary safety.[4] Therefore, monitoring the health and living environment of plants in sustainable agriculture is necessary for promoting the development of the economy and society.

To date, many technologies have been developed to monitor the health and living environment of plants. Traditional methods including molecular technology and chromatographic detection are regularly employed. For example, DNA amplification *via* polymerase chain reaction (PCR) and its derivatives, namely nested PCR, quantitative PCR, digital PCR, and multiplex PCR, enzyme-linked immunosorbent assay (ELISA), and loop-mediated isothermal amplification (LAMP) are scientific testing methods for plant diseases.[5,6] Also, ultra-performance liquid chromatography–tandem mass spectrometry (UPLC–MS/MS), gas chromatography–mass spectrometry (GC–MS), high performance liquid chromatography (HPLC) and other chromatographs are utilized to identify pesticide residues, soil or water contamination, and fruit nutrition.[7–10] However, these

[a] *State Key Laboratory of Green Pesticide, Key Laboratory of Green Pesticide and Agricultural Bioengineering, Ministry of Education, Center for Research and Development of Fine Chemicals, Guizhou University, Guiyang 550025, P. R. China. E-mail: gefei_hao@foxmail.com*

[b] *College of Chemistry, Huazhong Agricultural University, Wuhan 430070, China. E-mail: lijun1986@mail.hzau.edu.cn*

[c] *Department of Chemistry and Nanoscience, Ewha Womans University, Seoul 120-750, Korea. E-mail: jyoon@ewha.ac.kr*

† Equal contribution.

6992 | *Chem. Soc. Rev.*, 2024, **53**, 6992–7090

This journal is © The Royal Society of Chemistry 2024

procedures are laborious and time-consuming, often necessitating complex processes and proficient professionals for operation, and they fail to exhibit continuous monitoring. Consequently, due to their advantages of high sensitivity, simple operation, and spatiotemporal resolution, fluorescent chemosensors have gradually matured in exploring the connection between the health and living environment of plants.

In recent years, different types of fluorescent chemosensors including small-molecules and nano and supramolecular complexes have been used for monitoring plant health and their environment. The reasonable design of small-molecule fluorescent chemosensors using diverse chromophores such as naphthalimide, coumarin, BODIPY, rhodamine, and cyanine have been extensively applied for monitoring plant health owing to their low cost and favorable biocompatibility.[11,12] Furthermore, to increase the quantum yield (QY) and recyclability, fluorescent nano-chemosensors have been designed based on quantum dots, metal–organic frameworks, covalent organic frameworks and nanoclusters and used to analyze the

living environment and health of plants.[13–15] The fluorescent supramolecular chemosensors formed polymer and hydrogelator systems could realize recyclability and high-specificity monitoring of the living environment of plants and food security.[16–18] Consequently, fluorescence-based techniques have become one of the sustainable agriculture hotpots for monitoring plant health and their surroundings. Nevertheless, there is a lack of summary and critical reviews establishing the corresponding relationship between fluorescent chemosensors and the major issues in plant-environment interactions.

Herein, we present a comprehensive analysis on the progression and application of fluorescent chemosensors in monitoring the health and living environment of plants. The commonly used design strategies, mechanisms, and challenges associated with fluorescent chemosensors in monitoring and analyzing plant-environment interactions are introduced. Most importantly, we systematically discuss the application of small-molecule, nano and supramolecular fluorescent chemosensors in areas such as plant growth and development, abiotic and

Ting Wen, Yang-Yang Gao, Jie He (first row from left to right)
Xiao-Hong Li, Hong Wu, Jian-Hong Li (second row from left to right)

There are six authors in the photo including Ting Wen, Yangyang Gao, Jie He (first row from left to right), and Xiaohong Li, Hong Wu, Jianhong Li (second row from left to right). Yangyang Gao received her PhD degree from Shandong Agricultural University with Prof. Feng Liu and Prof. Wei Mu, and subsequently worked with Prof. Gefei Hao as a Postdoctoral Researcher at the State Key Laboratory of Green Pesticide in Guizhou University. She is interested in the areas of the interaction of plants and fungal pathogens and sustainable measures for maintaining plant health. Jie He and Xiaohong Li are currently pursuing a PhD degree at the State Key Laboratory of Green Pesticide in Guizhou University. Their research is focused on using nanotechnology to improve the stress resistance of plants and fluorescent chemosensors, respectively. Jianhong Li, Hong Wu, and Ting Wen are currently pursuing their Master's Degree at State Key Laboratory of Green Pesticide in Guizhou University. Their research focus is the design and synthesis of fluorescent probes, the design of biosensors based on genetic coding, and the application of imaging techniques for plant health analysis, respectively.

Jun Li

Jun Li earned his PhD in 2014 from Central China Normal University. Subsequently, he joined Prof. Juyoung Yoon's research group at Ewha Womans University as a Postdoctoral Fellow in 2015–2017. He is now an Associate Professor at Huazhong Agricultural University, P. R. China. His research interest mainly focuses on small-molecule-based fluorescent probes and their applications in plant imaging.

Ge-Fei Hao

Ge-Fei Hao, a Professor at Guizhou University, specializes in pesticide informatics research. Prof. Hao is a recipient of the National Science Fund for Distinguished Young Scholars and a chief scientist leading national key research and development projects. He has also been selected for the Ministry of Education's "Changjiang Scholars Reward Plan" for young scholars. He is focused on the key scientific issue of "the interaction between biomolecules and pesticides" in pesticide innovation. He established the world's first systematic pesticide informatics platform.
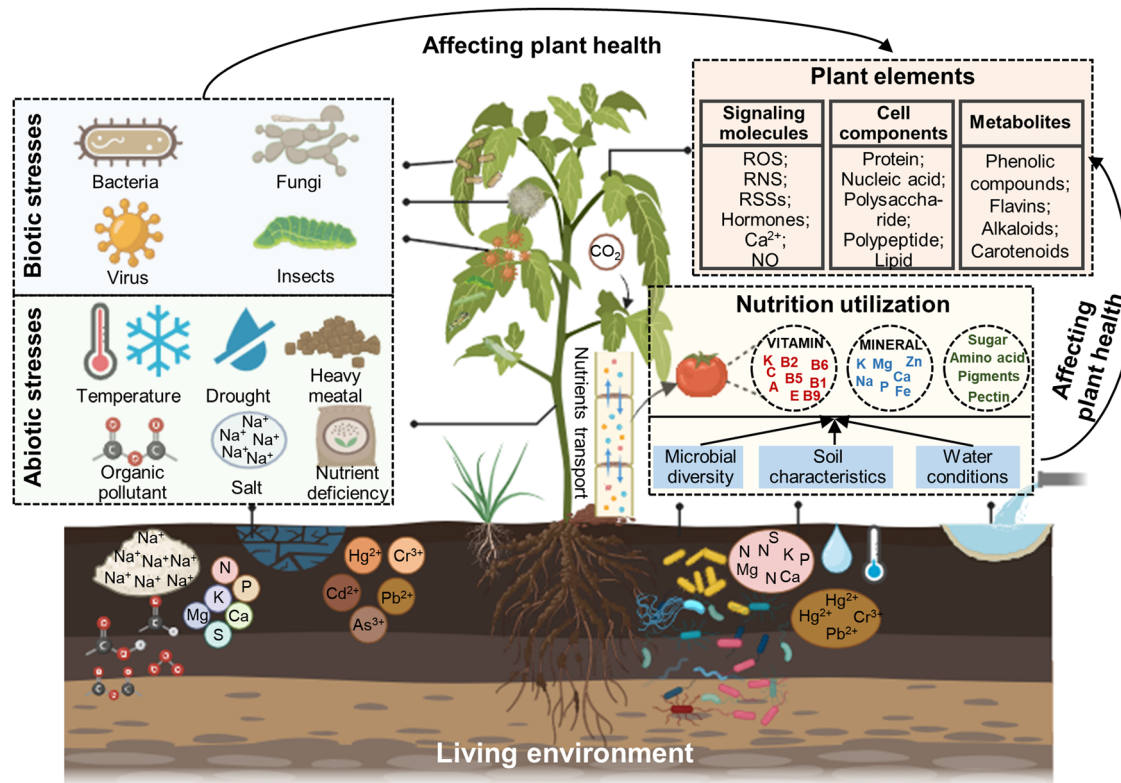
This journal is © The Royal Society of Chemistry 2024

Chem. Soc. Rev., 2024, **53**, 6992–7090 | **6993**

Fig. 1 Relationship between the health and living environment of plants. Biotic and abiotic stresses and nutrition utilization are major issues affecting plant health, which can reflect the changes in plant contents including signaling molecules (*e.g.* ROS, RNS, RSSs, hormones, Ca^{2+}, and NO), cell components (*e.g.* proteins, nucleic acids, polysaccharides, polypeptides, and lipids), metabolites (*e.g.* phenolic compounds, flavins, alkaloids, and carotenoids), metal ions and microenvironment (*e.g.* pH and pesticides).

biotic stresses, soil conditions, irrigation water quality and nutrition utilization. Meanwhile, we correlate the characteristics of chemosensors with their application, and then provide insights into designing efficient and suitable sensors. Lastly, we summarize the network of fluorescent chemosensors to promote the understanding of the connection between plant health and their environment. This work will provide guidance for the future development of efficient fluorescent chemosensors, thereby realizing the real-time monitoring of the health and living environment of plants in sustainable agriculture.

Juyoung Yoon is a distinguished Professor at the Department of Chemistry and Nanoscience, Ewha Womans University. His research interests include investigations of fluorescent chemosensors, activatable photosensitizers, phototherapy and theranostics. He was listed as a highly cited researcher in chemistry since 2014.

Juyoung Yoon

2. Monitoring plant health and their living environment in sustainable agriculture

2.1 The relationship between plant health and their environment

Plant health not only depends on the inherent potential of plants but also has a close relationship with environmental factors including abiotic and biotic stresses and nutrient utilization (Fig. 1).[19] Abiotic and biotic stresses mainly focus on evaluating the relationship between the elements and living environment of plants.[20] This is because abiotic (*e.g.* salinity, drought, temperature, heavy metals, and pesticides) and biotic stresses (*e.g.* phytoparasitic nematodes, fungi, and bacteria) are the most serious factors affecting plant growth and development. For example, drought and high temperature can cause wilting, leading to reduced photosynthesis, impaired nutrient uptake, protein denaturation, cellular damage, and ultimately plant death. Excessive levels of heavy metals can accumulate in plant tissues, disrupting cellular processes and inhibiting their growth. Biotic stresses can cause physical or tissue damage, nutrient deficiencies, and potentially mortality. During the interaction process of plants and an adverse environment, monitoring the changes in plant elements including signaling molecules (*e.g.* ROS, RNS, RSSs, hormones, Ca^{2+}, and NO), cell

6994 | *Chem. Soc. Rev.*, 2024, **53**, 6992–7090

This journal is © The Royal Society of Chemistry 2024

components (*e.g.* protein, nucleic acid, polysaccharide, and polypeptide, lipid), metabolites (*e.g.* phenolic compounds, flavins, alkaloids, and carotenoids), metal ions and microenvironments (*e.g.* pH and pesticides) can assess plant health, and then timely strategies applied to regulate the plant's response to various environmental stresses.[21,22] The efficiency of nutrient utilization is the determining factor of fruit quality, serving as the pivotal link between plant health and agricultural product supply chains. Nutrient utilization mainly depends on the diversity and equilibrium of beneficial microorganisms, nutrient sources and content, soil characteristics, water conditions, and plant health.[23] Therefore, monitoring the response of plants to abiotic and biotic stresses, their living environment, and nutrition supplication and utilization is essential for understanding the interactions between plants and their environment and promoting plant health in sustainable agriculture.

Currently, an array of techniques including visual assessment, PCR, immunological approaches, biochemical analysis technologies, chromatography and mass spectrometry methods, electrochemical sensors, visible light imaging, imaging spectroscopy, thermal infrared imaging and three-dimensional imaging have been used to monitor plant-environment interactions (Table 1). Visual assessment is a commonly utilized reliable strategy for evaluating plant stress phenotypes, although it has low sensitivity and is time consuming, as well as associated with subjectivity bias due to expert interpretation.[24] Alternatively, PCR and immunological techniques can effectively detect plant pathogens within smaller sample sizes, with increased sensitivity and precision, but involve higher testing expenses, intricate procedures, specialized operation, non-living surveillance and potential occurrence of false positives.[25] Biochemical analytical technologies are well-suited for analyzing the delicate, specific and trace analysis of plant health biomarkers in the laboratory, but their inability to conduct real-time detection and complex operation processes necessitate consideration.[26] Chromatography coupled with mass spectrometry techniques (*e.g.* UPLC–MS/MS, LC–MS and GC–MS) facilitate the precise determination of compound identity, quantification, and separation in complex samples, featuring high sensitivity and rapid analysis, but the required instruments are costly and the detection sensitivity can occasionally be affected by substrate interference.[27] Visible light imaging represents another alternative that employs digital images to capture plant phenotype at relatively lower costs, user-friendly operational pattern, and straightforward maintenance requirements, but its image quality can potentially be hindered by background factors and illumination conditions.[28] Imaging spectroscopy utilizes the interaction between the solar radiation generated from samples, providing high spatial resolution over a broad spectral range. However, the high cost and the significant data storage demands for multi-spectral and hyper-spectral imaging instruments should also be considered.[29] Thermal infrared imaging offers simplicity and high-resolution for quantifying the infrared radiation released by samples, though a difficulty is deciphering the infrared radiation released by samples. Meanwhile, deciphering the temperature of soil and

plants beneath sparse canopies under irregular environmental conditions is a persistent challenge.[30] Three-dimensional imaging can precisely quantify the electric or laser emission produced by specimens, exhibiting superior spatial resolution and robust resistance to interference, but the employed methodologies impose significant financial burden, necessitate extended scanning durations, and yield modest throughput rates.[31] Thus these issues, fluorescence-based technologies can counterbalance the above-mentioned disadvantages, which have developed rapidly and now extensively applied in monitoring the health and living environment of plants to promote the development of sustainable agriculture.

2.2 Advantages of fluorescent chemosensors

Compared with the above-mentioned technologies, fluorescence-based technology possesses advantages for visualizing plant health and their environment in some aspects, as follows:[32–34] (i) for easy detection, fluorescent chemosensors emit bright and distinct signals, facilitating the detection of the presence and localization of specific components in plants or in their living environment. (ii) For specificity, fluorescent chemosensors can be designed based on the characteristics of specific targets, molecules or compounds of interest. This allows the selective identification and quantification of specific markers for implying plant health. (iii) For real-time monitoring, fluorescent chemosensors facilitate the real-time monitoring of plant health indicators. By labeling specific molecules, changes in their concentration or distribution can be observed over time. (iv) For non-destructive analysis, fluorescent chemosensors can be applied externally or systemically absorbed by plants without causing significant damage. This allows repetitive measurement over time, reducing the necessity for destructive sampling and enabling longitudinal studies. (v) For high sensitivity, fluorescent chemosensors are highly sensitive, which can often detect low concentrations of target molecules. This attribute is particularly advantageous in detecting early signs of plant stresses or nutrient deficiencies. (vi) For multiplexing capability, fluorescent chemosensors can be designed with different emission wavelengths, allowing the simultaneous detection of multiple targets within the same sample and facilitating the evaluation of various aspects of plant health. (vii) In terms of high-throughput screening, fluorescent chemosensors are employed in high-throughput screening tests, enabling the expedited examination of an extensive array of plant samples. Therefore, fluorescent chemosensors have been widely used and progressively matured in the analysis of the correlation between plant health and environment.

2.3 The classification of fluorescent chemosensors

Fluorescent chemosensors are capable of monitoring plant health under abiotic and biotic stresses, various conditions of soil and water, and nutrient utilization rate. Currently, three major types of fluorescent chemosensors including small-molecule fluorescent chemosensors, fluorescent nano-chemosensors and fluorescent supramolecular chemosensors have been used in the visualization of plant health and their surroundings. Small-molecule fluorescent chemosensors are commonly used in plant imaging owing to their

This journal is © The Royal Society of Chemistry 2024

Chem. Soc. Rev., 2024, **53**, 6992–7090 | **6995**

Table 1 Conventional methods for monitoring plant health and their environment

Techniques	Principles	Advantages	Disadvantages
Visual assessment	Observing plant health status	Most reliable and accurate	Low sensitivity and timeliness
PCR-based methods	Amplification of one or a few copies of a particular sequence of DNA	Fewer samples, timeliness, high specificity and sensitive	Expensive, complicated steps, professional operation, and false positives
Immunology-based methods	Interaction between antibody and antigen	Timeliness and high specificity	Non-real-time detection, and false positive
Biochemical technologies	Biochemical reaction between biomarkers in samples and reagents	High sensitivity and specificity, and trace analysis	Non-real-time detection, and complex operation processes
Chromatography and mass spectrometry	Separation, identification and quantitative analysis of compounds in complex samples	Timeliness and high-throughput	High expensive cost, and professional operation
Electrochemical sensing	Monitoring the changes in current or potential of sample	High sensitivity and selectivity, low equipment cost	Lack of competitiveness
Visible light imaging	Using digital images to mimic human perception	Low cost, ease of operation and maintenance	False positive
Imaging spectroscopy	Imaging the solar radiation produced from samples	High spatial resolution and wide spectral range	Expensive, and large volume of data for processing
Thermal infrared imaging	Measuring the emitted infrared radiation from the surface of samples	High spatial resolution, and ease of operation	Influenced by environmental temperature or conditions
Three dimensional imaging	Imaging the electromagnetic or laser radiation produced by samples	High three-dimensional spatial resolution, and strong ant-interference capability	High cost, long scanning times, and low throughput

6996 | Chem. Soc. Rev., 2024, 53, 6992–7090

This journal is © The Royal Society of Chemistry 2024

biocompatibility and high spatial-temporal resolution. Most fluorescent nano-chemosensors have been used to monitor the living environment of plants, which is determined by their properties of recyclability and high sensitivity. Meanwhile, fluorescent supramolecular chemosensors are often used to detect fruit quality and the living environment of plants because of their recyclability, high selectivity and strong adaptability. In the following sections, we summarize and analyze the utility of three types of fluorescent chemosensors in monitoring the health and living environment of plants.

3. Applications of small-molecule fluorescent chemosensors

Small-molecule fluorescent chemosensors are powerful tools for visualizing plant health by changing their luminescence emission in response to specific analytes in plants under abiotic and biotic stresses. A variety of small-molecule fluorescent chemosensors based on different fluorophores such as coumarin, naphthalimide, rhodamine, fluorescein, NBD, BODIPY, Nile bule, and cyanine has been discovered and developed (Fig. 2).[35] When the parent structure of the fluorophore is modified, the emission spectrum is usually in the range of 500 to 600 nm. NIR fluorescence (near-infrared, 700–900) exhibits some advantages including deeper tissue penetration to circumvent photo-bleaching and minimal phototoxicity.[36] Each fluorophore has unique attributes that should be considered, which determine its suitability as a label for studying plant-environment interactions.

3.1 Coumarin derivatives

Coumarin is a bi-cyclic structure consisting of a phenyl unit encircled by a pyrone ring encompassing a rigid C═C bond, a C═O group and six peripheral C–H sites.[37] The parent coumarin molecule displays negligible or minimal fluorescence,

whereas numerous coumarin derivatives with various substitutes produce considerable fluorescence in the visible light spectrum (400–500 nm). Accordingly, hundreds of coumarin dyes have been engineered due to their increased fluorescent QY, adaptability of their emission wavelengths and responsiveness to their microenvironmental polarity. Observational research has explored the relationship between the photophysical attributes of coumarin derivatives and their chemical compositions, showing that substitutions on the coumarin fragment result in blue- or red-shifted fluorescence phenomenon.[38] In terms of electronic structure, the introduction of electron-withdrawing entities at positions 3 or 4, or electron-donor moieties at positions 6 or 7, induces a bathochromic shift in the emission wavelength curve (Fig. 2).[39] A vast majority of fluorescent chemosensors employing coumarin as a key group in combination with other functional receptors has been designed. Particularly, the coumarin moiety positioned at the 3- and 7-positions frequently serves as the structural backbone of the fluorophore, which has been widely used to monitor the distribution and concentration of ions, hormones and amino acids in plants, as well as assessing the quality of the soil in their living environment (Table 2).[40]

3.1.1 Fluorescent chemosensors derived from coumarin at 3-position or 7-position. Fluorescent coumarin derivatives at the 3-position or 7-position have been developed for detecting the distribution and concentration of ions and phytohormone in plants (Fig. 3). In 2021, Zhang *et al.* developed a coumarin derivative-based fluorescent chemosensor (**1**) linked by a Schiff base using straightforward synthesis and post-processing methods (Fig. 3a). **1** notably demonstrated remarkable aggregation stimulated luminescent amplification properties in the solvent environment ($V_{HEPES}:V_{EtOH}$), which was comprised of up to 40% aqueous portion. It showed proficiency in discerning the extraneous Zn^{2+} present within plant cells, exhibiting enhanced yellow-green fluorescence intensity at 515 nm (approximately two-fold) with a limit of detection (LOD) of
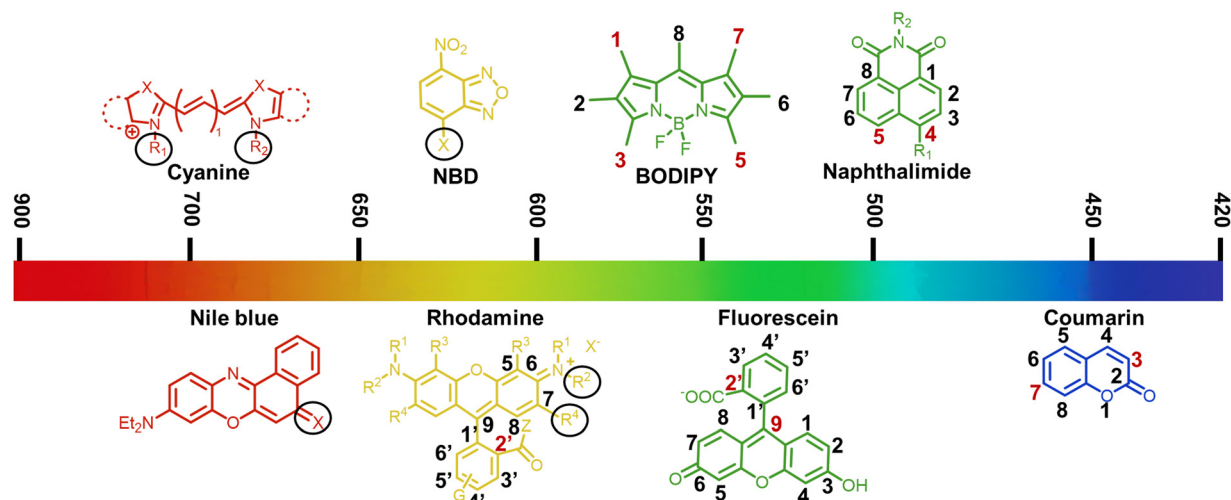

Fig. 2 Emission wavelength of small-molecule fluorescent chemosensors used in monitoring plant health. The fluorescent parents mainly include coumarin, naphthalimide, rhodamine, fluorescein, NBD, BODIPY, Nile bule, and cyanine. The numbers in red or black circle in the structure of the fluorescent parents are the modification sites for the fabrication of fluorescent chemosensors.

This journal is © The Royal Society of Chemistry 2024

Chem. Soc. Rev., 2024, **53**, 6992–7090 | **6997**

Table 2 Fluorescent coumarin derivatives for monitoring plant health and their environment

Classifications	Chemosensors	$\lambda_{ex}/\lambda_{em}$ (nm)	Solvents	Limit of detection (LOD)	Target analytes	Applications	Ref.
Coumarin derivatives at 3-position	1	425/515	$V_{HEPES}:V_{EtOH} = 1:1$, pH = 7.0	0.0260 μM	Zn^{2+}	Detecting exogenous Zn^{2+} in plant cells	41
Coumarin derivatives at 7-position	2	365/460	$V_{ethylene\ glycol}:V_{PBS} = 1:9$, pH = 7.3	52.0 ppb	Ethylene	Monitoring endogenous-induced changes in ethylene biosynthesis in plant	42
Coumarin derivatives at 3- and 7-positions	3	372/461	EtOH	—	Lignin	Visualizing the cell wall lignification process by labeling lignin	43
	4	428/505	$V_{DMSO}:V_{PBS} = 99:1$, pH = 7.4	0.930 μM	Cysteine	Detection of endogenous cysteine activities under external stimuli in live nematode and plant	44
	5	450/540–480	Aqueous solution	—	HClO	Tracking of exogenous/endogenous HClO variations in plant cell	45
	6	410/480 620/745	$V_{CH_3OH}:V_{PBS} = 4:6$, pH = 7.4	0.220 μM	CN^-	Detecting CN^- in flaxseed and bamboo shoots, and monitoring the viscosity of mitochondria	46

0.026 μM.[41] Another fluorescent coumarin derivative at the 7-position was developed by Chen *et al.* (2021) to monitor ethylene for evaluating the physiological state of plants (Fig. 3b). The fluorophore-tethered Rh[III]-based fluorogenic coumarin-ethylene chemosensor **2** exhibited superb sensitivity (LOD = 52 ppb) and instantaneous identification of ethylene in air (<2 min).

Upon reacting with ethylene, an associated organic activation process was verified, displacing rhodium to form a novel fluorescent entity, thereby manifesting the maximum fluorescence intensity at the mid-wavelength of 460 nm. Moreover, **2** showed superior ethylene selectivity, effectively avoiding potential interference from diverse unsaturated plant metabolite molecules. Given the pivotal role of ethylene in pathogen defense and external stress responses, this chemosensor not only offers a significant mechanism for deepening our comprehension of ethylene biosynthesis regulation and ethylene signaling transduction in plants, but also enables the monitoring of pathogen infections, which can provide guidance for preventing pathogen infection and studying the physiological process of ethylene in real time.[42] Coumarin-based fluorescent derivatives located at the 3- or 7-positions are expected to improve the emission spectrum for tracking small physiological molecules within plant cells. Furthermore, it is preferable for these probes, utilizing the coumarin fluorophore, to exhibit good water solubility.

3.1.2 Fluorescent chemosensors based on 3- and 7-positions of coumarin. Considerable effort has also been dedicated to exploring alternative positions of coumarins in fluorescent chemosensors targeting specific analytes. Four fluorescent chemosensors based on the 3- and 7-positions of coumarins can monitor plant components to evaluate plant health. The dimethylaminocoumarin-tagged guaiacyl monolignol chemosensor **3** was synthesized *via* a series of monolignol analogs γ-linked to fluorogenic aminocoumarin and nitrobenzofuran dyes, which could be inserted into the woody cell wall through a transpirational stream and biochemically integrated into lignins (Fig. 4a). Also, **3** showed high water solubility and membrane penetration, which was accurately and effectively reflected by staining unlabeled monolignol in plant tissue and the increase in fluorescent intensity at 461 nm, indicating its precise depiction of the integration of native lignin precursors, and hence monitoring tissue wall lignification processes in plants. This chemosensor is a useful tool for detecting the activity of lignification enzymes without destroying the plant environment and physiology, which is an important indicator for reflecting root ripeness and plant defense.[43] In 2019, Chen *et al.* reported the synthesis of fluorescent chemosensor **4** by integrating an acrylic acid ethyl ester moiety at the 3-position in the coumarin framework. This chemosensor exhibited high sensitivity towards cysteine (Cys) levels and activities with an LOD of 0.93 μM (Fig. 4b). The reactive thiol group of Cys could efficiently destroy the acrylate functionality through ring-closure reactions, generating a green fluorophore and ensuring an increase in fluorescence intensity at 505 nm. The dynamic alterations in the cellular Cys pool after exposure to oxidative stress triggers could be tracked using **4** in plants and nematodes, making it a significant diagnostic acid in probing the role of Cys in diverse biological events.[44] Longer emission wavelengths are beneficial for

6998 | *Chem. Soc. Rev.*, 2024, **53**, 6992–7090

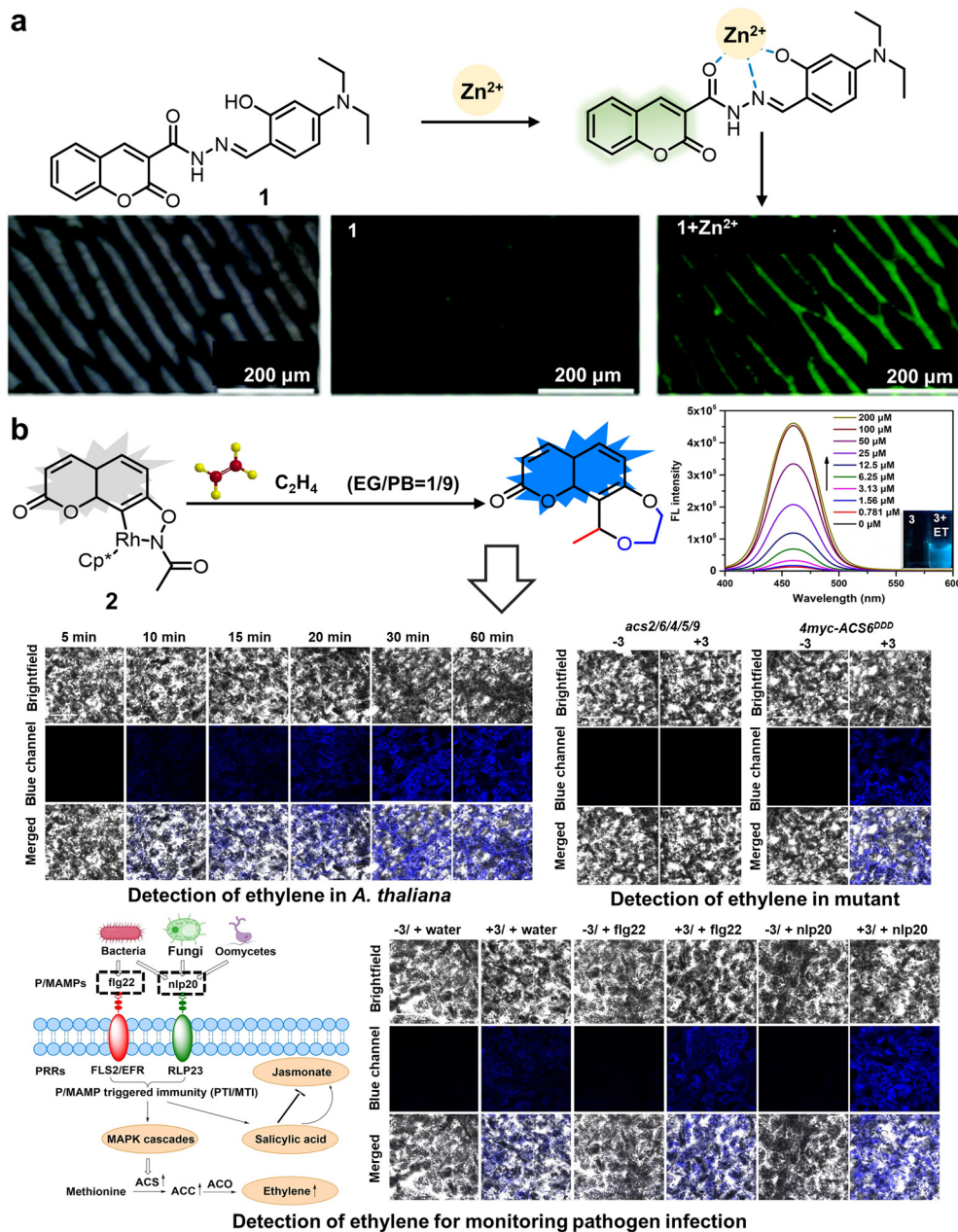This journal is © The Royal Society of Chemistry 2024

Fig. 3 Structure and application of fluorescent chemosensors **1** and **2** based on the 3-position or 7-position of coumarin for observing ions and hormones in plants. (a) Fluorescent chemosensor **1** synthesized using coumarin-2-hydrazine carbonate and 4-(diethylamino)-2-hydroxy-benzaldehyde can be used to monitor exogenous Zn^{2+} in plants.[41] Reproduced from ref. 41 with permission from The Royal Society of Chemistry. Copyright © 2021, The Royal Society of Chemistry. (b) Chemosensor **2** constructed utilizing the 7-position of coumarin, affording monitoring of stress-induced changes in ethylene biosynthesis and ethylene signal transduction.[42] Copyright © 2021, Wiley.

detection imaging given that they aid in reducing interference from background signals. In 2021, Wang *et al.* designed a highly specific colorimetric and ratiometric fluorescent chemosensor **5** comprised of coumarin aldehyde and HBT moieties. This chemosensor was responsive to HClO within 100 s due to the cleavage of the C=N bond (Fig. 4c). It sensed changes in extracellular or endogenous HClO levels inside plant cells within a short period (<100 s), causing a blue shift in fluorescence from the original green fluorescence (peak at 540 nm) to novel blue emission (peak at 480 nm). The LOD of **5** for the detection of HClO was 545 nM.

5 functioned as both a colorimetric and ratiometric chemosensor, enabling the imaging detection of HClO across diverse model systems. This highlights its broad spectrum of potential applications in the realm of plant science.[45] In 2023, Pan *et al.* developed a dual-responsive coumarin-derived NIR fluorescent chemosensor **6** for the simultaneous quantification of mitochondrial viscosity and cyanate (CN⁻). This chemosensor was synthesized using coumarin by expanding its double bond and linking benzindoles to enhance its conjugated structure (Fig. 4d). The significant increase in inner mitochondrial viscosity impeded the C=N bond rotation and

This journal is © The Royal Society of Chemistry 2024

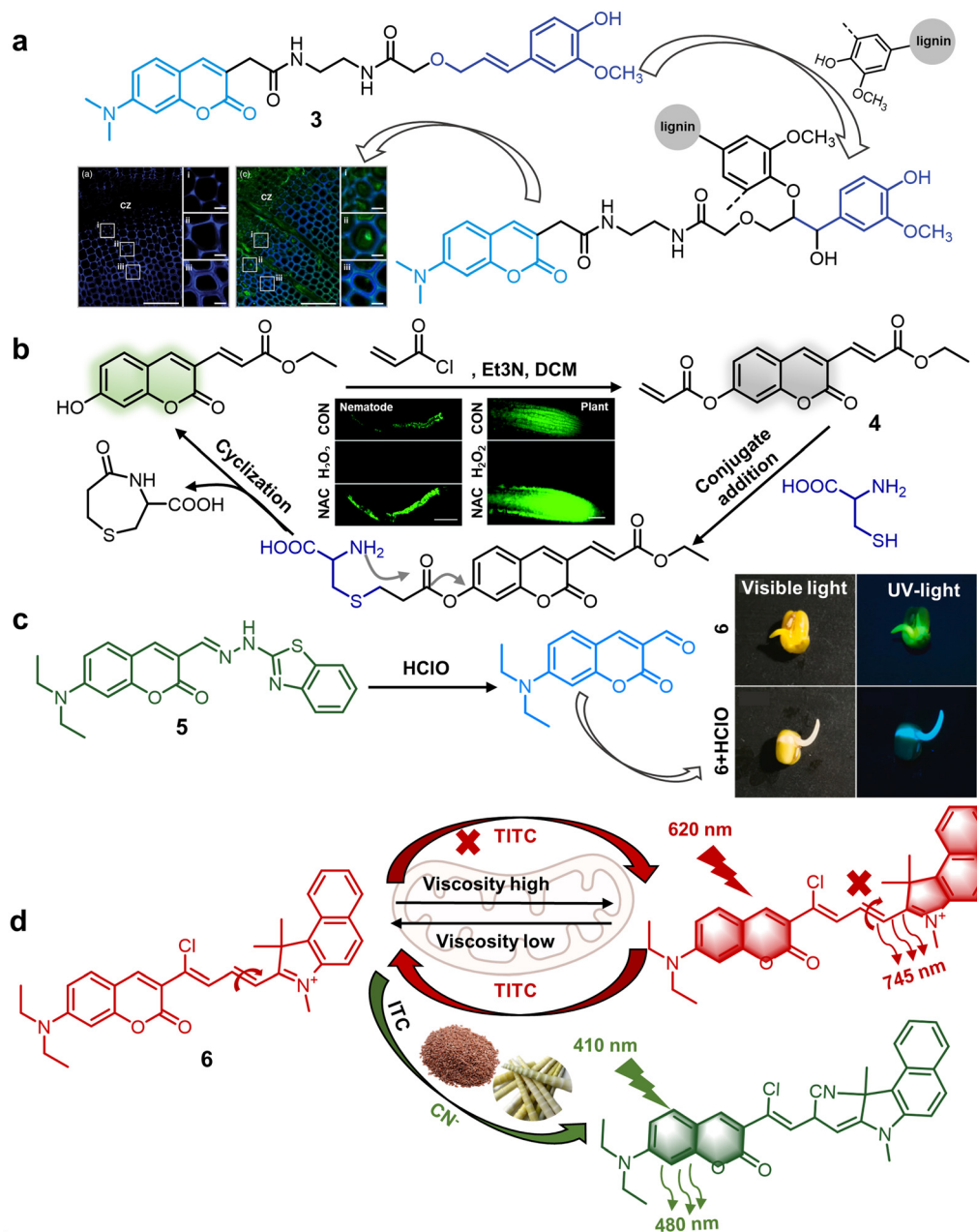*Chem. Soc. Rev.*, 2024, **53**, 6992–7090 | **6999**

Fig. 4 Structure and application of fluorescent chemosensors **3–6** based on the 3- and 7-positions of coumarin for monitoring the growth and components of plants. (a) Fluorescent chemosensor **3** can accurately detect the concentration of lignin to monitor plant cell wall lignification.[43] Copyright © 2013, Wiley. (b) Fluorescent chemosensor **4** can monitor cysteine changes in plants and nematodes under stress-induced oxidative stress.[44] Copyright © 2019, The Royal Society of Chemistry. Reproduced from ref. 44 with permission from The Royal Society of Chemistry. (c) Fluorescent chemosensor **5** can detect the concentration of HClO in plants.[45] Copyright © 2021, Elsevier. (d) Fluorescent chemosensor **6** can detect CN^- under different viscosity in the mitochondria in plants.[46] Copyright © 2023, Elsevier.

disrupted the organized conjugated system, thereby leading to a characteristic redshift of 125 nm (from 620 nm to 745 nm). Monitoring CN^- levels also resulted in the enhanced excitation of the chemosensor with peaks at the wavelength of 410 nm and 620 nm, which was caused by the nucleophilic addition reaction between the chemosensors and CN^-, disrupting the conjugated system and triggering a blue shift (410 nm/480 nm) at an LOD of 0.22 μM. Thus, **6** shows great promise for detecting CN^- under different mitochondrial viscosities in plants.[46] According to the proposed interaction mechanism, the carbonyl groups of the dicarboximide moiety with N_2H_4 resulted in liberated aromatic amines, which induced appreciable fluorescence shifts. These fluorescent chemosensors exhibited a large Stokes shift for fast response and high-selectivity monitoring of plant cell growth and the physiological state of mitochondria. Fluorescent chemosensors originating from the coumarin fluorophore have found extensive use in monitoring and imaging plant tissues and samples. Nonetheless, they have some limitations, such as longer emission wavelengths,

7000 | *Chem. Soc. Rev.*, 2024, **53**, 6992–7090

This journal is © The Royal Society of Chemistry 2024

elevated hydrophilicity, and minimal biological toxicity. Hence, the development and utilization of multifunctional fluorescent sensor materials, leveraging coumarin fluorophores with simple structures, versatility and high performance can facilitate the convenient detection of small molecule signals in plants.

Coumarin derivatives at the 3- and 7-positions have some advantages such as high solubility, photostability and large Stokes shift, and thus have been used for monitoring the health and living environment of plants. However, coumarin fluorescent chemosensors have certain drawbacks including high synthesis cost, complex synthesis process and environmental pollution. Therefore, further studies should focus on finding some new synthesis sites, recognition sites and mechanisms of action.

3.2 Naphthalimide derivatives

The naphthalimide family represents a traditional class of D–π–A fluorophores, wherein the naphthyl nucleus functions as a π bond, R1 denotes an electron donor moiety, and the imide fragment functions as an electrophilic region.[47] Naphthalimides inherently exhibit electron-deficient characteristics. Given the facile N-functionalization of the 1,8-naphthalic anhydride progenitor via the Gabriel phthalimide methodology, most of the existing reports in the literature focused on substitution reactions of non-polar alkyl substituents, leading to imide linkages, and thereby enhancing the solvent compatibility. Furthermore, there are some alternative reactive sites within the naphthalene moiety (Fig. 2),[48] which can be readily modified to achieve a large Stokes shift, superior fluorescence QY and exceptional photostability. Notably, the 4-position has predominantly been subjected to manipulations due to its convenience in synthesis and diminished synthesis costs (Table 3). These chemosensors have been widely utilized for detecting ions, amino acid, pesticides, and pathogens in plants, as well as the quality of soil and water.

3.2.1 Fluorescent chemosensors based on 4-position derivatives of naphthalimide.
The absorption and emission wavelengths of naphthalimides can be adjusted by altering the structure of the donating moiety, which is typically attached to the 4-position of the unit. Eight fluorescent naphthalimide derivatives at the 4-position were reported to evaluate the plant physiological status and irrigation water quality. In 2020, a two-photon (TP) ratiometric fluorescent chemosensor 7 was developed, which featured a TP fluorophore as the donor, an FA turn-on naphthalimide fluorophore as the acceptor, and a brief hydrazide linker (Fig. 5a). It displayed remarkable speed in detecting formaldehyde, exhibiting high sensitivity and exceptional selectivity within 65 s. Its noteworthy features included a 60-fold amplification at 550 nm (ex = 700 nm) and impressive LOD of 5.8 nM. Furthermore, 7 possessed good imaging resolution and deep tissue penetration, which are valuable for investigating the formaldehyde dynamics in living onion tissues through intramolecular charge transfer (ICT) and photoinduced electron transfer (PET).[49] In 2022, Kusano et al. synthesized a series of novel 1,8-naphthalimide-based chemosensors capable of selectively illuminating major subcellular structures such as the

Table 3 Fluorescent naphthalimide derivatives for monitoring plant health and their environment

Classifications	Chemosensors	$\lambda_{ex}/\lambda_{em}$ (nm)	Solvents	Limit of detection (LOD)	Target analytes	Applications	Ref.
Naphthalimide derivatives at 4-position	7	760/410, 550	$V_{DMSO}:V_{PBS} = 1:99$	5.80 nM	Formaldehyde	Investigating formaldehyde in living onion tissues	49
	8	405/540	Phosphate buffer solution, pH = 7.2	—	Plant intracellular compartments	Precise monitoring of subcellular behavior within the autophagic pathway	50
	9	420/560	$V_{PBS}:V_{DMSO} = 8:2$, pH = 7.4	16.3 nM	Cysteine	Detecting cysteine in plant roots, food samples and environmental water samples	51
	10	440/545, 565	Aqueous solution	—	The aggregation of anionic surfactants and bacteria	Monitoring the presence of cell membranes and bacteria	52
	11	420/520	Aqueous solution	—	Reduction products of azole in bacteria	Investigating the microbial degradation and transformation mechanism	53
	12	390/510	$V_{CH_3CN}:V_{HEPE} = 4:1$, pH = 7.4	6.60 nM for mesotrione, 7.37 nM for tembotrione, 10.2 nM for NTBC	HPPD inhibitors	Detecting HPPD inhibitors including mesotrione, tembotrione and NTBC in soil and water	54
	13	380/550	Acetonitrile	33.0 nM	F^-	Detecting F^- content in tea leaves and water	55
	14	420/520	Tris–HCl, pH = 7.01	2.00 nM	Hg^{2+}	Monitoring the concentration of Hg^{2+} in river water	56
Naphthalimide derivatives at 5-position	15	365/511	Aqueous solution	0.490 nM	2,4-Dinitrophenylhydrazine	The detection of 2,4-dinitrophenylhydrazine in real water and soil samples	57
	16	440/532	Aqueous solution	73.0 nM	Hg^{2+}	Recognition of Hg^{2+} in actual water, soil samples	58

This journal is © The Royal Society of Chemistry 2024

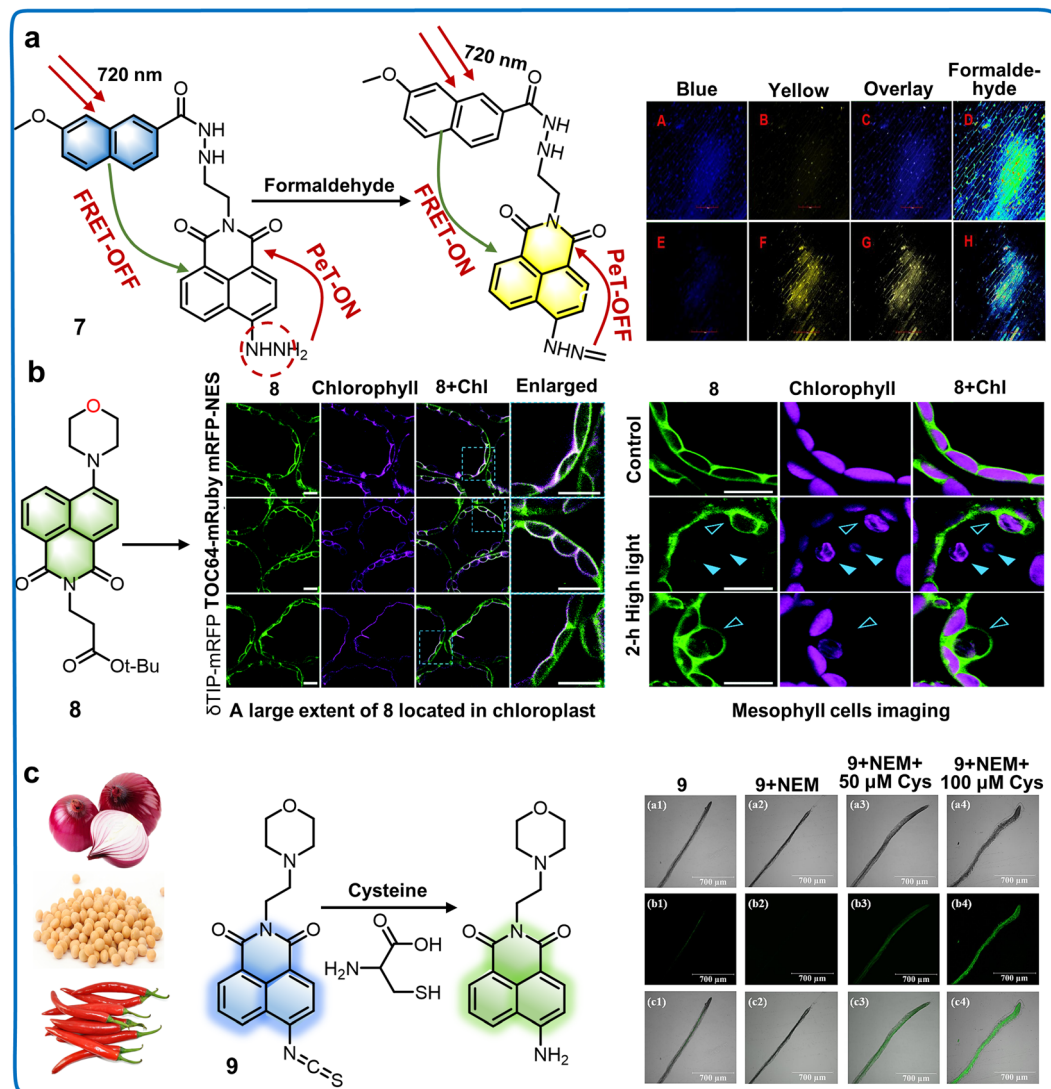*Chem. Soc. Rev.*, 2024, **53**, 6992–7090 | 7001

Fig. 5 Structure and application of fluorescent chemosensors **7–9** based on the 4-position of naphthalimide to monitor the subcellular structure and amino acid concentration in plants. (a) Fluorescent chemosensor **7** can detect formaldehyde rapidly in plants.[49] Copyright © 2023, Elsevier. (b) Fluorescent chemosensor **8** is capable of supervising the dynamic responses of plant organelle behaviors within an autophagic physiological process.[50] Copyright © 2021, The Royal Society of Chemistry. Reproduced from ref. 50 with permission from The Royal Society of Chemistry. (c) Concentration of cysteine in plants, food and water can be detected by fluorescent chemosensor **9**.[51] Copyright © 2023, Elsevier.

vacuolar membrane, the chloroplast envelope, and vacuolar lumen by modulating their spectral profiles (Fig. 5b). Among the chemosensors, the morpholino-substituted 1,8-naphthalimide (chemosensor **8**) demonstrated rapid cell wall permeation and subsequent accumulation in the chloroplast, allowing the examination of the chloroplast dynamics given that the degraded chloroplasts transported into the vacuolar lumen *via* chlorophagy remained unstained. These fluorescent chemosensors enabled the real-time assessment of organelle behaviors within an autophagy pathway.[50] In 2023, a novel lysosome-directed Cys fluorescent chemosensor (**9**) was synthesized by incorporating an isothiocyanate moiety as the Cys recognition site within the naphthalimide fluorophore and integrating it with a morpholine moiety for lysosomal targeting (Fig. 5c). **9** exhibited a large Stokes shift (420 nm → 560 nm), negligible cytotoxicity, and

marked selectivity for detecting Cys in plant roots, food samples and water samples with an LOD of 16.3 nM. The Stokes shift of **9** decreased the background interference, which increased its detection accuracy and sensitivity.[51] By incorporating an azetidine moiety in the aromatic nucleus of **10**, it served as an electron-donating structural element, and strategically locating a hydrophilic (2-(2-aminoethyl-amino)ethanol) moiety within the "*N*-imide site" of the core structure (Fig. 6a). This chemosensor showed enhanced fluorescent intensity at 560 nm, making it well suited for tracking the assembly pathway of negatively charged surfactants, which is primarily ascribed to its exceptional surface accumulation property. Meanwhile, it was effectively utilized to detect bacteria and cell membranes by exploiting their negatively charged surfaces, thus serving as essential tools for the rapid measurement of biological contamination in water. These results

7002 | *Chem. Soc. Rev.*, 2024, **53**, 6992–7090

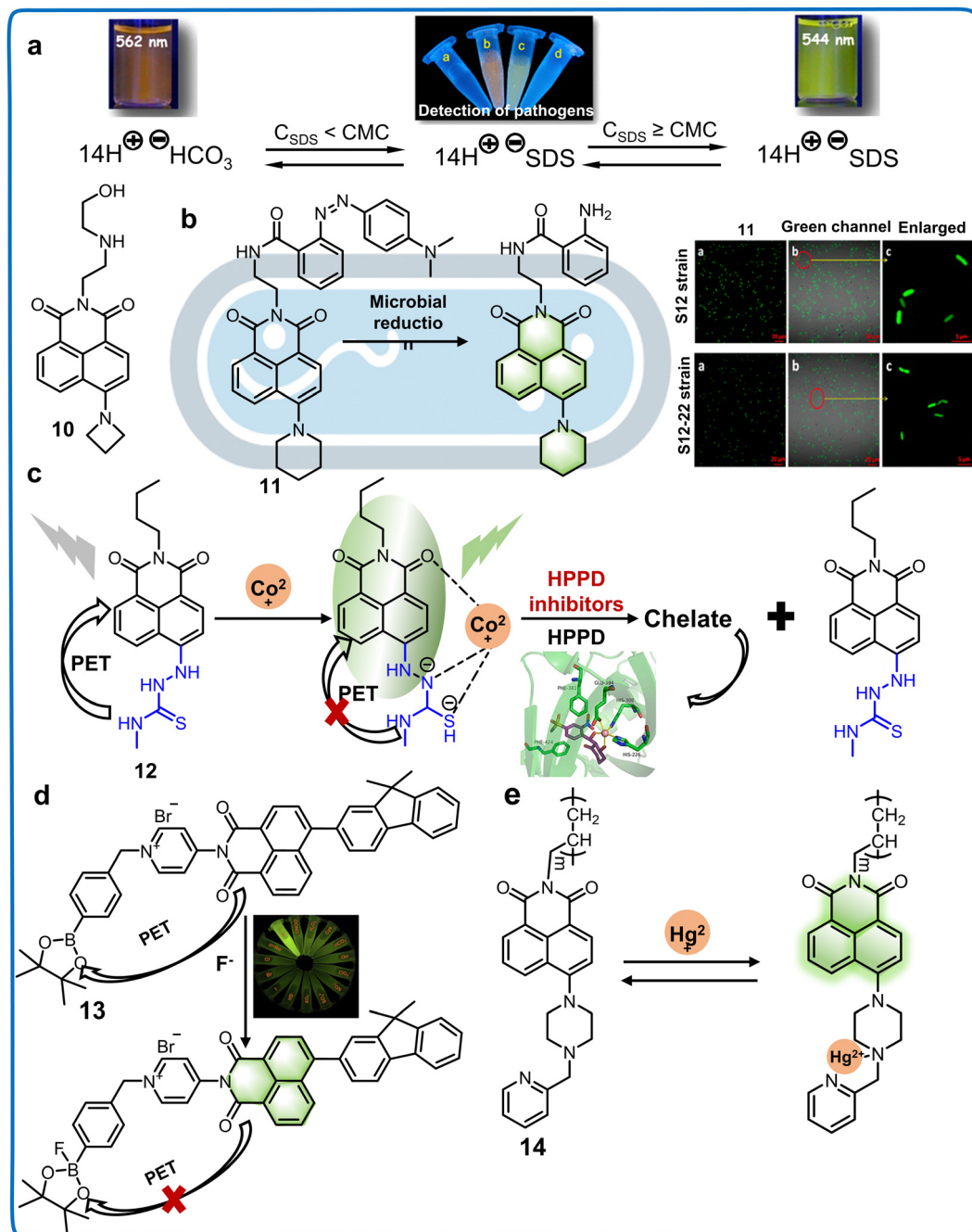This journal is © The Royal Society of Chemistry 2024

Fig. 6 Structure and application of fluorescent chemosensors **10–14** based on 4-position of naphthalimide to detect the pathogens, pesticides and ions in the living environment of plants. (a) Fluorescent chemosensor **10** can detect cell membranes of bacteria by detecting the viscosity and polarity of the medium.[52] Copyright © 2017, the American Chemical Society. (b) Fluorescent chemosensor **11** is a useful tool for understanding the degradation pathways of azo dyes in different microbial systems.[53] Copyright © 2015, the American Chemical Society. (c) Fluorescent chemosensor **12** exhibits remarkable potential for precisely detecting residual levels of HPPD inhibitors in water.[54] Copyright © 2021, Elsevier. (d) Fluorescent chemosensor **13** can detect F⁻ content in foods.[55] Copyright © 2022, Elsevier. (e) Fluorescent chemosensor **14** has a highly selective to response to Hg²⁺ in real water samples.[56] Copyright © 2013, Elsevier.

indicated that **10** has high potential for detecting microbial diversity in the living environment of plants.[52] Fluorescent chemosensor **11** designed based on 1,8-naphthalimide and azo dyes can trace the microbial degradation routes of azo dyes via fluorescence resonance energy transfer (FRET) (Fig. 6b). In *Pseudomonas stutzeri*, its inherent attributes such as low polarity

and hydrophobicity of the azo dye allowed it to be internalised within cells, where it underwent reduction processes, while the relatively more polar and hydrophilic azo dye was relegated to reduction outside the cells. This phenomenon could be observed by the changes in fluorescence from darker yellow to brighter yellow. This chemosensor can pioneer a novel research models

This journal is © The Royal Society of Chemistry 2024

Chem. Soc. Rev., 2024, **53**, 6992–7090 | 7003

for investigating microbial degradation and transformation mechanisms through the utilization of chemical fluorescent-labeling technology, which can provide guidance for engineering bacteria modification.[53] In 2021, the compound *N-n*-butyl-4-methylhydrazinecarbothioamide-1,8-naphthalimide (chemosensor **12**) was exclusively formulated and successfully manipulated to detect Co^{2+}, affording an exceptional LOD of 7.82 nM through its fluorescence-on response. As illustrated in Fig. 6c, this was achieved by employing a fluorescent complex, namely NMN–Co^{2+}, as a tool for identifying specific herbicide products known as HPPD inhibitors. Excitingly, these compounds exhibited a novel "turn-off" response with their sensing mechanism involving a competitive interaction between the chemosensor and HPPD in conjunction with Co^{2+}. Notably, the corresponding LODs for NTBC, tembotrione, and mesotrione (HPPD inhibitors) were 10.22 nM, 7.37 nM, and 6.60 nM in water and soil samples, respectively. NMN represents the first fluorescent probe to be employed for discerning HPPD inhibitors with exceptional selectivity and sensitivity, offering a promising avenue for detecting the residues of triketone HPPD inhibitors.[54] In 2022, a fluorescent chemosensor (**13**), constructed from 1,8-naphthalimide and an organoboron compound (4,4,5,5-tetramethyl-2-phenyl-1,3,2-dioxaborolane), functioning as a putative receptor of F^-, was identified (Fig. 6d). The robust Lewis acidic boron moiety of **13** enabled tight coordination with basic F^-, and then inhibiting direct PET linkage from the fluorophore to the boron site, thereby

elevating the fluorescence emission at 540 nm. The LOD of **13** for F^- was established as exceedingly low at 33 nM, which could be effectively applied for detecting F^- in tea leaves and water.[55] Additionally, naphthalimide fluorescent chemosensor **14** endowed with a terminal double bond was formed following reaction with an appropriate organoboron compound. The post-modification step involved photo-crosslinking with 2-hydroxyethyl methacrylate on a glass surface (Fig. 6e). It was applied for the quantification of Hg^{2+} in river water at 520 nm with an LOD of 2 nM.[56] Continued research may unveil more naphthalimide derivatives with superior capabilities in detecting and monitoring an extended range of hazardous substances in the environment, thereby promoting favorable conditions for plant growth.

3.2.2 Fluorescent chemosensors based on 5-position derivatives of naphthalimide. Modifications at alternative sites of naphthalimide have also been devised for the synthesis of fluorescent probes for plant-related detection. Two fluorescent naphthalimide derivatives at the 5-position were developed to evaluate the soil quality in the living environment of plants. "Turn-off" fluorescent chemosensor **15** was constructed by utilizing chitosan as its skeleton and naphthalimide as the fluorophore, which remarkably showed a distinct response to 2,4-dinitrophenyhydrazine (DNPH) in river and soil extracts, leading to a change in fluorescence color from green to colorless (Fig. 7a). The LOD for DNPH was equated to a threshold of 0.49 nM.[57] Another chitosan-naphthalimide fluorescent chemosensor **16** was
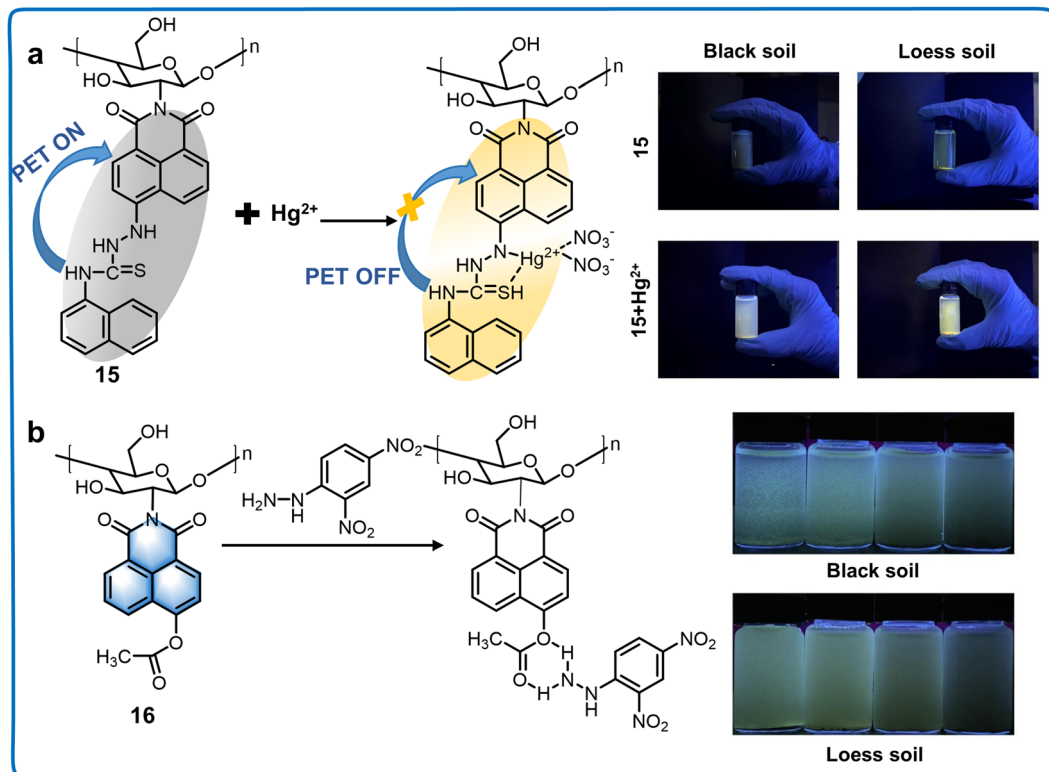

Fig. 7 Structure and application of fluorescent chemosensors **15** and **16** based on 5-position of naphthalimide for monitoring the quality of soil in the living environment of plants. (a) Fluorescent chemosensor **15** can be applied for the quantification of Hg^{2+} in irrigation water.[57] Copyright © 2021, Elsevier. (b) Fluorescent chemosensor **16** can monitor the concentration of DNPH in soil samples.[58] Copyright © 2023, Elsevier.

7004 | *Chem. Soc. Rev.*, 2024, **53**, 6992–7090

This journal is © The Royal Society of Chemistry 2024

synthesized based on chitosan and 4-bromo-1,8-naphthalic anhydride, which exhibited no fluorescence in the solution phase initially (Fig. 7b). Upon the detection of Hg^{2+}, an appreciable enhancement in fluorescence emission at 532 nm was observed, presenting a transformation from colourless to bright luminous yellow. This sensor displayed optimal properties with an LOD of 73 nM for recognizing Hg^{2+} in actual water and soil samples.[58] Furthermore, this type of fluorescent chemosensor could be used for monitoring the ion levels in plants and their response to external stresses owing to its good water solubility. As a result, environmentally friendly fluorescent chemosensors utilizing naphthylimide fluorophores have been developed, broadening the application scope of natural materials such as chitosan. These advancements have also aided in the development of fluorescent chemosensors for the detection of toxic substances over prolonged periods, allowing the observation of alterations in environmentally hazardous compounds.

Currently, 4-position naphthalimide derivatives with the advantages of photostability and good two-photon properties have been applied for monitoring plant health. However, are also some disadvantages to overcome, as follows: (i) the active site of naphthalimide is the 4-position, which limits the diversity of fluorescent chemosensors. Thus, to increase their diversity, novel recognition groups and various substituent units should be investigated. (ii) The low water solubility of naphthalimide derivatives decreases their sensitivity and responsiveness. (iii) The unstable and poor heat resistance of naphthalimide derivatives limit their application scope and accuracy.

3.3 Rhodamine derivatives

Rhodamine derivatives, part of the xanthene family together with fluorescein and eosin dyes, function as fluorophores with spectra relatively unaffected by pH changes within the range of 4–10.[59] Discovered in 1887, they have diverse applications in biotechnology, acting as fluorescent markers and aiding in the detection of small-molecules.[60] Since 1945, rhodamine-based chemosensors, capitalizing on analyte-induced spirolactam opening, have been designed for detecting metal ions and other biologically relevant species.[61] Rhodamine dyes, with moderate hydrophilicity, high absorption coefficient, elevated fluorescence QY, exceptional photostability, and visible light emission, have evolved beyond basic fluorescent labeling reagents into advanced fluorescent chemosensors.[62] This section focuses on rhodamine-derived chemosensors, especially those targeting the health and living environment of plants (Table 4).[63] The classical rhodamine dyes are predominantly employed in these applications, although in recent years, diverse modifications of rhodamine scaffolds have been performed for the visualization of plant components (Fig. 2).

3.3.1 Fluorescent chemosensors based on Z-position derivatives of rhodamine. Fluorescent chemosensors, utilizing Z-position rhodamine derivatives, have been extensively applied in detecting plant physiological signals and environmental parameters. For the detection of plant hormones, chemosensor **17**, employing rhodamine Z-position derivatives, showed

remarkable sensitivity with an LOD of 1 nM for salicylic acid (SA) (Fig. 8a).[64] It effectively detected the distribution and concentration of SA in plant callus tissues, serving as a sensitive tool for monitoring plant physiological states. Due to its promising performance and potential applications, **17** warrants further investigation for monitoring salicylic acid (SA) in the plant kingdom. This exploration may unveil novel immune activators for plant protection. For the detection of ions, an NIR fluorescence chemosensor (**18**) was engineered using the excellent fluorescence response platform of rhodamine dye, with a red-shifted emission wavelength to 695 nm (Fig. 8b).[65] Spectral experiments confirmed its fast response and high selectivity to Hg^{2+}, finding applications in the biological domain, particularly in plant cells. The long emission wavelength of **18** suggested that it has high potential for monitoring the concentration of ions in plant tissues owing to its deep tissue penetration and low background interference. The synthesis of a reversible Al^{3+}-specific fluorescent chemosensor (**19**) involved the conjugation of rhodamine B and pyridine-3-sulfonyl chloride, employing the molecular connector *o*-phenylenediamine (Fig. 8c).[66] This chemosensor exhibited exceptionally high sensitivity and a high selective response to Al^{3+}, which was effective for detecting low concentrations of Al^{3+} in plant tissues. Similarly, an activatable fluorescent chemosensor, rhodamine-based chemosensor **20**, was designed through an acylation reaction at high temperature (Fig. 8d).[67] Its reversibility with Fe^{3+} was confirmed by adding $Na_4P_2O_7$, proving useful for detecting Fe^{3+} in environmental water samples. Meanwhile, biological experiments confirmed that **20** could be used to detect Fe^{3+} in plant tissues, implying that **20** showed favorable water solubility and membrane penetration. Chemosensor **21**, with a 2-[(1*H*-pyrrol-2-ylmethyl)-(2-pyridinylmethyl)amino]-tripodal receptor integrated in its structure, exhibited unique characteristics, including photophysical spectral modifications, possessing specific affinity for Co^{2+}, a notably high association constant, accelerated metal-chemosensor reaction rates, and "on–off" signaling reversibility, together with a wide operational pH range. It was utilized in tracking the assimilation and accumulation of Co^{2+} within root and shoot tissues of *Hybanthus enneaspermus* (Fig. 8e). The results implied that **21** may be a useful tool for studying the accumulation of ions in plants or tracing the translation of ions from the environment to plants.[68] Integrating Z-position rhodamine derivatives into smart devices further facilitated the remote monitoring of various ions in the field and plants. Fluorescent sensors based on Z-position rhodamine derivatives offer unparalleled advantages such as their versatility across various plant species and capacity to rapidly convert endogenously produced chemical signals into detectable optical signals.

3.3.2 Fluorescent chemosensors based on 2′, Z-position derivatives of rhodamine. 2′, Z-position rhodamine derivatives have been proven to be versatile for detecting hormones and ions in plants. A recent breakthrough was chemosensor **22**, which was synthesized using benzothiazole and rhodamine, facilitating the visualization of SA in plant tissues. This chemosensor was proven to be effective in monitoring SA levels,

Table 4 Fluorescent rhodamine derivatives for monitoring plant health and their environment

Classifications	Chemosensors	$\lambda_{ex}/\lambda_{em}$ (nm)	Solvents	Limit of detection (LOD)	Target analytes	Applications	Ref.
Rhodamine Z-position derivatives	17	554/578	$V_{methanol}:V_{H_2O} = 9:1$	1.00 nM	Salicylic acid (SA)	Detecting the concentration and distribution of SA in plant callus tissues	64
	18	620/695	$V_{H_2O}:V_{EtOH} = 5:1$ (HEPES, 2.0 mM, pH = 7.0)	0.340 μM for Hg^{2+}; 1.63×10^5 M^{-1} for S^{2-}	Hg^{2+} and S^{2-}	Detecting Hg^{2+} in plant cells	65
	19	520/582	$V_{EtOH}:V_{H_2O} = 1:2$	14.2 nM	Al^{3+} and F^-	Detection of trace Al^{3+} ions in water and biological systems local river and lake water/plant tissues	66
	20	520/582	$V_{EtOH}:V_{H_2O} = 1:1$ (HEPES, 0.5 mM, pH = 7.3)	0.148 μM	Fe^{3+} and $Na_4P_2O_7$	The detection of Fe^{3+} in cells, and plant tissues	67
	21	500/580	$V_{THF}:V_{H_2O} = 8:2$ (HEPES, 0.01 M, pH = 7.4)	3.00 μM	Co^{2+}	Detecting Co^{2+} in root and shoot tissues of plant	68
Rhodamine 2′ and Z-position derivatives	22	565/590	$V_{MeCN}:V_{H_2O} = 2:3$	1.00 nM	Salicylic acid (SA)	Monitoring SA in plants and food	69
	23	560/700	$V_{EtOH}:V_{H_2O} = 1:1$	0.0770 μM for Hg^{2+}; 0.170 μM for S^{2-}	Hg^{2+} and S^{2-}	Detecting Hg^{2+} in living cells, animals and plant tissues	70
Rhodamine 2′, R2, R4-position and	24	515/555	$V_{Acetonitrile}:V_{HEPES} = 4:1$, pH 7.4	0.164 ppb	As^{3+}	Detecting As^{3+} from a series of wastewater specimens	71
2′-position derivatives	25	470/635	$V_{EtOH}:V_{PBS\ buffer} = 7:3$, pH = 7.4	29.0 nM for Cu^{2+}; 122 nM for Hg^{2+}	Cu^{2+} and Hg^{2+}	Visualization of Hg^{2+} and Cu^{2+} in soil and plants	72
	26	530/552	Ethanol	20.0 μM	Perillaldehyde	Detection of perillaldehyde in the leaves of plants	73
	27	530, 580/640	30% acetonitrile aqueous solution	26.2 nM	Ni and PPh$_3$	Detection of Ni and PPh$_3$ in plant and surroundings	74

with a rapid response time of less than 1 min, high sensitivity, photostability, and LOD of 1 nM. As the SA concentration increased from 0 to 1000 μM, the test strips changed color from colorless to pink, while the fluorescence color shifted gradually from blue to pink to purplish. This advancement holds promise for plant biology studies and effectively detecting excess SA in common foods such as grapes, bananas, and cucumbers, serving as a warning system for SA-sensitive individuals (Fig. 9a).[69] Another innovative design, chemosensor **23**, based on thiooxo-rhodamine B, involved sulfiding rhodamine spironolactam carbonyl groups to thiocarbonyl groups (Fig. 9b).[70] This fluorescent chemosensor exhibited a traditional reversible "turn-off–on" response with a uniform 1:1 binding stoichiometry. Notably, its C=S functional group served as a recognition group for Hg^{2+}, achieving an LOD of 0.077 μM. Its versatility extended to detecting Hg^{2+} in irrigation water and plant tissues. Chemosensors utilizing this fluorophore were utilized to detect and image cations, anions, and phytohormones in plant samples. Additionally, they have the potential to expand their application in plant health monitoring by detecting metabolites, reactive oxygen species (ROS), and other pertinent compounds.

3.3.3 Fluorescent chemosensors based on 2′, R2, R4-positions and 2′-position derivatives of rhodamine. 2′, R2, R4-position rhodamine derivatives are widely used for monitoring and quantifying the active constituents within plant samples and environmental samples, exhibiting versatile applications. Paul *et al.* demonstrated the arsenic-induced cleavage of the spirolactam ring in a cleft-shaped, electronically enriched rhodamine-derived chemoreceptor molecule, PBCMERI-23 (Fig. 10a).[71] Chemosensor **24**, derived from this structure, displayed a 2-fold optical response (chromogenic, colorless to reddish pink; fluorogenic, non-blooming fluorescence to yellow emission) *via* the ring-opening phenomenon of the developed chemoreceptor. It showed sparkling yellow illumination under a fluorescence microscope, confirming cell permeability and serving as a biomarker for intracellular investigation and As^{3+} imaging in plant samples. Erdemir *et al.* introduced red-emitting fluorescent chemosensor **25**, characterized by a substantial Stokes shift (about 220 nm), incorporating isophorone and rhodamine moieties (Fig. 10b).[72] This compound displayed outstanding linear responsiveness toward Thiram, Cu^{2+}, and Hg^{2+} in real soil samples, with LODs of 72.0 nM, 29.0 nM, and 122.0 nM, respectively. Moreover, the complex formed between the chemosensor and Cu^{2+} enabled the visualization of Thiram residues on a leaf surface, demonstrating the versatility of a singular probe. Zhao *et al.* developed chemosensor **26**, an innovative "turn-on" and dual-mode sensor platform for the quantification of perillaldehyde concentration (Fig. 10c).[73] Equipped with appropriate solid-state irreversible sensors, these diagnostic strips adeptly evaluated the level of perillaldehyde present in *Perilla frutescens* leaves, offering potential applications in smart agriculture. The modification of the benzene ring at the 2′-position of rhodamine derivatives facilitated the assessment of the living environment of plants, including irrigation water quality and soil condition. In response to the carcinogenic nature of nickel compounds, Wang
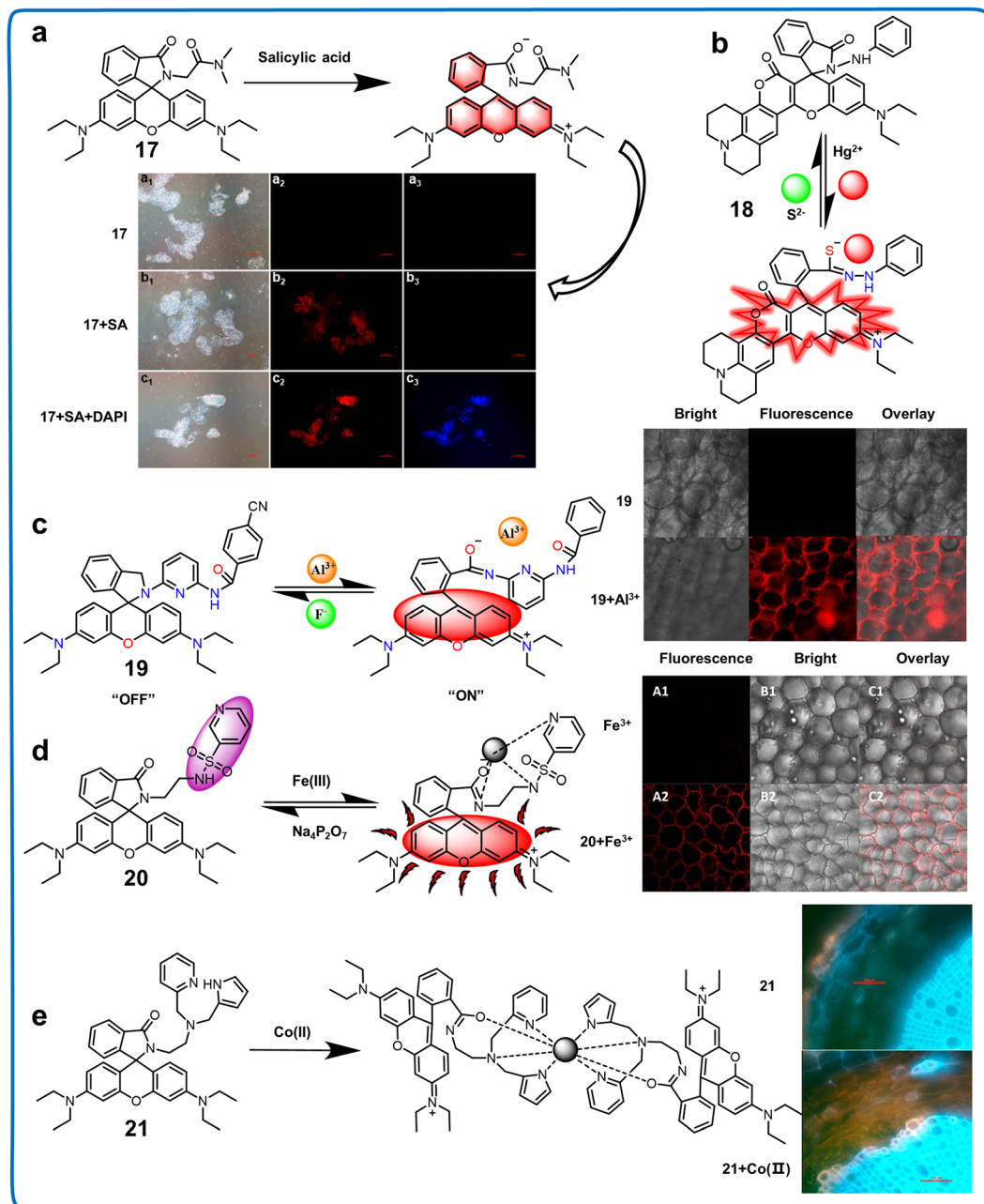
7006 | *Chem. Soc. Rev.*, 2024, **53**, 6992–7090

This journal is © The Royal Society of Chemistry 2024

Fig. 8 Structure, mechanism and application of fluorescent chemosensors **17–21** based on Z-position rhodamine derivatives in live cell imaging. (a) Fluorescent chemosensor **17** can monitor the distribution and concentration of SA in plant callus tissues.[64] Copyright © 2020, the American Chemical Society. (b) Fluorescent chemosensor **18** can detect Hg^{2+} in plant cells.[65] Copyright © 2022, Elsevier. (c) Fluorescent chemosensor **19** can detect trace Al^{3+} ions in local river/lake water samples and plant tissues.[66] Copyright © 2020, Elsevier. (d) Fluorescent chemosensor **20** can monitor Fe^{3+} in cells, *in vivo* and plant tissues.[67] Copyright © 2020, Elsevier. (e) Fluorescent chemosensor **21** could be utilized for the detection of Co^{2+} in different plant tissues.[68] Copyright © 2016, Elsevier.

et al. developed chemosensor **27**, an Ra–Ni ratiometric fluorescent chemosensor, sensitively detecting nickel ions with an LOD of 26.2 nM and rapid response (< 2 min) (Fig. 10d).[74] Its practical effectiveness in actual water samples emphasized its utility in environmental applications. In summary, rhodamine derivatives located at the 2′, R2, R4-positions, and the 2′-position offer efficient and simple tools for detecting ions, small molecules related to plant signaling, plant components, and pesticide residues. They present a novel and versatile approach for exploring physiological and pathological processes in plants. With their favorable performance, we anticipate the expansion of their applications for monitoring plant health.

Rhodamine derivatives have been widely used for monitoring the living environment and health of plants owing to their photostability, wide wavelength range and insensitivity to pH. However, they have some disadvantages, which should be
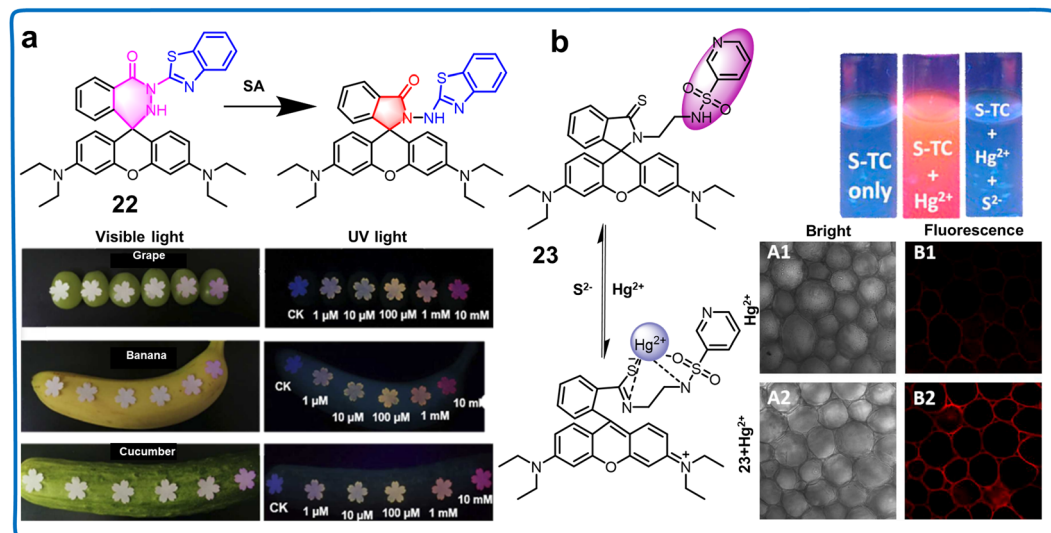
Fig. 9 Structure, mechanism and application of fluorescent chemosensors **22** and **23** based on 2′, Z-position rhodamine derivatives in monitoring phytohormone and ions in plants. (a) Fluorescent chemosensor **22** can monitor SA in plants and food.[69] Copyright © 2023, Elsevier. (b) Fluorescent chemosensor **23** can detect Hg^{2+} in plant tissues.[70] Copyright © 2019, Elsevier.

improved including (i) poor lipophilicity and poor penetration of cells, which make it difficult for *in vivo* imaging and (ii) low specificity and selectivity for specific binding, which decreases their detection accuracy. Thus, some specific recognition groups should be added to improve their selectivity.

3.4 Fluorescein derivatives

Fluorescein distinguishes itself as an eminently adaptable platform for diverse fluorescent chemosensors and markers, boasting high-intensity emission peaks, substantial molar absorption coefficients, and remarkable QY in aqueous media (Table 5).[75] Synthesized in 1871, fluorescein has gained significant attention and proven to be highly promising in various applications, particularly in smart sensors and bioimaging. The characteristic spirolactam structure of fluorescein enables a "close–open" transition with a "turn-on" fluorescence response in specific environments or events, making it an excellent dye for designing chemosensors.[76] Fluorescent chemosensors based on fluorescein offer the advantage of modification at two distinct moieties through organic synthesis, *i.e.*, the xanthene ring and benzoic acid moiety (benzene moiety).[77] This structure enables modifications at the 2′-position, alterations to the hydroxyl group, or replacement of the oxygen atom at the 9-position (Fig. 2). Typically, most derivatives undergo modifications at these sites, enhancing the versatility of the fluorescein structure in designing functional and adaptable chemosensors (Table 5).

Fluorescent chemosensors based on the 2′-position of fluorescein can be used to image and monitor physiological signals in the field of plant research. Potter *et al.* utilized a 2′-position fluorescein derivative to exploit the thiol-dependent quenching of fluorescein isothiocyanate (FITC) in developing a sulfide-specific assay. This innovative approach employed a polydimethylsiloxane (PDMS) membrane (chemosensor **28**), which is permeable to hydrogen sulfide while excluding larger charged

thiols (Fig. 11a).[78] They found that the formation of fluorescein dithiocarbamate (FDTC) upon reaction with sulfide could specifically interact with *S*-nitrosothiols (RSNO), regenerating FITC. This process acted as a specific, fluorogenic reagent capable of detecting picomolar levels of RSNO. These findings contribute to understanding the changes in plants induced by bio-thiols and peroxides.

Simultaneously, 9-position fluorescein derivatives have been applied in the detection of various plant components and signal changes in plants. In 2020, Takaoka *et al.* reported an innovative methodology involving fluorescence-imaging and utilization of fluorescein diacetate conjugated with Hoechst 33342, a well-known nuclear staining compound (chemosensor **29**), facilitating the rigorous qualitative quantification of stoma dynamic responses (Fig. 11b).[79] Using this method, the dynamic motion of stomata in *Arabidopsis thaliana* was interpreted through the straightforward surveillance of irregular changes in fluorescence intensity within the nuclear region of the stomata. The results indicated that **29** may be an alternative tool for regulating the drought response of plants or screening drought-resistant plants. Finally, a 9-position fluorescein derivative was valuable for the efficient detection of ions in food samples. Compounds functionalized with fluorescein and catechol (chemosensor **30**), synthesized through a Schiff base reaction, exhibited recognition capabilities for ClO^- in food items (Fig. 11c).[80] Based on its excellent selectivity, high sensitivity (LOD of 36.3 nM), "fast" response time (15 s), and large Stokes shift (353 nm), **30** was employed to detect exogenous ClO^- in potato sprouts. These fluorescein derivatives can be employed to detect small active molecules that are challenging to capture and to track kinetic processes in plants. The anticipated advantages of employing fluorescein in objective analyses include enhancing the capability for high-throughput examination of chemical repositories. This facilitates the development of
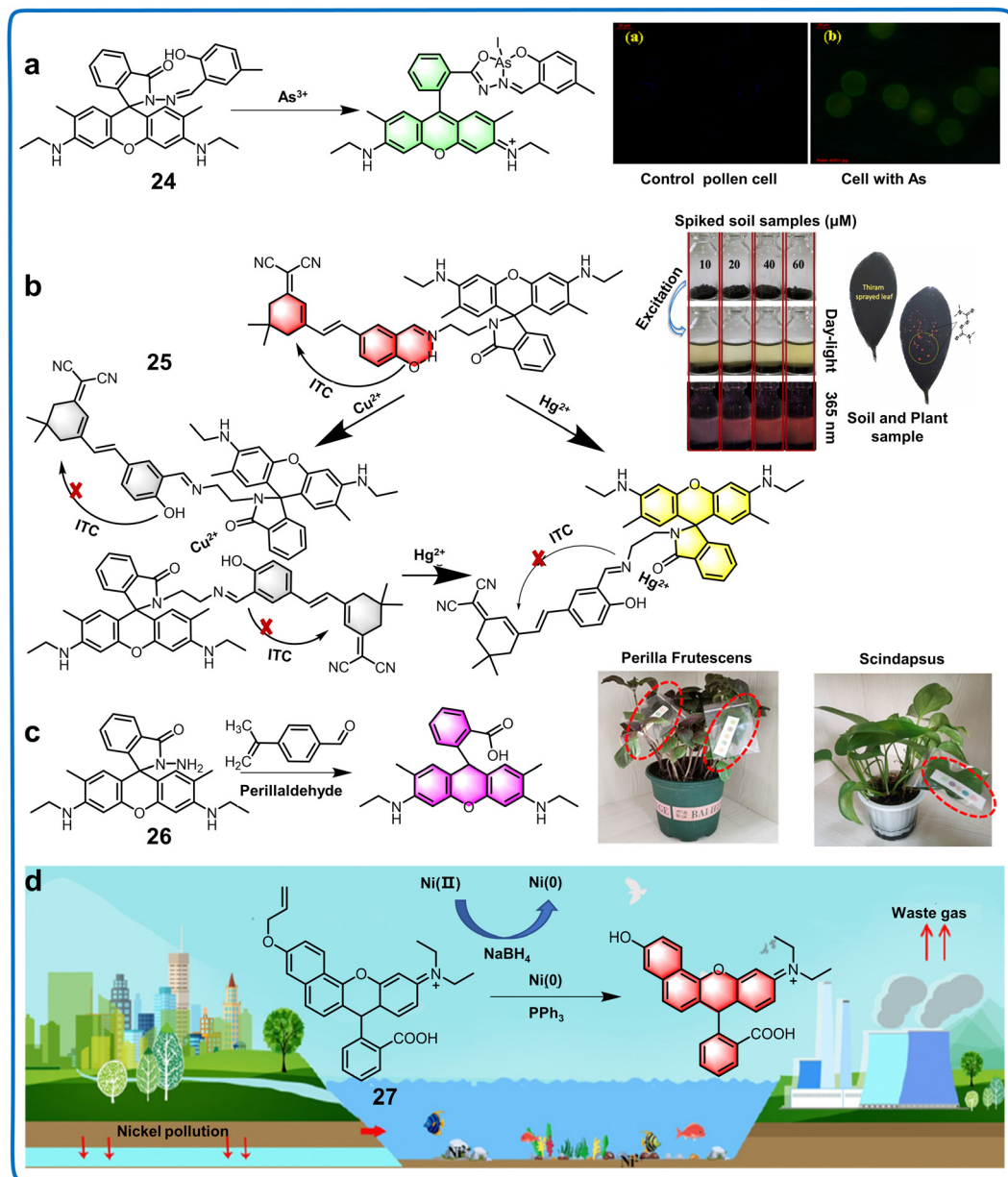
7008 | *Chem. Soc. Rev.*, 2024, **53**, 6992–7090

This journal is © The Royal Society of Chemistry 2024

Fig. 10 Structure, mechanism and application of fluorescent chemosensors **24–27** based on 2′, R2, R4-position and 2′-position rhodamine derivatives in soil samples and plants. (a) Fluorescent chemosensor **24** can detect As(III) in a series of water specimens.[71] Copyright © 2019, the American Chemical Society. (b) Fluorescent chemosensor **25** can be used for the visualization of Hg^{2+} and Cu^{2+} in soil and plant.[72] Copyright © 2023, Elsevier. (c) Fluorescent **26** can be utilized for the detection and evaluation of perillaldehyde in the solution phase and plant leaves.[73] Copyright © 2022, the American Chemical Society. (d) Fluorescent chemosensor **27** can detect Ni and PPh$_3$ in the living environment and tissues of plants.[74] Copyright © 2022, Elsevier.

innovative chemical chemosensors and provides insights into biosensors. The utilization of fluorescein-based chemosensors has the potential to deepen our comprehension of plant responses to environmental changes.

Fluorescein derivatives show high water solubility and QY but they also have some disadvantages, as follows: (i) their light stability is poor and their fluorescence is easily quenched after long irradiation. Further studies should focus on modifying and optimizing the structure of fluorescein derivatives to improve their stability. (ii) They are very sensitive to pH and their fluorescence intensity can change under different pH

conditions, which decrease their application scope and detection accuracy.

3.5 NBD derivatives

In 1968, Ghosh and Whitehouse reported the synthesis of 4-chloro-7-nitro-2,1,3-benzoxadiazole (NBD-Cl), an ingeniously conceived fluorogenic reagent exclusively engineered for the detection of amino acids and various amines. Since its discovery, compounds featuring the NBD framework are prevalent in biochemical studies and chemical biological explorations, marking their significance in various research domains.[85] The

This journal is © The Royal Society of Chemistry 2024

Chem. Soc. Rev., 2024, **53**, 6992–7090 | **7009**

spectral range of the emission from *N*-monoalkyl NBD amines (NBD-NHR) extends beyond 420 nm, with their fluorescence arising from ICT transitions.[86] In NBD-NHR assemblies, the amino function serves as the ICT donor, while the nitro site, a potent electron-withdrawing moiety, operates as the acceptor.[87] Notably, donor–acceptor (also known as push–pull)-type dipolar fluorophores generally exhibit strong emission in organic solvents but are often less effective in aqueous media due to the hydrogen bond interactions between water and the 2-oxa-1,3-diazole moiety of NBD, leading to nonradiative dissociation channels. Consequently, NBD-NHR species in aqueous solutions tend to have lower QYs.[88] However, the distinct advantages such as water solubility, eco-sensitivity, and concise dimensions of NBD-NHR fluorophores make them highly valuable, facilitating biomolecular interactions and self-assembly, especially in living systems (Table 5). The structural characteristics of the latter two compounds are commonly harnessed in the visualization of plant health (Fig. 2).

NBD derivatives are some of the most used fluorophores for live plant imaging owing to their simplicity, high efficiency, high sensitivity and low detection limits in fluorescence analysis. FluorA I and II, fluorescent conjugates of 2,4-D with NBD, served as promising auxin chemosensors (31), mimicking known auxin distribution patterns in distinct developmental processes. These conjugates displayed potential for visualizing auxin distribution in plant roots and apical hooks (Fig. 12a).[81] Additionally, the probe revealed the presence of fluorescent analogues in specific organelles such as the ER and endosomes. This toolkit provided high spatiotemporal resolution support for elucidating the mechanisms governing the precise, local regulation of auxin distribution in living materials. Tobimatsu *et al.* reported the synthesis of a range of monolignol analogs, γ-conjugated with substrates such as fluorogenic aminocoumarin and nitrobenzofuran dyes (chemosensor 32), which were examined for potential application as imaging chemosensors. They proved to be valuable for visualizing the cell wall lignification process in *A. thaliana* and *Pinus radiata* under diverse feeding conditions (Fig. 12b).[43] An NBD derivative, chemosensor 33, was applied for the detection of pH, anions, cations, and biothiols in plants. 33 exhibited exclusive affinity for Hg^{2+} with an activation of emission wavelength at 543 nm. Its reversible fluorescence response, coupled with a low detection limit (19.2 nM) in the pH range of 6.0–7.5, positions NBDP as a prospective option for detecting Hg^{2+} in neutral aqueous settings. This phenomenon was attributed to the impediment of the photo-electron transfer (PET) mechanism upon complex formation with Hg^{2+} (Fig. 12c).[82] This chemosensor with high water solubility was effectively employed for fluorescence imaging in plant tissue. Furthermore, NBDP demonstrated Hg^{2+} recognition ability in live tissues of *A. thaliana via* fluorescence imaging. NBD-NHR-based fluorescent chemosensors have been widely employed in plant detection. Yu *et al.* ingeniously devised a new molecular pH sensing agent, chemosensor 34 (NBD-pbz), which was formed through the strategic combination of 2-piperazin-1-yl-1,3-benzothiazole (pbz) and 7-nitro-1,2,3-benzoxadiazole (NBD) elementary units (Fig. 12d).[83] 34 enabled the precise monitoring of pH variations spanning the range of 3.2–7.6, demonstrating a pK_a

Table 5 Fluorescent fluorescein and NBD derivatives for monitoring plant health and their environment

| Classifications	Chemosensors	$\lambda_{ex}/\lambda_{em}$ (nm)	Solvents	Limit of detection (LOD)	Target analytes	Applications	Ref.
Fluorescein 2′-position derivatives	28	365/543	HEPES buffer (0.1 M, pH = 6.5)	200 pmol	S-Nitrosothiols and hydrogen sulfide	Visualization of intracellular RSNO in plans seedling roots	78
Fluorescein 9-position derivatives	29	—	—	—	—	Assessment of stomatal dynamics in *A. thaliana*	79
	30	350, 507/650	$V_{H_2O}:V_{THF} = 7:3$	86.7 nM	Exogenous ClO⁻	Monitoring of exogenous ClO⁻ in potato sprouts and industrial effluents	80
NBD-N derivatives	31	—	—	—	Auxin	Visualising the distribution of auxin in plants at cellular or subcellular levels	81
	32	488/500–650	Aqueous solution	—	Monolignols	Understanding the plant cell wall lignification process	43
	33	495/543	Aqueous solution (containing 0.4% DMSO)	19.2 nM	Hg^{2+}	The Hg^{2+} recognition in live tissues of *A. thaliana*	82
NBD-O derivatives	34	450/540	PBS buffer (1% DMSO)	—	pH	Tracking of pH changes in mung bean sprouts	83
	35	480, 550/625	PBS buffer (pH = 7.4, containing 20% CH₃CN, v/v)	0.0820 μM for GSH / 0.0610 μM for Cys/Hcy	Cys/Hcy and GSH	Detecting Cys/Hcy and GSH in *A. thaliana*	84
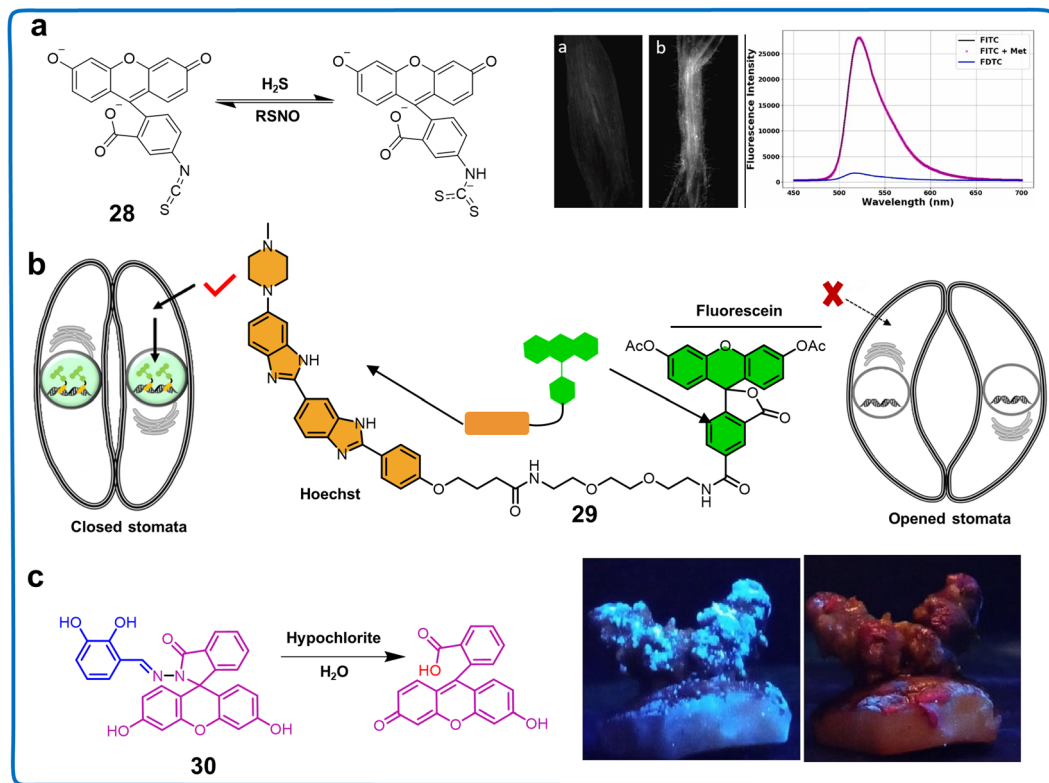
Fig. 11 Structure, mechanism and application of fluorescent chemosensors **28–30** based on 2′-position fluorescein derivatives in imaging water samples and plants. (a) Fluorescent chemosensors **28** for the visualization of intracellular RSNO in plant seedling roots.[78] Copyright © 2022, Elsevier. (b) Fluorescent chemosensors **29** is employed to assess the stomatal dynamics in *A. thaliana*.[79] Copyright © 2020, Springer Nature. (c) Fluorescent chemosensors **30** for monitoring exogenous ClO⁻ in potato sprouts.[80] Copyright © 2023, Elsevier.

value of 5.51, as observed in mung bean sprout tissues. This functionality was enabled by utilizing a fluorometric activation response together with an ICT-based operating mechanism methodology. This type of structure was versatile for detecting anions, cations, and biothiols in environmental samples. Fluorescent chemosensors based on the 2-oxa-1,3-diazole of NBD were also extensively utilized in plant detection and could sensitively detect biothiols (such as amino acids or sulfide) in plants, real environments, and food samples. For instance, Huang *et al.* synthesized NBD-O-1 (chemosensor **35**), which was capable of detecting endogenous compounds such as Cys/Hcy and GSH in *A. thaliana* (Fig. 12e).[84] The fluorescence emission amplitude of NBD-O-1 at 550 nm and 625 nm significantly increased upon exposure to Cys/Hcy with superior selectivity and LOD of 0.061 μM. The experiment demonstrated the utility of **35** in exploring the conversion and metabolic pathways of thiols in plants. NBD, known for its low molecular weight, high QY, and stability, presents numerous advantages. It has found extensive use in plant imaging to observe physiological processes within plant cells. This effort seeks to enhance our comprehension of physiological processes from the standpoint of subcellular organelles in plants, which play an important role in plant health management. Hence, the introduction of NBD derivatives can provide a new perspective to study the changes of physiological signals within the plant system.

The low molecular weight, high solubility, biocompatibility and relatively easy synthesis process of NBD derivatives have led to their use in plant imaging. However, they also have some disadvantages, as follows: (i) their emission spectrum is located in the range of 500–560 nm, which overlaps with some spontaneous fluorescence in biological systems, causing fluorescence interference and (ii) the relatively low structural diversity of NBD derivatives limit their application scope. Thus, more substituent or recognition groups should be added to NBD.

3.6 BODIPY derivatives

The BODIPY molecule, also known as 4,4-difluoro-4-bora-3*a*,4*a*-diaza-*s*-indacene, has been attracting increasing interest due to its minimal Stokes shift, substantial absorbance, narrow absorption and emission spectra, elevated QY, insensitivity to variations in polarity and pH, and consistent chemical structure and mechanism, making it a highly favored fluorescent dye.[89,90] Developed by Treibs and Kreuzer in 1968, research related to the BODIPY compound underwent a period of inactivity spanning over a decade, only regaining prominence in the late 1980s.[91] In recent years, BODIPY has found extensive application in biochemistry, materials science, engineering, physics, electronics, therapeutic applications, and various other fields. The inherent adaptability of 4,4-difluoro-4-bora-3*a*,4*a*-diaza-*s*-indacene-based BODIPY derivatives allow significant alterations, making them optimal candidates for use as photodynamic therapy (PDT) agents, including low dark toxicities, cellular uptake, high extinction coefficients, and low photobleaching. This versatility allows for modifications,
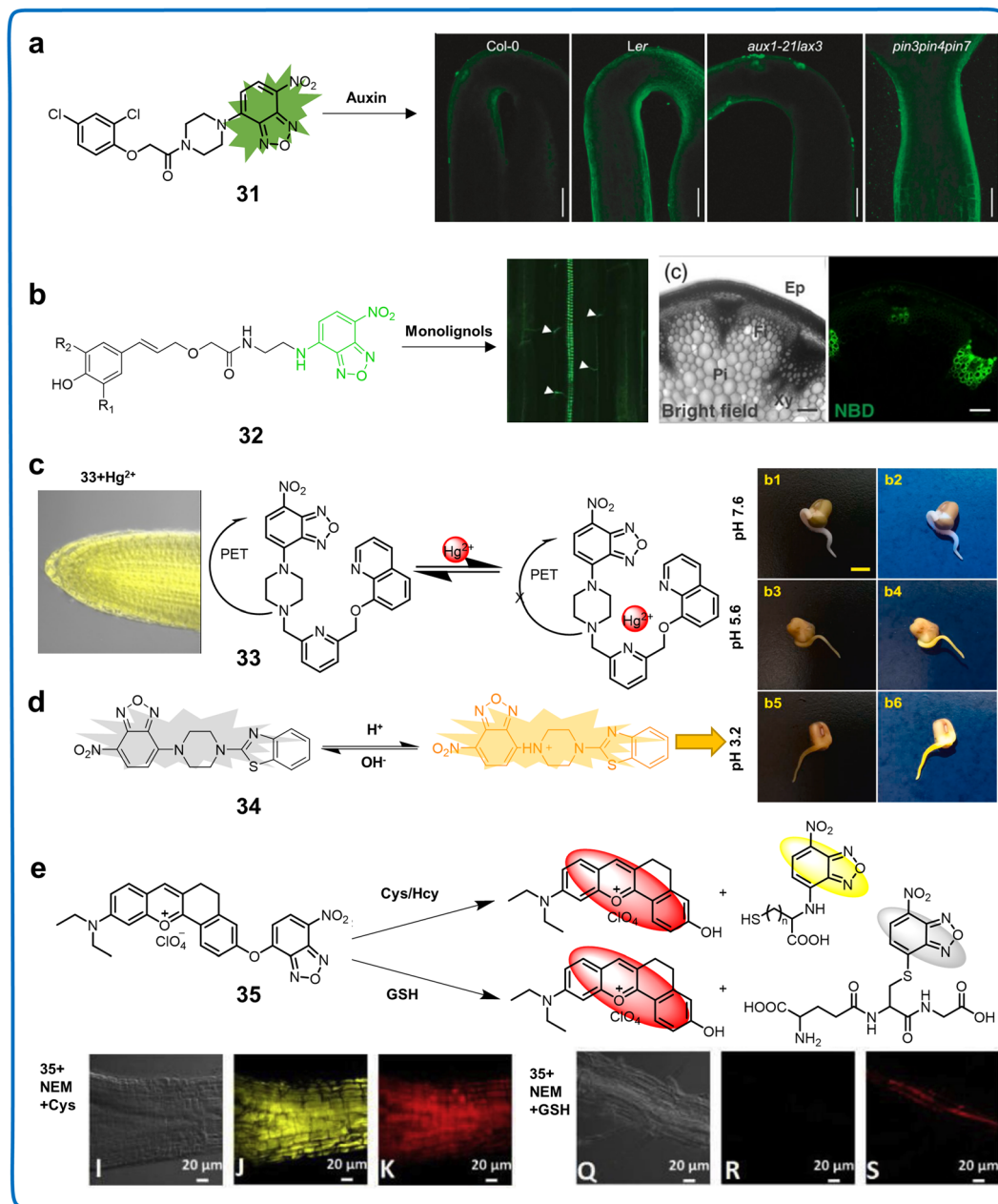
Fig. 12 Structure, mechanism and application of fluorescent chemosensors **31–35** based on NBD-N for visualising plant growth. (a) Fluorescent chemosensor **31** for visualising auxin distribution within different plant tissues at the cellular or subcellular levels.[81] Copyright © 2021, Wiley. (b) Fluorescent chemosensor **32** for understanding the intricacies of cellular wall lignification in plants.[43] Copyright © 2013, Wiley. (c) Fluorescent chemosensor **33** for Hg²⁺ recognition in live tissues of *A. thaliana*.[82] Copyright © 2020, Elsevier. (d) Fluorescent chemosensor **34** for tracking pH changes in mung bean sprouts.[83] Copyright © 2021, Elsevier. (e) Fluorescent chemosensor **35** for detecting Cys/Hcy and GSH in *A. thaliana*.[84] Copyright © 2019, Elsevier.

enabling absorbance at long wavelengths.[92] Acting as an acceptor, the optical properties of BODIPY can be finely tuned through facile structural modifications on its core.[93] The core of BODIPY allows functionalization at its *meso*-, α-, β-positions and B(III) center, and thus the introduction of substituents with varying electron densities and adjusting its conjugation length with suitable spacers or π-linkers (Fig. 2). The extensive synthetic methodologies and diverse functionalization options of BODIPY make it one of the most extensively studied organic fluorophores (Table 6).

3.6.1 Fluorescent chemosensors based on 3,5-position derivatives of BODIPY. Numerous 3,5-position BODIPY derivatives have played crucial roles in monitoring food security and plant components. Zhang *et al.* developed an innovative borate-functionalized BODIPY-based fluorescent paper chemosensor (**36**) with heavy metal ion responsiveness employing solid phase extraction technology (SPE). **36** showed both superior selectivity and sensitivity in the quantification of minimal traces of Cd²⁺ in rice with an LOD of 0.5 μM, which is useful for monitoring

7012 | *Chem. Soc. Rev.*, 2024, **53**, 6992–7090

This journal is © The Royal Society of Chemistry 2024

Table 6 Fluorescent BODIPY, Nile blue, cyanine derivatives and chemosensors with AIE property for monitoring plant health and their environment

Classifications	Chemosensors	$\lambda_{ex}/\lambda_{em}$ (nm)	Solvents	Limit of detection (LOD)	Target analytes	Applications	Ref.
BODIPY 3,5-position derivatives	36	—	Aqueous solution	0.500 μM	Cd²⁺	Detection of Cd²⁺ in real rice samples	94
	37	—	—	—	Viscosity	Imaging microviscosity in key plant cell structures	95
BODIPY 1,3,5,7-position derivatives	38	640/790	$V_{H_2O}:V_{DMF} = 7:3$	2.66×10^{-4} mol L⁻¹	Mercury	Marking the level of Hg²⁺ pollution in A. thaliana	96
	39	495/505	DMSO	—	Brassinosteroids (BRs)	Monitoring BRs epidermal cells of A. thaliana	97
	40	505/600	$V_{PBS}:V_{CH_3CN} = 1:1$, pH = 7.4	11.2 nM	Cys	Detecting Cys in food samples	98
Nile blue derivatives	41	580/675	PBS buffer (100 mM, pH = 7.4)	HP-1 (0.700 μg mL⁻¹ and 4.53 μg mL⁻¹), HP-2 (0.800 μg mL⁻¹ and 2.41 μg mL⁻¹)	HPPD	Monitoring AtHPPD, HPPD of A. thaliana	99
	42	620/675	$V_{EtOH}:V_{PBS} = 3:2$, pH = 7.4	1.80 nM	Toxic thiophenol	Determining ArSH in industrial wastewater	100
	43	652/692	PBS buffer (10 mM, pH = 7.4)	9.50 nM	Selenol	Detecting selenol in foodstuff	101
Cyanine derivatives	44	680/790	PBS buffer	170 and 448 μM	NaCl	Monitoring Salt Stress of plants	102
	45	340, 385/440, 490	Triton X-100/HEPES buffer pH = 6.0	0.540 nM	CN⁻	Monitoring CN⁻ in water	103
	46	510, 640; 520–800, 650–850	ACN	0.0800 ppb	Phosgene	Monitoring phosgene in soil	104
	47	515, 637/816	PBS buffer (10 mM, pH = 8.0 containing 15% DMSO)	0.240 μg mL⁻¹	DDVP residues	Determination of BChE and detection of DDVP residues in food samples	105
Chemosensors with AIE property	48	492/614	—	—	Lignin	Distinguishing the meristematic zone in root tissue and primary xylem in stem tissue.	106
	49	300–350/675	—	—	Plasma membranes	Imaging the morphological changes of plasma membranes	107

food safety (Fig. 13a).[94] In 2020, Michels et al. introduced an imaging microviscosimetry toolbox (chemosensor 37) of molecular rotors, which was designed for the comprehensive microviscosity mapping of cells and tissues. These molecular rotors precisely targeted the cytosol, vacuole, plasma membrane, and cell wall of plant cells (Fig. 13b).[95] Operating based on BODIPY, these molecular rotors exhibited rigidochromicity, linking the rate of intramolecular rotation, influenced by their direct surrounding mechanics, with their fluorescence lifetime. Despite the typically low intracellular levels of physiological parameters in plants and environmental parameters, detecting them remains a challenge. In this case, the combination of fluorescent imaging with chemosensing exhibits unparalleled utility in plant experiments, yielding elevated sensitivity, direct on-site evaluation, and minimal damage.

3.6.2 Fluorescent chemosensors based on 1,3,5,7-position derivatives of BODIPY. The remarkable specificity and sensitivity of fluorescent chemosensors based on 1,3,5,7-position BODIPY derivatives have fundamental advantages in botanical investigations. In 2022, Chen et al. innovatively utilized a BODIPY core as an NIR fluorophore, paired with an aza-containing macrocyclic thioether recognition ligand to create novel chemosensor 38 with outstanding photostability. 38 was employed for the specific recognition of Hg²⁺, emitting NIR light at 753 nm (Fig. 14a).[96] Importantly, its emission effectively avoided interference from chlorophyll fluorescence in A. thaliana, ensuring the accurate quantification of Hg²⁺ levels, with an LOD of 2.66×10^{-4} mol L⁻¹. Fluorescence imaging of A. thaliana seedlings revealed that 38 can monitor the heavy metal pollution in plants, thus providing an efficient molecular tool for determining the Hg²⁺ levels and translocation in living biosystems. For the precise, non-invasive detection of brassinosteroids (BRs) in plants, Starodubtseva's team synthesized a BODIPY-conjugated epibrassinolide (chemosensor 39). 39 could not only assess bioactivity but also serve as a fluorescent tool for the in vivo visualization of BR. Mimicking the effects of eBL, this chemosensor is suitable for both short- and long-term applications and holds high potential for use in cell biology studies, especially it may be an effective tool for studying the physiological function of BR in plant resistance to biotic or abiotic stresses (Fig. 14b).[97] In Cys detection, Yang et al. ingeniously synthesized "turn-on" fluorescent chemosensor 40 utilizing the BODIPY platform specifically for detecting Cys in food samples (Fig. 14c).[98] This chemosensor, with a brief reaction time (10 min) and distinctive color response (blue to pink), boasted a high signal-to-noise (S/N) ratio (3150-fold) and sensitivity (LOD = 11.2 nM) towards Cys. Conveniently deposited on test strips, it became a robust tool for analyzing the Cys levels in food samples and complex biological systems. Consequently, these dynamic molecules derived from BODIPY play crucial surveillance and visualization roles in the complex procedures of plant growth, development, and stress responsiveness. These chemosensors also have utility in detecting and visualizing hazardous substances, analyzing food and environmental samples, and studying intricate living systems.

The advantages of BODIPY derivatives include their favorable QY, high molar extinction coefficient, and insensitivity to
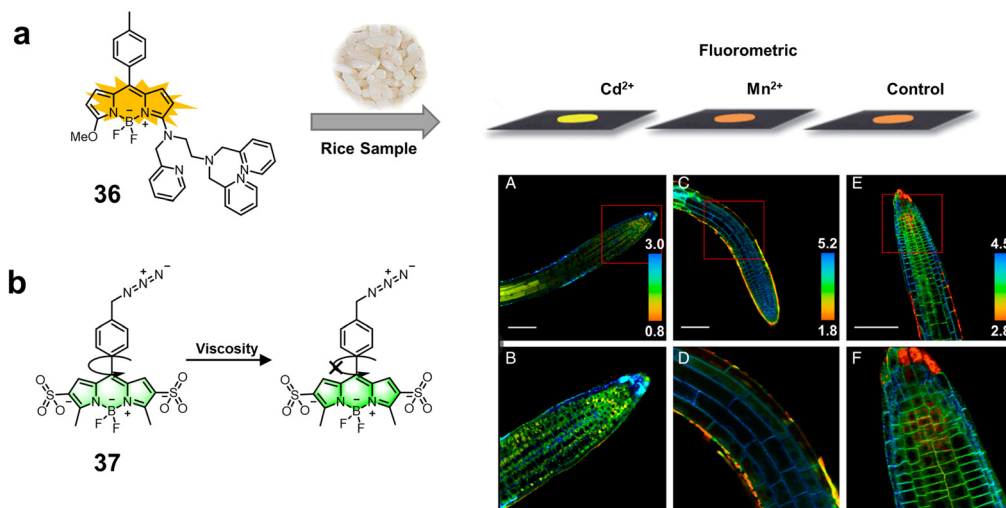
This journal is © The Royal Society of Chemistry 2024

Chem. Soc. Rev., 2024, **53**, 6992–7090 | **7013**

Fig. 13 Structure and mechanism of fluorescent chemosensors **36** and **37** based on 3,5-positions derivatives of BODIPY for monitoring ions and viscosity in plant cells. (a) Fluorescent chemosensor **36** for the specific quantification of Cd^{2+} in real rice samples. Copyright © 2014, The Royal Society of Chemistry.[94] Reproduced from ref. 94 with permission from The Royal Society of Chemistry. (b) Fluorescent chemosensor **37** for imaging microviscosity in key plant cell structures.[95] Copyright © 2020, PNAS.
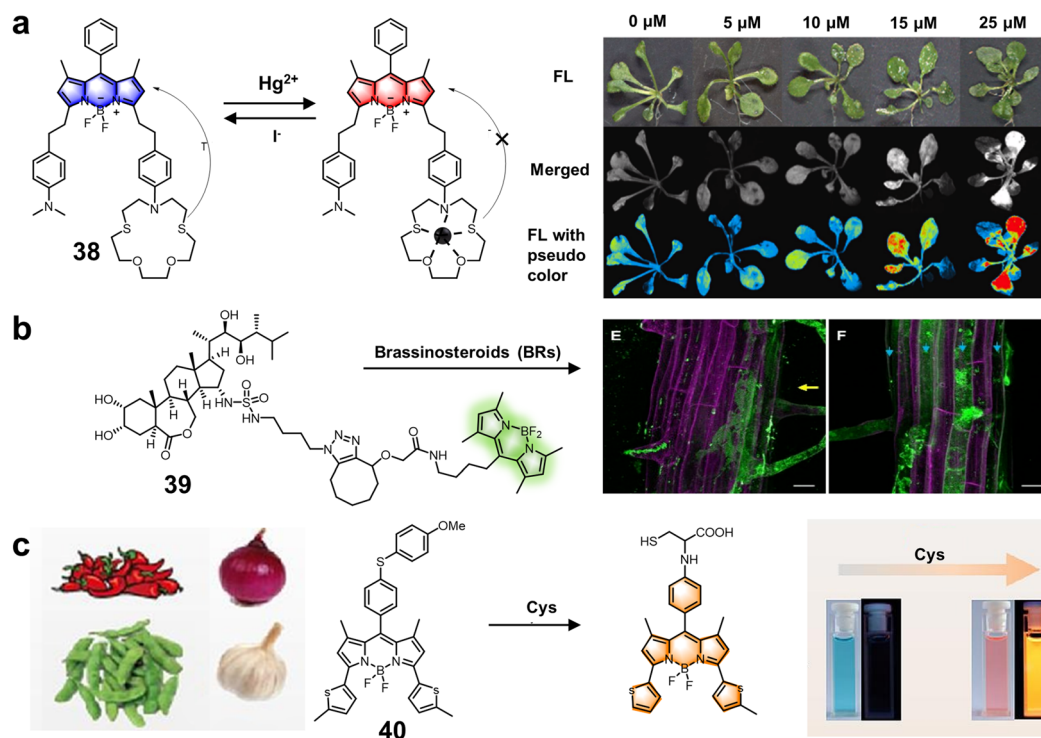

Fig. 14 Structure and mechanism of fluorescent chemosensors **38–40** based on 1,3,5,7-position BODIPY derivatives for the evaluation of ions, hormones and amino acids in plants. (a) Fluorescent chemosensor **38** for marking the level of Hg^{2+} pollution in *A. thaliana*.[96] Copyright © 2022, Elsevier. (b) Fluorescent chemosensor **39** for monitoring BR epidermal cells of *A. thaliana* roots.[97] Copyright © 2021, MDPI. (c) Fluorescent chemosensor **40** for detecting Cys in food samples.[98] Copyright © 2023, Elsevier.

pH. However, they also have some disadvantages, as follows: (i) the low water solubility of BODIPY derivatives limits their application in *in vivo* imaging and (ii) their relatively low photostability and easy photobleaching can reduce their detection accuracy, which implies the important of timeliness of sample preparation.

3.7 Nile derivatives

Nile blue, discovered by scientist Lorrain Smith in 1908, serves to distinguish neutral fats, specifically staining fatty acids deep blue and triglycerides and steroids reddish-pink. It is comprised of oxazine sulfate (true Nile blue) and oxazone (Nile red) and is soluble in water and ethyl alcohol.[108] Nile pink, its

7014 | *Chem. Soc. Rev.*, 2024, **53**, 6992–7090

This journal is © The Royal Society of Chemistry 2024

oxazone form, results from the spontaneous oxidation of Nile blue A in an aqueous solution or refluxing Nile blue A with dilute sulfuric acid (Fig. 2).[109] It exhibits high solubility in neutral lipids, showing fluid characteristics at the required staining temperature. Although Nile blue is inherently hydrophobic, modifications to facilitate its water solubility are possible.[110] However, its synthesized analogs evaluated thus far show fluorescence in the NIR region with a low QY in aqueous systems or in the presence of proteins (Table 6).

4-Hydroxyphenylpyruvate dioxygenase (HPPD), which plays a pivotal role in the biosynthesis of vitamin E and plastoquinone in plants, has been regarded as a key herbicide target for over 30 years. Recently, it was recognized as a marker for plant health under abiotic stresses. Fu *et al.* introduced chemosensor **41**, a tool for precise visualization and PL in *in vivo* studies, for the exceptionally effective identification of an HPPD-targeted inhibitor (Fig. 15a).[99] **41** exhibited an approximately 16-fold enhancement in fluorescence levels upon exposure to HPPD,

showing excellent specificity for imaging HPPD in complex environments. Importantly, it allowed the visual tracking of HPPD activity in plants spatially and temporally, overcoming the inconsistency between molecular-level HPPD-based bioevaluation and weed control efficiency.[111] Zeng *et al.* proposed a fluorescence labelling method for HPPD, avoiding interference with normal plant growth. The innovative bioorthogonal strategy visualized HPPD in *A. thaliana*, integrating the evaluation of the adaptive response of plants to diverse abiotic stresses, while simultaneously monitoring the *in vivo* concentration and subcellular localization of HPPD in plants. Additionally, they executed a systematic molecular construction for a highly specific HPPD-reactive fluorescent chemosensor, demonstrating excellent capability for monitoring the presence of HPPD in *A. thaliana* and detecting dynamic fluctuations occurring under varying levels of temperature stress coupled with Cd^{2+} stress.[112] These results indicated that this chemosensor may be an effective tool for investigating abiotic stress mechanisms associated with HPPD,
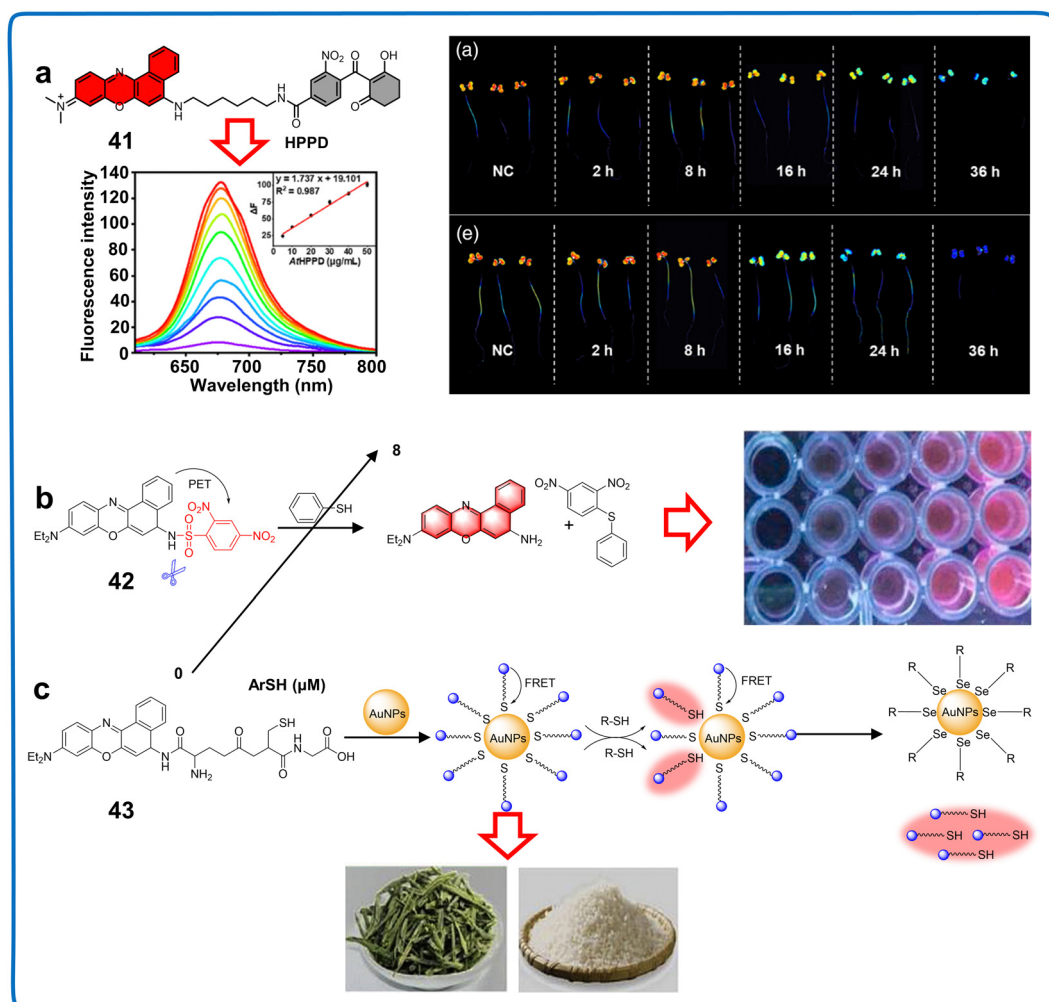

Fig. 15 Structure, mechanism and application of fluorescent chemosensors **41–43** based on Nile blue for monitoring water quality and plant components. (a) Fluorescent chemosensor **41** for monitoring *At*HPPD, HPPD in *A. thaliana*.[99] Copyright © 2022, Wiley. (b) Fluorescent chemosensor **42** for determining ArSH in water.[100] Copyright © 2019, Elsevier. (c) Fluorescent chemosensor **43** for detecting selenol in foodstuff.[101] Copyright © 2020, Elsevier.

This journal is © The Royal Society of Chemistry 2024

Chem. Soc. Rev., 2024, **53**, 6992–7090 | **7015**

detecting herbicidal compounds, evaluating enzymatic activity and elucidating uncharacterized biological functions.

The Nile blue fluorophore is extensively used in evaluating food and environmental samples. Wu *et al.* introduced an innovative NIR fluorescent chemosensor (**42**) for detecting thiophenols in environmental water samples. Through a single-step condensation process using 2,4-dinitrobenzenesulfonyl chloride in combination with Nile blue (Fig. 15b), this sensor demonstrated a remarkable chromogenic reaction and NIR fluorescent "turn-on" response against thiophenols, offering exceptional sensitivity, prompting a rapid response (12 minutes), and impressive LOD of 1.8 nM.[100] Nile blue-DN effectively monitored the thiophenol levels in water with good recoveries ranging from 90% to 110%, which offered a robust strategy for facilitating highly precise measurements of the thiophenol levels in environmental water samples. Further studies should explore the integration of **42** with enzyme-responsive groups, which can increase its pesticide detection sensitivity and reduce the complex processes for enzyme activity analysis. Nile blue is also employed for detecting components in food samples. Selenocysteine (Sec), a crucial reactive selenium species, was the focus of the study by Guo *et al.* They reported the synthesis of a chemosensor (**43**) comprised of oxidized glutathione (GSH) and Nile blue ligands immobilized in gold nanoparticles (AuNPs) (Fig. 15c).[101] The developed chemosensor displayed remarkable sensitivity and specificity towards Sec, facilitating the visualization of both endogenously present and externally administered Sec within plant cells *via* confocal fluorescence microscopy. This proposed analytical device hold substantial promise for the detection of selenol in foodstuffs such as selenium-rich rice and tea, exhibiting an impressive LOD of 9.5 nM, holding great potential for advancing the detection of selenol and unraveling its role in organisms. The results indicated that **43** can also be used as an indicator to analyze the redox balance in plants. Customizing these chemosensors for the precision targeting of distinctive biologically active compounds within plants, including reactive species, metal ions, signal-transducing molecules, and harmful substances, enables the precise and quantitative detection of these indispensable active substance.

Compared with other fluorescent chemosensors, NIR chemosensors have less background interference, strong tissue penetration and high solubility, making them more suitable for *in vivo* imaging. However, their rational structural modification, specific recognition groups and simple synthesis process should be explored to improve their specificity and sensitivity.

3.8 Cyanine derivatives

Cyanine (CY), a classical cyanine dye, features two nitrogen-containing heterocycles and a conjugated chain of methyl chloroform $(CH)_n$, with an odd or even number of n.[113] Manipulating the length of the poly(hypomethyl)-bridge allows the control of its absorbance and fluorescence wavelengths, resulting in higher absorbance and emission wavelengths (Fig. 2). Quinones, distinguished according to the number of carbon atoms with their carbonaceous backbone, include monomethyl (CY_1, $n = 0$), trimethyl (CY_3, $n = 1$), pentamethyl (CY_5, $n = 2$), and

heptamethyl (CY_7, $n = 3$) (Table 6). CY offers several advantages for the synthesis of phloroglucinol dyes: (1) a narrow spectrum and robust signal; (2) a molar absorption coefficient surpassing that of other fluorescent dyes; (3) easy dissolution in water and low toxicity to tissues and cells, making it suitable for plant bioimaging experiments; and (4) a fluorescence band with enhanced tissue transmittance in the NIR region.[114]

Effective methods for analyzing plant stress responses, hazardous substances, and environmental conditions are crucial. In 2022, the *N*-benzyloxycarbonyl-based Cy-CO2Bz (chemosensor **44**) exhibited a strong fluorescence response to NaCl, serving as a sensitive indicator for discerning salt stress within live root tips and whole plants (Fig. 16a).[102] NaCl induced the assembly of *N*-benzyloxycarbonyl Cy-CO2Bz into a J-aggregate with absorption at 890 nm. This fluorescence response implied its potential as a chemosensor for tracing salt stress in plants. The construction of J-aggregates induced by NaCl implies that it can sensitively and selectively monitor the presence of NaCl. Thus, more J-aggregates should be constructed or more functions of this system discovered for effectively monitoring other indicators to manage the health and living environment of plants. Additionally, the novel π-conjugated indolium salt fluorescent chemosensor **45** based on cyanine derivatives could detect CN^- in real water samples. With an increase in the concentration of CN^-, the fluorescence intensity of **45** was enhanced with an LOD of 0.54 nM. The combination **45** with gel- or paper-based indicators showed sensitivity to 1 μM of CN^-, which could be observed by the naked eye, implying that this chemosensor is a useful tool for monitoring the changes in CN^- in the living environment of plants (Fig. 16b). Real-time detection of chemical warfare agents (CWAs) in irrigation water and soil can mitigate their threatening effects on plant growth and development.[103] A reversible, colorimetric, and fluorescent sensor for the detection of phosgene based on the cyanine scaffold (chemosensor **46**) in an aqueous system was synthesized (Fig. 16c).[104] The rapid dual response of **46** was constructively employed for monitoring phosgene in the environment through strip tests and soil analysis, providing up to ppb (LOD of 0.08 ppb) level detection with distinct color and fluorescence. The NIR fluorescence response of **46** indicated that it has high potential for *in vivo* imaging owing to its strong tissue penetration and low background interference.

For the detection of pesticides, NIR fluorescent chemosensor **47** was developed, utilizing a cyanine scaffold to generically endorse intrinsic NIR fluorescence and circumventing interference arising from bioluminescence changes (Fig. 16d).[105] An intriguing structural transformation occurs during the sensing event in this protocol, causing a reduction in conjugation. This results in a striking fluorescence change from the near-infrared (816 nm) to the red (637 nm) region, facilitating the proposed ratiometric assay. This receptor also demonstrated capability in monitoring dichlorvos (DDVP) residue in food samples with superior sensitivity and precision, showing potential as a viable substitution for detecting pesticide pollution. Collectively, the literature analysis reflects the universal utility of cyanine derivatives in detecting plant physiological stress responses, ions, and pesticides.

7016 | *Chem. Soc. Rev.*, 2024, **53**, 6992–7090

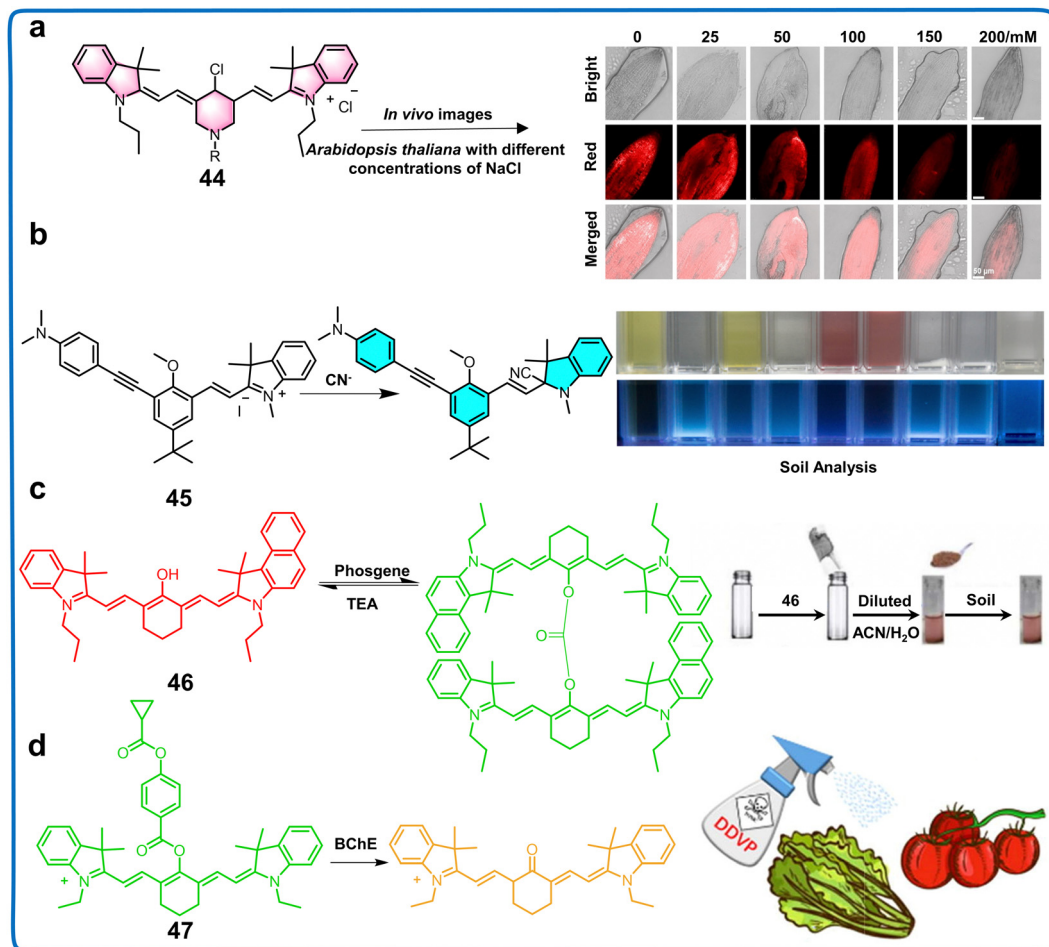This journal is © The Royal Society of Chemistry 2024

Fig. 16 Structure, mechanism and application of fluorescent chemosensors **44–47** based on cyanine derivatives in live plant imaging, water, soil samples and food. (a) Fluorescent chemosensor **44** for monitoring salt stress of plants.[102] Copyright © 2020, Wiley. (b) Fluorescent chemosensor **45** for monitoring CN⁻ in water.[103] Copyright © 2017, Elsevier. (c) Fluorescent chemosensor **46** for monitoring phosgene in soil.[104] Copyright © 2022, Elsevier. (d) Fluorescent chemosensor **47** for the determination of BChE and detection of DDVP residues in food samples.[105] Copyright © 2023, Elsevier.

Cyanine derivatives have some advantages including favorable molar absorption coefficient, low background interference, high specificity and sensitivity. Alternatively, the defects of these chemosensors mainly include low photostability and aggregation quenching. Therefore, their structure should be modified or the aggregation quenching mechanism exploited to expand the application of cyanine derivatives in plants.

3.9 Chemosensors with AIE property

The phenomenon of aggregation-induced emission (AIE) arises due to the restraint of molecular rotations involving rotatable entities such as the phenyl moiety.[115] The low-frequency transitions of rotor-bearing fluorophores in dilute solutions result in weak emission within their excited states.[116] Conversely, upon aggregation, their rotations are obstructed by intermolecular steric interactions, thereby facilitating radiative pathways.[117] Unlike traditional fluorophores that succumb to aggregation-induced quenching, AIE emits high levels of light persistently, demonstrating remarkable resilience under challenging bioimaging circumstances prevalent within plant cells.[118]

Fluorescent chemosensors with AIE property have been used to analyze the subcellular events of plants because of their superior S/N ratios, intense fluorescence levels and fluorescent stability. In 2017, an AIE based chemosensor (**48**) was synthesized using diphenylimidazole-In (DPI-In) and saponin (Fig. 17a).[106] **48** could specifically label lignin in plant roots with specific ''turn-on'' emission properties due to its hydrophobicity. This property was effectively utilized to monitor the composition of lignin and morphological modifications that occur during plant growth and developmental stages. Meanwhile, **48** distinguished the meristematic zone in root tissue and primary xylem in stem tissue. Compared with other commercial dyes, **48** showed greater photostability and higher sensitivity, which inspired the modification of the AIE property to manage plant health by bioimaging. In 2023, an AIE-active chemosensor (**49**) featuring NIR emission was developed, which was capable of four-dimensional spatiotemporal imaging of the morphological changes in plant cell plasma membranes on the subcellular level (Fig. 17b).[107] **49** was designed based on the principles of similarity and intermiscibility, a robust imperviousness strategy, and intense electrostatic

This journal is © The Royal Society of Chemistry 2024

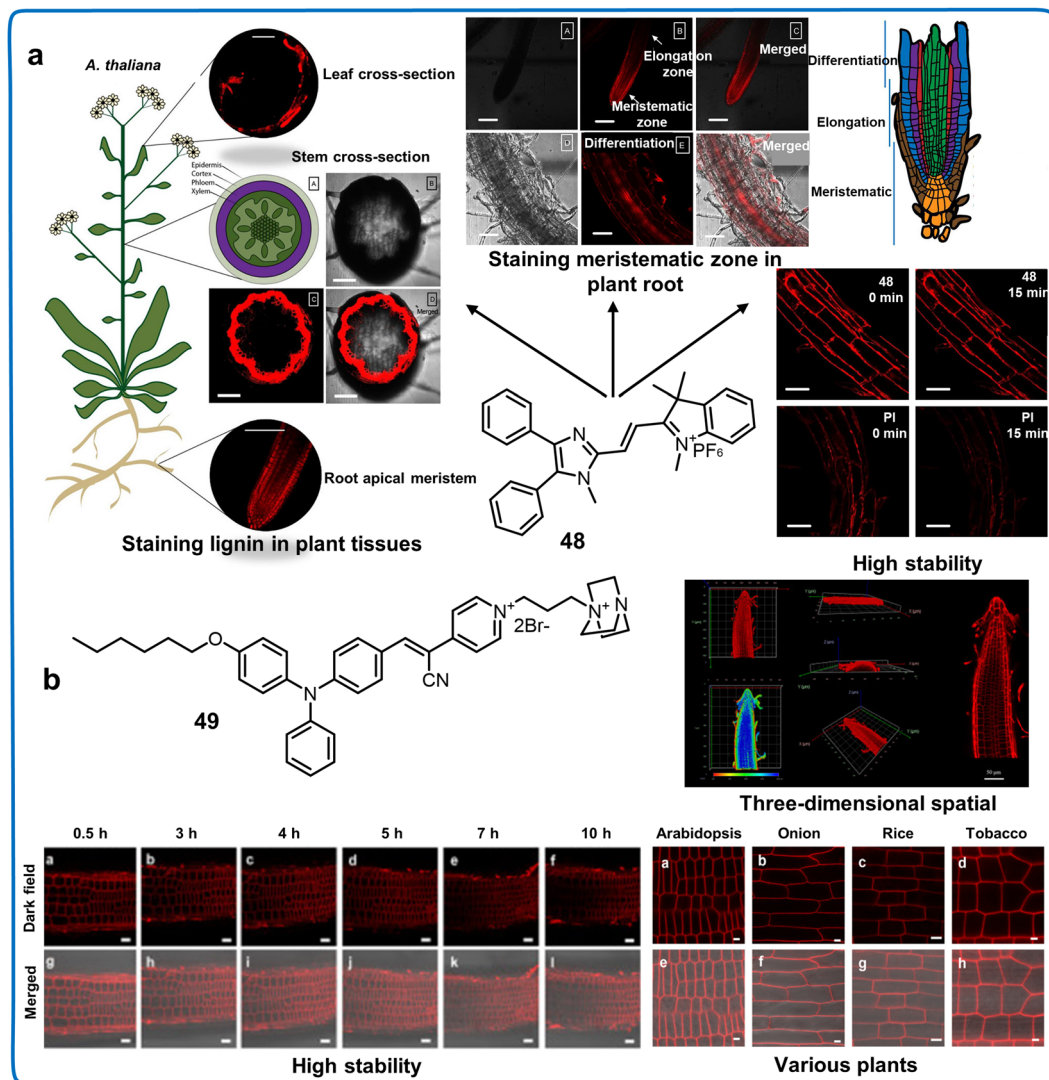*Chem. Soc. Rev.*, 2024, **53**, 6992–7090 | 7017

Fig. 17 Fluorescent chemosensors with AIE property for imaging subcellular events in plants. (a) Fluorescent chemosensor **48** monitoring concentration of lignin in root and distinguishing the meristematic zone in root tissue and primary xylem in stem tissue.[106] Copyright © 2017, the American Chemical Society. (b) Fluorescent chemosensor **49** monitoring the morphological and structural alterations of plasma membranes of plant.[107] Copyright © 2023, The Royal Society of Chemistry.

interactions, making it capable of selectively adhering to plant membranes across diverse plant cell types and plant species. **49** could quickly penetrate the cell wall and stain the cell membrane for up to 10 h and image its integrity. This makes it a highly useful tool for visually tracking plasma membrane-related events in an intuitive and real-time manner. Meanwhile, the favorable imaging performance of **49** for different plant cells indicated that it can be employed to monitor the physiological processes of plasma membranes in different plant species and cell types. We hope that more chemosensors with AIE property be designed to perform more unique and original research into plant bioluminescence imaging.

In summary, modifying the fluorophore modifiable sites in the original series of ancient dyes has revitalized this dye class, offering versatile structures, unique properties and biocompatibility, which have been widely used for imaging plants.

Fluorescent chemosensors mainly developed based on the collaborative efforts between chemists and biologists have led to breakthrough progress in developing fluorescent chemosensors, particularly NIR fluorescent ones, despite ongoing challenges, as follows: (i) the majority of NIR chemosensors exhibit limited stability and low QY, making them less suitable for precise and sensitive biological imaging. (ii) Compared to chemosensors with short-wavelength emission, their NIR counterparts often have larger molecular structures, potentially compromising their water solubility. Therefore, the imperative task is to develop small molecular structure NIR dyes and chemosensors with high QY and biocompatibility. Novel heteroatom substitution strategies may represent the most viable approach for constructing these NIR dyes. (iii) To avoid interference from the plant background, it is a necessary to develop NIR-II fluorescent chemosensors or improve their QY. Equipped

7018 | *Chem. Soc. Rev.*, 2024, **53**, 6992–7090

This journal is © The Royal Society of Chemistry 2024

with potent fluorophores for investigating the intricate aspects of hazardous substances, plant physiology, adaptation mechanisms, and responses to environmental stimuli, innovative chemosensors will promote advancements in both plant science and agricultural research.

4. Applications of fluorescent nano-chemosensors

Nano-based fluorescent chemosensors exhibit great potential in monitoring the health and living environment of plants because of their enhanced surface activity, excellent recyclability, considerable surface area, robust adsorptive capability, outstanding catalytic proficiency, and substantial QY.[33,119] Nanosensors are used to detect the presence of chemical species on the nanoscale, which are combined with a fluorophore to significantly enhance their fluorescence efficiency and broaden their range of applications.[33] To date, various nanomaterials including quantum dots (QDs), metal organic frameworks (MOFs), covalent organic frameworks (COFs) and nanoclusters (NCs) have been used to design chemosensors to detect plant components implying plant health and environmental pollutants.[13] In the following sections, we elaborate the applications of various types of nano-based fluorescent chemosensors in monitoring the health and living environment of plants.

4.1 Quantum dots

Quantum dots (QDs), which are comprised of a group of nanocrystals, exhibit stable photoluminescence (PL), tunable optical properties, and good light stability. Recently, the exceptional optical properties and biocompatibility of QDs have facilitated their use as fluorescent chemosensors for the accurate identification of substances such as hormones, proteins, harmful heavy metals, anions, and pesticide residues, which can imply plant health (Table 7).[120] Various types of QDs including semiconductor QDs, carbon quantum dots (CQDs), graphene quantum dots (GQDs), silicon quantum dots (SiQDs), sulfur quantum dots (S QDs), molybdenum disulfide quantum dots (MoS$_2$ QDs), and MXene QDs are widely used in the detection of these substances.[121] Due to the effectiveness of chemosensor-based QDs in monitoring the health and living environment of plants, we analyze their applications in detail (Fig. 18).

4.1.1 Semiconductor quantum dots. Semiconductor QD chemosensors are mainly composed of semiconductor nanocrystals of group II–VI, IV–VI and III–V, which mainly include CdSe QDs, CdTe QDs, CdS QDs, ZnS QDs, and perovskite QDs.[190] Since 1980, they have gradually become an important tool for replacing organic dyes because of their excellent optical and physicochemical properties. They have been extensively employed for detecting various proteins, hormones and metal ions in plants.

CdSe quantum dots. Among the various semiconductor QDs, CdSe QD chemosensors have been widely used to monitor plant components and irrigation water quality. For the first time, a CdSe QD fluorescent chemosensor (**50**) was used to label γ-aminobutyric acid (GABA) in plants, and thus determine its distribution in plant protoplasts.[122] Furthermore, its emission efficiency was improved by conjugating a ZnS shell layer to the surface of the CdSe core QD. Due to the increase in the size of the CdSe core QD, its emission peaks were red-shifted (5–20 nm). **50** penetrated and adhered to the cell membrane and specifically bind to the GABA binding pocket on the surface of plant protoplasts, dramatically reducing the fluorescence intensity of the chemosensor. This medium type of chemosensor labeling of GABA in plants provided strong evidence for the presence of the binding site of metabotropic (GABAb) at plant cell membrane (Fig. 19a).[122] Meanwhile, **50** exhibited substantial biological capability in regulating Ca^{2+} signaling within the cell by preventing GABA from permeating the cell, which indicated that it has high potential for regulating plant development and protecting plants from stresses. A thiourea-encapsulated CdSe QD chemosensor (**51**) was prepared through an aqueous photochemical approach utilizing 300 nm UV light in a solution containing acetone, sodium selenosulfate, *etc.*, which could detect the concentration of Hg^{2+} in water. The PL efficiency of this chemosensor decreased with an increase in temperature and pH. Among the many toxic metal ions, only Cu^{2+}, Cd^{2+}, and Hg^{2+} could significantly quench the fluorescence intensity of the chemosensor, with the LODs of 27.6 μM, 196.0 μM, and 279.2 μM, respectively (Fig. 19b).[123] **51** could distinguish various oxidation states of metal ions such as Hg and Cr owing to the photochemically mediated electron transfer between the QDs and metal ions, which implied that **51** can analyze environmental conditions by monitoring the oxidation state of metals. The fluorescent CdSe QD (chemosensor **52**) prepared using RNA *via* a bottom-up method could also be used to detect Hg^{2+} in water, whereas it has characteristics of fluorescence quenching.[124] Therefore, CdSe QD chemosensors show low selectivity and fluorescence intensity in the detection of metal ions, which can be improved by eliminating the interference from the sample matrix and light scattering.

CdTe quantum dots. CdTe QDs, which are water-soluble sulfhydryl-capped QDs, have a narrower emission band in the NIR region than CdSe QDs, making them attractive materials for detecting plant metabolites and water quality for plant survival. A ratiometric QD-based fluorescent chemosensor (**53**) was recently reported to monitor the distribution and concentration of glucose in plants. **53** was designed based on CdTe/CdS QDs capped with boronic acid (BA)-coupled QDs (BA-QDs) as sensing modules. Upon the addition of glucose, it could catalyze the aggregation of **53** utilizing the covalent bonding between BA and two pairs of *cis*-diols from glucose. It exhibited impressive fluorescence intensity between 500 and 600 nm, which could monitor the glucose levels in individual chloroplast organelles of *A. thaliana*. **53** exhibited good sensitivity for glucose detection in plants, and the portable QD glucose sensing method has immense promise to be utilized for the study of photosynthesis and energy transformation in non-model plant species (Fig. 20a).[125] The ability of GSH-modified CdTe QDs (chemosensor **54**) to monitor Cu^{2+} in water

This journal is © The Royal Society of Chemistry 2024

Chem. Soc. Rev., 2024, **53**, 6992–7090 | **7019**

Table 7 Application of QD-based chemosensors in monitoring the health and environment of plants

QD probe types	Chemosensors	Name	$\lambda_{ex}/\lambda_{em}$ (nm)	Linear range	Limit of detection (LOD)	Target analytes	Applications	Ref.
Semiconductor QDs	50	CdSe QDs	—	1.0×10^{-6}–1.0×10^{-3} M	—	γ-Aminobutyric acid	Label of gamma-aminobutyric acid in plant protoplasts	122
	51	CdSe QDs	—	—	27.6 μM	Cu^{2+}	Detection of Cu^{2+} in water	123
					196 μM	Cr^{6+}	Detection of Cr^{6+} in water	
					279 μM	Hg^{2+}	Detection of Hg^{2+} in water	
	52	CdSe QDs	430/585	—	1.00 nM	Hg^{2+}	Detection of Hg^{2+} in water	124
	53	BA-QD/TGA-QD	—	500–1000 μM	500 μM	Glucose	Detecting the distribution and concentration of glucose in plant leaf tissue (A. thaliana)	125
	54	GSH-CdTe QDs	365/575	20–1100 nM	10.1 nM	Cu^{2+}	Detection of Cu^{2+} in water	126
	55	CdTe/ZnS	—	—	1.00×10^{-12} M	Hg^{2+}	Detection of Hg^{2+} in water	127
	56	CdTe QDs	390/530	0.01–1.00 μg mL^{-1}	0.008 μg mL^{-1}	$Cr(VI)$	Detection of $Cr(VI)$ in water	128
	57	CdTe QDs	589/611	15–80 μM	10.4 nM	CN^-	Detection of CN^- in cassava, lake, river water	129
	58	CdTe QDs	450/520	0.1 nM–10 μM	5.50 ppb	Chlorpyrifos	Monitoring the chlorpyrifos residue in apples	130
	59	CdTe QDs	—	0–10^{-3} M	3.40×10^{-8} M	Acetamiprid	Detection of acetamiprid in water	131
	60	CdTe QDs	400/600	4.49–896 nM	4.49 nM	Dichlorvos (DDVP)	Detecting the dichlorvos (DDVP) residue in apple	132
	61	CdS QDs	365/505	1.0–90 ng mL^{-1}	0.220 ng mL^{-1}	Cu^{2+}	Detection of Cu^{2+} in laker	133
				8.0–30 ng mL^{-1}	5.80 ng mL^{-1}	Hg^{2+}	Detection of Hg^{2+} in laker	
				6.0–90 ng mL^{-1}	1.60 ng mL^{-1}	Mg^{2+}	Detection of Mg^{2+} in laker	
	62	L-Cy-CdS QDs	380/475	0.05–5 ng mL^{-1}	39.0 ng mL^{-1}	2,4,6-Trinitrophenol (TNP)	Detection of 2,4,6-trinitrophenol (TNP) in water	134
	63	CdS QDs	390/600	—	49.8 μM	Glufosinate-ammonium	Detection of Glufosinate-ammonium in water	135
	64	CIS@ZnS QDs	430/600	—	0.200 nM	Cu^{2+}	Detection of Cu^{2+} in water	136
					5.00 nM	Hg^{2+}	Detection of Hg^{2+} in water	
	65	Mn:ZnS QDs	310/450	0.19–0.95 μM	0.0200 μM	Methyl parathion (MP)	Detection of methyl parathion (MP) in laker, apple	137
	66	ZnS:Mn^{2+} QDs	—	50 nM–2.5 μM	25.0 nM	Thiram	Detection of thiram in apple	138
	67	Cs$_3$Bi$_2$Br$_6$:Eu^{3+}Pe QDs	446/620	5 nM–3 μM	10.0 nM	Cu^{2+}	Detection of Cu^{2+} in water	139
	68	CsPbBr$_3$@CTAB PQD	370/436	5–100 μM	30.3 nM	Pendimethalin	Monitoring the concentration of pendimethalin in potatoes and apples	140
	69	MIP@CsPbBr$_3$QD	—	50–400 ng mL^{-1}	18.8 ng mL^{-1}	Omethoate (OMT)	Detection of omethoate (OMT) in vegetables and soil	141
Carbon QDs	70	CDs	320/388	—	—	V. mali	Detecting the infection of V. mali in plants	142
	71	CDs	420/680	—	0.375 nM	Cu^{2+}	Detection of Cu^{2+} in onion roots	143
	72	CDs	305/400	—	5.05 μM	Pb^{2+}	Detection of Pb^{2+} in water	144
	73	Fe$_3$O$_4$/CDs	360/435	0.003–0.01 μM	0.300 nM	Hg^{2+}	Detection of Hg^{2+} in water	145
	74	MAB-CDs	280/398	0.5 μM–10 mM	0.100 μM	Ni^{2+}	Detection of Ni^{2+} in water	146
	75	CDs	610/670	0–70 μM	15.0 nM	Cd^{2+}	Detection of Cd^{2+} in water	147
	76	CQDs	340/412	5–100 ppb	0.0860 ppb	Arsenite	Detection of arsenite in water	148
	77	CDs	320/420	0.01–1.0 μg mL^{-1}	3.00 ng mL^{-1}	Chlorpyrifos	Detecting the concentration of chlorpyrifos on cabbage leaves	149
	78	CDs	423/524	—	0.220 μM	Paraoxon-ethyl	Monitoring the distribution of paraoxon-ethyl in cabbages	150
	79	CDs	348/433	1.0×10^{-10}–1.0×10^{-4} M	4.80×10^{-11} M	Methyl parathion	Detecting the concentration of methyl parathion in cabbage	151
	80	CDs	325/450	—	0.250 ng mL^{-1}	Diazinon	Detection of diazinon in tomatoes	152
	81	Tb-CDs	360/463	0.5–15 μM	50.0 nM	ppGpp	Monitoring the concentration of ppGpp in plant	153
	82	MnO$_2$CD	340/425	0–100 nM	5.75 nM	Arsenic	Detection of arsenic in water and emerald plants	154
	83	NCDs	370/450	0.01–1 μM	4.80 nM	Hg^{2+}	Detection of Hg^{2+} in water	155
				0.001–1 μM	1.00 nM	Ag^+	Detection of Ag^+ in water	
	84	S-CQDs	360/435	25–250 μM	0.960 μM	Fe^{3+}	Detection of Fe^{3+} in water	156
	85	N-CDs	—	11.24–241 μg L^{-1}	7.45 μg L^{-1}	Cd^{2+}	Detection of Cd^{2+} in lake	157
	86	N, s-CQDs	350/450	—	500 ppb	Carbaryl	Monitoring the carbaryl residue in apples	158
	87	N, Cl-CDs	400/570	0.3–1000 μg L^{-1}	30.0 ng L^{-1}	Organophosphorus	Detection of organophosphorus pesticides in soil	159

7020 | Chem. Soc. Rev., 2024, 53, 6992–7090

This journal is © The Royal Society of Chemistry 2024

Table 7 (continued)

QD probe types	Chemosensors	Name	$\lambda_{ex}/\lambda_{em}$ (nm)	Linear range	Limit of detection (LOD)	Target analytes	Applications	Ref.
	88	N-CD-Fla	400/502	1.0–2000 nM	0.36 nM	Fenitrothion	Monitoring the concentration of fenitrothion in rice	160
	89	N-CDs	420/500	5 pM–7 nM	3.00 pM	Atrazine	Monitoring the concentration of atrazine in cucumbers	161
	90	N-CDs	—	10–1000 μg L⁻¹	3.50 μg L⁻¹	Methiocarb	Monitoring the concentration of methiocarb in cabbage	162
	91	N-CDs	370/450	0–5×10^{-4} M	1.00×10^{-7} M	p-Nitroaniline	Detection of p-nitroaniline in soil and water	163
	92	NCQDs@Co-MOFs@MIPs	—	1–800 ng mL⁻¹	0.350 ng mL⁻¹	Jasmonic acid (JA)	Monitoring the distribution and concentration changes of Jasmonic acid (JA) in plant	164
Graphene QDs	93	GQDs	320/440	—	1.17 μM; 2.46 μM; 2.01 μM	Hg^{2+}; Cd^{2+}; Pb^{2+}	Detection of Hg^{2+} in water; Detection of Cd^{2+} in water; Monitoring the concentration of Pb^{2+} in water	165
	94	PEI-GQDs	390/460	0–1 μM	—; —	Fe^{2+}; Cu^{2+}	Detection of Fe^{2+} in water; Detection of Cu^{2+} in water	166
	95	GQDs	300/456	9.9–435.0 nM	0.600 nM	Pb^{2+}	Detection of Pb^{2+} in water	167
	96	GQDs/AuNPs	320/516	—	0.520 μM	CN-	Monitoring the distribution of CN^- in plant	168
	97	B-/N-GQD	320/425	—	0.00620 mg L⁻¹	Paraquat	Detection of paraquat in water	169
	98	N-GQDs	320/423	0.1–17 nM	0.041 pM	Omethoate	Detection of omethoate in cabbage leaves and water	170
	99	GQDs–AgNPs	260/460	—	9.00 ng mL⁻¹	Glyphosate	Monitoring the glyphosate residue in peas	171
	100	GQDs/AChE/CHOx	362/467	0.1–10 ppm	0.172 ppm	Dichlorvos	Detection of dichlorvos in the lake	172
	101	Si QDs	350/470	10–150 μM	0.430 μM	Chlorogenic acid (CGA)	Monitoring the concentration changes of chlorogenic acid (CGA) in plant	173
Silicon QDs	102	S-SiQDs	345/425	1–20 μM	0.210 μM	Fe^{3+}	Detection of Fe^{3+} in water	174
	103	N-SiQDs	347/440	0.1–4 μM	24.0 nM	Hg^{2+}	Detection of Hg^{2+} in water	175
	104	Si QDs-AuNPs-CdTe QDs	—	66–200 μM	16.3 nM	Carbaryl	Detection of carbaryl in water, soil, and cabbage	176
Molybdenum disulfide QDs	105	Eu–MoS₂ QDs	310/410	50 nM–25 μM	23.8 μM	ppGpp	Detection of ppGpp in plant	177
	106	MoS₂QDs–MnO₂	360/430	0.33–5.00 μM	39.0 nM	Ascorbic acid	Monitoring the distribution of ascorbic acid in hawthorn and red dates	178
	107	MoS₂QDs	360/440	3.3×10^{-7}–8×10^{-3} M	50.0 μM	Pb^{2+}	Detection of Pb^{2+} in water	179
	108	B-MoS₂QDs	335/415	0.005–41 μM	1.80 nM	Hg^{2+}	Detection of Hg^{2+} in lake water	180
	109	β-CD-MoS₂QDs	289/400	0.01–18.0 ppm	3.30 ppb	Parathion-methyl (MP)	Detection of parathion-methyl (MP) in water	181
Sulfur QDs	110	SQDs	320/431	5–50 μM	4.51 μM	Co^{2+}	Monitoring the concentration of Co^{2+} in roots and stems of Salvia miltiorrhiza	182
	111	Apt-SQDs	—	10^{-15}–10^{-7} M	0.300 fM	Hg^{2+}	Detection of Hg^{2+} in laker, river	183
	112	r-SDs	360/440	1.0–50.0 μmol L⁻¹	0.560 μmol L⁻¹	Cu^{2+}	Detection of Cu^{2+} in laker	184
	113	RhB-SQDs	455/580	0.050–0.500 μg mL⁻¹	17.3 ng mL⁻¹	2,4-Dichlorophenoxyacetic acid (2,4-D)	Detection of 2,4-dichlorophenoxyacetic acid (2,4-D) in water	185
MXene QDs	114	Ti₃C₂MQDs	350/442	0–1.7 μM	5.20 nM	Mn(vii)	Detection of Mn(vii) in laker, plant leaves	186
	115	Ti₃C₂QDs	380/470	—	30.0 mM	Cr^{3+}	Detection of Cr^{3+} in water	187
	116	N-Ti₃C₂ MXene QDs	330/453	0–2000 μM	10.0 μM	Cu^{2+}	Detection of Cu^{2+} in water	188
	117	N-MQDs	420/580	0–80 μM	1.21 μM	Alizarin red (ARS)	Detection of alizarin red (ARS) in water	189
	118	UA@Ti₃C₂QDs	360/420	0.01–40 μM	9.58 nM	2,4,6-Trinitrophenol	Detection of 2,4,6-trinitrophenol in water	189

This journal is © The Royal Society of Chemistry 2024

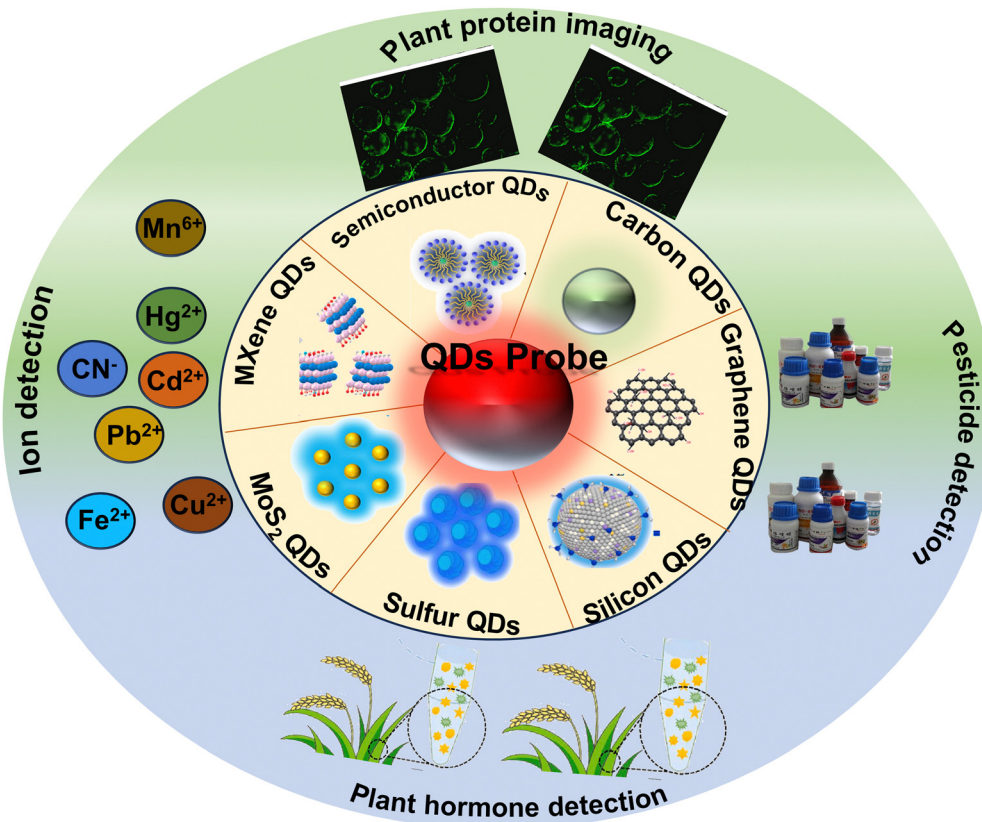*Chem. Soc. Rev.*, 2024, **53**, 6992–7090 | 7021

Fig. 18 Application of quantum dot-based fluorescent chemosensors for monitoring the living environment and elements of plants.

was recently reported. When the excitation wavelength was 365 nm, a fluorescence emission peak appeared at 575 nm. The QY of the chemosensor markedly diminished with an increase in the concentration of Cu^{2+}. An excellent correlation was observed between Cu^{2+} concentration and the fluorescence decay of **54**, spanning the concentration range of 20 to 1100 nM with an LOD of 10.56 nM (Fig. 20b).[126] Also, it was successfully used for the detection of Cu^{2+} in lake water and plants, which has great potential for monitoring food safety and water quality. Some heavy metals such as Hg^{2+} and Cr^{6+} were also detected by CdTe QD chemosensors (**55** and **56**).[127,128] **55** was comprised of MSA-functionalized CdTe/ZnS core/shell (CS) QDs, which showed high selectivity for monitoring Hg^{2+} by electron transfer. To promote the application of **55** in the detection of water quality, a preliminary electronic apparatus should be established. The GSH capping layer of **56** can bind with Cr^{6+}, realizing the detection of different ions by changing the crystallite dimensions of QDs. This strategy makes it easy to obtain QDs chemosensors. For instance, N-acetyl-L-Cys (NALC) CdTe QDs (chemosensor **57**) could also be synergized with carbon dots (CDs) for the detection of CN^-. **57** exhibited unique absorbance and emittance wavelengths at 589 nm and 611 nm, respectively. CDs and CdTe QDs showed bright blue and red colors under UV light, respectively. The fluorescence from **57** was first quenched by the introduction of Cu^{2+}, while the fluorescence of **57** significantly recovered upon the addition of CN^-. Ultra-LODs as low as 10.35 nM were achieved for CN^- concentrations in cassava and water samples in the range of 0.02–10 μM and 15–80 μM,

respectively (Fig. 20c).[129] This ratiometric chemosensor could realize the highly sensitity detection of CN^- at the nM level and accurately determine its concentration in real samples. In addition, a CdTe QD chemosensor (**58**) was developed to detect the residue levels of organophosphorus pesticides in apples. The surface coordination of thiourea in the basal medium strongly inhibited the green emission of **58** through the FRET mechanism, and its fluorescence was gradually restored upon the addition of chlorpyrifos. The fluorescence of **58** was linear at concentrations in the range of 0.1 nM to 10 μM with an LOD of 0.1 nM for apples (Fig. 20d).[130] Based on this type of chemosensor, it was also possible to realize the accurate detection of anilinophos and dichlorvos in water (chemosensor **59** and **60**, respectively).[131,132] The detection mechanism of **60** was based on the inhibition of enzymatic activity (AchE) but the stability of AchE may limit its application in practice. This phenomenon indicates that an automatic biochemical analyzer should be developed for combination with **60**. CdTe QD chemosensors have been widely used in detecting water pollution but improving their detection performance remains a challenge.

CdS quantum dots. CdS QDs have unique optical and electronic properties such as high fluorescent emission and light bleaching resistance, which can be used to monitor the quality of irrigation water. For example, a yellow fluorescent CdS QD chemosensor (**61**) was reported for the detection of Cu^{2+}, Hg^{2+}, and Mg^{2+} in water samples. The peak values for the excitation

7022 | *Chem. Soc. Rev.*, 2024, **53**, 6992–7090

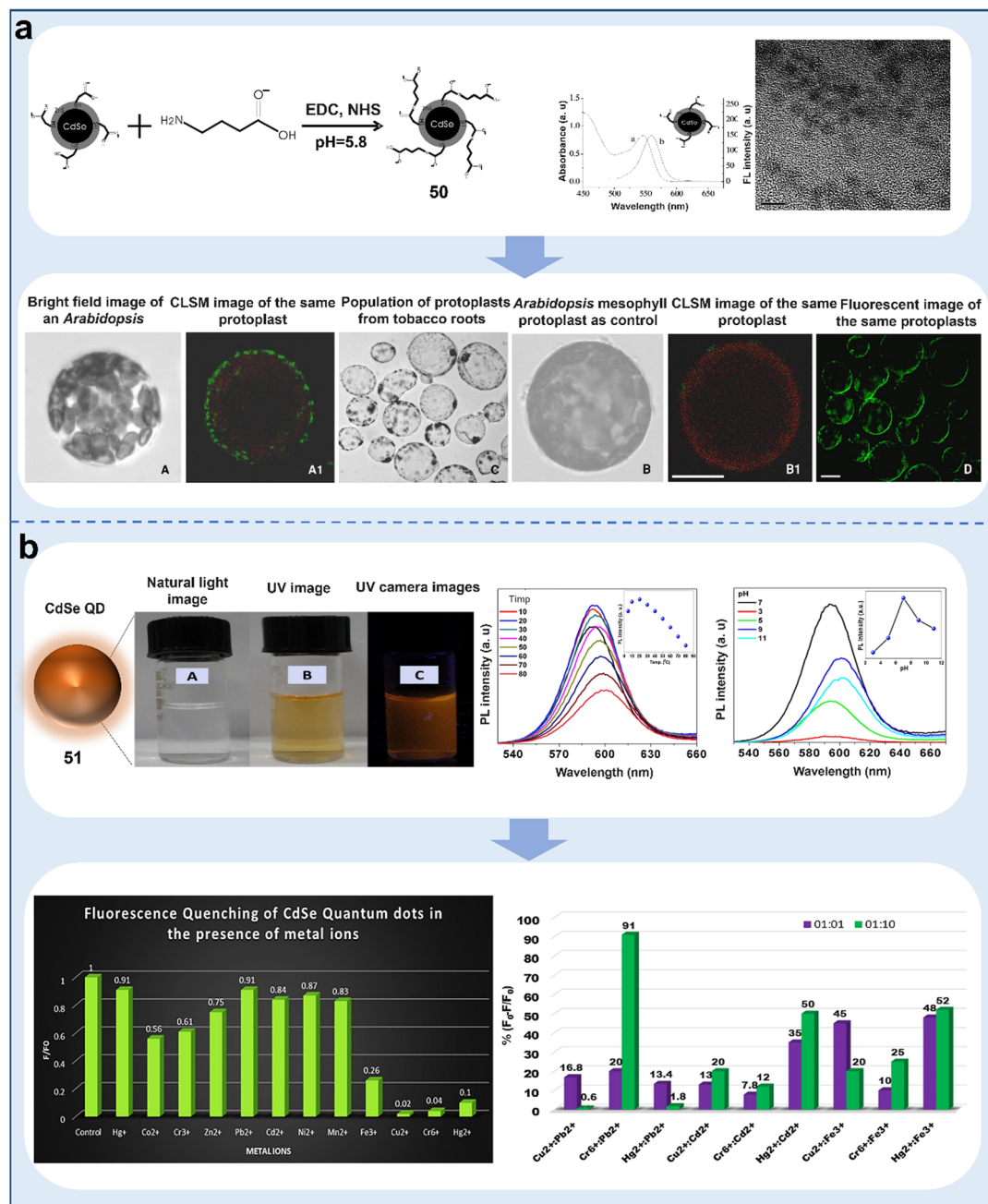This journal is © The Royal Society of Chemistry 2024

Fig. 19 Schematic representation of CdSe QD-based chemosensors for the visualization of plant protein level and ions in water. (a) Specific recognition and detection of GABA on the surface of plant protoplasts based on ZnS outer shell layer and CdSe inner core QD.[122] Copyright © 2006, Elsevier. (b) Detection of heavy metal Hg²⁺ in water based on starch-capped CdSe QDs.[123] Copyright © 2020, Elsevier.

and emission wavelengths of **61** were recorded to be 365 nm and 505 nm, respectively, and the color under UV irradiation was an intense yellow. **61** could be linearly quenched by Cu^{2+}, Hg^{2+}, and Mg^{2+} in aqueous solution with LODs of 0.22, 5.8 and 1.6 ng mL^{-1}, respectively (Fig. 21a).[133] In the presence of GSH, the fluorescence intensity of **61** increased 1.5-fold, which implied that **61** can be used to monitor the stress damage caused by ions in plants. The ability of L-Cys-coated cadmium sulfide QDs (L-Cys-CdS QDs) (chemosensor **62**) with strong fluorescence was reported to detect 2,4,6-trinitrophenol (TNP)

in environmental water samples. Particularly, the PL emission peak of **62** remained unaffected by a change in the excitation wavelength. The emission spectrum was strongest upon excitation at the wavelength of 365 nm. It was highly selective for TNP, and an apparent reduction in fluorescence intensity of CdS QDs was observed with an increase in TNP concentration, and its quenching effect was better under weakly acidic conditions. The linear range of TNP concentration was determined to be 0.05–5 μg mL^{-1} with the LOD of 39 ng mL^{-1} (Fig. 21b).[134] Furthermore, a program for the accurate, discerning detection

This journal is © The Royal Society of Chemistry 2024

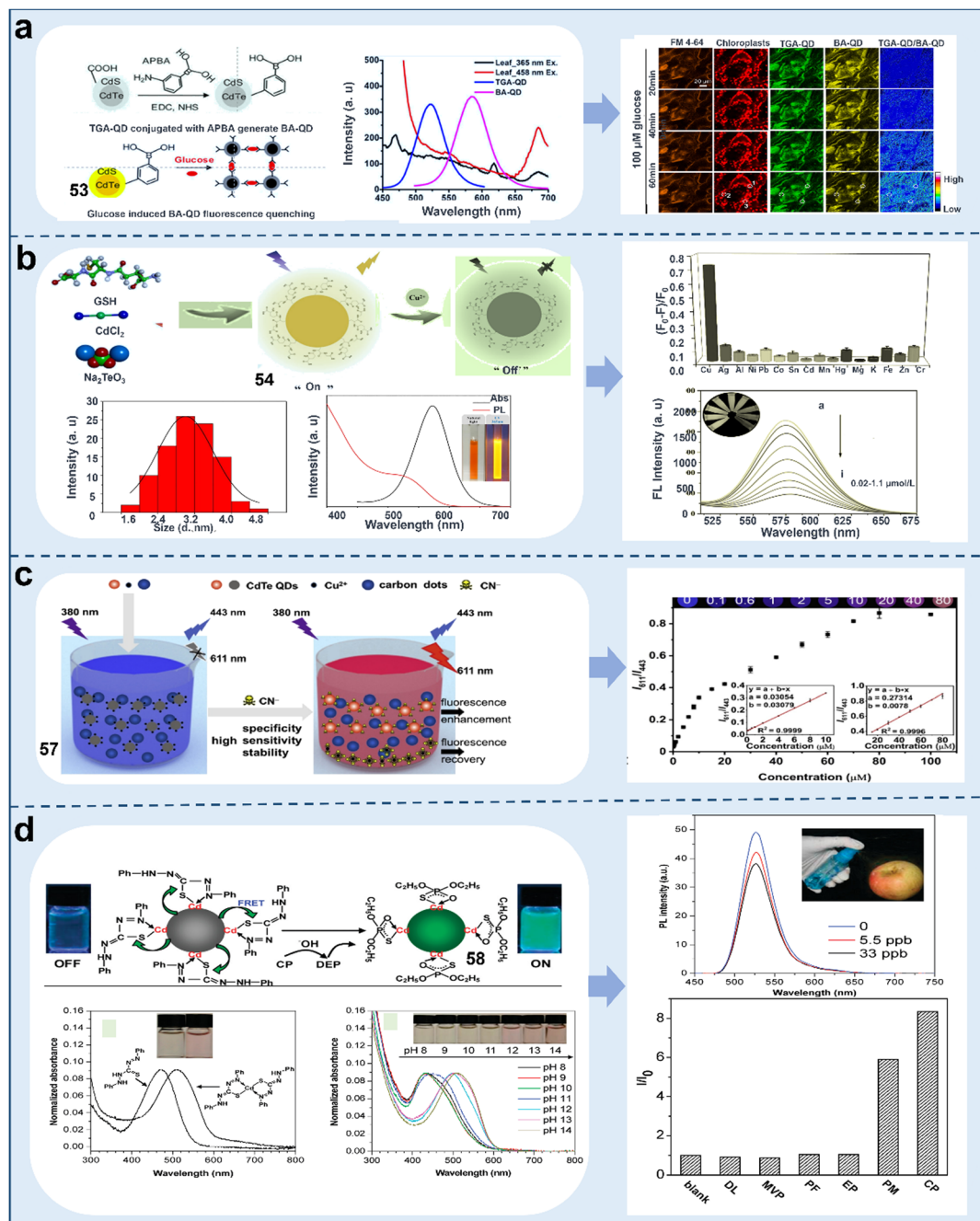*Chem. Soc. Rev.*, 2024, **53**, 6992–7090 | **7023**

Fig. 20 Schematic representation of CdTe quantum dot-based chemosensors for detecting ions and pesticides in plants and water. (a) Ratiometric fluorescent chemosensors based on TGA-QD and BA-QD for monitoring the glucose content in plant chloroplast organelles.[125] Copyright © 2018, the American Chemical Society. (b) Detection of heavy metal Cu^{2+} in environmental water samples by glutathione-modified CdTe QD.[126] Copyright © 2023, Elsevier. (c) Detection of cyanide anions based on synergistic interaction of N-acetyl-L-Cys-capped CdTe QDs and CDs.[129] Copyright © 2019, Elsevier. (d) Detection of the organophosphorus pesticide chlorpyrifos in apples based on CdTe QD fluorescent chemosensor.[130] Copyright © 2010, the American Chemical Society.

methodology for quantifying trace levels of TNP in water was developed. In addition, the CdS QD chemosensor (**63**) also enabled the accurate monitoring of dichlorvos (DDVP), paraquat, and glufosinate in environmental water samples with LODs of 0.23 mM, 1.44 μM and 49.8 μM, respectively.[135] Paraquat possesses the capacity to quench the fluorescence of QDs, DDVP significantly enhances their fluorescent intensity, and glufosinate induces a blue-shift and increase in fluorescence intensity. Based on these results, we can develop software for use with a smartphone to realize the fast detection of various pesticides in the environment. Future studies should focus on improving the biocompatibility of CdS QD chemosensors to expand their imaging in plant tissues.

ZnS quantum dots. Compared with other semiconductor quantum dots, ZnS QDs are more stable, non-toxic, and ecologically safe, and thus widely used in biosensing and toxic
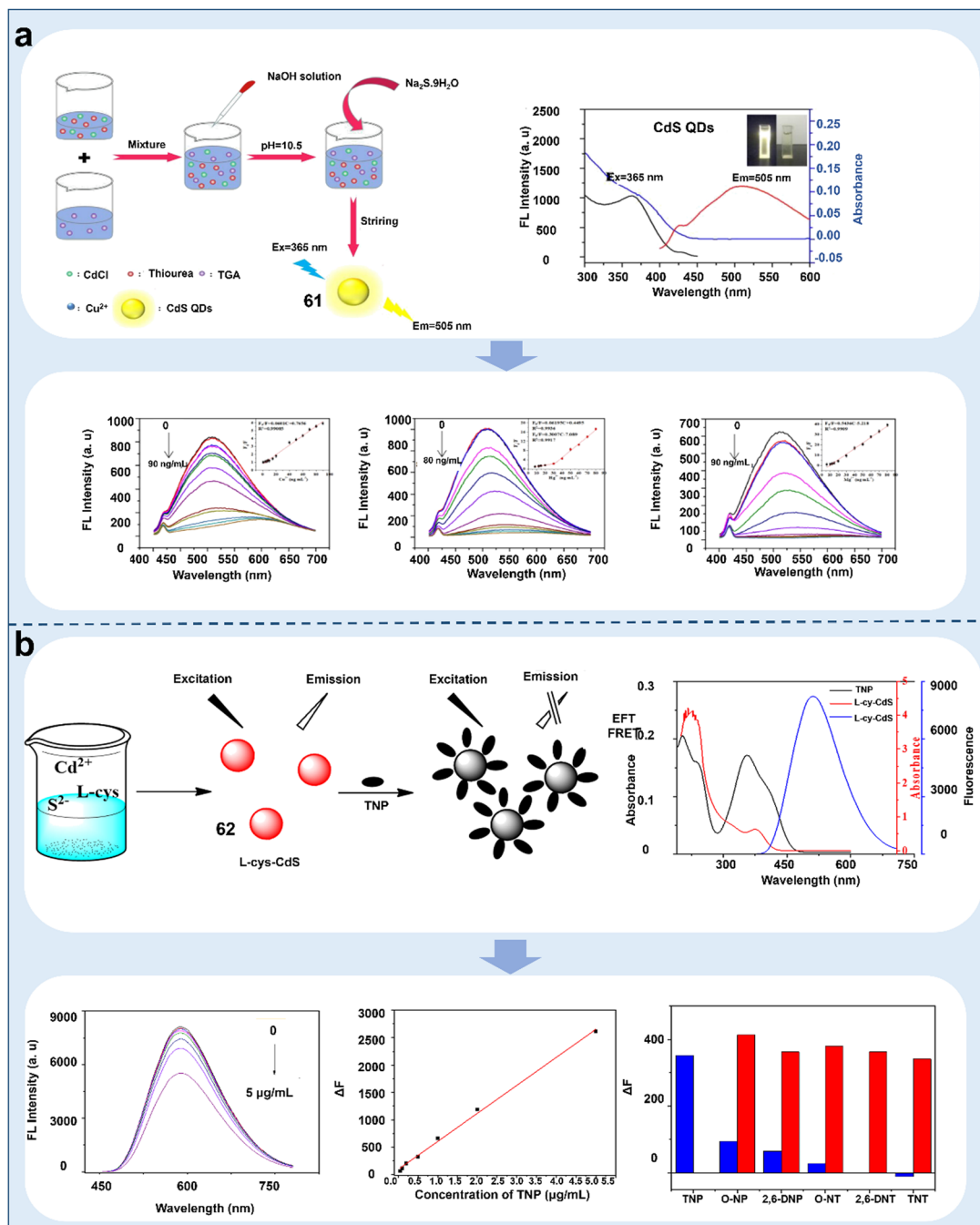
Fig. 21 Schematic representation of CdS quantum dot-based chemosensors for monitoring irrigation water quality. (a) GSH-CdS QD chemosensor for the accurate detection of Cu^{2+}, Hg^{2+}, and Mg^{2+} in water.[133] Copyright © 2022, Elsevier. (b) Detection of TNP in environmental water samples based on L-cysteine-coated cadmium sulfide quantum dot chemosensor.[134] Copyright © 2019, Elsevier.

substance detection technologies.[191] For example, $CuInS_2$@ZnS (CIS@ZnS) (chemosensor **64**) core–shell QDs were reported for the sensitive detection of heavy metals in water. **64** showed a PL excitation peak at 450 nm and emission peak at 620 nm, and the core–shell QDs exhibited blue shifts with a significant increase in emission intensity. The QY of their PL was 95%. By adding various heavy metals such as Ar^{3+}, Cd^{2+}, Co^{2+}, Cu^{2+}, Fe^{2+}, Hg^{2+}, and Zn^{2+}, which are commonly found in water, to aqueous dispersions of **64**, it was found that the PL of the chemosensor was quenched by the

test metal ions at the nM level, such as Cu^{2+} and Hg^{2+}, with an LOD of 0.22 nM in evaluating water quality (Fig. 22a).[136] Besides the detection of ions, **64** could also monitor changes in cholesterol and citric acid, implying its potential as a tool to evaluate fruit quality. A proportional fluorescent chemosensor based on double-emitting Mn-doped ZnS QDs (Mn:ZnS QDs) (chemosensor **65**) was demonstrated for the detection of Pb^{2+} and methyl parathion (MP). **65** was designed to show blue fluorescence at 400–500 nm, which was highly sensitive as a proportional fluorescent chemosensor for the

This journal is © The Royal Society of Chemistry 2024
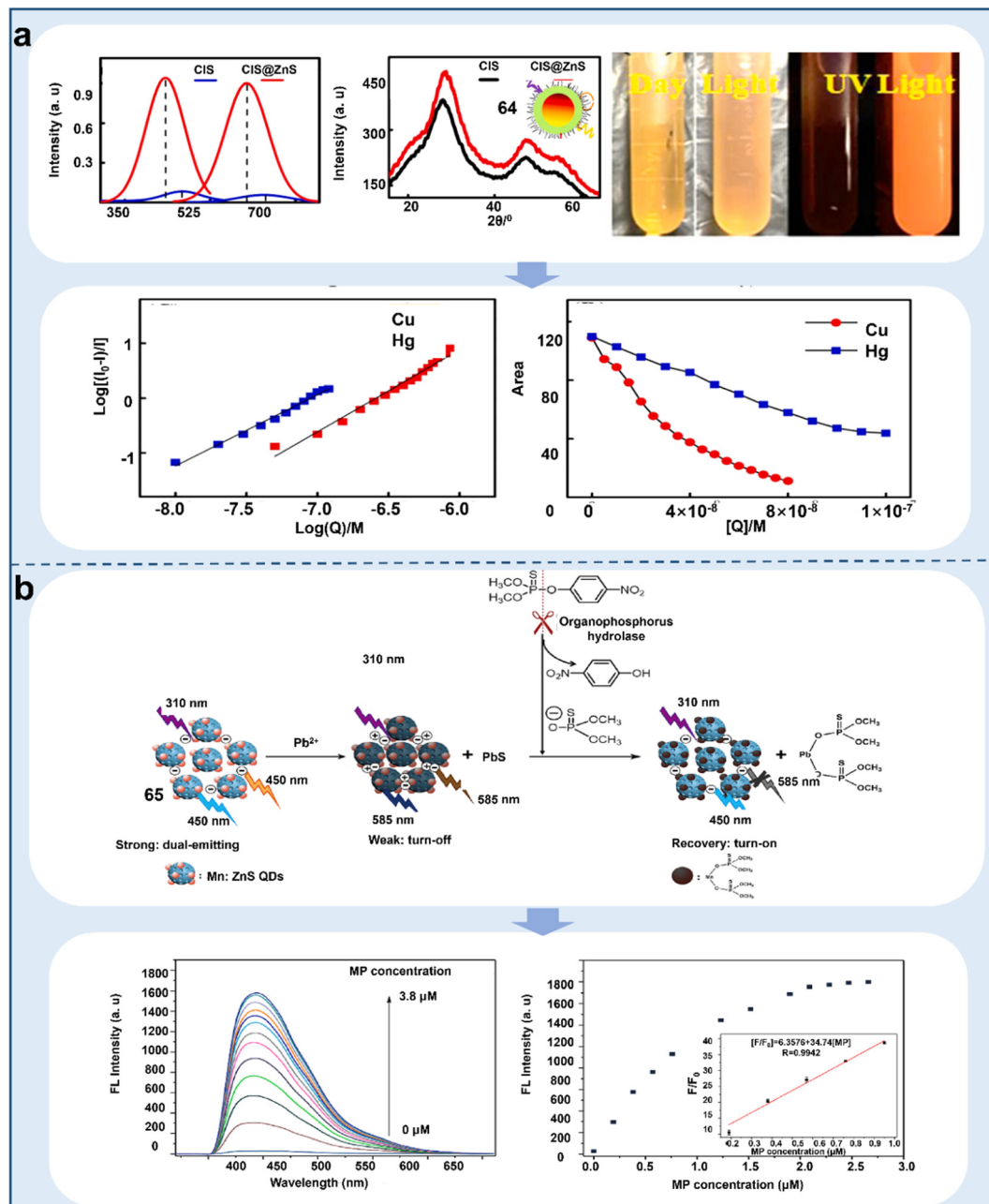
Chem. Soc. Rev., 2024, **53**, 6992–7090 | 7025

Fig. 22 Schematic representation of ZnS quantum dot-based chemosensors for detecting ions and pesticides in water. (a) Efficient detection of copper and mercury in water quality based on CIS@ZnS QD chemosensor.[136] Copyright © 2021, Elsevier. (b) Novel proportional fluorescent chemosensor based on luminescent manganese-doped ZnS QD (Mn:ZnS QD) for the detection of Pb^{2+} and methyl parathion (MP).[137] Copyright © 2019, Elsevier.

detection of Pb^{2+}. This chemosensor showed good concentration linearity between 10 nM and 60 nM for Pb^{2+}, with an LOD of 0.5 nM. Also, **65** served as a "turn-on" fluorescent chemosensor for detecting the concentration of MP. The fluorescence response of this chemosensor showed an excellent linear response for MP in the concentration range of 19.0–450.0 μM, with LOD of 0.02 μM (Fig. 22b).[137] This sensor system was employed to identify MP residues in apples and lake water. Considering the complexity of environmental samples and unknown interferences, a specific response structure or recognition moiety should be combined with **65**. In addition, a ZnS QD-based chemosensor (**66**) also enabled the accurate detection

of thiram in environmental water samples and fruit peels.[138] In the presence of thiram, the Ag^+ in **66** could form an Ag-thiram complex, which could suppress the phosphorescence quenching, indicating that a UV lamp can be used to easily realize pesticide detection. Therefore, compared with other semiconductor quantum dots, ZnS has lower toxicity and better stability, which has broader prospects for plant imaging in the future.

Perovskite quantum dots. Perovskite QDs are recently developed semiconductor QDs that have great potential for detecting heavy metals in soil and water. For example, the ability of Eu^{3+}-

7026 | *Chem. Soc. Rev.*, 2024, **53**, 6992–7090

This journal is © The Royal Society of Chemistry 2024

doped lead-free $Cs_3Bi_2Br_9$ Pe QDs (chemosensor **67**) to detect Cu^{2+} in real water samples on was reported. The UV-vis absorption spectra of **67** and **67**:Eu^{3+} showed that the absorption band edge of the bare **67** was at 389 nm. The absorption band shifted towards a higher wavelength with an increase in the concentration of Eu^{3+}. **67**:Eu^{3+} was characterized by high QY, non-toxicity, robust stability and multi-color emissions, thereby conferring heightened sensitivity and selectivity for detecting metal ions in environmental water. Notably, the exciton emission at 446 nm was rapidly perturbed upon the introduction of

Cu^{2+}, which has excellent detection efficiency for Cu^{2+} in the concentration range of 5 nM to 3 μM, with an LOD of 10 nM (Fig. 23a).[139] PS-$CsPbBr_3$@CTAB PQDs (chemosensor **68**) acted as a sensor, exhibiting blue fluorescence under UV light. **68** could be used to detect dimethoate in water, and the addition of the pesticide dimethoate resulted in the fluorescence shutdown of **68**. Notably, linear quenching was achieved with an increase in the concentration dimethoate in the range of 5–100 μM with an LOD of 5.0 nM. The developed method exhibited higher sensitivity compared with analytical instruments
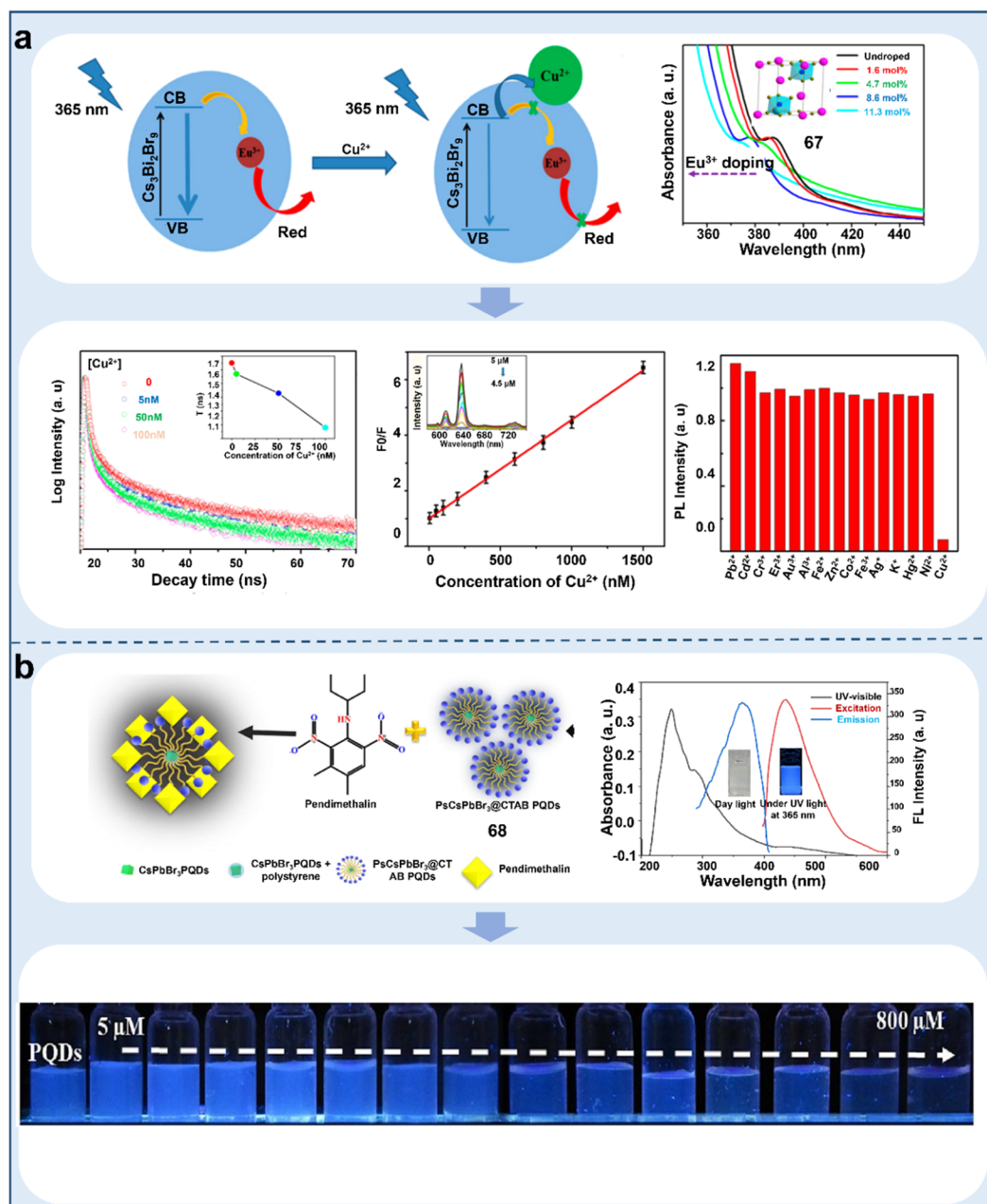

Fig. 23 Schematic representation of chalcogenide-based quantum dot chemosensors for monitoring the concentration of ions and pesticides in water. (a) Eu^{3+}-doped lead-free $Cs_3Bi_2Br_9$ Pe QD fluorescent chemosensor for the detection of Cu^{2+} in real water samples.[139] Copyright © 2019, the American Chemical Society. (b) Detection of the pesticide dimethoxybenzoate by the introduction of polystyrene and cetyltrimethylammonium bromide as an encapsulated assembly system prepared as $CsPbBr_3$@CTAB PQD.[140] Copyright © 2019, Elsevier.

(Fig. 23b).[140] In addition, the fluorescent sensor prepared by combining a molecularly imprinted polymer (MIP) with luminescent perovskite (CsPbBr$_3$) (chemosensor 69) encapsulated in (3-aminopropyl) triethoxysilane (APTES) could sensitively detect oxidized lecithin in soil with an LOD of 18.8 ng mL^{-1}.[141] However, the low water-soluble of perovskite QDs is a challenging task, and thus focusing on improving their stability and water solubility will increase their application scope in the biological field.

Although semiconductor QDs have been widely used to monitor pollutants in the living environment of plants, their application in plant imaging is limited, which is mainly attributed to the following factors: (i) the *in vivo* imaging technology of semiconductor QDs is constantly improving, but the sensitivity of fluorescence imaging for deep tissues is low; (ii) the inertness of semiconductor QDs *in vivo* may cause enduring toxicity to organisms; and (iii) semiconductor QDs have high surface activity, which make them easily agglomerate to form larger agglomerates.

4.1.2 Carbon quantum dots. CQDs are novel and green carbon nanoparticles, characterized by particle dimensions generally smaller than 10 nm. CQDs also exhibit interesting fluorescence properties because of their excellent fluorescence properties and physicochemical properties such as good water solubility, low toxicity, and great biocompatibility.[192] Thus, non-doped CQD chemosensors, metal-doped CQD chemosensors and non-metal-doped CQD chemosensors have been used as chemical and biological sensors to achieve the precise detection of substances affecting plant health.

Undoped carbon quantum dots. CQDs are mainly prepared from some natural plants and biomolecules, which are widely used in monitoring fungi, reactive oxygen species, and heavy metals in plants because of their impressive biocompatibility, negligible toxicity and remarkable stability.[193] For example, fluorescent CQDs (chemosensor 70) were designed for the first time for monitoring pH changes in plant cells. 70 exhibited excitation-dependent fluorescence behavior, and its fluorescence emission intensity changed with pH. The gradual increase in fungal concentration in infected apple tissues led to a transient decrease in pH in plant cells, which caused the fluorescence intensity to increase. Consequently, the fluorescence imaging of the pathogenic fungus *Valsa mali Miyabe et Yamada* in apple tissues was realized (Fig. 24a).[142] Meanwhile, the fluorescence of 70 in dead cells was quickly quenched because of the absence of cellular pH regulation, implying that this chemosensor can be developed into a kit for the visualization of pH regulation in plants or distinguishing live or dead cells. Accurate monitoring of Cu^{2+} in plants could be realized based on fluorescent R-CDs (chemosensor 71). The fluorescent carbon dots were well dispersed and water-soluble. 71 exhibited bright-red emission at 680 nm when excited at 420 nm. The red emission of 71 was found to decay upon interaction with Cu^{2+} in solution by incubating 71 with bean sprouts, and then transferring them to a solution of Cu^{2+}. The LOD was 25 nM in plants. 71 was capable of overcoming the influence from the

internal environment of the plant and had excellent immunity to interference, implying that this chemosensor can monitor the stress in plants in practice with nondestructive nature (Fig. 24b).[143] Also, the accurate detection of Pb^{2+}, Ni^{2+}, Hg^{2+}, Fe^{3+}, Cr^{6+}, and Cd^{2+} in environmental water samples could be realized based on fluorescent CQDs (chemosensor 72–75).[144–147] Among them, 73 showed the lowest detection limit of 0.3 nM, which can effectively coordinate with Fe$_3$O$_4$/CDs by electrostatic interactions, and then quench their fluorescence signal. The results indicated that 73 can not only detect Hg^{2+} in the actual environment but also remove Hg^{2+}. A CQD chemosensor (76) could detect arsenite in environmental water samples. 76 showed the strongest emission wavelength at 412 nm when excited at 340 nm and its solution appeared blue under UV light. The SH-groups of 76 could selectively interact with arsenite, which enabled the sensitive detection of arsenite in environmental water with a good response in the range of 5–100 ppb and LOD (3 s) of 0.086 ppb (Fig. 24c). However, considering that the excitation wavelength of 76 in the UV region, it is not suitable for *in vivo* imaging of Hg^{2+}.[148] In addition, it was reported that CDs (chemosensor 77) synthesized by burning waste paper as a carbon source could detect chlorpyrifos pesticide in vegetables. The fluorescence spectrum of 77 reached its optimum emission peak at 420 nm with an excitation wavelength of 320 nm. Its fluorescence was quenched by Fe^{2+} and recovered upon the introduction of chlorpyrifos. The linear concentration range extended from 0.01 to 1.0 μg mL^{-1}, featuring an LOD of only 3 ng mL^{-1}, which was used for imaging chlorpyrifos in vegetables (Fig. 24d). The fluorescence of 77 depended on the transformation between Fe^{2+} and Fe^{3+} by H$_2$O$_2$ and the production of H$_2$O$_2$ was inhibited by acetylcholinesterase activity, implying that this chemosensor can quantitatively detect organophosphorus pesticides and monitor enzymatic activity.[149] In addition, fluorescent chemosensors (78–80) based on CDs also enabled the accurate detection of some pesticides in plants such as parathion-ethyl, cyfluthrin, glyphosate, methomyl and methyl parathion.[150–152] Among them, 79 showed the lowest detection limit of 4.8 × 10^{-11} M owing to its detection mechanism, where methyl parathion can decrease the enzyme activity of tyrosinase. Therefore, the excellent fluorescence properties based on fluorescent CQDs enable them to be used more often as chemosensors in plants, consequently enabling an in-depth understanding of plant growth conditions and patterns.

Metal-doped carbon quantum dots. In recent years, doping different metal elements is an important way to enhance the physicochemical attributes of CQDs to make them more stable, and they are widely used in sensing applications. For example, Tb^{3+}-doped CDs (CD-Tb) (chemosensor 81) showed bright-blue fluorescence emission under a 365 nm UV lamp with a relatively high QY of 54.8%. Subsequently, its sensitivity to guanosine 3′-diphosphate-5′-bisphosphate (ppGpp) was evaluated. The ppGpp molecular phosphate group was found to be able to bind to the rare-earth Tb^{3+}, and thus effectively improved the emission intensity of 81. Paper-based sensors were developed to realize simple and intuitive ppGpp detection. A linear

7028 | *Chem. Soc. Rev.*, 2024, 53, 6992–7090

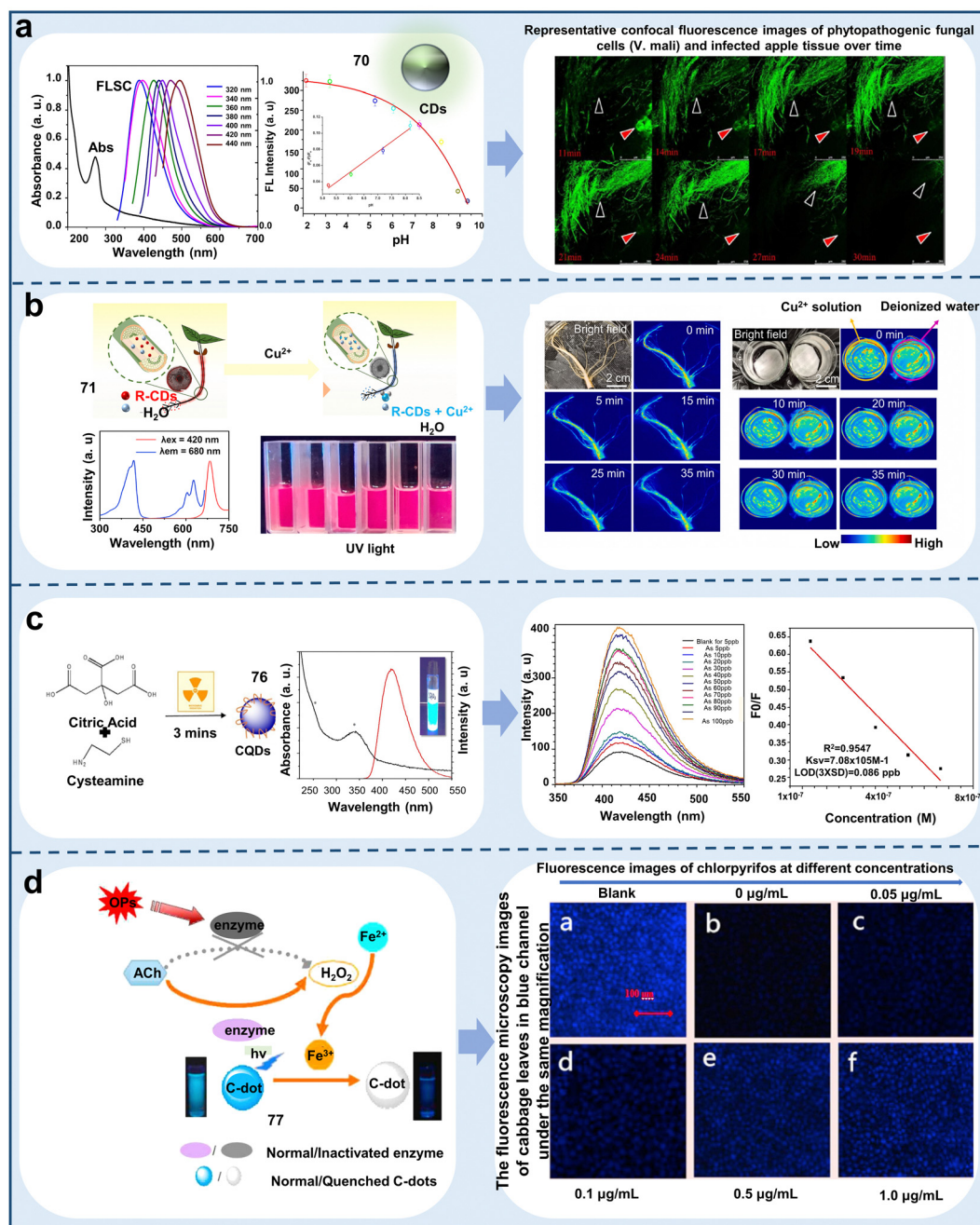This journal is © The Royal Society of Chemistry 2024

Fig. 24 Schematic representation of the application of undoped carbon quantum dot-based chemosensors for detecting pathogens and water pollution. (a) Hydrothermal preparation of pH-sensitive fluorescent CDs for the detection of the pathogenic bacterium *Valsa mali Miyabe et Yamada* in apple tissues.[142] Copyright © 2015, Elsevier. (b) Fluorescent sensors of red fluorescent R-CDs enable Cu^{2+} concentration monitoring in plant roots.[143] Copyright © 2014, Elsevier. (c) Fluorescent sensor of blue fluorescent CDs enables the sensitive detection of arsenite in environmental water samples.[148] Copyright © 2017, Elsevier. (d) Detection of chlorpyrifos levels in cabbage leaves by a blue fluorescent CD sensor.[149] Copyright © 2018, Elsevier.

relationship emerged in a broad concentration range of 25 to 750 μM (Fig. 25a). Among the tested amino acids, **81** could selectivity detect ppGpp owing to the production of antenna and coordination binding.[153] This scheme confirmed the great potential of rare earth ion-modified CDs as a novel proportional FL chromophore. An MnO_2-doped carbon QD chemosensor (MnO_2CD) (**82**) was prepared by a hydrothermal methodology based on the combination of citric acid and $KMnO_4$. This

chemosensor exhibited good photostability with no discernible alteration in its PL spectra, even in the presence of elevated NaCl concentrations up to 2.5 M. No change in its PL peak position was observed with a change in pH conditions. Importantly, **82** enabled the first visual identification of arsenic-containing compounds in rice and green plants. The luminescence signal of **82** was mainly presented in the vascular system of the roots, and As^{3+} was linearly correlated in the concentration range of 0–0.991 μM. The LOD of

arsenite in the chlorotic plants reached 9.2 μM (Fig. 25b).[154] Thus, **82** showed good translocation properties in lateral and green rice plants, demonstrating its potential for detecting the deposition of arsenic within plant root structures. The temperature-sensitive fluorescent properties of the chemosensor of MnO_2CD establish its potential for use as a nano-temperature meter in physiological environments. Therefore, the introduction of metal ions increases the detection range of CQDs.

Nonmetal-doped carbon quantum dots. Compared with metal element doping, nonmetal-doped CQD chemosensors with low toxicity, good biocompatibility, and high-intensity PL have been used in biosensing and environmental monitoring. For example, nitrogen-doped carbon QDs (NCDs) (chemosensor **83**) prepared using uronic acid were reported to be capable of detecting Hg^{2+} and Ag^+ in water. **83** exhibited a light transparent color under daylight conditions and a bright-blue color under 365 nm excitation. The fluorescence intensity of **83** could
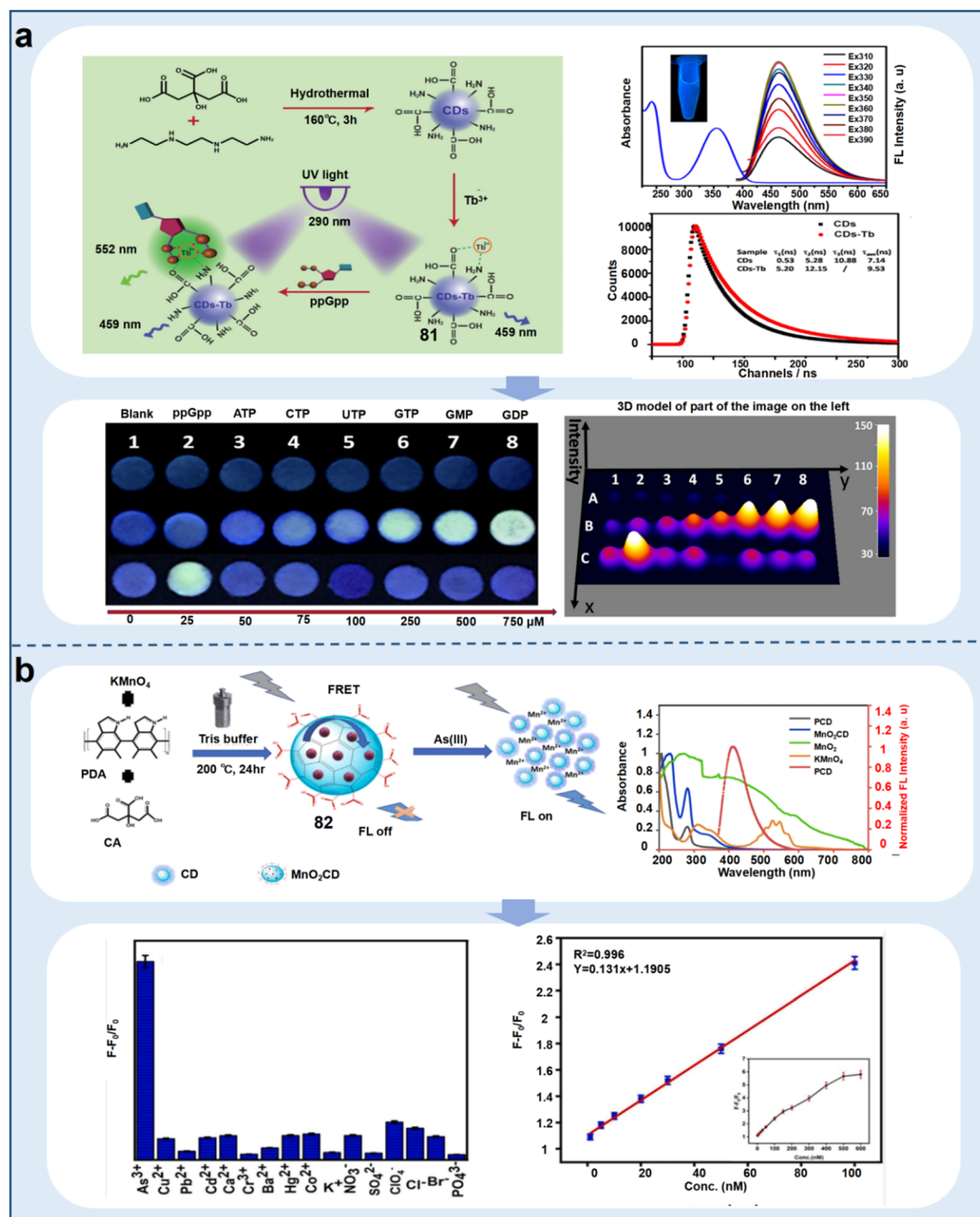

Fig. 25 Schematic representation of metal-doped carbon quantum dot-based chemosensors for monitoring the living environment of plants. (a) Terbium-modified fluorescent CD chemosensor for the detection of ppGpp.[153] Copyright © 2018, the American Chemical Society. (b) Detection of As(III) in environmental water samples by MnO_2 CD fluorescent chemosensor synthesized by hydrothermal decomposition.[154] Copyright © 2022, Elsevier.

7030 | *Chem. Soc. Rev.,* 2024, **53**, 6992–7090

This journal is © The Royal Society of Chemistry 2024

be linearly quenched in the presence of Hg^{2+} and Ag^+ in water with LODs of 4.8 nM and 1 nM, respectively (Fig. 26a). Furthermore, **83** could be recovered by EDTA solution, indicating that this chemosensor may be a potential tool for sensing Hg^{2+}/Ag^+ in the real environment because of its recyclability.[155] NCD chemosensors enabled accurate detection of Fe^{3+}, Pb^{2+}, Cr^{2+}, and Cu^{2+} in water (chemosensors **84** and **85**).[156,157] Among them, **85** is an electrochemical sensor that could sensitively

detect Pb^{2+} and Cr^{2+} owing to its electroactive surface and oxygen-functional groups. CQDs based on N, S co-doping (N, S-CQDs) (chemosensor **86**) also accurately detected carbaryl in apples. **86** achieved a QY of 12.5% with a PL lifetime of 2.8 ns, and carbaryl could quench its fluorescence in the presence of acetylcholinesterase. The linear concentration range was 6.3×10^{-9} g L^{-1} to 6.3×10^{-4} g L^{-1}, with the lowest detection limit of 5.4×10^{-9} g L^{-1} because of its dual enzyme response
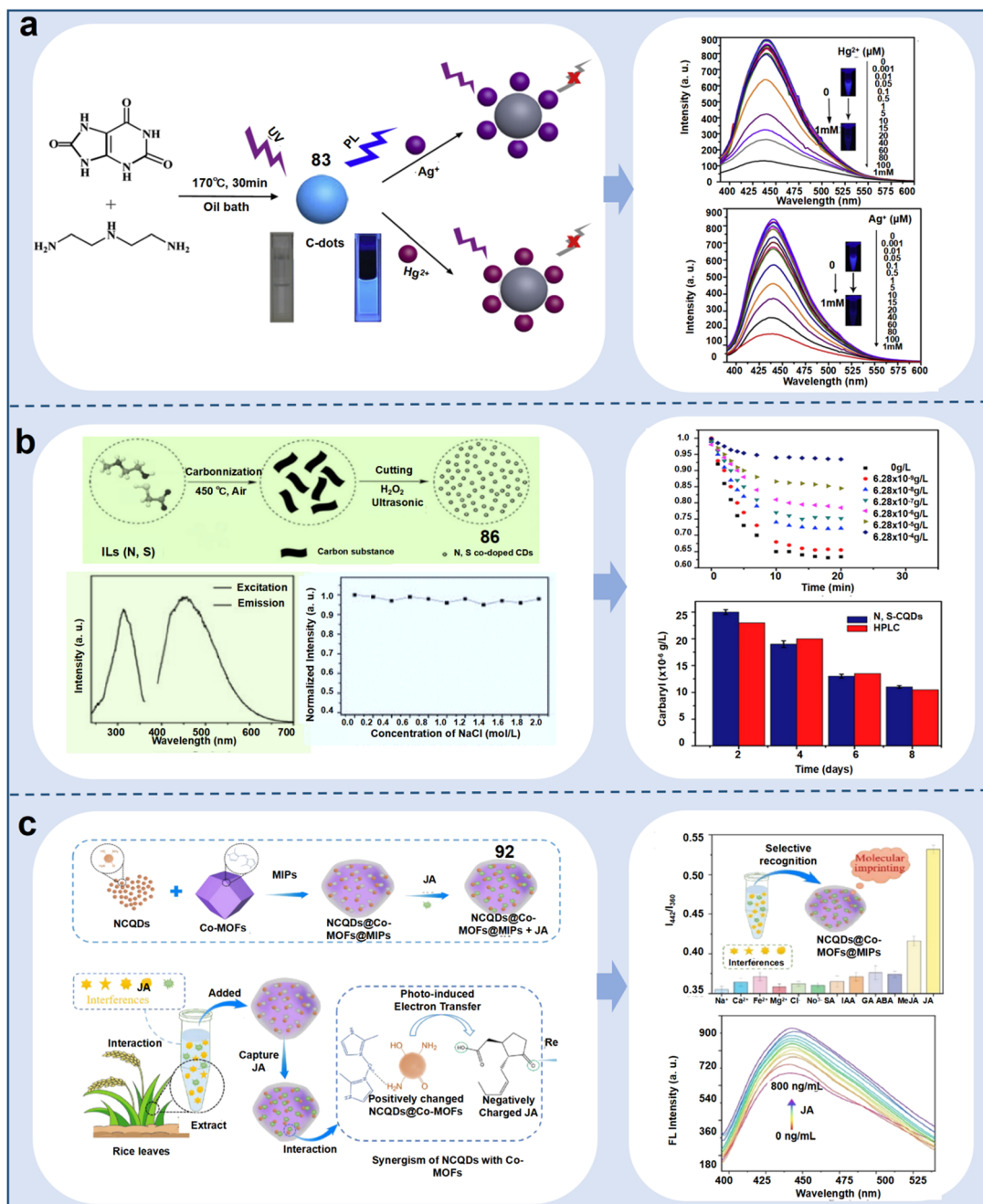

Fig. 26 Schematic representation of non-metal doped carbon quantum dot-based chemosensors for monitoring ions in water, pesticides and hormones in plants. (a) Fluorescent chemosensors with N-doped carbon dots for the detection of Hg^{2+} and Ag^+ in water samples.[155] Copyright © 2017, Elsevier. (b) Fluorescent chemosensors of N, S co-doped carbon quantum dots were used for the detection of the pesticide carbaryl in fruit samples.[158] Copyright © 2016, Elsevier. (c) Detection of phytohormone jasmonic acid based on NCQD@Co-MOFs@MIP ratiometric fluorescent chemosensor.[164] Copyright © 2023, Elsevier.

This journal is © The Royal Society of Chemistry 2024

Chem. Soc. Rev., 2024, **53**, 6992–7090 | **7031**

mechanism (AChE and ChOx enzymes) (Fig. 26b).[158] N, S-CQD chemosensors also enabled the fluorescence detection of para-oxon, p-fenitrothion, dithiopyr, aflatoxin, methimazole, and fenitrothion in soil, water or vegetable samples (chemosensors 87–91).[159–163] Among them, 88 was been proven to detect fenitrothion, dinoseb, dithianon, and their analogues, which was attributed to the electron transition of C=N in flavonoids. Additionally, fluorescent NCDs, metal–organic frameworks, and molecularly imprinted polymers, in conjunction with a proportional fluorescent sensor NCQD@Co-MOFs@MIPs (chemosensor 92), were proposed for the accurate quantification of the jasmonic acid (JA) content in plants. This groundbreaking study represented the first instance integrating fluorescent carbon dots with these composites. Co-MOF and MIPs acted synergistically in trapping the JA molecule, improving the sensitivity and selectivity for monitoring the distribution of JA. Upon the incorporation of JA in 92, it formed a chemical interaction with the NCQDs via PET, leading to changes in the fluorescence signal of 92. The LOD reached 0.35 ng mL^{-1}, offering new insights for developing low-cost and highly sensitive methods for monitoring phytohormones.

Implying that 92 is useful for monitoring the response of plants to biotic and abiotic stresses (Fig. 26c).[164] Therefore, the combination of non-metallic doped quantum dot chemosensors and smartphones and composites is an important approach to improve the detection efficiency and practical applications.

Compared with semiconductor QDs, CQDs have some advantages such as low cytotoxicity, high biocompatibility, and fluorescence stability, but CQDs also have some disadvantages, as follows: (i) the fluorescence wavelength of CQDs is 400–520 nm, and most of them require UV excitation. This short-wavelength has low penetration depth in biological tissues and easily causes photodamage to biological tissue. (ii) Short-wavelength can cause strong autofluorescence in biological tissues, resulting in serious fluorescence background, which interferes with the analysis of fluorescence signals.

4.1.3 Graphene quantum dots. GQD chemosensors, a class of carbon-based QDs, have been used to monitor the water quality for plant survival and non-metal ions in plants. For example, using graphene oxide as a precursor, GQD (Chemosensor 93) was prepared via a simple hydrothermal method for monitoring various heavy metal ions in water. Due to the different functional groups in 93, the particles were different sizes and had surface states, which showed different excitation and emission spectra. In aqueous medium, its fluorescence intensity gradually decreased with an increase in the concentration of Hg^{2+}, Cd^{2+} and Pb^{2+} due to the effective energy transfer. Metal ions exhibited a "turn-off" fluorescence response when they were coordinated with the functionalities of 93. The LODs for the three metal ions were 1.171 μM, 2.455 μM and 2.011 μM, respectively, confirming the feasibility of 93 as promising material for the detection of heavy metal ions in water samples (Fig. 27a). However, its same emission wavelength decreased its selectivity for detecting ions, implying that we should introduce attractive or specific sensing units for distinguishing different ions.[165] Heavy metals and pesticides in soil or water can also

affect the survival of plants, and GQD chemosensors have also been widely used for the accurate detection of Cu^{2+}, Pb^{2+}, Fe^{3+}, and Cr^{3+} (chemosensors 94 and 95).[166,167] The major component of 94 and 95 was coffee grounds and graphene, respectively, which showed good reproducibility, implying that we can develop opto-electronic devices or photocatalysis to increase their application scope. This type of chemosensor also enabled the real-time monitoring of cyanide in plant species. The strategy involved using GQD/gold nanoparticles (AuNPs) coupling to sense and image endogenous bio-cyanide in plants. The GQDs were assembled on the surface of AuNPs by π–π stacking of the GQDs and peptides to form an AuNP-PEP@GQD (chemosensor 96) nanosensor. In the absence of CN^-, the fluorescent emission of GQD was significantly diminished due to FRE facilitated by AuNPs, while the addition of CN^- led to the disassembly of 96 and the fluorescence recovery of GQDs. The LOD under optimal conditions was 0.52 μM (Fig. 27b).[168] In addition, a fluorescent chemosensor (97) based on BN co-doped GQDs (BN-GQDs) could sensitively detect paraquat in environmental water. Under UV light irradiation, the samples emitted different colors including green (B0), light green (B1), light blue (B2), and blue (B3). With an increase in the concentration of paraquat, the fluorescence intensity of 97 gradually diminished with the LOD of 0.0062 mg L^{-1} (Fig. 27c). 97 could specifically recognize paraquat by forming 97-(paraquat)$_x$ intermediates, causing aggregation-caused quenching owing to π–π stacking.[169] Fluorescence sensing based on graphene quantum dot chemosensors was also capable of detecting fenoxycarb, furan, glyphosate, and methyl-phosphate in water or vegetable samples with high efficiency (chemosensors 98–100).[170–172] Among them, 99 showed the highest sensitivity for the detection of glyphosate. After the addition of glyphosate, the fluorescence of cysteine-capped AgNPs of 99 was quenched, implying that this chemosensor has high potential for testing enzymatic activity. Therefore, the low toxicity and high biocompatibility of GQDs provide an important tool for detecting factors that affect plant health.

GQDs show strong fluorescence characteristics, high solubility, excellent biocompatibility, low toxicity and photostability, but they also have some disadvantages, as follows: (i) the structure of GQDs is too small, and then not enough QY can be produced by chemosensors; (ii) the redox reaction and coordination of recognition parts cause GQDs to have weak anti-interference and poor specificity; and (iii) the synthesis process of GQDs is complex and requires many solvents that can increase their synthesis cost and toxicity.

4.1.4 Silicon quantum dots. Si QDs are a new type of fluorescent chemical sensing material with high fluorescence QY, which have been widely used in monitoring plant metabolites, heavy metals and pesticides in water.[194] For example, in recent years, it has been reported that a cyanine-colored luminescent Si QD chemosensor (chemosensor 101) could accurately monitor the endogenous plant metabolite chlorogenic acid (CGA) with good stability and fast response. The optimal engagement and emissive radiation wavelengths for 101 were 350 nm and 470 nm, respectively. Chlorogenic acid quenched the fluorescence of 101 through the synergistic action of static
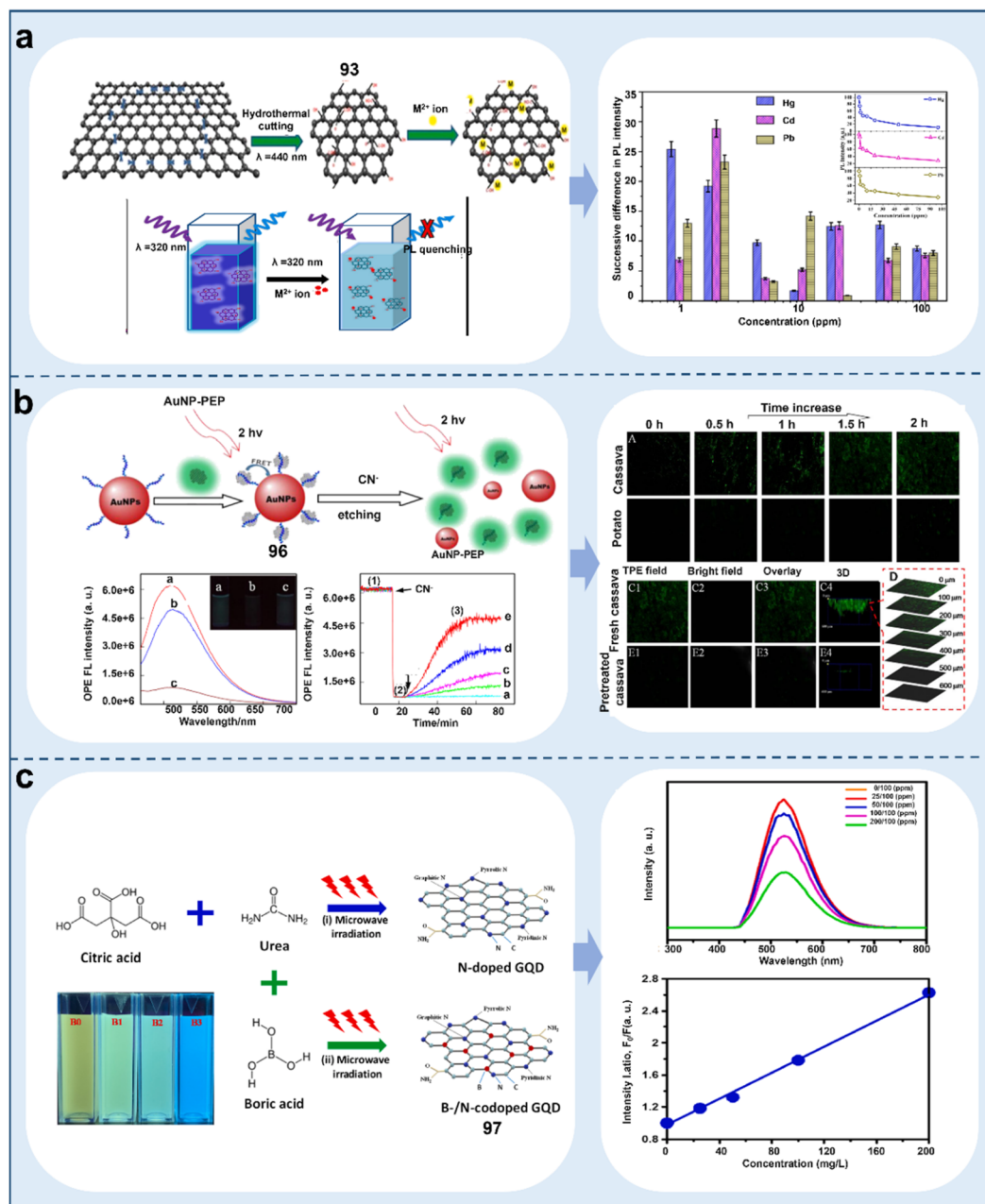
7032 | Chem. Soc. Rev., 2024, 53, 6992–7090

This journal is © The Royal Society of Chemistry 2024

Fig. 27 Schematic representation of graphene-based quantum dot chemosensors for detecting water pollution. (a) Hydrophilic graphene quantum dot chemosensor for the detection of heavy metals Hg^{2+}, Cd^{2+}, and Pb^{2+} in water.[165] Copyright © 2021, Elsevier. (b) Novel dual-photo-excitation nanofluorescent sensor with GQD/AuNP conjugates for the detection of CN^- in plants.[168] Copyright © 2015, the American Chemical Society. (c) Microwave synthesis of boron and nitrogen co-doped graphene quantum dot fluorescent chemosensors for the detection of paraquat in aqueous media.[169] Copyright © 2023, Elsevier.

and dynamic quenching, and it was used for the *in situ* detection of chlorogenic acid in coffee beans. The LOD was 0.43 μmol L^{-1} and the recoveries were in the range of 99.96–109.20% (Fig. 28a).[173] Novel S-doped Si QDs (chemosensor **102**) capable of detecting Fe^{3+} in water were reported, which exhibited an optimal emission of 425 nm at an excitation wavelength of 345 nm, and blue fluorescence under UV illumination. When subjected to numerous metal ions, Fe^{3+} exhibited a linear quenching effect on the fluorescence intensity of **102**, which

was utilized to detect Fe^{3+} in water. The linear range was 1–20 μM and the LOD was 0.21 μM (Fig. 28b).[174] Fluorescent chemosensor (**103**) based on Si QDs also enabled the accurate detection of Hg^{2+} and Cu^{2+} in water.[175]

Upon the addition of Hg^{2+}, the fluorescence intensity of **103** decreased rapidly, which could be recovered by coordination with glutathione. The linear range for the detection of glutathione and Hg^{2+} was 0.1–5 μM and 0.1–4 μM, with LODs of 55 nM and 24 nM, respectively. The results indicated that the

This journal is © The Royal Society of Chemistry 2024

Chem. Soc. Rev., 2024, **53**, 6992–7090 | **7033**

chemosensor can monitor plant health under ion stresses. In addition, sensing centers based on Si QDs, gold nanoparticles (AuNPs) and CdTe QDs (chemosensor **104**) detected carbaryl in lake water and in apples. The blue Si QDs showed an emission spectrum at 460 nm, whereas the red-light emitting CdTe QDs showed an emission peak at 650 nm. Carbaryl exhibited a tendency to adsorb on AuNPs, eliciting a gradual increase in

the fluorescence emission intensity of the Si QDs, while simultaneously inducing a notable reduction in the fluorescence emission intensity of **104**. The LOD of carbaryl in lake water and vegetable samples containing carbaryl was 3.3 nM in the concentration range of 80–200 μM. Importantly, it could be detected in real-time by a smartphone sensing platform (Fig. 28c).[176] Therefore, the proposed sensing scheme enables
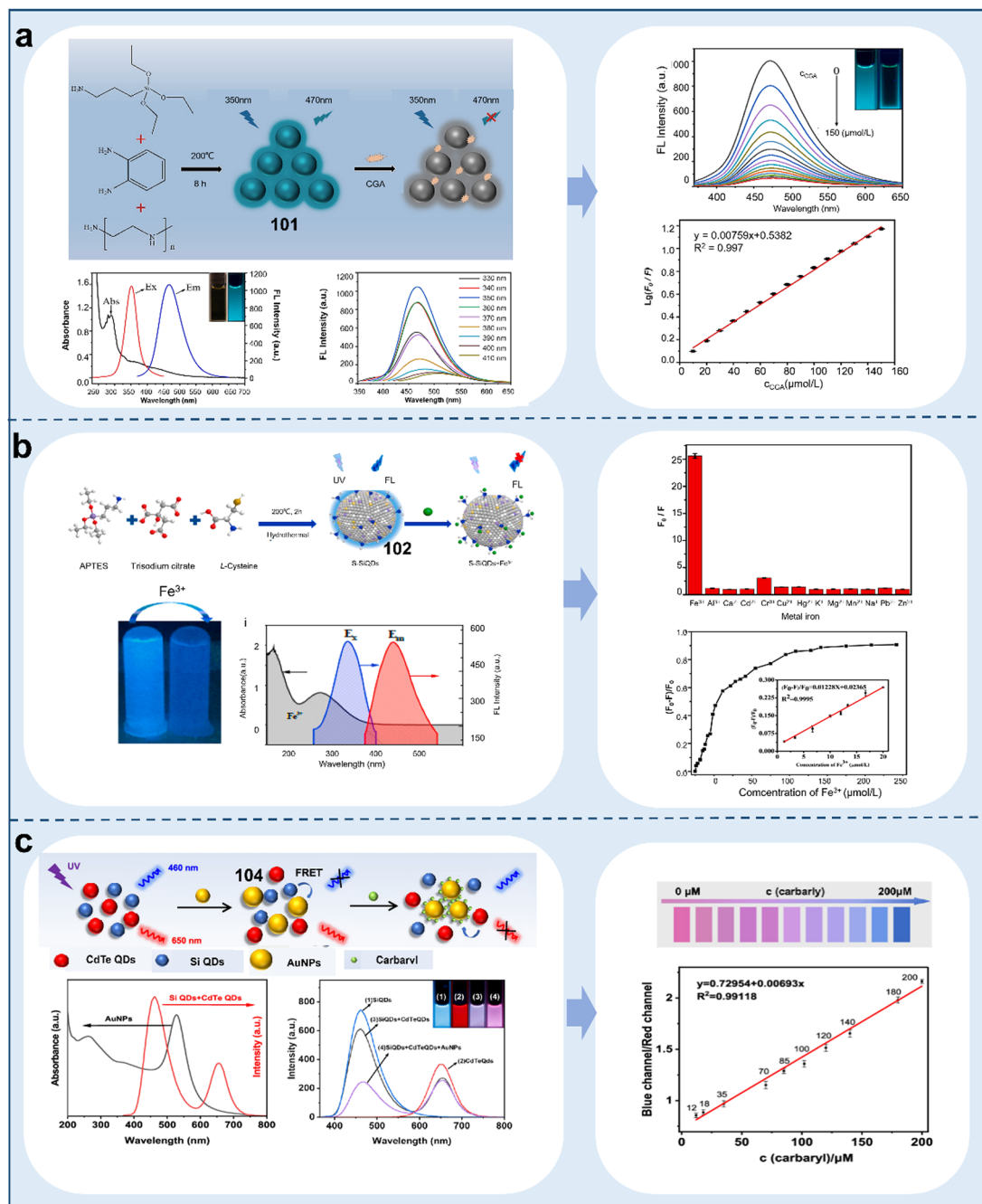

Fig. 28 Schematic representation of silicon quantum dot-based chemosensors for monitoring the living environment and quality of plants. (a) Cyanoluminescent Si quantum dot fluorescent chemosensor for the detection of chlorogenic acid.[173] Copyright © 2023, Elsevier. (b) Detection of Fe^{2+} in water by S-doped Si quantum dot chemosensor.[174] Copyright © 2020, Elsevier. (c) Detection of carbaryl in vegetables by a fluorescent sensor with amino-modified gold nanoparticles, blue-emitting silicon quantum dots and red-emitting cadmium telluride quantum dots.[176] Copyright © 2023, the American Chemical Society.

new proportional fluorescence detection with satisfactory specificity and sensitivity, paving the way for implementing smart phone-centric pesticide detection platforms.

Si QDs have some advantages such as high QY, abundant silicon source, low toxicity and environmentally friendly nature, but they also have disadvantages, as follows: (i) the low water solubility of Si QDs limit their application in biological imaging and decrease their sensitivity and (ii) the poor stability and easy coacervation of Si QDs can affect their fluorescence efficiency, which can be improved by modifying their surface.

4.1.5 Molybdenum disulfide quantum dots. MoS_2 QDs are two-dimensional (2D) inorganic graphene analogs that have been used to identify phytohormones, heavy metals and pesticides in the living environment of plants.[195] For example, novel Eu^{3+} ion-functionalized fluorescent molybdenum sulfide QDs ($Eu–MoS_2$ QDs) (chemosensor **105**) were used for the effective detection of guanosine 3′-diphosphate-5′-diphosphate (ppGpp). **105** showed bright-blue fluorescence with optimal excitation and emission wavelengths of 310 and 410 nm, respectively. The electrostatic interaction of the negatively charged ppGpp with positively charged $Eu–MoS_2$ was stronger for these QDs than for other QDs, and thus the substantial enhancement in red fluorescence was rapid when ppGpp was added to the solution with an LOD of 23.8 μM (Fig. 29a).[177] MoS_2 QDs can also be combined with manganese dioxide using nanosheets to design "off-on" chemosensor **106** to determine trace levels of ascorbic acid (AA).[178] Upon the addition of ascorbic acid, the fluorescence of **106** was gradually restored, which mainly depended on the reducibility of ascorbic acid. Considering that there are many reducing substances in plants, a specific reaction unit should be added to increase the selectivity of **106**. Another MoS_2 QD chemosensor (**107**) was also able to achieve the sensitive detection of Pb^{2+} in water. When excited at 440 nm, the MoS_2 QDs exhibited the maximum intensity at 360 nm, which redshifted with a change in the excitation wavelength. The linear detection range in aqueous solution was 3.3×10^{-7} to 8×10^{-3} M with an LOD of 3.5×10^{-3} M (Fig. 29b).[179] This type of chemosensor also enabled the fluorescence detection of Hg^{2+} in water (chemosensor **108**).[180] Compared with the substitution reaction mechanism, **108** combined with Hg^{2+} showed a synergistic effect for the reaction between TMPyP and Co^{2+}, which caused an evolution in its optical characteristics and promoted the Hg^{2+} sensing to the nM level. A β-cyclodextrin-functionalized MoS_2 QD nanochemosensor (**109**) was reported for the sensitive fluorescence detection of methylthiophene (MP). **109** showed shifted excitation and emission peaks compared to MoS_2. The fluorescence intensity of **109** gradually decreased with an increase in MP concentration, and there was good linearity in the MP concentration from 0.01 ppm to 18.0 ppm with an LOD of 3.3 ppb (Fig. 29c).[181] Therefore, MoS_2 QDs need to be continuously explored to find more robust and effective methods for improving their biological applications.

MoS_2 QDs have been widely used to detect ions and pesticides in the living environment of plants owing to their high QY, biocompatibility, and low toxicity, but their applications are limited due to the following facts: (i) most MoS_2 QD-based biosensors are turn-off fluorescence sensors, and their fluorescence signal is susceptible to the detection system, which may lead to incorrect detection results and (ii) the processes for the synthesis of MoS_2 QDs are complex, which lead to a low yield, size various, and difficult removal of organic solvents.

4.1.6 Sulfur quantum dots. S QDs consist of a polymer core of sulfur and substantial surface functional groups, presenting superior optical stability and tunability, which have been employed for detecting heavy metals in plants.[196] S QDs (chemosensor **110**) with good water solubility and stability were prepared *via* a simple one-step method. UV irradiation at 320 nm resulted in **110** showing the maximum emission peak at 431 nm and blue fluorescence with a QY of about 71%. The distinct reduction in the blue fluorescence emission intensity of **110** was noticeable due to the presence of Co^{2+}. The feasibility of the assay was evaluated using the rhizome of *Salvia miltiorrhiza* as a sample, and the protocol was found to have good recoveries and relative standard deviations for the determination of Co^{2+}. The LOD was 4.51 μM when the concentration of Co^{2+} was 5–50 μM (Fig. 30a).[182] Fluorescence sensing technology based on S QDs could also selectively detect Hg^{2+}, Fe^{3+} and Cu^{2+} in water samples (chemosensor **111** and **112**).[183,184] **111** showed excellent reducibility and it could reduce Cu^{2+} and Fe^{3+} to Cu^+ and Fe^{2+}, respectively, which indicated that **111** may be an effective tool for detecting the redox state transition of ions.[183,184] In addition, the first hydrothermal preparation of S QDs combined with rhodamine B (RhB) resulted in a novel sensing platform (chemosensor **113**) with dual-emission, which could be used to quantitatively monitor 2,4-dichlorophenoxyacetic acid (2,4-D) in vegetables. When excited at 380 nm, **113** produced two emission peaks at 455 nm and 580 nm. The SQD and RhB-SQD solutions appeared transparent light-yellow and light-pink under the sunlight, respectively, and blue or pink-purple color under 365 nm UV irradiation. **113** was successfully used to determine the content of 2,4-D in vegetable and water samples with an LOD of 17.3 ng mL^{-1} (Fig. 30b).[185] This enzymatic inhibitor-based analytical technology provides an uncomplicated efficient way for evaluating the concentration of pesticides in vegetables.

S QDs have been widely used to image ions in plants owing to their high fluorescence intensity, low toxicity and photostability, while they also have some disadvantages, as follows: (i) the temperature instability of S QDs implies that they can be developed as a temperature sensor and (ii) the excitation wavelength of S QDs is mainly in the blue region, which limits their application in biological imaging.

4.1.7 MXene quantum dots. Recently, the emerging development of MXene QDs, mainly in combination with smart devices, has enabled the real-time monitoring of heavy metals and harmful organics in the living environment of plants.[197] For example, a two-dimensional MXene QD-based fluorescent chemosensor (**114**) could simultaneously monitor and remove the heavy metal Mn(VII) from plant leaves. Upon exposure to 365 nm excitation, **114** showed predominant bright blue-green fluorescence with emission and excitation peaks located at 473 nm and 320 nm, respectively, which was primarily ascribed to both its inner core and inherent defects. **114** exhibited ultra-
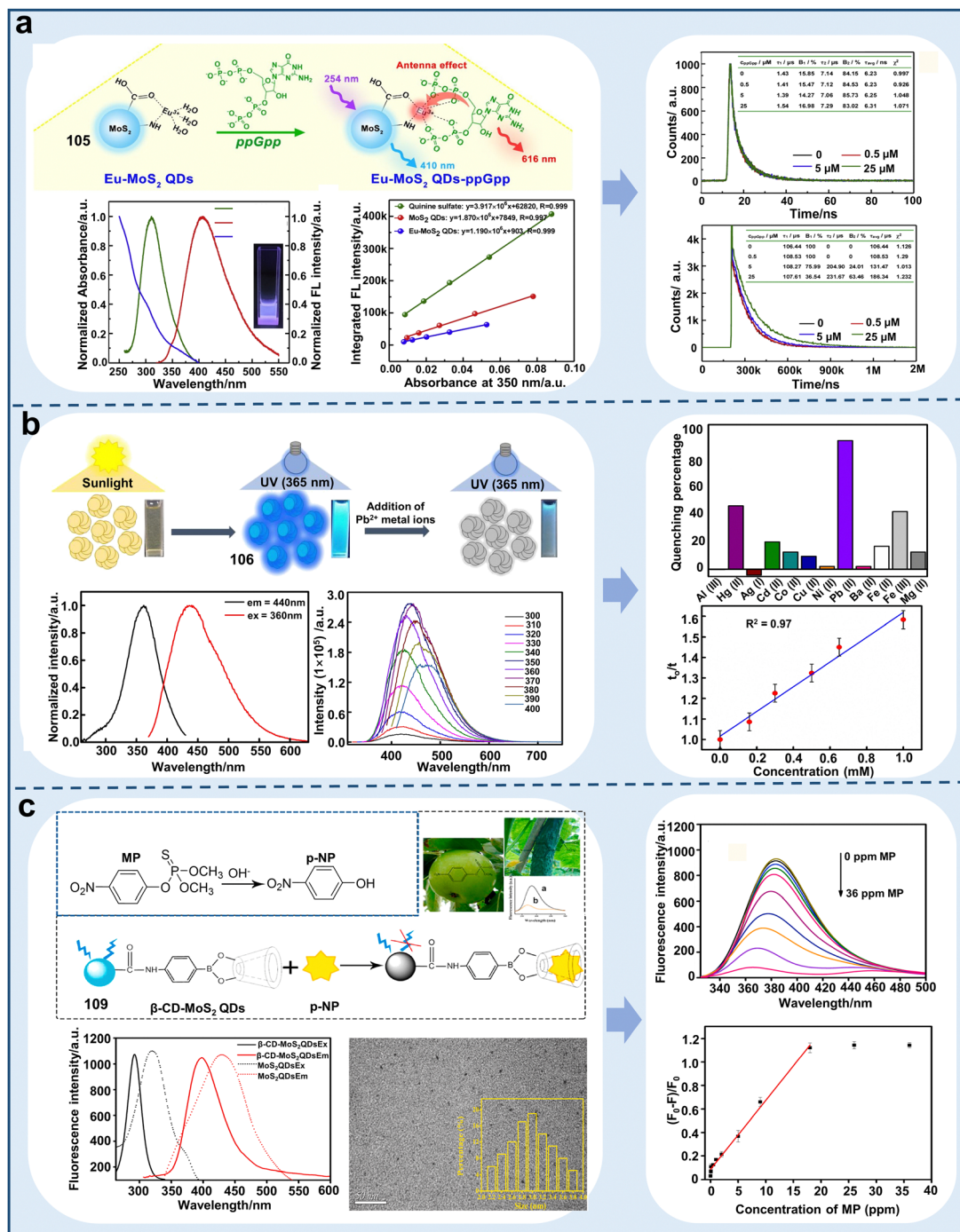
This journal is © The Royal Society of Chemistry 2024

Chem. Soc. Rev., 2024, **53**, 6992–7090 | **7035**

Fig. 29 Schematic representation of molybdenum disulfide-based quantum dot chemosensors for detecting ions and pesticides in plants or the environment. (a) Eu-doped MoS$_2$ quantum dot fluorescent chemosensor developed for paper sensor detection of ppGpp.[177] Copyright © 2020, Elsevier. (b) Functionalized molybdenum disulfide quantum dot fluorescent chemosensor for the detection of Pb^{2+} in water to determine its quality.[179] Copyright © 2020, Elsevier. (c) Detection of p-methyl parathion in fruits by β-cyclodextrin-functionalized molybdenum disulfide quantum dot fluorescent chemosensor.[181] Copyright © 2021, Elsevier.

sensitivity and selectivity towards Mn(VII), which resulted in a marked diminution in its fluorescence intensity. **114** exhibited bright fluorescence in the leaves, which disappeared upon the injection of Mn^{7+}. The results revealed that **114** is an effective fluorescent chemosensor for detecting the concentration and distribution of Mn^{7+} in plants with an LOD of 230 nM. The efficacy of Mn^{7+} elimination employing **114** was ascribed to its

self-reductive potential, thereby facilitating the removal of Mn^{7+} (Fig. 31a).[186] The results indicated that **114** has dual function for monitoring the presence of heavy metals and removing heavy metals from the environment or plants. Fluorescence sensing based on MXene QD chemosensors also enabled the accurate detection of Cr^{3+} and Cu^{2+} in water (chemosensors **115** and **116**, respectively).[187,188] **115** was composed of N-doped

7036 | Chem. Soc. Rev., 2024, **53**, 6992–7090

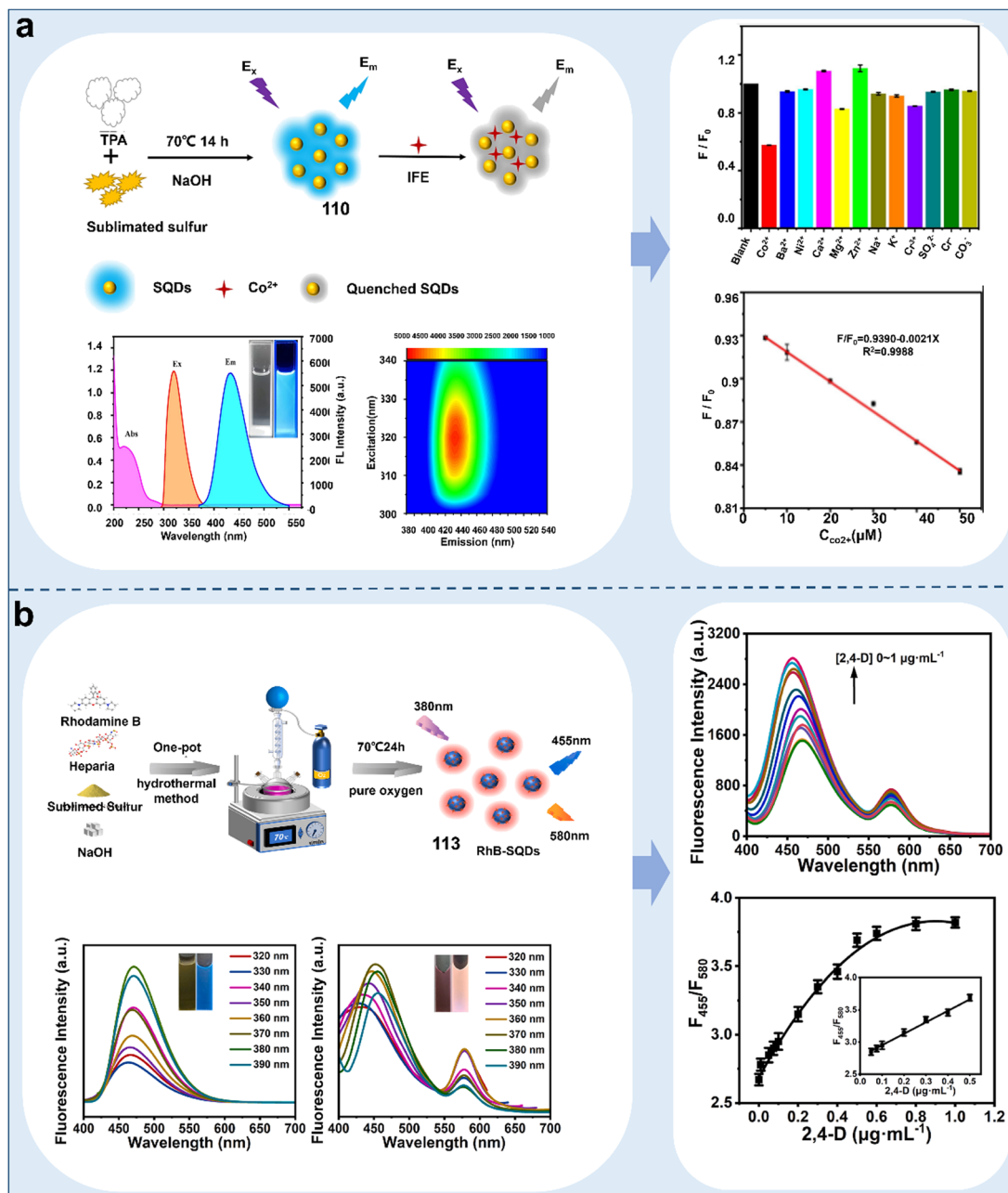This journal is © The Royal Society of Chemistry 2024

Fig. 30 Schematic representation of sulfur-based quantum dot chemosensors for detecting ions and pesticides in plants and water. (a) Detection of Co^{2+} in water by a sulfur quantum dot fluorescent chemosensor.[182] Copyright © 2023, Elsevier. (b) Novel dual-emission sulfur quantum dot fluorescent chemosensor enables the accurate detection of 2,4-dichlorophenoxyacetic acid.[185] Copyright © 2023, Elsevier.

Ti_3C_2 MXene QDs and N doping showed a positive correlation with the size of QDs. **115** showed different fluorescence quenching by interaction with various metal ions, which could specifically recognize Cu^{2+} based on the static fluorescence-quenching mechanism. Recently, nitrogen-doped MXene QDs (chemosensor **117**) were reported for the detection of alizarin red (ARS) in water at 420 nm when excited at 580 nm. The MQD solution was light yellow in daylight and showed strong yellow fluorescence at 365 nm UV. As the concentration of alizarin red increased, the fluorescence of **117** gradually decreased due to the inner-filter effect (IFE). The linear range and LOD were

0–80 μM and 1.21 μM in real water samples, respectively (Fig. 31b).[198] In addition, Ti_3C_2 MXene QDs (chemosensor **118**) based on uronic acid encapsulation also enabled the fluorescence detection of 2,4,6-trinitrophenol in water.[189] TNP could significantly quench the fluorescence of **118** by the IFE, showing a good linear concentration range of 0.01–40 μM and LOD of 9.58 nM. Considering the more environmentally friendly and water-soluble nature of **118**, further studies should focus on combining a smartphone with this fluorescent system, which can realize the easy and convenient detection of 2,4,6-trinitrophenol in the environment. The novel material, MXene

This journal is © The Royal Society of Chemistry 2024

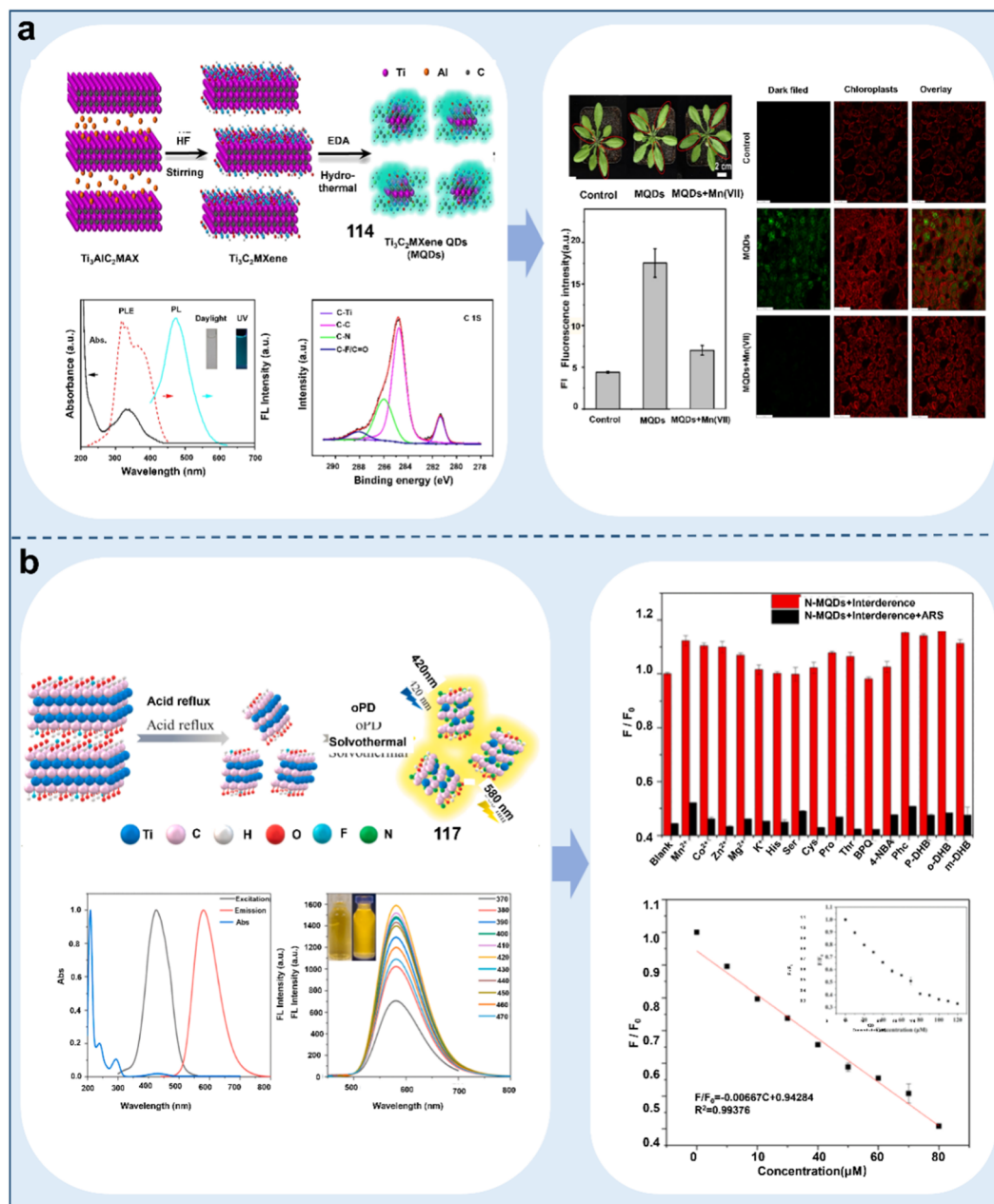Chem. Soc. Rev., 2024, **53**, 6992–7090 | **7037**

Fig. 31 Schematic diagram of the application of MXene quantum dot-based chemosensors for the detection of ions in water and plants. (a) Accurate detection of Mn(VII) in water and plants based on MQD fluorescent chemosensors.[186] Copyright © 2023, Elsevier. (b) Solvothermal synthesis of N-MQD fluorescent chemosensors for the detection of ARS in real water samples.[198] Copyright © 2021, Elsevier.

QDs, offers an important solution for both monitoring and removing metal ions in the environment, which has great potential for improving the quality of the living environment of plants.

We summarized the application of MXene QD chemosensors in detecting the factors affecting or reflecting plant health, which showed good detection efficiency in these areas.[199] However, there are some disadvantages that need to be improved, as follows: (i) almost all MXene QD chemosensors showed UV or blue excitation light, which can reduce the application of these chemosensors for detecting plant hormones, proteins, or enzymes; (ii) the synthesis

strategies for MXene QDs chemosensors should be improved such as fluorine-free or high efficiency and stability of catalyst, which can reduce the toxicity of MXene QD chemosensors and increase their application scope; and (iii) combining MXene QD chemosensors with smart devices to improve the detection and removal efficiency, which will be the future development direction.

4.2 Metal–organic frameworks (MOFs)

MOFs are a class of coordination polymers self-assembled with metal centers (clusters) and organic ligands through coordination bonds. Due to their superiorities of adjustable metal ion

7038 | Chem. Soc. Rev., 2024, 53, 6992–7090

This journal is © The Royal Society of Chemistry 2024

species, diverse functional sites and clear structure, MOFs have emerged as exciting sensing and detection materials.[200,201] A distinctive approach for the fabrication and design of luminescent MOFs (LMOFs) involves utilizing the porous nature of the MOF host to encapsulate diverse luminescent guests (LG), leading to the formation of a composite system known as "LG@MOF".[202] LG are mainly derived from metallic constituents, organic linkers and encapsulated guest entities (*e.g.*, lanthanide ions, organic dyes and QDs) within MOFs.[203] Besides, organic ligands with versatile reactive functional groups such as free pyridyl, imidazole, hydroxyl, and carboxyl groups, have been skillfully immobilized on the pore surfaces of fluorescent MOFs. This strategy aims to amplify the fluorescence sensing ability of MOFs by facilitating a wide array of host–guest interactions.[204] Based on the differences in guest molecules, the main types of LG-MOFs include organic dyes@-MOF, metal ions@MOF, metal nanoclusters@MOF, quantum dots@MOF and perovskites@MOF.[204–207] Thus far, LMOF-based detection platforms have been developed to evaluate the living environment of plants (Fig. 32). Table 8 lists some classic examples of various developed MOF-based fluorescent chemosensors applied in this field.

4.2.1 Metal ion@MOF-based fluorescent chemosensors. Luminescence in metal ions is primarily observed in lanthanide ions, which is attributed to their substantial Stokes shift values, prolonged fluorescence lifetimes, visually discernible colors, superior quantum efficiency and narrow emission spectra. The distinctive fluorescence characteristics of Ln-MOFs originate from not merely from their 4f–4f electron transitions, but are additionally comprised of ligand-to-metal energy transfer (LMET), commonly referred to as the "antenna effect".[240] The organic linker of MOFs offers great tunability, enabling the effective interaction between MOFs and Ln ions. This interaction promotes energy transfer or establishes an optical antenna effect, thereby increasing the luminescent efficiency of Ln ions. Importantly, the inherent porous structure of MOFs offers a conduit for encapsulating guest materials, and the synergistic interplay between the host framework and the guest, including π–π interaction, hydrogen bonding, and coordination bonds, exhibit exceptional analytical sensitivity towards target analytes.[241] Together, these factors have potential to significantly enhance the QY to approximately 14–30%.[218] Eu^{3+} and Tb^{3+} are the commonly used Ln ions to construct LMOFs. Non-Ln ions such as Zr^{2+}, Al^{3+}, Zn^{2+}, and Cu^{2+} have also been documented for use as metal centers or transition components of MOFs. According to the investigations in the literature, LMOFs based on metal ions predominantly specialize in environmental monitoring, particularly in detecting pesticides, anions and cations (*e.g.*, heavy metal ions).[209,212,242]

Eu^{3+}@MOF-based fluorescent chemosensors. Among the metal ions, Eu^{3+} ions are most commonly used to dope MOFs or as
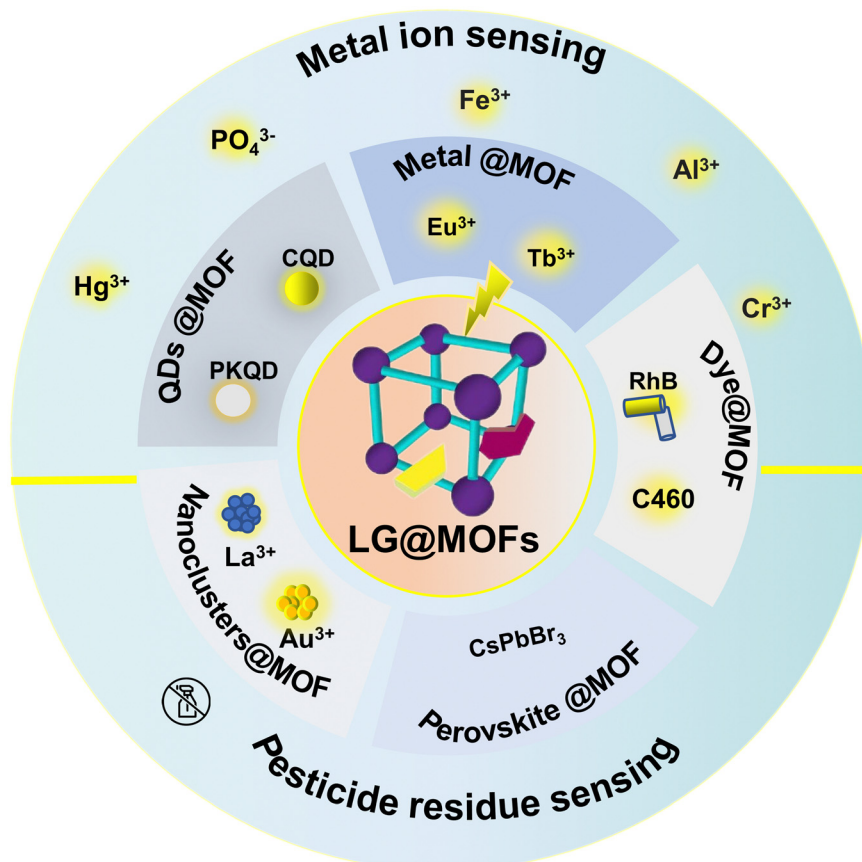

Fig. 32 Classification and synthesis of LG@MOF-based chemosensors and their applications in monitoring the living environment of plants.

Table 8 Examples of metal@MOF-based sensors for monitoring the living environment of plants

Nanofluorescence sensors	Chemosensors	Name	Linear range	Limit of detection (LOD)	Target analytes	Applications	Ref.
Metal ions@MOF	Lanthanide irons	Eu-MOF	—	0.280 μM for Fe^{3+}, 0.150 μM for Cr_2O_7	Fe^{3+}, Fe^{2+}, $Cr_2O_7^{2-}$	Detection of Fe^{3+}, Fe^{2+}, and $Cr_2O_7^{2-}$ in water	208
	120	Eu-MOF	0–110 and 0–90 μM	0.120 μM for Fe^{3+}, 0.360 μM for Al^{3+}	Fe^{3+}, Al^{3+}	Monitoring the concentration of Fe^{3+} and Al^{3+} water	209
	121	Eu-MOF	0.02–200 μM	2.60 nM	Hg^{2+}	Detection of Hg^{2+} in water	210
	122	Eu-MOF	—	10^{-5} mol L^{-1}	PO_4^{3-}	Detection of PO_4^{3-} in water	211
	123	Eu-MOF	—	0.170 μM	Pesticide DCNA	Monitoring the concentration of pesticide DCNA in water	212
	124	Tb-MOF	0.06–4 and 4–40 μg mL^{-1}	18.0 ng mL^{-1}	Carbendazim (CBZ)	Detection of CBZ in apples and tea	213
	125	Tb-MOF	0–80 μg L^{-1}	0.271 μg L^{-1}	Thiabendazole (TBZ)	Detection of TBZ in orange samples	214
	126	Tb-MOF	10–1000 ng mL^{-1}	3.41 ng mL^{-1}	Chlorpyrifos	Detecting CPF in fruit juice	214
	127	Eu, Tb-MOF	—	—	Flavonoids, stilbenes, anthraquinones	Monitoring the concentration changes of saponins, flavonoids, stilbenes, anthraquinones in plant	215
	128	Tb-MOF	—	4.50 ppm	PO_4^{3-}	Detection of PO_4^{3-} in water	216
	129	Tb-MOF	10^{-6} to 10^{-3} M	0.100 ppm	PO_4^{3-}	Detection of PO_4^{3-} in water	217
	130	Ce-MOF	0.02–30 μg mL^{-1}	0.00620 μg mL^{-1}	Glyphosate	Detection of glyphosate in water	218
	131	Al-MOF	—	102 nM	Pd^{2+}	Detection of Pd^{2+} in water	219
	132	Zn/Fe-MOF	0.001–100 mg L^{-1}	0.340 μg L^{-1}	Paraquat (PQ)	Monitoring the content of PQ in lettuce, cabbage and agriculture irrigation water	220
	133	UiO-66(Zr MOF)	0–200 μM for $Cr_2O_7^{2-}$, 0–220 μM for CrO_4^{2-}	0.160 μM for $Cr_2O_7^{2-}$, 0.170 μM for CrO_4^{2-}	Cr^{3+} ($Cr_2O_7^{2-}/CrO_4^{2-}$)	Detecting the concentration of Cr^{3+} in food	221
	134	Mn/Fe-MOF	10^{-9}–10^{-7} M	0.850 nM or 0.290 ppb	Glyphosate	Detection of glyphosate in water	222
Quantum dots@MOF	135	Cu-MOFs@CDs	0.0307–0.769 μmol L^{-1}	3.67 nmol L^{-1}	Thiophanate-methyl (TM)	Microcystin-LR	223
	136	MOF-5@$CH_3NH_3PbBr_3$ CDs	—	—	Al^{3+}, Bi^{3+}, Co^{2+}, Cu^{2+}, Fe^{3+}, Cd^{2+}	Monitoring various ions in water	224
	137	MOF-derived In_2O_3 hollow tubulars @Ti_3C_2 QDs	0.5–4 × 10^5 pmol L^{-1}	0.169 pmol L^{-1}	Photoelectrochemical (PEC)	Detection of PEC in water	225
	138	ZIF-8@ZnS QDs	0–80 μM	0.890 μM	Chlorpyrifos	Detection of CPF in water	226
	139	ZIF-67@ZnSQDs	3–500 nM	0.960 nM	Cu^{2+}	Detection of Cu^{2+} in water and soil	227
Organic dyes@MOFs	140	RhB@Zr-MOF	—	1.60 μM for Fe^{3+}, 0.200 μM for nitenpyram	Fe^{3+}, nitenpyram	Detecting the content of Fe^{3+} and nitenpyram in water	228
	141	RhB@HNU-48	—	0.590 ppb	Alachlor	Monitoring the concentration of alachlor in paddy water and soil, polished rice and cucumber	229
	142	RhB@Zr-MOF	—	6.27 for $Cr_2O_7^{2-}$, 5.26 ppb for CrO_4^{2-}	$Cr_2O_7^{2-}$, CrO_4^{2-}	Detection of $Cr_2O_7^{2-}$ and CrO_4^{2-} in water	230
	143	Doxorubicin@AzoMOF	0–5 μg mL^{-1}	2.96 ng mL^{-1}	Dufulin	Detection of dufulin in water	231
	144	Curcumin@MOF-5	—	3.10 μM for A-curcumin@MOF-5, 2.84 μM for B-curcumin@MOF-5	Al^{3+}	Monitoring the concentration of Al^{3+} in lettuce extract and water sample	232
Metal clusters@MOFs	145	AuNCs@ZIF-8	3–30 nM	1.00 nM	Hg^{2+}	Detection of Hg^{2+} in food	233
	146	AuNCs@Zr-MOF	—	193 pM	Hg^{2+}	Detection of Hg^{2+} in water	234

7040 | Chem. Soc. Rev., 2024, 53, 6992–7090

This journal is © The Royal Society of Chemistry 2024

Table 8 (continued)

Nanofluorescence sensors	Chemosensors Name		Target analytes	Limit of detection (LOD)	Linear range	Applications	Ref.
	AuNCs@ZIF-8	147	OPs	0.300 µg L⁻¹	0.75 µg L⁻¹–100 mg L⁻¹	Detection of OPs in water	235
	AgNCs@Zr-MOF	148	Hg²⁺	1.80 µg L⁻¹	0.010–0.5 µg mL⁻¹	Detection of OPs in water	236
	CuNCs@MOFs UiO-66-(COOH)₂	149	Cu²⁺	178 nM	1–30 µM	Detection of Cu²⁺ in water	237
Perovskite@MOFs	LaNCs@MOFs	150	Fe³⁺	16.6 µM	16.6–167 µM	Detection of Fe³⁺ in water	238
	Eu³⁺@CsPbBr₃ nanocrystal	151	Hg²⁺	0.116 nM	0–1 µM	Detection of Hg²⁺ in water	239

atomic centers for the construction of single emission or double emission fluorescent chemosensors to detect harmful anions and cations in the living environment of plants.[240] For instance, Xu *et al.* introduced Eu^{3+} in the MIL124 MOF to develop a highly selective and sensitive single-emission chemosensor (Eu^{3+}@ MIL124, **119**) for the detection of Fe^{2+}, Fe^{3+}, and $Cr_2O_7^{2-}$ *via* the exceptional fluorescent quenching exhibited by Eu^{3+} and MOF compared to other metal ions.[208] However, although the single luminescence based on MOFs is easily measured,[204] their intensity is often interrupted by the concentration and environment of chemosensors. In this case, the incorporation of two or more emitting sites resulting from the dual emission or bimetallic properties of Ln metal ions and organic ligands can effectively avoid false responses, thereby improving the S/N ratio.[240] For example, Xia *et al.* successfully developed a novel dual-emission MOF incorporating Eu^{3+} ions and 2-hydroxyterephthalic acid ($H_2BDC-OH$) in a UiO-66-type MOF material (chemosensor **120**).[209] **120** displayed dual emission peaks at 450 and 614 nm and exhibited good anti-interference characteristics for Fe^{3+} and Al^{3+} in the complex aquatic environment. Besides, **120** exhibited remarkable selectivity and sensitivity towards Fe^{3+} and Al^{3+}, and their detection linear range was 0–110 and 0–90 µM, respectively (Fig. 33a). Additionally, Hao *et al.* successfully synthesized a dual-emission Ln-MOF material (Eu-Ca-MOF) by incorporating Eu^{3+} ions in the channels of a Ca-MOF parent framework (chemosensor **121**).[210] **121** exhibited excellent PL properties, in tandem with precise capacity to detect trace levels of Hg^{2+} in water, achieving an LOD of 2.6 nM (Fig. 33b). Besides, a novel Eu-based three-dimensional framework was obtained based on the 1,3,5-benzenetribenzoate (H_3BTB) ligand with high C_3 symmetry (chemosensor **122**).[211] **122** demonstrated remarkable thermostability and water stability for the detection of PO_4^{3-} ions among various colorless anions. This work represents a pioneering example of regenerable MOF-based luminescent chemosensors for detecting PO_4^{3-}. Besides monitoring harmful ions, Eu–MOF-based chemosensors have also been used for detecting pesticide residues. For example, Qin *et al.* designed ultrathin fluorescent Eu^{3+}@Zn-MOF nanosheets (Eu^{3+}@Zn-MOF-NS, chemosensor **123**) to rapidly detect the residues of organic pesticides.[211] In the synthesis of **123**, 2,6-dichloro-4-nitroaniline (DCNA) was employed, utilizing Zn^{2+} as the metal node and pyridine and 1,4-benzenedicarboxylate (H_2BDC) (Py) as the organic ligands. **123** offered a unique combination of benefits of both MOFs and 2D nanomaterials simultaneously. Notably, its LOD and K_{sv} were 0.17 µM (35 ppb) and 3.2×10^5 M⁻¹ in water, respectively. **123** could potentially be applied for the rapid, *in situ*, and visualized detection of DCNA residues on fresh vegetables (Fig. 33c). The intense PL exhibited by **123** could be significantly quenched by DCNA in water, without any interference from other amino acids, small organic molecules, pesticides, or commonly encountered anions and ions. Interestingly, the as-obtained Eu^{3+}@Zn-MOF-NS probe in this work is promising for the visual, rapid, and *in situ* detection of DCNA residues on fresh vegetables. This work provides meaningful information on using Eu^{3+}-based MOF probes for the effective detection of

This journal is © The Royal Society of Chemistry 2024

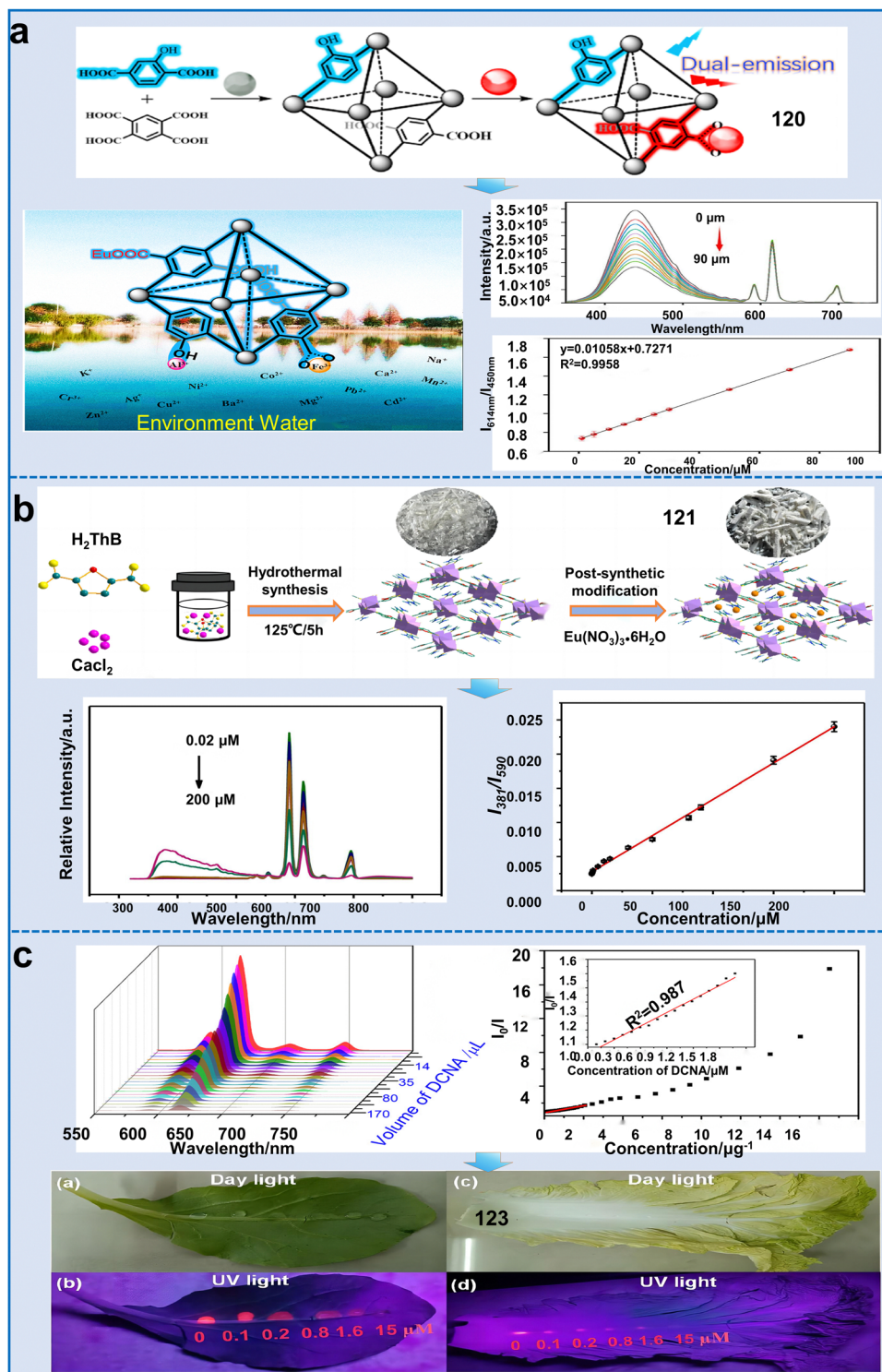Chem. Soc. Rev., 2024, **53**, 6992–7090 | 7041

Fig. 33 Applications of Eu^{3+}-based sensors for monitoring the living environment of plants. (a) Synthesis of a highly water-stable dual-emission Eu^{3+}-loaded MOF (EuUCH) and its detection of Fe^{3+} and Al^{3+} metal ions.[210] Copyright © 2022, Elsevier. (b) Synthesis of Eu-Ca-MOF fluorescence sensor and its detection sensitivity for Hg^{2+} in water.[211] Copyright © 2022, Elsevier. (c) Detection sensitivity of Eu^{3+}@Zn-MOF for pesticide and its sensing effect in actual samples.[211] Copyright © 2022, the American Chemical Society.

pesticide residues in practical applications. However, although Eu^{3+}-based sensors have been applied in environment monitoring, related studies on bioimaging in plants are still lacking.

Tb^{3+}@MOF-based fluorescent chemosensors. In addition to the incorporation of Eu^{3+} ions mentioned earlier, other commonly used Ln ions such as Tb^{3+} have been extensively employed in the

construction of LMOFs to detect natural metabolites, metal ions and pesticide residues. For example, Wang *et al.* successfully fabricated a fluorescent nanosheet of a two-dimensional terbium-based MOF (2D Tb-MOF) for the detection of carbendazim (CBZ) (chemosensor **124**).[213] The 2D Tb-MOF nanosheets, synthesized with 5-borono-1,3-benzenedicarboxylic acid (BBDC) and Tb^{3+} ions as the precursors, demonstrated outstanding optical features. After the addition of CBZ, the fluorescence of the Tb-MOF nanosheets was quenched due to dynamic quenching and the inner filter effect (IFE). **124** offered two linear ranges of 0.06–4 μg mL^{-1} and 4–40 μg mL^{-1} with an LOD of 17.95 ng mL^{-1} (Fig. 34a). Furthermore, the developed sensing platform was effectively utilized to detect CBZ in apples and tea samples, yielding satisfactory results. However, in the presence of other coexisting substances such as NH_4^+, glucose and fipronil, the

reaction between Tb-MOF and CBZ was slightly hindered. Another study constructed a highly selective luminescent sensor (chemosensor **125**) for monitoring thiabendazole (TBZ) in oranges based on a Tb^{3+}-functionalized Zr-MOF (Tb^{3+}@1). **125** with high selectivity exhibited a good linear range of 0–80 μM, rapid response time (less than 1 min) and LOD of 0.271 μM. Additionally, this sensor presented good recoveries from 98.41% to 104.48% when used for detecting TBZ in real orange samples and this process only took 35 min (Fig. 33b). Coupling anti-bodies or aptamers with Tb-MOFs was helpful for the detection selectivity and sensitivity by providing specific recognition sites to match the target analyte molecules.[214] Another mesoporous molecular imprinted polymer (mMIP) layer imprinted Tb-MOF (MOF-76) fluorescent chemosensor (**126**) was constructed for the analysis of chlorpyrifos in fruit juice and the environment.[214] **126**
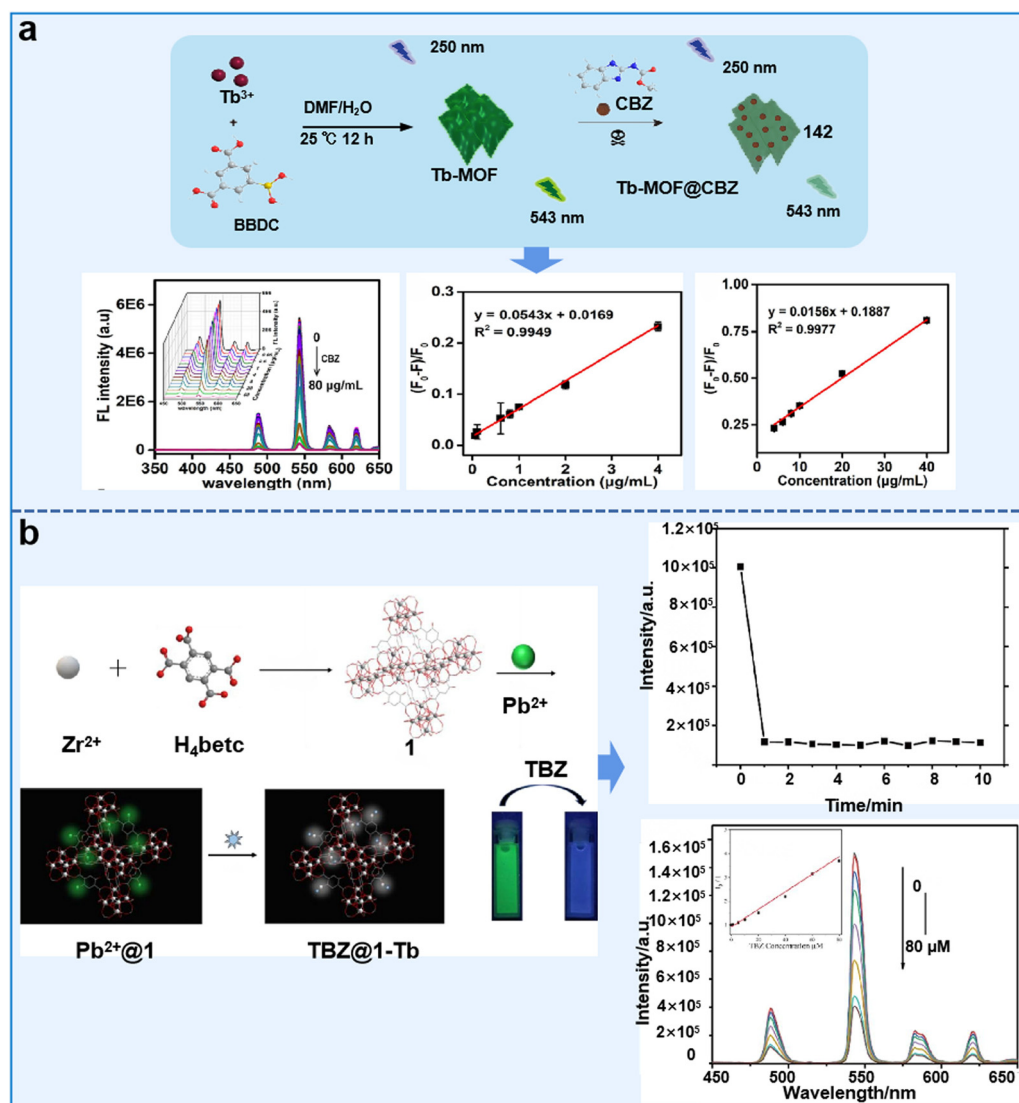

Fig. 34 Examples of Tb-MOF chemosensors for sensing pesticide residues. (a) Synthesis process of Tb-MOF@CBZ and its sensing effect and sensitivity for CBZ.[213] Copyright © 2023, Elsevier. (b) Synthesis process of Tb^{3+}-functionalized Zr-MOF and its sensing mechanism and sensitivity for TBZ.[214] Copyright © 2021, Elsevier.

This journal is © The Royal Society of Chemistry 2024

Chem. Soc. Rev., 2024, **53**, 6992–7090 | 7043

contained specific sites for the adsorption of chlorpyrifos, ensuring the selectivity of the designed chemosensor. It exhibited a linear response in the concentration range of 10–1000 ng mL^{-1} for chlorpyrifos, with an LOD of 3.41 ng mL^{-1}. These studies provide useful analytical tools for the rapid and sensitive detection of CPF in the living environment of plants.

Besides the detection of pesticides, Tb-MOF chemosensors have also been used to monitor the distribution and concentration of inorganic anions and plant metabolites. For example, Yin *et al.* designed a fluorescent chemosensor (**127**) that incorporated Eu^{3+} and Tb^{3+} ions within an MOF. **127** enabled the rapid identification of various natural compounds, including 7 flavonoids, 12 saponins, 4 anthraquinones and 3 stilbenes.[215] **127** possessed powerful identification and analysis ability, and

the detection accuracy of each type of compound was up to 100% (Fig. 35a). Another study developed a Tb-MOF-based fluorescent chemosensor (**128**) for the detection of PO$_4^{3-}$.[216] **128** was demonstrated to be an exceptional luminescent chemosensor with a low detection limit, rapid response time, and an extensive detection range. Its versatile capabilities enabled the recognition of anions in water or other highly polar solvents, providing exciting prospects for various applications. Ji *et al.* encapsulated the Tb^{3+} cation into a 3D microporous MOF to construct a fluorescent-functionalized Tb@Zn-MOF (chemosensor **129**).[217] **129** showed both excellent chemical stability and the characteristic emission of Tb^{3+}. **129** emerged as an advantageous photoluminescent reagent demonstrating exceptional specificity and precision for the quantitative analysis of
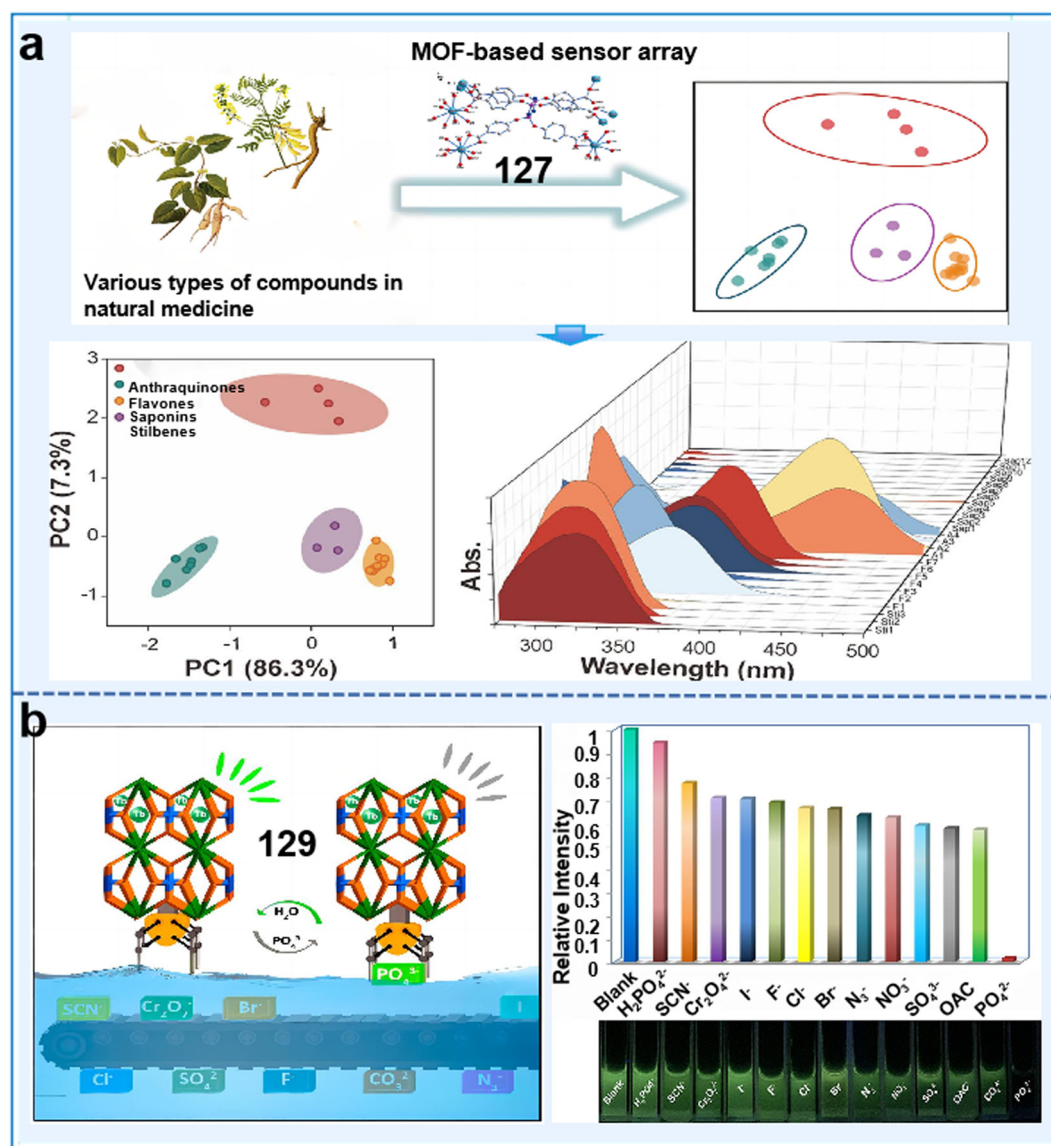

Fig. 35 Examples of Tb-MOF chemosensors for sensing ions and plant metabolites. (a) Schematic diagram of Ln-MOF-based sensor arrays for the identification and detection of natural compounds.[215] Copyright © 2021, the American Chemical Society. (b) Sensing sensitivity of Tb-MOF chemosensor for inorganic anions.[217] Copyright © 2018, the American Chemical Society.

7044 | *Chem. Soc. Rev.*, 2024, **53**, 6992–7090

This journal is © The Royal Society of Chemistry 2024

PO_4^{3-}. It presented a swift response time of only 10 s with a noteworthy LOD of 0.1 ppm. This investigation served as the pioneering prototype of a competent excitable fluorescent sensor to quantitatively assess the concentration of PO_4^{3-} in simulated biological systems and detecting its presence in aquatic environments with a broad concentration range of 10^{-6} to 10^{-3} M (Fig. 35b). This sensor offers a new approach for identifying inorganic anions, which is highly significant in both physiological and ecological settings. It is evident that metal ion@LMOF sensors with high efficiency and sensibility for the detection of phosphorus anions in the living environment of plants are still lacking.

Other metal ion@MOF-based fluorescent chemosensors. In addition to Eu^{3+} and Tb^{3+}, some other metal ions have also been doped in MOFs to construct fluorescent chemosensors. For example, a study prepared a nanocomposite LMOF, incorporating UiO-67 nanoparticles within the pores of carbonaceous materials isolated from a novel Ce-MOF (Ce-PC) for the fluorescent sensing of glyphosate (chemosensor **130**).[218] The prevalent oxygen-bearing hydroxyl moiety (M–O–H) present in UiO-67/Ce-PC was capable of recognizing the phosphoryl moieties (–PO_3H_2) in glyphosate *via* ligand substitution and exhibited specificity toward glyphosate (Fig. 36a). Findings revealed that glyphosate could be reliably detected in cereal specimens
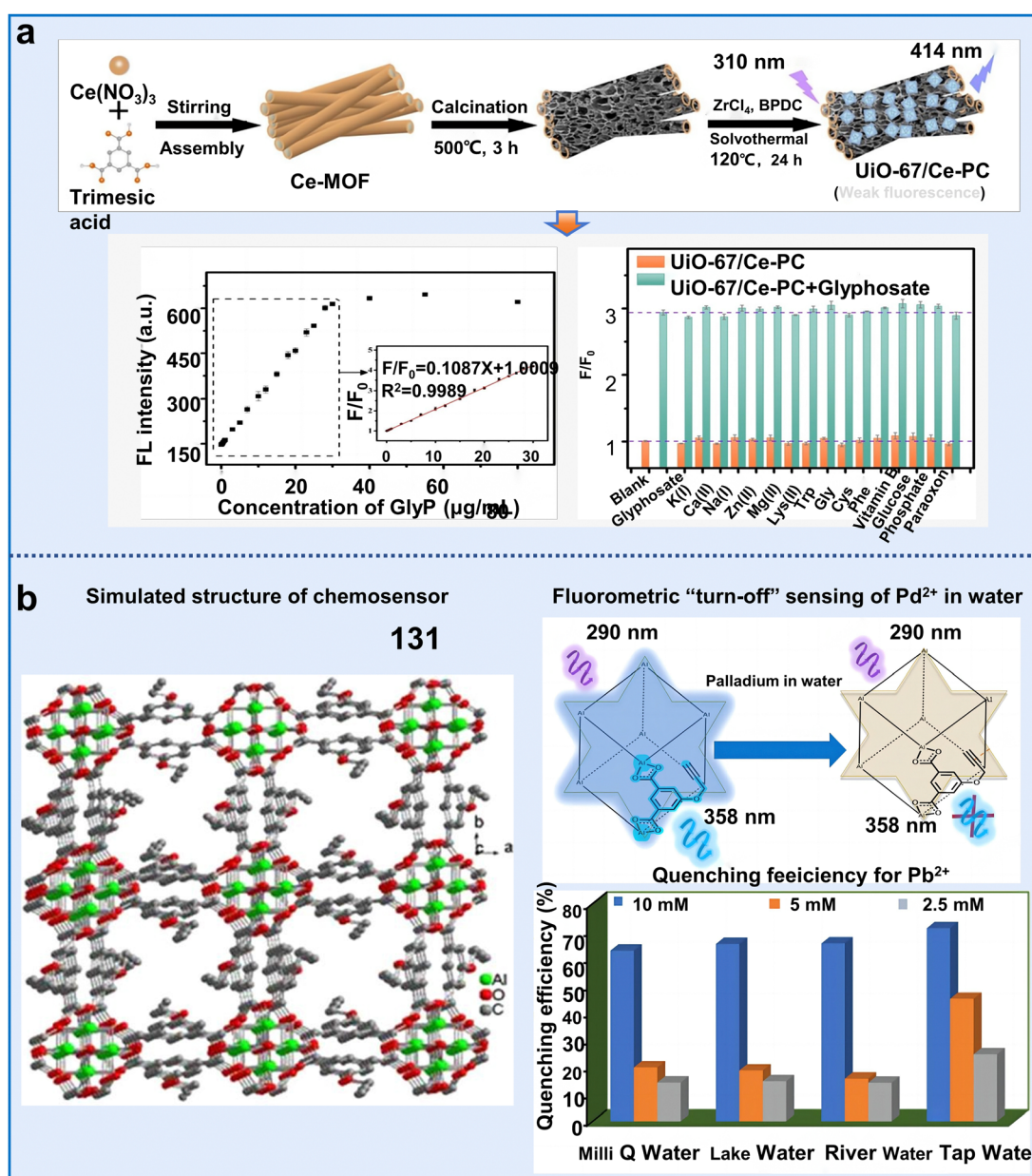

Fig. 36 Examples of Tb-MOF chemosensors for sensing ions and plant metabolites. (a) Schematic diagram of Ln-MOF-based sensor arrays for the identification and detection of natural compounds.[218] Copyright © 2021, the American Chemical Society. (b) Sensing sensitivity of Tb-MOF chemosensor for inorganic anions.[219] Copyright © 2018, the American Chemical Society.

This journal is © The Royal Society of Chemistry 2024

Chem. Soc. Rev., 2024, **53**, 6992–7090 | 7045

in the concentration range of 0.02 to 30 μg mL^{-1} with an LOD of 0.0062 μg mL^{-1}. These findings represent a promising approach for developing MOF-derived nanocomposite materials for the precise trace analysis of pollutants in the living environment of plants. Chakraborty *et al.* introduced an innovative ultrafast Al(III)-MOF chemosensor (**131**) for the detection of Pd^{2+}.[219] **131** demonstrated the lowest response time (30 s) and a remarkable low LOD of 102 nM, which is the shortest response time for MOF-based Pd^{2+} sensing thus far. Compared to the previously reported palladium sensors based on MOFs, **131** exhibited excellent recyclability, maintaining consistent effectiveness and selectivity for Pd^{2+} detection over five cycles in real water with the same efficiency (Fig. 36b). The quick response, sensitivity, and selectivity of this sensor make it an excellent choice for the selective detection of Pd^{2+} ions in water. More importantly, we believe that this work based on the alkyne–π interaction concept will inspire studies in diverse areas, particularly the development of various functionalized MOF-based sensors for detecting other hazardous heavy metal ions. Besides single metal doping, bimetallic-doped MOF-based sensors are promising to improve the sensing signal and sensitivity. For instance, Wu *et al.* developed an innovative electrochemical method for the detection of paraquat through the use of a modified glassy carbon electrode. The modification involved the incorporation of a Zn/Fe dual-metal ZIF-generated nanoporous carbon composite (Zn/Fe-ZIF-NPC) with Ni hexacyanoferrate nanoparticles (NiHCF-NPs) on the electrode substrate (chemosensor **132**).[220] NiHCF-NPs functioned as the dedicated signal chemosensor, whereas Zn/Fe-ZIF-NPC promoted swift electron transfer and powerfully amplified the discernible signal originating from NiHCF-NPs. Consequently, the modified electrode exhibited a linear concentration range of 0.001 to 100 mg L^{-1} and with an impressive LOD of 0.34 μg L^{-1}. These outcomes provide strong evidence supporting the high reliability and application of the proposed methodology for discerning PQ contamination in actual vegetables and agricultural irrigation water. Besides the above-mentioned chemosensors, some other chemosensors based on metal-MOF could also detect anions, cations, and pesticides in the environment (chemosensors **133** and **134**).[221,222]

In summary, these results offer some available strategies for future studies to develop more effective and sensitive fluorescent chemosensors based on metal ion MOFs for monitoring the living environmental conditions of plants. However, although considerable results have been achieved, there are still some concerns in their actual application, as follows: (i) the use of Ln ions for constructing LMOFs is currently limited to a narrow range of options, and the Earth's supply of Ln ions is also restricted. These factors present obstacles to the widespread application of Ln-based MOFs.[204] (ii) The efficiency of exciting Ln ions through the excitation light is limited due to the forbidden nature of the 4f–4f electronic transition, and the generation of higher external quantum efficiency is hindered for Ln-ions. (iii) Most of the studies on metal ion@MOF sensors mainly focus on detecting pollutants and bio-small molecules in the living environment of plants, but there is still a lack of

research on biological detection, such as plant hormones. (iv) To ensure successful sensing in water or other sensing media, it is crucial to enhance the stability of LnMOF-based sensors, particularly their water stability. This improvement is necessary to prevent structural breakdown or degradation before the sensing process is completed.[240]

4.2.2 Quantum dot@MOF fluorescent sensors. The chief design for QD-MOFs is a specific class of MOFs, wherein QDs are intercalated into the framework of MOFs or reside within their pores. The surface of the QDs offers multiple interaction sites, which substantially manifest alterations in their fluorescence intensity, serving as an integral component in the sensing mechanism.[243] Nevertheless, combining QDs with MOFs can mitigate agglomeration issues that may arise during precipitation and drying. This integration effectively suppresses electronic transition and cavitation, enhancing the stability of the QDs within the MOF framework.[204] To date, a diverse range of QDs, such as carbon QDs, perovskite QDs, ZnS QDs, and Ti$_3$C$_2$ QDs, has been successfully integrated in MOFs.[224] The following parts will elaborate on the application of these quantum dot-based MOF chemosensors in fluorescence detection.

In recent years, carbon dots (CDs) have attracted significant research interest in the field of sensing due to their remarkable attributes including low toxicity, tunability and robust fluorescence emission stability.[244] The abundant functional groups on the surface of CDs facilitate their direct chemical coordination with MOFs.[223] These phenomena indicate that integrating CDs with MOFs is a promising and efficient strategy for the detection of harmful substances in plant surroundings. For example, a simple and efficient ratiometric fluorescence chemosensor, CDs@Cu-MOF (**135**), was constructed for the detection of pesticide thiophanate-methyl (TM). This chemosensor was formed by coordinating the –COO– groups present on the surface of CDs with Cu^{2+} ions of Cu-MOF.[223] **135** demonstrated excellent selectivity and accuracy for detecting TM in food samples, which was achieved through the interplay of π stacking and Cu^{2+} chelation between TM and Cu-MOFs and exhibited a remarkable LOD of 3.67 nmol L^{-1}. Therefore, CD-based MOF sensors present a novel and effective strategy for pesticide detection, offering potential applications in monitoring plant health.

Hybrid organic–inorganic halide perovskites, such as CH$_3$NH$_3$PbX$_3$ (X = Cl, Br, and I), have attracted significant interest in recent years. However, the practical use of CH$_3$NH$_3$PbX$_3$ is limited due to the intrinsic susceptibility of its organic cation CH$_3$NH$_3^+$. Under diverse environmental conditions such as UV light, moisture, high temperatures, and oxygen this cation degrades rapidly.[224] Accordingly, integrating CH$_3$NH$_3$PbX$_3$ QDs in MOFs can significantly improve their stability, and perovskites QD-based MOF fluorescent chemosensors have been successfully implemented to detect pesticides and heavy metal ions in the environment. Zhang *et al.* developed an innovative methodology for enhancing the stability of CH$_3$NH$_3$PbX$_3$ perovskite QDs by encapsulating them within MOF-5 microcrystals. This was achieved by adding PbBr$_2$ and CH$_3$NH$_3$PbX$_3$ precursors in a stepwise manner to create a stable CH$_3$NH$_3$PbX$_3$@MOF-5 composite (chemosensor **136**).[224] **136** demonstrated significantly

7046 | *Chem. Soc. Rev.*, 2024, **53**, 6992–7090

This journal is © The Royal Society of Chemistry 2024

enhanced water resistance and thermal stability compared to $CH_3NH_3PbX_3$ QDs, which was useful for detecting various metal ions in water including Al^{3+}, Bi^{3+}, Co^{2+}, Cu^{2+}, Fe^{3+}, and Cd^{2+} (Fig. 37a). However, although this work improves the relative stability of perovskite QDs, the exploration of the fundamental properties, operating principles, and prospective applications of $CH_3NH_3PbX_3$ QDs encapsulated in MOFs remains a limited and challenging area of research.

In addition to CQDs, Ti_3C_2 QDs are also excellent candidates for constructing fluorescent chemosensors due to their inherent hydrophilicity and conductivity originating from 2D MXene. Moreover, they offer advantages such as abundant active sites, enhanced redox activity, and excellent stability. Studies indicated that microcystin-LR (MC-LR) can inhibit the growth and reproduction of bacteria, aquatic animals, and some phytoplankton in water bodies, and thus the effective detection of MC-LR is very important. Yan et al. developed a self-powered aptasensing platform for the detection of MC-LR, which utilized a dual-mode approach combining photoelectrochemical (PEC) and photofuel cell (PC) techniques (chemosensor 137).[225] The platform utilized an In_2O_3–In_2S_3–Ti_3C_2 (IO–IS–TC) composite assembled on the base of MOF-derived In_2O_3 hollow tubulars, with Ti_3C_2 QDs serving as a photoelectrode matrix to enhance the PEC performance. Aptamer-based recognition was employed for the efficient capture of MC-LR molecules, enabling highly sensitive detection. The PC aptasensor exhibited a detection range of 5–50×10^5 pmol L^{-1} and LOD of 17.4 pmol L^{-1}, while the PEC aptasensor achieved a detection range of 0.5–4×10^5 pmol L^{-1} and LOD of 0.169 pmol L^{-1} (Fig. 37b). This work established a foundation for the formulation of photoelectrode-centric PFC applications, significantly enhancing the scope for the establishment of highly sensitive PEC environmental analytical methodologies.

Phosphorescence, with its longer lifetime compared to fluorescence, is a relatively uncommon luminescent phenomenon. This unique characteristic allows the examination signal to successfully counteract the interference of the matrix autofluorescence and disseminated light.[226] ZnS QDs have attracted substantial interest and research emphasis with favorable phosphorescent emission characteristics, which are widely used as phosphorescent chemosensors for detecting pollutants in the living environment of plants. For example, a pioneering phosphorescent sensor was engineered utilizing a technologically advanced core–shell structure, Mn:ZnS QD@ZIF-8@MIP (chemosensor 138), for the highly sensitive and selective detection of CPF.[226] Under the optimal operating parameters, 138 displayed the rapid detection of CPF within 5 min. It also exhibited a consistent, linear correlation over a concentration scope extending from 0 to 80 μM. Besides, the recoveries of CPF ranged from 92% to 105% in water samples with an LOD of 0.89 μM. This sensor combined the benefits of phosphorescent emission and molecular imprinting, significantly reducing the potential interferences from competing substances, scattered light, and background fluorescence. This innovation lays the foundation for the sensitive and selective detection of water pollutants using molecularly imprinted phosphorescent sensors.

Another study prepared a novel and highly fluorescent MOF-based host–guest hybrid system (ZnSQD@ZIF-67) for the detection of Cu^{2+} by incorporating polyethylene glycol (PEG)-coated ZnS QDs in ZIF-67 (chemosensor 139).[227] The PEG-ZnS QD@ZIF-67 nanohybrids combined the accumulation effect of ZIF-67 and ZnS QDs showed a highly selective and sensitive fluorescence response to specifically detect Cu^{2+}. This allowed the detection of Cu^{2+}, spanning a broad concentration range of 3–500 nM with an LOD of 0.96 nM (Fig. 37c). Compared to fluorescent sensors based on QDs without MOFs, nanohybrid 139 exhibited a significant enhancement in fluorescent QY. Therefore, ZnS QD-based sensors have shown substantial potential towards the comprehensive evaluation of the health and surroundings of plants.

However, although QDs have attracted significant attention due to their robust photobleaching stability, broad excitation range, and enhanced photostability, there are still some challenges that need to be addressed, as follows: (i) occasionally, it becomes imperative to modify QDs to enhance their stability and luminescent QY when coated within MOFs. Concurrently, the inclusion of an encapsulating agent during modification can efficaciously counteract the aggregation of QDs, although it may introduce complexities in the operational process. (ii) Inorganic semiconducting QDs routinely incorporate hazardous substances such as cadmium and lead, which can pose toxicity concerns when utilized for biological detection. (iii) Studies on QDs@MOF fluorescence chemosensors for biological detection are still lacking.

4.2.3 Organic dye@MOF-based fluorescent sensors. Fluorescent dyes have gained significant attention due to their low cost, easy availability, enhanced QY, robust optical attributes, and broad emission wavelength spectrum.[204] However, although organic dyes offer luminous benefits, they are prone to aggregation, which lead to multi-chromophoric interactions that alter their color quality and suppress their fluorescence emission.[228] In this case, encapsulating dyes in MOFs reduces their self-aggregation tendency. MOF materials possess adjustable skeleton structures and uniform pores, making them ideal for protecting fluorescent dyes and preventing fluorescence quenching due to aggregation. Furthermore, the interaction between dyes and MOFs allows the regulation of fluorescence properties.[203] To date, the commonly used small-molecule fluorescent dyes including coumarins, doxorubicin and rhodamines have been integrated in MOFs to develop organic dye@MOF fluorescent chemosensors for the detection of pesticides, pH and metal ions.

Rhodamine B (RhB) is the most widely used fluorescent dye for constructing luminescent chemosensors to detect anions, cations and pesticide residues in the environment. For instance, a novel RhB@Zr-MOF composite exhibiting dual-emission capabilities was developed (chemosensor 140).[228] This unique construct was attributed to the interaction between the luminescent host Zr-MOF and the fluorescent guest RhB, enabling it to specifically recognize Fe^{3+} and nitenpyram. The introduction of RhB greatly improved the thermal stability, recyclability and low LOD (Fe^{3+} was 1.6 μM and nitenpyram was 0.2 μM) for sensing various analytes. Li et al. successfully

This journal is © The Royal Society of Chemistry 2024

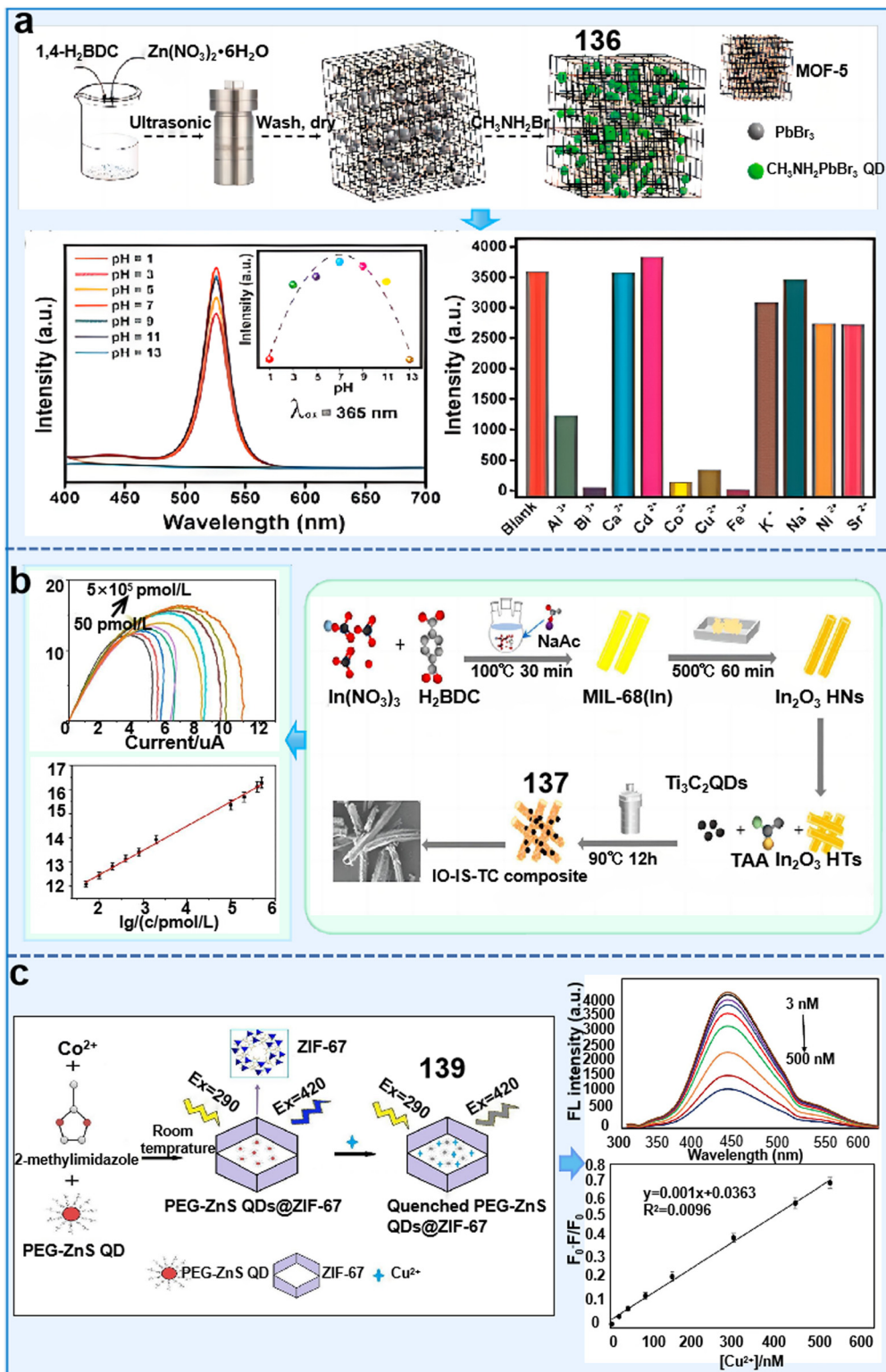Chem. Soc. Rev., 2024, 53, 6992–7090 | 7047

Fig. 37 Examples of quantum dot@MOF-based fluorescent sensors for monitoring the living environment of plants. (a) Emission intensities and selectivities of $CH_3NH_3PbBr_3$@MOF-5 composite for sensing various ions.[224] Copyright © 2018, Elsevier. (b) Synthesis process of Ti_3C_2 QD@MOF chemosensor and its detection sensitivity for PEC.[225] Copyright © 2022, ACS Appl. Mater. Interfaces. (c) Synthesis process of ZnSQDs@ZIF-67 and the detection sensitivity for CPF.[227] Copyright © 2019, Elsevier.

7048 | *Chem. Soc. Rev.*, 2024, **53**, 6992–7090

This journal is © The Royal Society of Chemistry 2024

Review Article

designed a dual-emission fluorescent sensor by introducing RhB in the framework of HNU-48 (named RhB@HNU-48, chemosensor **141**).[229] The addition of RhB led to a significant improvement in the sensing sensitivity of alachlor, achieving an ultra-LOD of 0.59 ppb. This enhancement was due to the host–guest interactions, which influenced the excitation and emission spectra of the composite (Fig. 38a). This work was the first report on the use of a dual-emission fluorescence probe for

the detection of alachlor, and the detection capability of RhB@HNU-48 is higher than that of most sensors reported thus far. Furthermore, the practical application of this sensor was confirmed through its sensing performance in river and soil samples. This study created a logic gate using the sensing ability of RhB@HNU-48 to assess alachlor residue safety levels. Importantly, it presented a promising strategy for developing tailored sensors for agricultural residues. Li *et al.* developed an
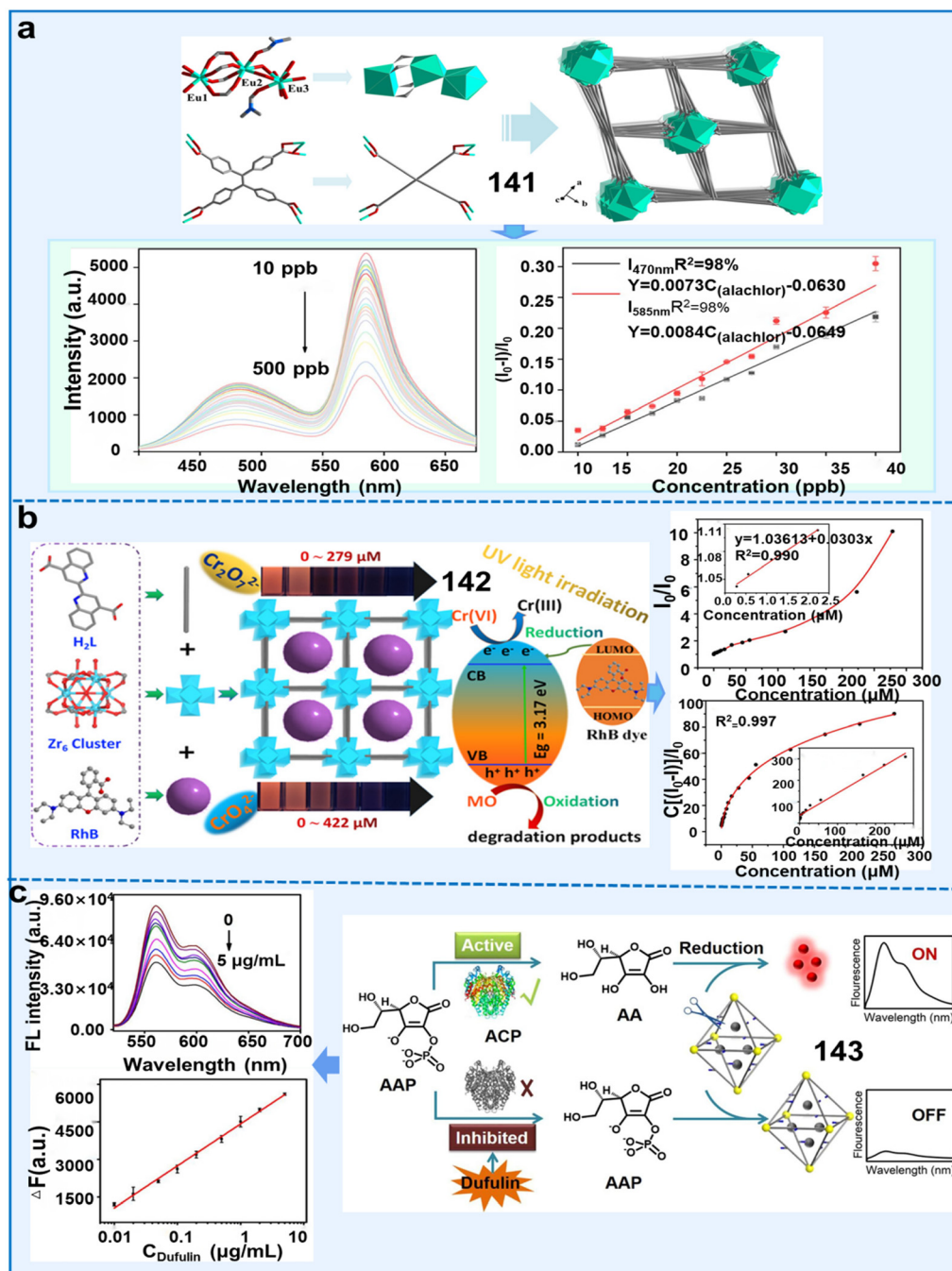

Fig. 38 Examples of organic dye@MOF-based fluorescent sensors for monitoring the living environment of plants. (a) Process for the synthesis of RhB@HNU-48 chemosensor and its detection sensitivity for alachlor.[229] Copyright © 2022, ACS Appl. Mater. Interfaces. (b) Detection mechanism of RhB@Zr-MOF composites for sensing ions of $Cr_2O_7^{2-}$ and CrO_4^{2-}.[230] Copyright © 2022, ACS Appl. Mater. Interfaces. (c) Process for the synthesis of DMOF chemosensor and its detection sensitivity for dufulin.[231] Copyright © 2022, Elsevier.

This journal is © The Royal Society of Chemistry 2024

Chem. Soc. Rev., 2024, **53**, 6992–7090 | **7049**

orange-yellow fluorescence sensor assembled by in situ-encapsulating rhodamine B (RhB) in a zirconium-biquinoline-based MOF (chemosensor **142**).[230] This approach effectively prevented the aggregation fluorescence quenching (ACQ) effect of RhB molecules within the RhB@Zr-MOF structure. The efficient electron transfer in RhB@Zr-MOF significantly enhanced its sensitivity in detecting $Cr_2O_7^{2-}$ and CrO_4^{2-} ions, achieving ultra-LODs of 6.27 and 5.26 ppb, respectively. Compared to the pristine Zr-MOF, the sensitivity of RhB@Zr-MOF increased by approximately 6 and 9 times for $Cr_2O_7^{2-}$ and CrO_4^{2-} ions, respectively (Fig. 38b). The aggregation fluorescence quenching (ACQ) effect of RhB molecules was effectively overcome. Importantly, RhB@Zr-MOF exhibited a rapid fluorescence quenching response toward Cr(vi) ions with high selectivity, sensitivity, and anti-interference resistance. This research offers a new approach for modulating the fluorescent detection sensitivity and photochemical removal efficiency for heavy metal ions and dyes. In addition to RhB, some other fluorescence dyes including coumarin, curcumin and doxorubicin have also attracted attention from researchers. The inclusion of 7-diethylamino-4-methyl coumarin (C460) within the pores of MOFs effectively mitigated the aggregation-induced quenching of dyes, without altering the original structure of the MOFs. For example, Liu *et al.* designed a dye-encapsulated zoterephthalate MOF-structured fluorescent chemosensor (**143**), specifically engineered for precise dufulin recognition.[231] **143** exhibited excellent sensitivity and linearity for the detection of dufulin and demonstrated a robust concentration-response relationship in the range of 0 to 5 μg mL^{-1} with an LOD of 2.96 ng mL^{-1} (Fig. 38c).

Importantly, **143** was successfully employed for examining the content of dufulin in cucumbers, polished rice, soil, and water. This investigation clearly demonstrated the practicality and untapped potential of MOF-derived nanosensors for detecting pesticides in the environment and food. Additionally, this work also opens up an avenue for the design of enzyme-based probes for pesticide sensing in environmental assessment and food safety. Zhong *et al.* synthesized a curcumin@MOF-5 composite *via* two methods (chemosensor **144**),[232] which showed highly selective fluorescence enhancement responses to Al^{3+} with LODs of 3.10 μM and 2.84 μM for A-curcumin@MOF-5 and B-curcumin@MOF-5, respectively.

In conclusion, multiple fluorescent dyes have been used for the fluorescence detection recently; however, some limitations hinder their applications, as follows: (i) organic dyes frequently exhibit aggregation behavior, leading to a significant reduction in their luminescent intensity; (ii) the parameters including pH, temperature, and other substances modulate the fluorescent stability of organic dyes; and (iii) although introducing them in MOFs can improve their performance, studies on the detection of substances related to plant health are still lacking.

4.2.4 Metal nanocluster@COF-based fluorescent sensors.
Metal nanoclusters (NCs) have recently attracted increasing attention because of their remarkable longevity, large Stokes shift, good photostability, and efficient electrocatalysis. In comparison to conventional fluorescent materials such as organic dyes and QDs, NCs are characterized with lower toxicity.[245]

However, their lower QY limits their further development. In this case, the incorporation of metal nanoclusters in MOFs to create composite materials effectively decreases aggregation and clustering, thereby enhancing their fluorescence detection ability and stability. At present, some metal ions including Ag, Au, Cu, and La have been encapsulated in MOFs to prepare metal cluster@MOF composites, which show great detection efficiency for metal ions and pesticides in the environment.

Among the above-mentioned metal nanoclusters, gold nanoclusters (AuNCs) have attracted tremendous interest owing to their distinctive properties and high application value in biosensing. For example, ZIF-8 was utilized to enwrap both CDs and gold nanoclusters (CDs/AuNCs@ZIF-8), subsequently producing an aggregate for the ratiometric fluorescence determination of Hg^{2+} (chemosensor **145**).[233] **145** enabled the highly sensitive detection of Hg^{2+}, where the fluorescence intensity ratio (I_{640}/I_{440}) exhibited a distinct decreasing trend with an increase in the concentration of Hg^{2+} in the concentration range of 3 to 30 nM, achieving an LOD of 1 nM. In another study, AuNCs were synthesized within a Zr-MOF (AuNCs@UiO-66) for monitoring the concentration of Hg^{2+} in water (chemosensor **146**).[234] This nanocomposite exhibited exceptional sensitivity for detecting Hg^{2+} in real water samples, achieving an LOD of 193 pM. Compared with the above-mentioned chemosensor, this composite showed higher detection sensitivity. **146** with stable and high fluorescence could be easily fabricated using a simple method. Its properties make it valuable not only for detecting various metal ions but also for applications in the field of biology. Additionally, Cai *et al.* successfully constructed a dual-signal chemosensor of AuNCs@ZIF-8 for the detection of organophosphorus pesticides (chemosensor **147**).[235] **147** exhibited strong fluorescence with a fluorescence lifetime and QY of 6.83 μs and 4.63%, respectively. The MOF carrier restricted the molecular mobility of AuNCs, leading to the manifestation of the AIE effect. As a result, the composite exhibited a robust fluorescence signal, characterized by a fluorescence lifetime of 6.83 μs and QY of 4.63%. In addition, an innovative smartphone application (app) was designed to ensure real-time monitoring of pesticide contamination. The gray values of the solution were determined using a smart phone app, subsequently yielding calculated recoveries of OPs in the range of 85.2% to 113.8% (Fig. 39a). Compared to conventional single-signal biosensors, this chemosensor exhibited higher sensitivity and reliability. The reasons for this improvement are as follows: (1) encapsulating AuNCs with an AIE effect into ZIF-8 restricts their molecular movement and amplifies their fluorescence signal. (2) By inhibiting the enzymatic hydrolysis product, H_2O_2, using the decomposition effect of H_2O_2 on ZIF-8 and the peroxidase mimic activity of AuNCs, a dual signal detection is achieved through fluorescence and color changes. Furthermore, a colorimetric test paper was developed for the visual detection of OPs. Additionally, the gray values of the solution were obtained using a smartphone app for the on-site quantitative detection of OPs with an LOD of 0.4 μg L^{-1}.

This method exhibited higher sensitivity and reliability compared to traditional single-signal biosensors. Besides

7050 | *Chem. Soc. Rev.*, 2024, **53**, 6992–7090

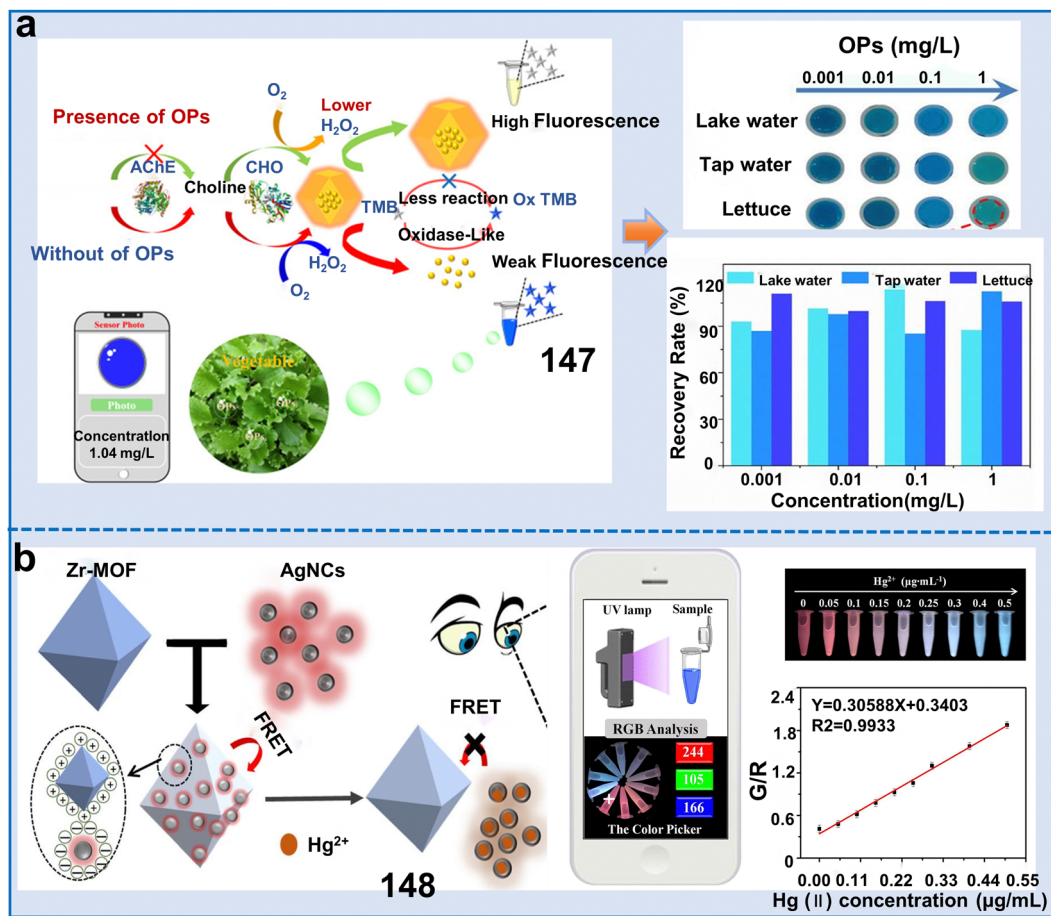This journal is © The Royal Society of Chemistry 2024

Fig. 39 Application of metal nanocluster@COF-based sensors for monitoring the living environment of plants. (a) Schematic diagram of the synthesis of AuNCs@ZIF-8 and the mechanism for the detection of OPs.[235] Copyright © 2022, ACS Appl. Mater. Interfaces. (b) Schematic diagram of the synthesis of Zr-MOF sensor and its mechanism for the detection of Hg^{2+}.[236] Copyright © 2022, Elsevier.

AuCNs, AgNCs, CuNCs and LaNCs have also gained attention for fluorescence imaging. For instance, a dual-emission ratiometric fluorescence chemosensor (**148**) based on Zr-MOF and AgNCs was constructed for the accurate and intuitive detection of Hg^{2+}.[236] Upon exposure to Hg^{2+}, the AgNCs in the chemosensor underwent aggregation, causing a decrease in fluorescence. In contrast, the fluorescence intensity exhibited by Zr-MOFs demonstrated a slight increase because of the diminished FRET interaction between AgNCs and Zr-MOFs. This sensor demonstrated excellent sensitivity in the concentration range of 0.010 to 0.5 μg mL^{-1}, achieving an LOD of 1.8 μg L^{-1} (Fig. 39b). This simple, fast, and highly sensitive fluorescence probe provides a promising approach for assessing the safety of food contaminated with Hg^{2+}. Another study synthesized a new dual-emission fluorescent sensor (chemosensor **149**) CuNCs@Tb@UiO-66-(COOH)$_2$ for the detection of Cu^{2+}.[237] The fluorescence ratio and Cu^{2+} concentration showed a good linear relationship when fitted in the range of 1–30 μM, with an LOD of 178 nM. This study offers a novel approach to design multifunctional ratiometric fluorescent sensors using a one-pot method with MOFs as support materials. Abdelhamid *et al.* synthesized a series of new isostructural lanthanide-based

MOFs based on the trimolecular linker of 2,4,6-tri-*p*-carboxyphenyl pyridine (H$_3$L$_2$), together with La^{3+} as their select metal cluster (chemosensor **150**).[238] The fluorescence emission intensity exhibited a linear decrease in the concentration range of Fe^{3+} from 16.6 to 167 μM, and the Stern–Volmer analysis further verified linearity and revealed an LOD of 16.6 μM. This study introduced a novel platform with potential applications in biosensing. Therefore, NC-based fluorescent sensors possess great efficiency and performance for the detection of metal ions and pesticide residues, but only a few types of metal ions has been reported for designing fluorescent sensors currently. Moreover, further endeavors are necessary to enhance the sensitivity and selectivity of materials for improved performance in future applications.

4.2.5 Perovskite@MOF fluorescent sensors. Perovskite materials have attracted increasing attention due to their advantageous characteristics, including high QY, tunable optical properties and low cost. However, the stability of hybrid perovskites remains a concern given that it can lead to their degradation, affecting their long-term performance. Accordingly, they can be combined with some relatively stable MOFs for the construction of robust perovskite@MOF assemblies that

This journal is © The Royal Society of Chemistry 2024

Chem. Soc. Rev., 2024, **53**, 6992–7090 | **7051**

exhibit enhanced chemical stability and luminescence.[241] Besides, by integrating dopant-modified perovskites within MOFs, it is feasible to fabricate ratiometric fluorescent sensors boasting diverse emission profiles as a result of the distinctive PL of these two substances.[239] In the past few years, $CsPbBr_3$, $MAPbBr_3$, and $CH_3NH_3PbBr_3$ have been doped in MOFs for the construction of fluorescence chemosensors. However, their applications in monitoring the health and surrounding of plants are still lacking.

Recently, only one study reported the function of perovskite@MOFs for the identification of substantial heavy metal ions. Subsequently, this research disclosed an innovative methodology that was pioneering in incorporating bisected inorganic perovskite nanocrystalline components in lanthanide MOFs, which constructed a ratiometric fluorescent chemosensor (151) for the determination of Hg^{2+} in aquatic medium (Fig. 40).[239] 151, consisting of $CsPbBr_3$@Eu-BTC, exhibited exceptional stability and fluorescence output in water. When exposed to Hg^{2+}, the fluorescence of $CsPbBr_3$ emitting at 520 nm was instantaneously depleted via an electronic transfer mechanism. However, the red emission from Eu-BTC peaking at 616 nm remained unaffected. Meantime, this color change was easily observed by the naked eye, providing a visual indication of the existence of Hg^{2+}. The $CsPbBr_3$@Eu-BTC fluorescent chemosensor could rapidly, sensitively and selectively detect Hg^{2+} and exhibited a linear concentration range of 0 to 1 μM and impressive LOD of 0.116 nM. Therefore, introducing perovskites in MOFs effectively improves the analytical proficiency of MOF-based sensors, but studies on the design and application of perovskite-based MOF fluorescent sensors are still lacking.

In summary, the application of perovskite-containing MOF materials for fluorescence sensing is still somewhat restricted owing to a few key challenges, as follows: (i) the strategies for combining and incorporating perovskite nanocrystals with luminescent MOFs are still complex and not fully understood and (ii) the primary obstacle hindering the practical sensing applications of perovskite@MOF fluorescent sensors in water is their poor fluorescence and water stability.

4.3 Covalent organic frameworks (COFs)

COFs have become attractive materials for fluorescence sensing due to their high fluorescence QY, extendable framework, and excellent chemostability and thermostability.[246] The luminescence properties of COFs are determined by the presence of abundant π-conjugation structures within their skeleton, which are created through a broad array of chemical bindings and affinities resulting from the unique monomer constituents of the material. The diverse functional groups in COFs as chromophores also have potential to promote their luminous efficiency.[247] Nevertheless, the poor intrinsic conductivity and weak electrocatalysis of most COFs obviously limit their application. Thus, to amplify the sensitivity of COF-based materials, various desirable modifications have been implemented, including metal encapsulation, incorporation of carbon-based nanomaterials, and the fabrication of COF composites with other porous nanostructures.[248] According to previous reports, COF-based fluorescent sensors have made great achievements in detecting pesticide residues, anions and cations in the living environment of plants (Fig. 41). In the following parts, we elaborate the applications of functional COF-based fluorescent chemosensors including various linkage types of COFs and COF-based composites in the detection of plant-related aspects (Table 9).

4.3.1 Specific linkage types of COFs for fluorescence detection. Different connection units forming various types of functional COFs with outstanding characteristics and great application potential in fluorescence detection have been widely studied. Comprehending and pinpointing the fundamental components and linkage systems present in COFs have opened the path to engineering materials with specifically customized attributes suitable for distinct applications.[254] At present, COFs
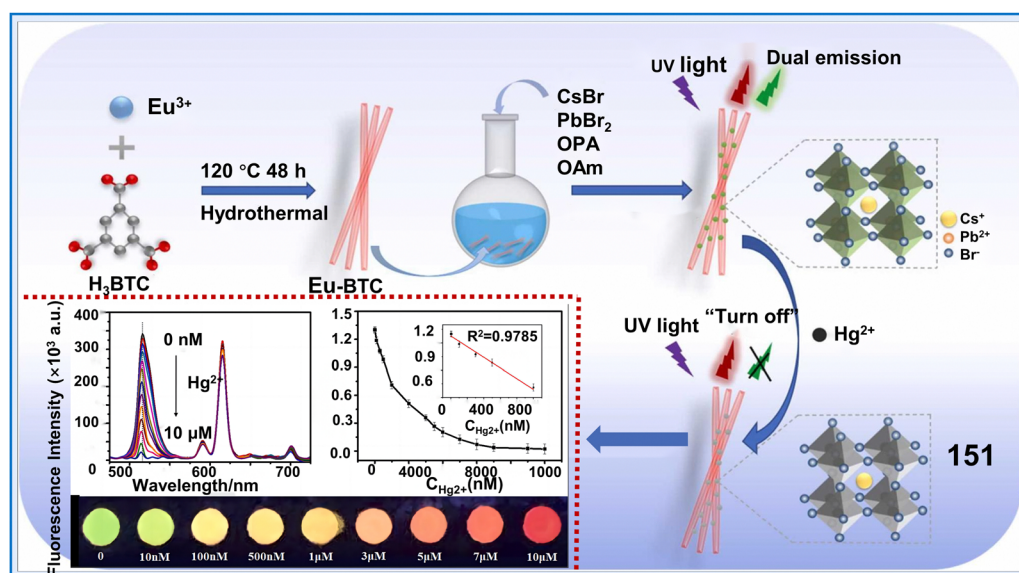

Fig. 40 Application of $CsPbBr_3$@Eu-BTC for the visualization of Hg^{2+}.[239] Copyright © 2022, Elsevier.

7052 | Chem. Soc. Rev., 2024, 53, 6992–7090

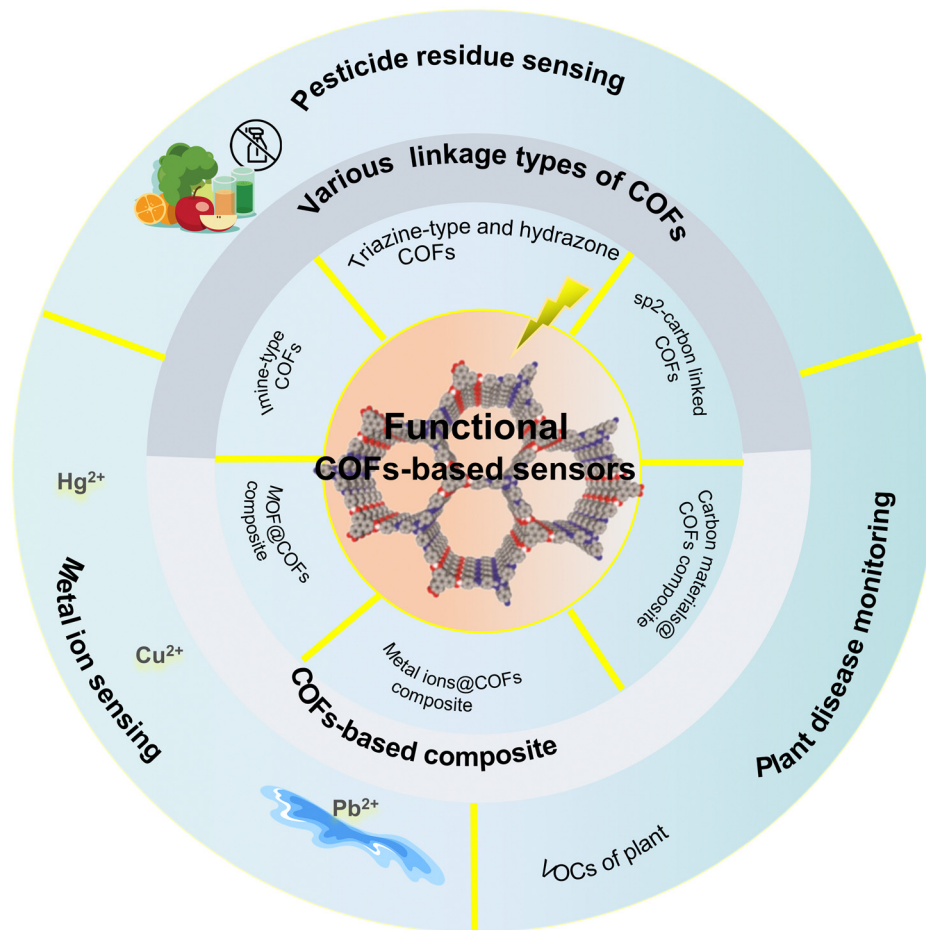This journal is © The Royal Society of Chemistry 2024

Fig. 41 Classification of functional COF-based sensors and their application in the detection of pesticide residues, metal ions and plant disease monitoring.

based on Schiff base, triazine and hydrazone groups and other types such as sp² carbon-conjugated COFs have been used for the detection of pollutants in the living environment of plants.

Imine-type COFs, known as "Schiff bases", are synthesized through an esterification response between aldehydes and amines.[248] This reaction leads to the formation of the Schiff base functionality (–C=N–), which is characteristic of imine linkages in the COF structure. This chemical union imparts noticeably high stability and robustness to the ensuing framework, presenting imine-type COFs with potential usage in the detection of pesticides and metal ions.

For example, a luminescence sensor was engineered by fabricating a novel imine-bonded conjugated COF (IC-COF) through the reaction between 2,4,6-tris(4-formylphenoxy)-1,3,5-triazine and 1,5-diaminonaphthalene (chemosensor **152**). **152** demonstrated remarkable selectivity towards PO_4^{3-} and an LOD of 0.61 μM (Fig. 42).[249] Furthermore, the exceptional recycling capability of IC-COF display substantial potential for reutilization without a discernible degradation in performance (5.2% decrease post 5 recycling cycles). The persistent issue with imine-based COFs is the propensity for nonradiative transition in response to π–π stacking interactions, giving rise to the aggregation-caused quenching (ACQ) effect. This triggered a reduction or complete cessation of COF luminescence emission.[250] Thus, to solve this problem, Song *et al.* synthesized an electrochemical luminescent material with properties to mitigate the ACQ event. Subsequently, they synthesized an imine-linked COF (TFPPy-TPh-COF) with high electrochemiluminescence (ECL) emission and the capability of eliminating the ACQ effect and further constructed an ECL sensor for the detection of malathion (chemosensor **153**). The efficient quenching of ECL was achieved by electrochemiluminescence resonance energy transfer (ERET) from the excited state of TFPPy-TPh-COF to zeolite imidazolate framework-8 (ZIF-8) and the steric hindrance of ZIF-8. **153** exhibited an extremely low LOD of 2.44 pg mL⁻¹ together with a broad dynamic concentration range of 0.01 to 1000 ng mL⁻¹. It could be effectively employed for the detection of other OPs (*e.g.*, paraoxon, methidathion, and chlorpyrifos) and utilized for the measurement of malathion in apples, lettuce, and pakchoi. This research offers a new opportunity for the synthesis of ECL materials with high performance and the development of new ECL sensors for the detection of various pesticides.

Besides, triazine-type and hydrazone-linked COFs possess several remarkable properties such as chemical stability, good thermal stability, and high nitrogen content. These properties make them promising for various applications, particularly fluorescence detection in the study of plant-environment interactions. For

This journal is © The Royal Society of Chemistry 2024

Chem. Soc. Rev., 2024, **53**, 6992–7090 | **7053**

Table 9 The application of COF-based fluorescent sensors in monitoring the living environment of plants

Classifications	Chemosensors	Name	Target analytes	Response range	Limit of detection (LOD)	Applications	Ref.
Special linkage types of COFs	152	IC-COF	PO_4^{3-}	—	0.610 μM	Detection of PO_4^{3-} in water	249
	153	TFPy-TPh-COF	Malathion	0.01–1000 ng mL^{-1}	2.44 pg mL^{-1}	Monitoring the concentration of malathion in pakchoi, lettuce, and apples	250
	154	Triazine-COF	Glyphosate	0.1–10 μM	96.0 nM	Detecting the distribution of glyphosate in water and soil	251
	155	Bth-Dma COF	Fe^{3+}	0–100 μM	0.170 μM	Monitoring the concentration of Fe^{3+} in water	252
	156	sp^2-carbon-linked COF	Cu^{2+}	0–150 μM	1.43 μM	Monitoring the concentration of Cu^{2+} in water	253
	157	Bpy-sp^{2}c-COF	Hg^{2+}, Ni^{2+}, Cu^{2+}, Co^{+}	0–20 nM	Hg^{2+}: 2.42 nM, Ni^{2+}: 2.73 nM, Cu^{2+}: 1.47 nM, Co^{+}: 2.20 nM	Detection of various ions including Hg^{2+}, Ni^{2+}, Cu^{2+}, and Co^{+} in water	254
COF-based composite fluorescent sensors	158	AuNPs@COF	OPs	10–800 ng mL^{-1}	0.610 ng mL^{-1}	Monitoring the concentration of OPs in food and water	255
	159	MnO$_2$@COF	Chlorpyrifos	—	0.0632 and 0.108 ng mL^{-1} by two treatments	Detecting the residue of chlorpyrifos in water and vegetables	256
	160	CDs@TDCOFs@PNIPAM	Pyrethroids	5–400 μg L^{-1}	4.88 μg L^{-1}	Monitoring the pyrethroids concentration in cabbage, cauliflower, and apple	257
	161	CDs@COF	Hg^{2+}	10–100 μg L^{-1}	0.750 μg L^{-1}	Detection of Hg^{2+} in water	258
	162	Dye/MOFs@COFs	VOCs	0.1–1 mg L^{-1}	—	Monitoring the VOCs from wheat scab	259

example, a study constructed a triazine-COF-derived electrochemical chemosensor (**154**), which was designed to facilitate specific non-covalent interactions with glyphosate (GLY) for detecting GLY.[251] **154** exhibited a wide linear operation range of 0.1 μM to 10 μM of glyphosate and demonstrated an LOD of 96 nM and a limit of quantification (LOQ) of 320 nM. This work shows significant potential for further improvements and commercialization as a versatile disposable sensing platform specifically designed for the detection of glyphosate in water and fruits. Chen *et al.* designed and successfully synthesized two stable crystalline hydrazone-linked COFs containing functional O,N,O′-chelating sites by Schiff-base condensation reactions (chemosensor **155**) (Fig. 43).[252] The as-synthesized Bth-Dma COF exhibited strong fluorescence in both the solid state and aqueous suspension and demonstrated exceptional sensitivity for detecting Fe^{3+} in water with an LOD of 0.17 μM. The recognition process can be attributed to the coordination interaction with Fe^{3+}. This groundbreaking study introduced the first instance of utilizing a robust luminescent COF material with pre-designed O,N,O′-chelating sites for the detection of Fe^{3+}. This research may lay the foundation for developing luminescent COF sensors with targeted binding sites to detect specific metal ions. Therefore, triazine-type and hydrazone-linked COFs have shown great efficiency for the detection of ions and pesticides in the environment, but related studies on their applications in the monitoring of the health and environment of plants are still lacking.

Additionally, COFs with sp^2-carbon chains exhibited commendable photoelectric attributes that make them effective in the fields of luminescent material production and chemical detection systems. Notable, they have been harnessed for plant habitat monitoring purposes also. For instance, Yan *et al.* constructed an AIE-active unit-containing and sp^2-carbon-linked COF (chemosensor **156**).[253] The conjugated backbone of sp^2-TPE-COF, interlinked by olefinic bonds, functioned as a highly informative sensor for detecting metal ions. **156** significantly improved the dispersion of COFs and finely modulated their sensitivity towards Cu^{2+}, resulting in a remarkably increased Stern–Volmer constant (K_{sv}) value of 15.15 × 10^4 m^{-1} (Fig. 44a). The present investigation underscored the considerable promise inherent in employing surfactant-modulated, extensively π-conjugated COFs for sensor technology applications. This work can open up opportunities for creating more fully conjugated COFs to detect a wider range of water-soluble toxic analytes. Zhu *et al.* reported a fully π-conjugated COF with dual binding sites, Bpy-sp^{2}c-COF, which demonstrated commendably swift fluorescence recognition and substantially amplified adsorption tendencies toward divalent heavy metal ions (chemosensor **157**) (Fig. 44b).[254] XPS analysis confirmed the concurrent coordination between metal ions and both cyano and bipyridine groups in Bpy-sp^{2}c-COF, leading to its efficient fluorescence recognition and adsorption capabilities for Cu^{2+}, Hg^{2+}, Ni^{2+} and Co^{2+}. The fully π-conjugated COF, demonstrating dual ligand binding sites, offered a promising and innovative method for formulating sensors possessing exceptional attributes. At present, exploration into robustly π-conjugated COFs for fluorescent sensing and contaminant remediation remain
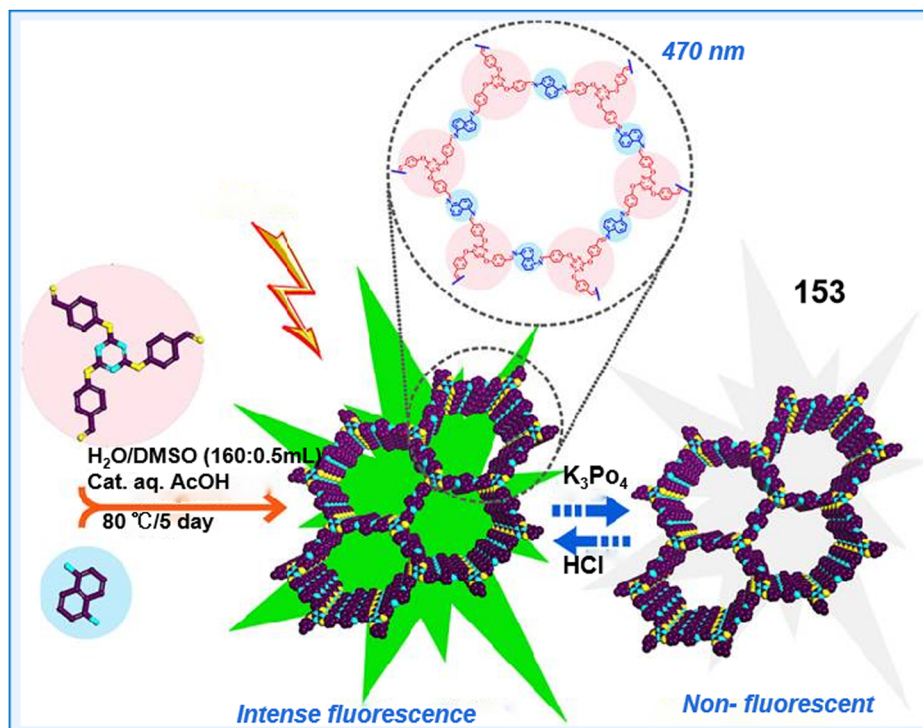
7054 | *Chem. Soc. Rev.*, 2024, **53**, 6992–7090

This journal is © The Royal Society of Chemistry 2024

Fig. 42 Precipitation methodology for IC-COF and the influence of phosphate ions on its fluorescence properties.[249] Copyright © 2023, the American Chemical Society.
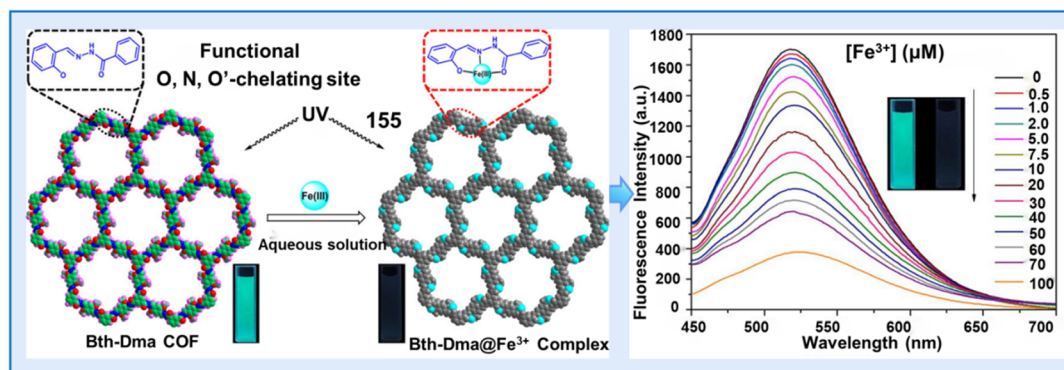

Fig. 43 Schematic illustration of the designed synthesis of Bth-Dha and Bth-Dma COFs, as well as their functional O,N,O′-chelating sites.[252] Copyright © 2019, the American Chemical Society.

scarce, primarily owing to their intricate synthetic procedures, which typically result in relatively modest success rates. Thus, further efforts should be focused on sp^2 c-COFs and their versatile applications.

4.3.2 COF-based composite fluorescent sensors. Metal nanoparticles (MNPs) have gained significant attention recently due to their exceptional catalytic attributes. Unfortunately, the aggregation of MNPs (*e.g.*, AuNPs, PtNPs, and PdNPs) is a common issue due to their high surface energy, resulting in decreased catalytic efficiency and difficulties in their extended storage. Research indicates that by leveraging the expansive porous structures and remarkable stability of COFs, there have been successful efforts to combine MNPs such as AuNPs,

PtNPs, and PdNPs with COFs. COF-MNP composites offer the synergistic benefits of the excellent catalytic activity of MNPs and the unique advantages of COFs, and can be utilized for detecting pollutants in plants and their surrounding environment.[260] For example, Li *et al.* developed a novel core–shell nanocomposite, PB@Fe-COF@Au, for the highly efficient detection of OP residues (chemosensor **158**) (Fig. 45a).[255] The PB nanoparticle (PBNP) cores with Fe^{2+} and Fe^{3+} exhibited peroxidase-like activity, while metallated porphyrins and AuNPs also acted as peroxidase-mimicking catalytic sites. Therefore, PB@Fe-COF@Au possessed satisfactory triplet peroxidase-like catalytic efficiency (Fig. 45a). The use of the triple nanozyme enhanced the sensitivity of the sensor and effectively reduced
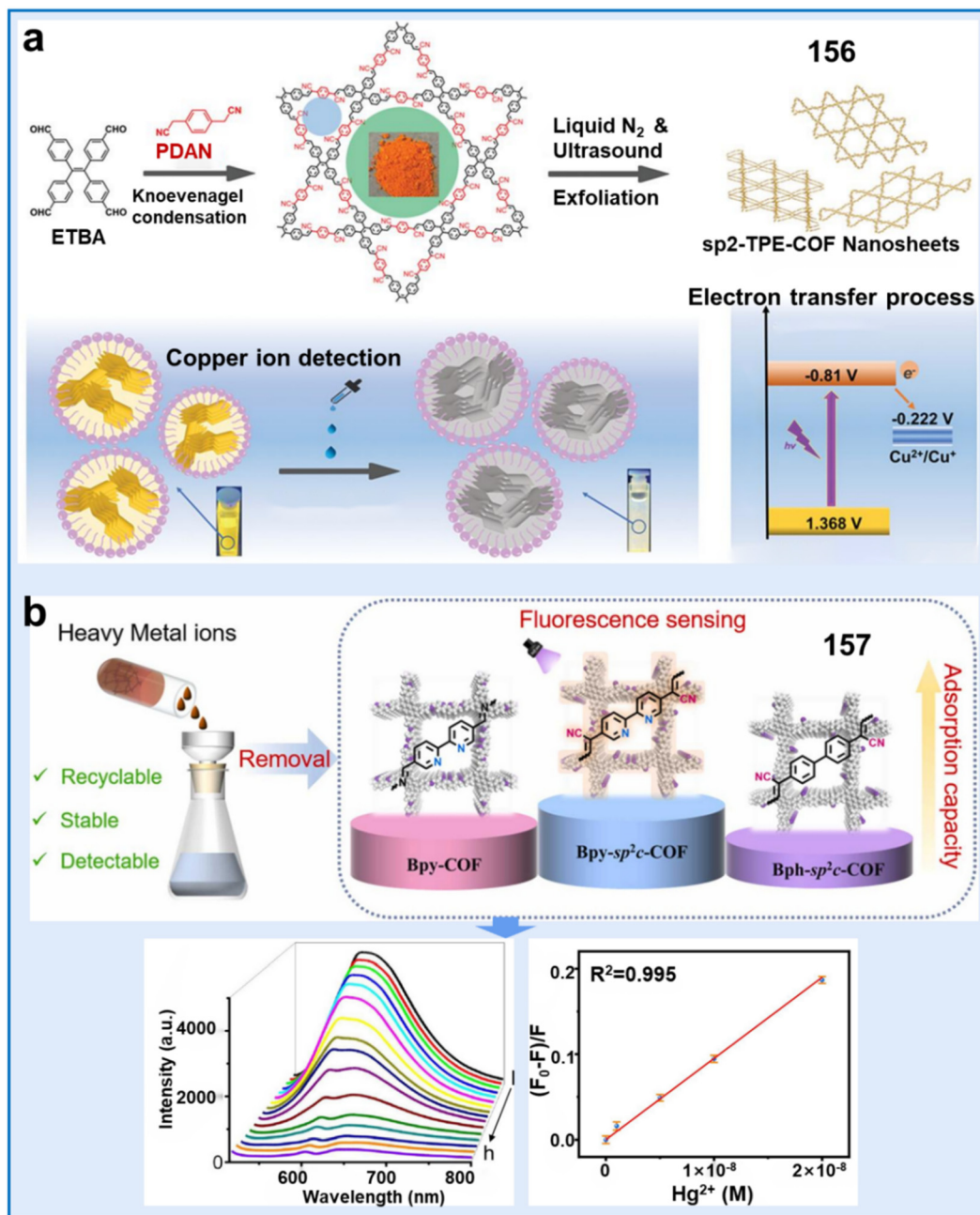
This journal is © The Royal Society of Chemistry 2024

Chem. Soc. Rev., 2024, **53**, 6992–7090 | **7055**

Fig. 44 Application of sp^2-carbon-linked COFs for monitoring the living environment of plants. (a) Synthesis of sp^2-TPE-COF, copper ion detection, and its electron transfer process during copper ion sensing with sp^2-TPE-COF.[253] Copyright © 2022 Wiley-VCH GmbH. (b) Schematic illustration of Bpy-sp^{2}c-COF for the detection and removal of divalent heavy metal ions.[254] Copyright © 2022, Elsevier.

interference in the detection of OP. In comparison to previous studies, this sensor achieved a broader linear range (10–800 ng mL^{-1}) and a lower detection limit (0.61 ng mL^{-1}) for chlorpyrifos. These improvements were directly linked to the synergistic interplay among the triple catalytic sites of PB@Fe-COF@Au, which also functioned as its triple responsive sites for OPs. This research offers a novel approach for the design and application of efficient nanozymes for on-site monitoring of pesticides.

Besides, metal oxide MnO$_2$ NPs have also been introduced in COFs to improve their catalytic efficiency due to their expansive

surface area, substantial adsorptive potential and superior biocompatibility. For example, Wen *et al.* developed a cutting-edge COF/methylene blue@MnO$_2$ (COF/MB@MnO$_2$) composite, which demonstrated superior signal amplification, a unique binding entity, and robust oxidase-mimicking activity (chemosensor 159).[256] In the absence of OPs, the MnO$_2$ coating on the surface could detect thiocholine (TCh) due to the enzymatic breakdown of acetylthiocholine (ATCh), catalyzed by acetylcholinesterase (AChE). The inhibitory activity of OPs against AChE and their impact on the generation of TCh

7056 | *Chem. Soc. Rev.*, 2024, **53**, 6992–7090

This journal is © The Royal Society of Chemistry 2024

provided the basis for the accurate detection of chlorpyrifos. The detection could be achieved through complementary electrochemical and photothermal measurements, with LODs of 0.0632 ng mL^{-1} and 0.108 ng mL^{-1}, respectively. Moreover, this sensor demonstrated exceptional selectivity and robust anti-interference capability for the precise detection of chlorpyrifos in diverse environmental and biological samples, effectively distinguishing it from interfering substances (Fig. 45b). This study offered a dual-mode detection method for OPs that is convenient and suitable for on-site testing in various scenarios. Additionally, it broadened the practical utilization range of COF-derived multifunctional composites for application in multimodal sensing systems. Therefore, introducing metal oxides into MOFs is another effective strategy to improve the detection efficiency.

COFs employed together with carbon nanomaterials can avoid the lack of electron conductivity. However, only a few studies reported the combination of CDs in COFs to detect pesticide residues and heavy metal ions in the environment. CDs, as quasi-spherical fluorescent nanoparticles based on carbon, possess excellent chemical stability, abundant low-cost sources, and strong resistance. These attributes make them highly promising for selective detection applications. However, the nanoscale size of CDs leads to intrinsic self-aggregation, resulting in the quenching of AIE.[257] Therefore, to prevent self-aggregation, a viable and intelligent approach is to encapsulate CDs within the channels or pores of COFs. For example, Zhang *et al.* created a fluorescent composite called CDs@TDCOFs@PNIPAM by encapsulating CDs within 1,3,5-tris(4-formylphenyl)benzene (TFB)/2,5-dihydroxyterephthalohydrazide grafted with thermally responsive poly(*N*-isopropylacrylamide) (PNIPAM) (CDs@TDCOFs@PNIPAM, chemosensor **160**) (Fig. 46).[257] **160** demonstrated a temperature-reactive "on/off" detection module for pyrethroids through
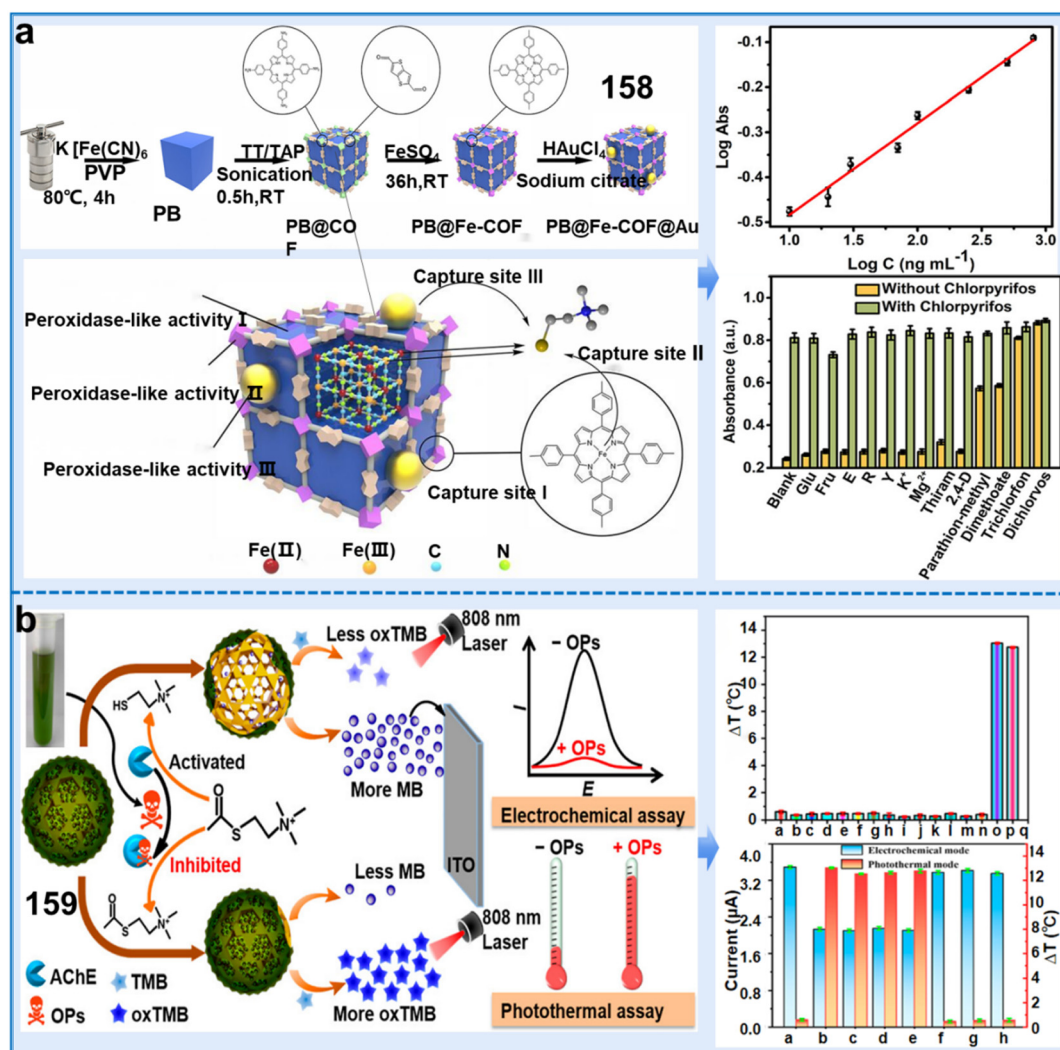

Fig. 45 Fluorescence sensors based on metal and metal oxide NP composites for the detection of OPs in the environment. (a) Synthesis of PB@Fe-COF@Au composite and its diagrammatic sketch of triplet peroxidase-like active sites and multiple capture sites.[255] Copyright © 2023, the American Chemical Society. (b) Synthesis of the COF/MB@MnO$_2$ composite and its detection mechanism, selectivity and anti-interference capacity of OPs (from a to p: blank, Fe^{2+}, Fe^{3+}, Cu^{2+}, Pb^{2+}, Cd^{2+}, Hg^{2+}, As^{5+}, glucose, methionine, arginine, glycine, citric acid, thiamine nitrate, chlorpyrifos, and a mixture of all the above-mentioned substances, respectively).[256] Copyright © 2023, the American Chemical Society.

This journal is © The Royal Society of Chemistry 2024

Chem. Soc. Rev., 2024, **53**, 6992–7090 | **7057**

target-catalyzed electron exchange. The model manifested an expansive linear measurement range of 5 to 400 μg L^{-1} with an LOD of 0.69 μg L^{-1}. Concurrently, CDs@TDCOFs@PNIPAM, equipped with red, green, and blue (RGB) fluorescent emissions, was combined with a smartphone-assisted apparatus, facilitating the visually discernible and astute quantification analysis of pyrethroids, exhibiting an LOD of 4.875 μg L^{-1} (Fig. 46). Another study designed and synthesized an innovative composite of imine-bonded COF doped with CDs for the analytical monitoring of Hg^{2+} in environmental water (chemosensor **161**), which exhibited superior sensitivity and discriminative fluorescence response to low concentrations of Hg^{2+} in water.[258] The analytical threshold of the sensor was in the range of 10 to 100 μg L^{-1}, presenting an LOD of 0.75 μg L^{-1}. This cost-effective and simple-to-construct fluorescent COF offers promising prospects for the precise detection and efficient removal of diverse pollutants present in irrigation water.

MOFs are traditionally known as a family of structurally aligned substances affiliated with COFs, exhibiting comparable essential characteristics to COFs such as high surface area, tunable accessibility and extended crystalline structure. COFs possess strong covalent linkages, which endow them with the exceptional thermal and chemical stability vital for chemical detection under harsh conditions.[261] Integrating MOFs with COFs presents a promising strategy to elevate the performance and expand the application scope of COFs.[260] Currently, only one study reported an MOF@COF composite as a chemical fluorescence sensor to detect the substances related to plant health. Furthermore, the practical application of colorimetric sensor arrays still face challenges, including environmental

humidity interference and insufficient sensitivity towards minute traces of target volatile organic compounds (VOCs).[259] Thus, to address these challenges, Wang *et al.* developed a solution by creating dye/MOF@COF core–shell composites *via* the application of hydrophobic COF overlayers on top of MOFs loaded with dyes (chemosensor **162**).[259] The composite-based sensor, benefiting from the uniform dispersion of dyes across the porous MOF structure, exhibited enhanced sensitivity at sub-ppm levels for the detection of VOCs compared to conventional dye sensors. The developed dye/UiO@TPB-DVA-COF composites exhibited excellent sensing capabilities for the differentiation and detection of eight plant VOCs.

This array facilitated the precise and timely detection of wheat scab, even as early as one day after inoculation (Fig. 47). This study suggested that MOF@COF composites offer a versatile platform for constructing colorimetric sensing arrays exhibiting exceptional humidity sensing capabilities and robustness. These arrays hold significant promise for practical application scenarios, particularly in monitoring the health of plants.

In summary, although considerable achievements have been made in the development of COF-based sensors, the synthesis of COFs and their composite counterparts encounters significant hurdles, as follows: (i) the exorbitant expense associated with precursor materials, together with the ecological risks posed by these substances and the organic solvents utilized throughout the process pose significant obstacles in their large-scale industrial production; (ii) enhancing the operational duration and performance of COF-modified electrodes is crucial, and there is a pressing need to develop materials that offer high loading efficiency and excellent conductivity; (iii) further
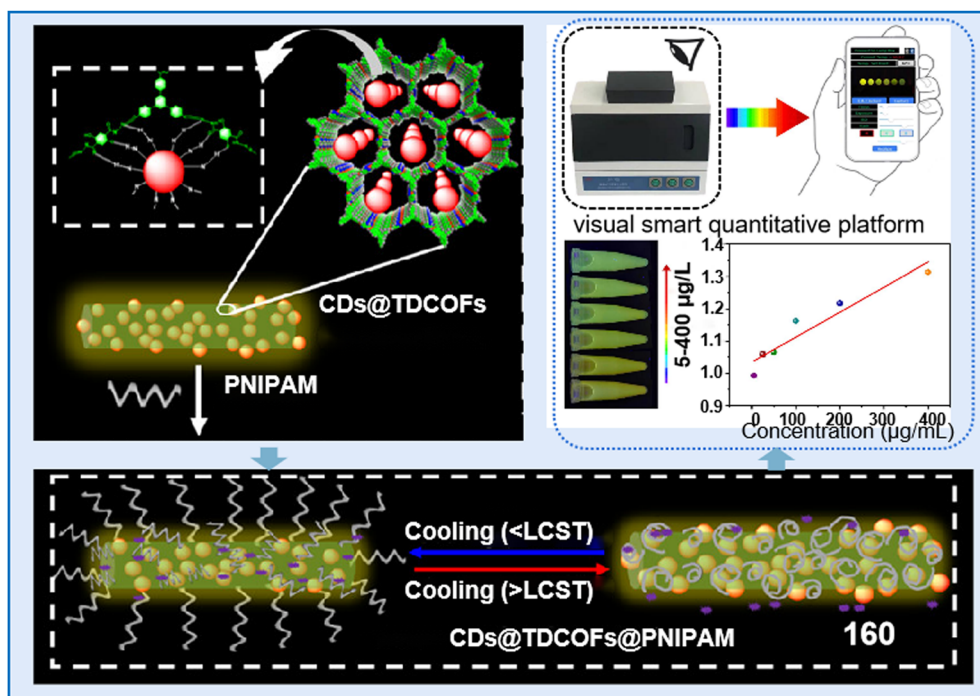

Fig. 46 Process for the synthesis of CD@TDCOF@PNIPAM composite and CD@TDCOF@PNIPAM-based smartphone readout analysis of LCY in real samples.[257] Copyright © 2022, the American Chemical Society.
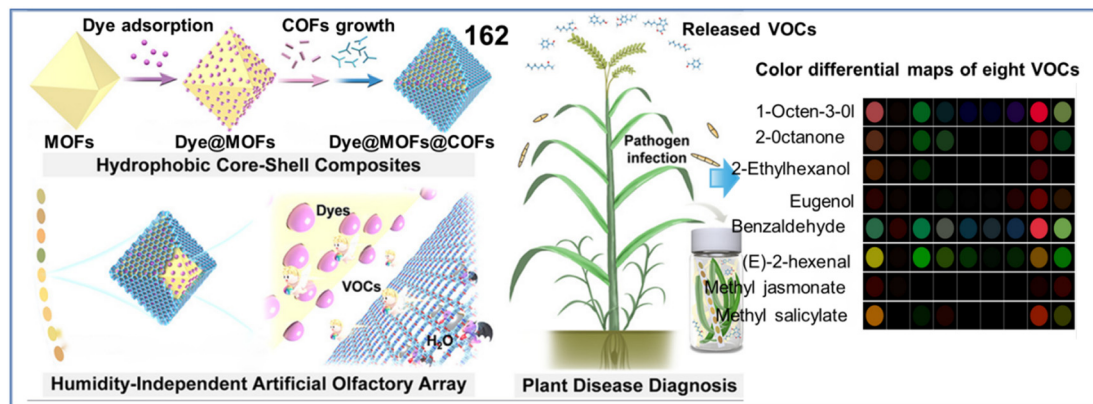
Fig. 47 Schematic diagram of the synthesis of dye/MOF@COF core−shell composite and the detection of the released VOCs by pathogens for the diagnosis of diseases in plants.[259] Copyright © 2022, the American Chemical Society.

innovation is required in the methods and means of functionalizing COFs; and (iv) their application range is still limited, especially in the field of monitoring plant health. Thus, designing COFs with better biocompatibility and adaptability is imperative to further expand the application scope of electrochemical sensors.

4.4 Nanoclusters

Nanoclusters (NCs), typically consisting of a single or multimetal core with a diameter of less than 2–3 nm, have attracted significant attention due to their broad Stokes shifts, very intense fluorescence bands, good biocompatibility and strong PL.[262] Additionally, NCs are known for their simple preparation and low toxicity, making them a preferred choice compared to other fluorescent materials such as toxic QDs and organic dyes.[263] Nanoclusters can be categorized into single metallic clusters and bimetallic clusters based on the composition of species within their cores.[262] Thus far, these NC-based fluorescent sensors have been widely used for monitoring the living environment of plants (Fig. 48). Here, we introduce the applications of single NCs, bimetallic NCs and NC-based fluorescent chemosensors in the above-mentioned aspects in detail (Table 10).

4.4.1 Single metal NC-based sensors. Metal nanoclusters (MNCs) consist of a few to several hundred metal atoms, exhibiting discrete energy levels because of their nanoscale size. This characteristic gives rise to exceptional optical properties in MNCs. Besides, MNCs possess attractive properties such as ultra-small size, excellent biocompatibility, and outstanding photostability, making them an ideal choice for fluorescent materials.[268] Among the various types of MCNs, AuNCs, CuNCs and AgNCs are the most widely used MCNs for developing fluorescent sensors. In the following parts, we elaborate the applications of these three single NCs in monitoring the living environment of plants.

Gold nanoclusters (AuNCs), an exclusive subset of metallic NCs, demonstrate a marked Stokes shift, adjustable emission response, and commendable biosafety, which are emerging as a cutting-edge subclass of fluorescent materials for developing high-performance sensors.[278] Fluorescent AuNCs have been

successfully employed for the identification of various pollutants, including pesticide residues and metal ions in the living environment of plants. For example, Li *et al.* synthesized hydrolysate-response disulfide bond-functionalized gold nanoclusters (S-S-AuNCs, chemosensor **163**).[205] Remarkably, S-S-AuNCs exhibited a distinct response to low pH values and thiol compounds, enabling their application as highly efficient sensors for organophosphates (OPs). This sensing mechanism relied on the AChE-facilitated hydrolysis of acetylthiocholine in thiocholine and CH_3COOH, with OPs inhibiting the activity of AChE (Fig. 49a). In addition, S-S-AuNCs were implemented for the meticulous examination of the distribution, residue and metabolization of methidathion within pakchoi. Another study also developed a novel dual-signal fluorescent sensor for detecting OPs in vegetables based on GSH-synthesized AuNCs (GSH-AuNCs, chemosensor **164**).[264] **164** is based on the catalytic activities of acetylcholinesterase (AChE) and choline oxidase (ChOx), which convert acetylcholine (ACh) into choline and generate hydrogen peroxide (H_2O_2). This process leads to increased cyan fluorescence due to aggregation. Besides a mobile application called ''RGB Color Picker'' was employed to visually detect organophosphates (OPs) by recognizing the RGB values of fluorescent colors associated with different OP concentrations. This sensor exhibited a linear dynamic range of 10–2000 ng mL^{-1} with a detection limit of 2.05 ng mL^{-1}. This sensor demonstrated the ability to detect a wide range of organophosphates (OPs), but it lacked specificity in distinguishing individual types of OPs.

Besides the detection of pesticides, several studies reported that AuNCs can also detect metal ions in the environment. For instance, Zhang *et al.* developed a simple fluorescent chemosensor (**165**) using a single AuNC chemosensor for the rapid discrimination of heavy metal ions (HMIs).[265] **165** was synthesized by chemically reducing the gold precursor, $HAuCl_4$, using 2-mercapto-1-methylimidazole (MMI) in the presence of polyvinylpyrrolidone (PVP). The resulting PVP/MMI-AuNC exhibited significant responsiveness towards diverse metal ions. This resulted in a distinctive fluorescent response at both wavelengths of 512 nm and 700 nm (Fig. 49b). The observed changes in fluorescence could serve as a unique fingerprint, enabling
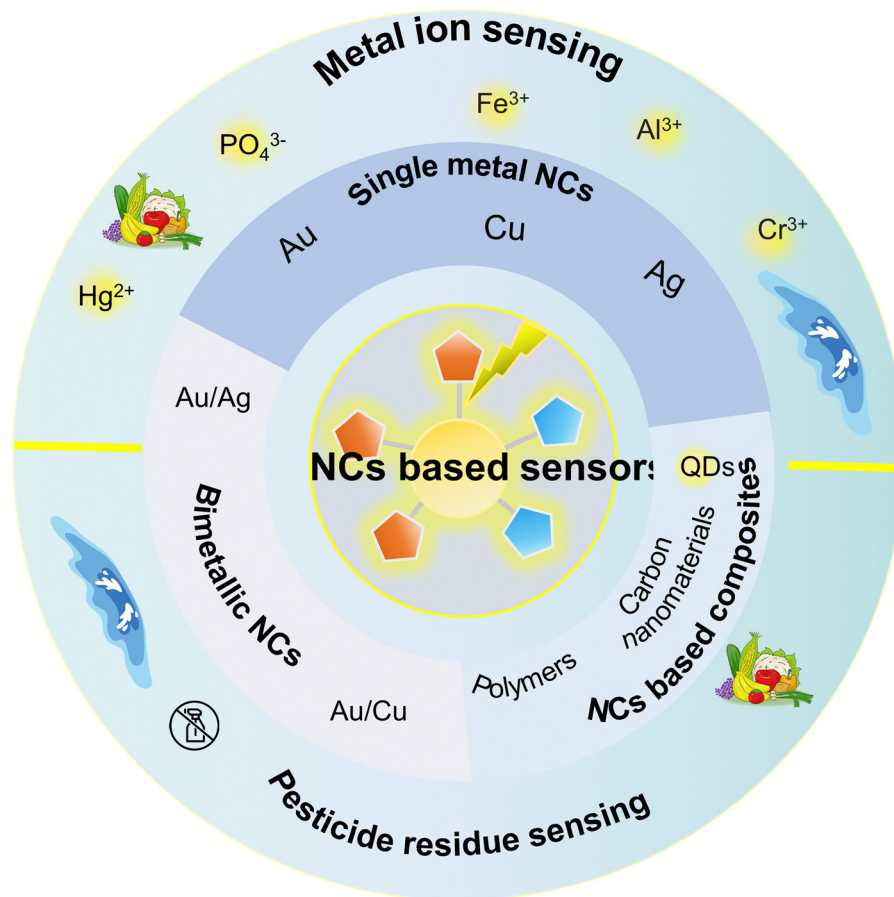
This journal is © The Royal Society of Chemistry 2024

Chem. Soc. Rev., 2024, **53**, 6992–7090 | 7059

Fig. 48 Classification and applications of NC-based sensors in plant-related environment monitoring.

the accurate discrimination of metal ions. By utilizing this newly developed PVP/MMI-AuNC-based fluorescent sensor array as our primary receptor, we could detect and unequivocally identify numerous heavy metals such as Ag^+, Fe^{3+}, Fe^{2+}, Mn^{2+}, Sn^{2+}, Pb^{2+}, and Hg^{2+}. Hada *et al.* achieved the successful synthesis of photoluminescent His-AuNCs, enabling the quantification of hazardous levels of Fe^{2+} in low-volume samples (chemosensor **166**).[266] Importantly, it exhibited high selectivity and accuracy for detecting Fe^{2+}, achieving an LOD of 3.2 μM. Finally, the realized transportable sensor was ascertained for its functionality in authentically assessing the Fe^{2+} levels in water samples that had been spiked with 35 μM Fe^{2+}. This portable sensing platform could monitor the concentration of heavy metals in water samples. Hence, AuNC-based sensors exhibit excellent selectivity and accuracy for detecting ions and pesticides in the environment and can monitor their toxicity level in the real environment.

In addition to AuNCs, CuNCs and AgNCs also have very intense fluorescence signals, which have been applied in the field of fluorescence detection.[279] For example, Xu *et al.* developed the first CuNC-based fluorescent sensor array (chemosensor **167**) to identify 12 metal ions (Pb^{2+}, Fe^{3+}, Cu^{2+}, Cd^{2+}, Cr^{3+}, Co^{2+}, Ni^{2+}, Zn^{2+}, Ag^+, Fe^{2+}, Hg^{2+}, and Al^{3+}) and various organic compounds, such as humic substances, lipids, fatty acids, amino acids, and lignans.[267] These 12 metal ions could be detected at a

concentration limit of 1.5 μM. Furthermore, the developed method allowed for the quantification of metal ions even at a low concentration of 0.83 μM (Zn^{2+}) (Fig. 49c). This constitutes the pioneering fluorescent sensor array constructed with CuNCs for the sensitive detection of various metal ions in water. The array was also employed to distinguish seawater and riverine samples from various regions, showcasing its potential for water quality evaluation. Chen *et al.* accomplished the development of a dual-emission nanocomposite using His-AgNCs for the detection of Cu^{2+} (chemosensor **168**).[268] It showed high detection sensitivity, good selectivity and anti-interference, and LOD of 0.4 ppm. In addition, this work designed a polymer film to load a dual-emission nanochemosensor, which meant that the visual detection of Cu^{2+} is possible. This work indicates the potential application prospects of dual-emission fluorescent nanochemosensors in the analysis of the living environment of plants.[269]

4.4.2 Bimetallic NC-based sensors. Bimetallic NCs have attracted great attention in the past few years due to their better catalytic activity, strong luminescence and higher sensitivity due to the synergistic effect of two types of metal atoms.[271] Thus far, bimetallic NC-based fluorescent sensors including Au/Ag, Au/Cu and bimetallic composite NCs have been used for the monitoring of the living environment of plants. Here, we introduce the application of these bimetallic NC-based chemosensors in this field.

7060 | *Chem. Soc. Rev.*, 2024, **53**, 6992–7090

This journal is © The Royal Society of Chemistry 2024

Table 10 The applications of NC-based fluorescent sensors in the detection of pollutants in the living environment of plants

Classifications	Name	Chemosensors	Response range	Limit of detection (LOD)	Target analytes	Applications	Ref.
Single NC-based sensors	Au NCs	163	0.05–20 ng mL⁻¹	0.0150 ng mL⁻¹	Methidathion	Detecting the methidathion residue in foods	205
		164	10–2000 ng mL⁻¹	2.05 ng mL⁻¹	OPs	Monitoring the concentration of OPs in vegetables	264
		165	Ag^+: 0.050–1.00 μM / Fe^{3+}: 0.100–25.0 μM / Sn^{2+}: 0.100–10.0 μM	17.0 nM for Ag^+	Ag^+, Fe^{3+}, Fe^{2+}, Mn^{2+}, Sn^{2+}, Pb^{2+}, and Hg^{2+}	Detection of metal ions in water	265
	Cu NCs	166	—	3.20 μM	Fe^{2+}	Detection of Fe^{2+} in water	266
		167	—	1.50 μM	Pb^{2+}, Fe^{3+}, Cu^{2+}, Cd^{2+}, Cr^{3+}, Co^{2+}, Ni^{2+}, Zn^{2+}, Ag^+, Fe^{2+}, Hg^{2+}, and Al^{3+}	Detection of 12 metal ions in water	267
	Ag NCs	168	0–10 ppm / 0–3.0 μM	0.400 mg L⁻¹ / 21.0 nM	Cu^{2+} / Glyphosate	Monitoring the concentration of Cu^{2+} in foods / Detecting the glyphosate residue in lettuce and *A. thaliana*	268 / 269
Bimetallic based sensors	Au/Cu NCs	169	50 nM–1 mM	10.0 nM	Cr^{3+}	Detection of Cr^{3+} in water	270
		170	Two linear range of 5.0×10^{-7}–7.0×10^{-6} M and 7.0×10^{-6}–1.0×10^{-4} M	0.100 μM	Fe^{3+}	Detection of Fe^{3+} in water	271
		171	Hg^{2+}: 10–100 μM / Cu^{2+}: 0–50 μM	2.45 nM for Hg^{2+}, 1.92 nM for Cu^{2+}	Hg^{2+} and Cu^{2+}	Monitoring the distribution of Hg^{2+} and Cu^{2+} in water and food	272
NC-based composite-based sensors	CQDs@CuNCs	172	10 to 500 nM for thiram, 5 to 100 nM for paraquat	7.49 nM for thiram, 3.03 nM for paraquat	Thiram and paraquat	Detecting the occurrence and concentration of thiram and paraquat in water	268
	N-GQDs	173	Cu^{2+}: 8×10^{-8} mol L⁻¹ × 10^{-6} mol L⁻¹, Cd^{2+}: 1×10^{-6} mol L⁻¹ × 10^{-5} mol L⁻¹	4.12×10^{-9} mol L⁻¹ for Cu^{2+}, 9.43×10^{-7} mol L⁻¹ for Cd^{2+}	Cu^{2+} and Cd^{2+}	Monitoring the concentration changes of Cu^{2+} and Cd^{2+} in food	273
	Blue-emitting CDs	174	Cu^{2+}: 0–600 nM / Hg^{2+}: 0–2000 nM	5.00 nM for Cu^{2+}, 7.00 nM for Hg^{2+}	Cu^{2+} and Hg^{2+}	Monitoring Cu^{2+} and Hg^{2+} in water	274
	WS₂-QDs	175	0.3 to 3 μM	0.120 μM	Cu^{2+}	Detection of Cu^{2+} in water	275
	AuNC@nanogel	176	0.625 to 125 ng mL⁻¹	0.590 ng mL⁻¹	Chlorpyrifos	Monitoring the concentration of chlorpyrifos in food	276
	BiNCs@AB	177	3.0 ng L⁻¹ to 1.0 mg L⁻¹	1.00 ng L⁻¹	Pb^{2+}	Detection of Pb^{2+} in water	277

This journal is © The Royal Society of Chemistry 2024

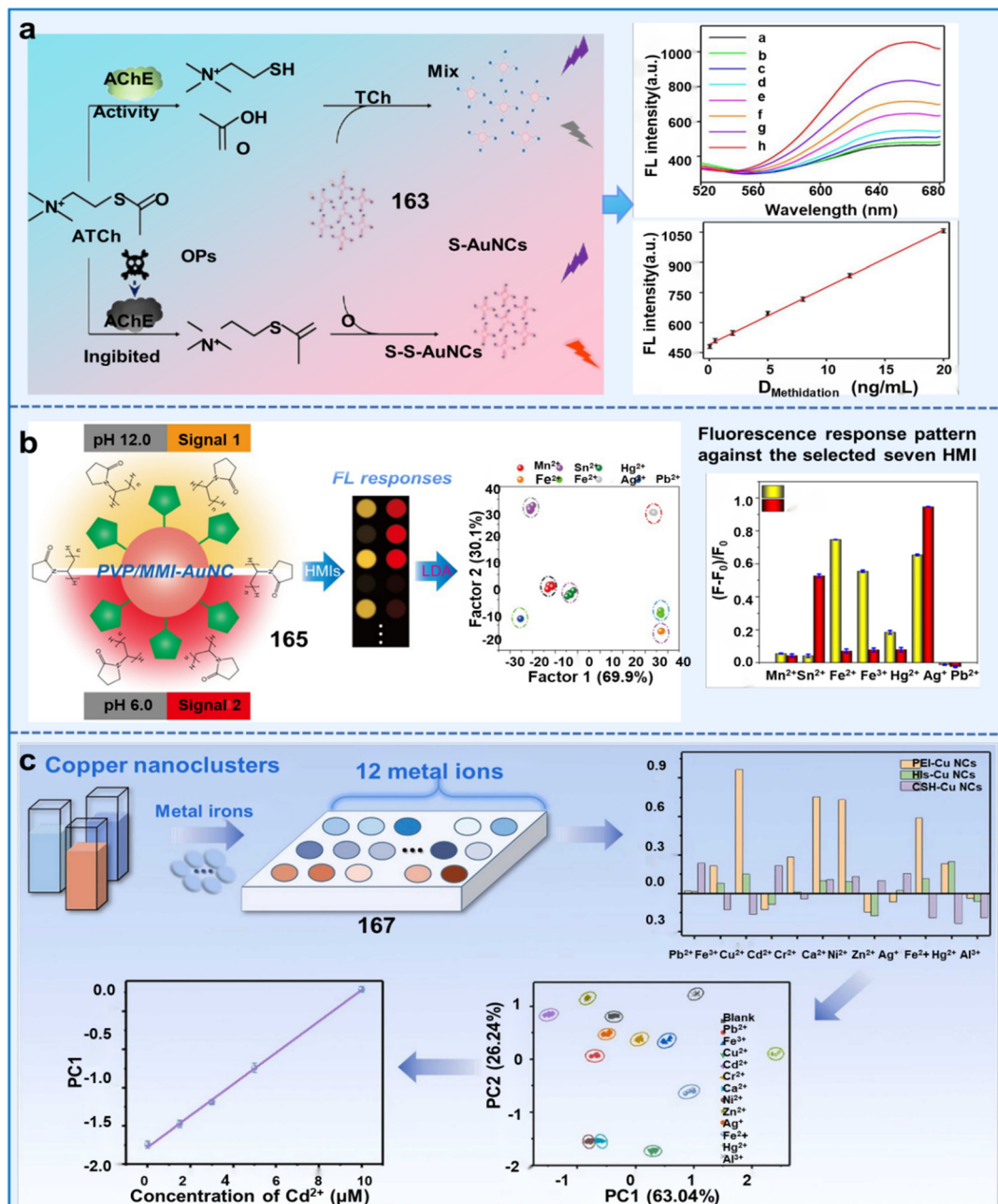*Chem. Soc. Rev.*, 2024, **53**, 6992–7090 | **7061**

Fig. 49 Single-metal NCs based fluorescent sensors used for monitoring the living environment of plants. (a) Sensing mechanism and application of S-S-AuNCs for detecting OPs.[205] Copyright © 2021, the American Chemical Society. (b) Schematic illustration of the CuNC-based fluorescent sensor array for detecting different metal ions.[265] Copyright © 2022, Elsevier. (c) Schematic representation of the PVP/MMI-AuNC-based fluorescent sensing system for identifying various HMIs.[267] Copyright © 2021, Elsevier.

Au-based bimetallic NCs are widely utilized for the detection of metal ions in soil and irrigation water. For example, Nie *et al.* prepared highly luminescent Cu/Au bimetallic nanoclusters (BNCs) by employing GSH for not only the reduction process but also as an enveloping shield, thus circumventing the aggregation of the synthesized nanoclusters (chemosensor 169).[270] When excited at 380 nm, Cu/Au BNCs showed an emission peak at 450 nm. Selective quenching of Cu/Au BNCs by Cr^{3+} facilitated the implementation of an analytical approach benefiting from their broad linear dynamic range of 50 nM to 1 mM and superior

sensitivity (LOD = 10 nM, S/N = 3). Shojaeifard *et al.* utilized the remarkable metallophilicity and PL properties of Au and Cu clusters to design a chemosensor based on bimetallic gold-copper nanoclusters (PA-AuCu bi-MNCs, 170).[271] The fluorescence intensity of PA-AuCu bi-MNCs was selectively quenched in the presence of Fe^{3+}, resulting in the hindrance of their emission. This work demonstrated an LOD of 0.1 μM and highlighted the independence from most interferences, making it an important feature of the study. Therefore, compared to single NCs, Au-based bimetallic NCs show high selectivity and anti-interference.
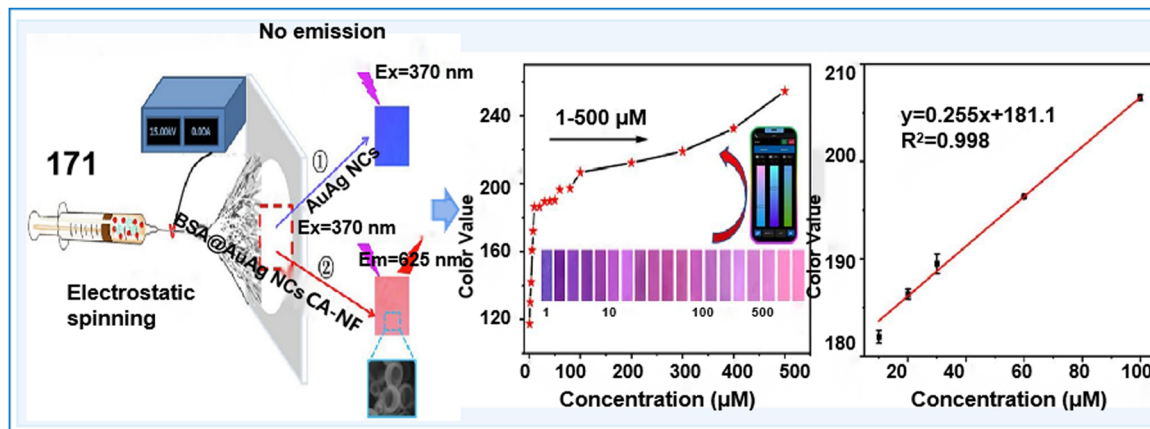
7062 | *Chem. Soc. Rev.*, 2024, 53, 6992–7090

This journal is © The Royal Society of Chemistry 2024

Fig. 50 Schematic illustration of the fabrication of AuAg–ENM and its sensing process.[272] Copyright © 2023, Elsevier.

Additionally, using other materials for the immobilization of bimetallic NCs has gained great attention due to their improved fluorescence performance for the trace identification of metal ions and pesticides in food and water. For example, Wu *et al.* synthesized a ratiometric fluorescent system (chemosensor **171**) by integrating AuAgNCs within electrospun cellulose acetate nanofibrous membranes (ENM). This strategy enabled the facile, rapid and visual detection of both Cu^{2+} and Hg^{2+} in Petri dishes under diverse conditions.[272] It was successfully utilized for detecting amino acid L-histidine (His) sequentially, a pivotal stem that integrated His analysis with a smartphone platform for quantitative on-site monitoring. This sensor exhibited exceptional performance in detecting traces of Hg^{2+} and Cu^{2+}, with LODs of 12.36 nM and 25.90 nM, respectively. The high selectivity of the AuAg-ENM system further enhanced its capability for monitoring and controlling the safety standard of Hg^{2+} and Cu^{2+} in multiple applications (Fig. 50). This developed system was validated using real environmental water samples, demonstrating its practicality for on-site detection using a smartphone with convenient operation.

4.4.3 NC-based composite-based sensors. To overcome the inherent tendency of MCNs to aggregate, incorporating diverse ligands/templates in NCs to form NC-based composites has been proven effective to greatly enhance their fluorescence properties, sensitivity and stability towards metal ions.[263] At present, various ligands including QDs, carbon nanomaterials, polymers and other porous materials have been used to stabilize MNCs, which show great detection efficiency for metal ions and pesticides in the environment.

QDs have been introduced in NC sensors to improve their detection efficiency and sensitivity through their exceptional optical attributes, robust photochemical stability, prolonged fluorescence lifetime, low toxicity, and stable emission. For example, a ratiometric fluorescent sensing system (chemosensor **172**) was constructed by leveraging red-emitted CuNC complexes and blue-radiating N-CQDs to effectively assess the concentrations of thiram and paraquat with LODs of 7.49 nM and 3.03 nM, respectively (Fig. 51a).[269] At the same time, the ratiometric fluorescence probe achieved satisfactory recovery

results, ranging from 82% to 114%, for actual food measurements. More interestingly, thiram and paraquat could be swiftly and visually detected *via* a smartphone-enabled colorimetric evaluation, offering an efficient methodology for the real-time monitoring of pesticide residues in fruits. Another study constructed a ratiometric fluorescence nanomixture of GQDs-AuNCs specifically for the quantitative analysis of Cu^{2+} and Cd^{2+} in fruits (chemosensor **173**).[273] Under the optimal conditions, the fluorescence intensity ratio (I_{565}/I_{403}) of the GQD-AuNC system showed a linear relationship with the concentration of Cu^{2+} or Cd^{2+} in the range of 8×10^{-8} M–6×10^{-6} M and 1×10^{-6} M–4×10^{-5} M, respectively. Also, its detection limits were 4.12×10^{-9} M and 9.43×10^{-7} M, respectively. When Cu^{2+} and Cd^{2+} were present, the paper-based visual sensor exhibited detectable fluorescent color changes, enabling rapid on-site detection. The findings suggest that the ratiometric fluorescence sensor holds great significance in food safety and biological analysis. Babaee *et al.* designed an innovative dual-emissive ratiometric nanohybrid chemosensor comprised of red-emitting (Ag/Au)@insulin NCs and blue-emitting CDs for the sensitive and selective ratiometric determination of Hg^{2+} and Cu^{2+} (chemosensor **174**).[274] The LODs for the determination of Cu^{2+} and Hg^{2+} were estimated to be 5 nM and 7 nM, respectively. Interestingly, the selectivity of this probe towards these two ions could be easily controlled by adjusting the pH of the probe solution without requiring any chelating agents. This unique feature allowed the selective detection of Cu^{2+} and Cd^{2+} ions by simply modifying the pH of the probe solution without the need for any additional reagents. Another study introduced a ratiometric fluorescent nanosensor (NCs/QDs, chemosensor **175**) for the detection of Cu^{2+} ions by combining the stable optical properties of AuAgNCs and WS2-QDs.[275] The addition of WS2-QDs could avoid the interference from Pb^{2+} and Cd^{2+} in the process of detecting Cu^{2+} due to their advantages of simple synthesis and stable luminescence properties. This sensor exhibits significant potential for detecting Cu^{2+} in river samples, offering great application potential in practical environmental monitoring. Therefore, QD-based NCs can achieve the fast and visual detection of ions and pesticides in the environment.

This journal is © The Royal Society of Chemistry 2024

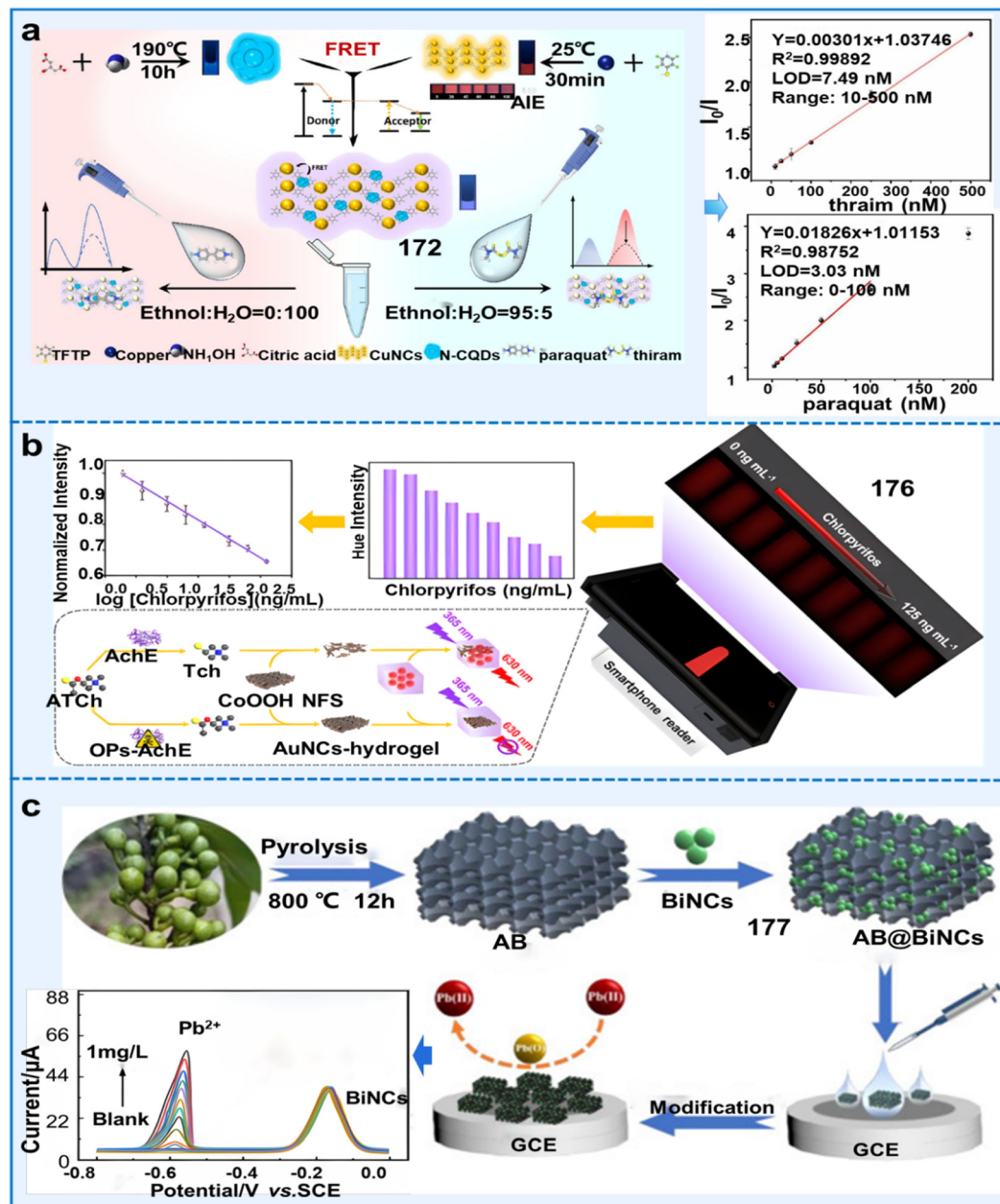*Chem. Soc. Rev.*, 2024, **53**, 6992–7090 | 7063

Fig. 51 Applications of NC-based composite-based fluorescent sensors in monitoring the living environment of plants. (a) Schematic representation of the ratiometric fluorescent sensor for the detection of pesticides using N-CQDs@CuNCs.[268] Copyright © 2023, Elsevier. (b) Schematic illustration of the portable fluorescent hydrogel test kit for the on-site quantitation of chlorpyrifos.[276] Copyright © 2021, the American Chemical Society. (c) Process for the fabrication of the BiNC@AB composite sensor for the sensing of Pb^{2+}.[277] Copyright © 2021 The Authors. Published by the American Chemical Society.

Hydrogels, as stable 3D networks with environmentally friendly properties, have gained considerable interest for immobilization and encapsulation purposes in sensor technology. Hydrogels, serving as water-holding networks, offer nanometer-scale porous structures that enable the passage of small molecules by providing physical encapsulation to trap nanoparticles.[276] The effective integration of the excellent performance of hydrogels with NCs can greatly enhance the accuracy and stability of sensors. For example, Wang *et al.* developed a portable handheld platform integrated with smartphones for the on-site detection of OPs

(chemosensor **176**).[276] Cobalt oxyhydroxide nanoflakes (CoOOH NFs) could effectively suppress the fluorescence originating from AuNC hydrogel systems through the FRET effect (Fig. 51b). By converting the fluorescent colors into digital information by using self-made auxiliary devices and smartphones, the on-site monitoring of the concentration of chlorpyrifos was achieved with an LOD of 0.59 ng mL^{-1}. This sensor presented good selectivity, anti-interference, high sensitivity and capability due to the encapsulation of the hydrogel into specific AuNC signatures in practical analysis, offering huge potential for on-site applications.

7064 | *Chem. Soc. Rev.*, 2024, **53**, 6992–7090

This journal is © The Royal Society of Chemistry 2024

Besides, a highly porous activated biochar (AB), exhibiting superior electrical conductivity, extensive surface area, and robust chemical stability, was selected as a support material to assist NCs in enhancing their excellent conductivity and electrocatalytic efficiencies. As demonstrated by Zou *et al.*, a ratiometric electrochemical chemosensor (**177**) was constructed using the BiNC@AB-modified electrode to analyze Pb^{2+}.[277] BiNCs were capable of not only forming an alloy with Pb^{2+} to enhance the affinity of Pb^{2+} towards the electrode interface, but also generating reference signals crucial in the precise and accurate process of electrochemical detection using a ratiometric approach (Fig. 51c). The prepared sensor exhibited an excellent electrocatalytic performance towards Pb^{2+}, with a satisfactory linear range and detection limit, which was attributed to the synergistic effect of these advantages. Therefore, AB as the support material can greatly improve the detection efficiency of NCs, but related studies are still limited.

In conclusion, despite the significant progress in the development of nanoclusters, many hurdles persist when advancing and endorsing the practical utilization of COFs for electrochemical analysis. (i) Reports regarding the utilization of metal nanoclusters as sensors for detecting Na^+, K^+, and Ca^{2+} ions are rare, mainly because of the suboptimal binding affinity displayed by the core of metal nanoclusters towards these ions; (ii) controlling the size regulation of nanoclusters remains challenging with the aim to enhance their photochemical attributes such as quantum efficiency and mitigate the complexities associated with post-synthesis purification tasks;[280] (iii) the incomplete understanding of the internal assembly process involved in metal nanocluster synthesis, thereby exacerbating the intricacy associated with enhancing their photochemical attributes; (iv) primary utilization of nanoclusters typically occurs within water samples, as opposed to plant samples where further detection utilities still exist and demand exploration in this field.

5. Applications of fluorescent supramolecular chemosensors

To provide accurate information for managing plant health, fluorescent supramolecular chemosensors with the advantages of recyclability, high sensitivity, selectivity and adaptability are suitable for a wide range of on-site environments.[281] To date, there are two types of fluorescent supramolecular materials, polymers and hydrogels, which are excellent tools for monitoring the health and living environment of plants (pesticides, ions and plant components). In the following section, we summarize and analyze the application of fluorescent supramolecular chemosensors in these aspects.

5.1 Polymer systems

Fluorescent polymers are specific due to the properties of their fluorophores such as photovoltaic properties and non-covalent bonding that stimulate reactivity and reversibility.[282] The non-covalent linkages affect the luminous characteristics of chromophores given that they have the ability to control the aggregation states and energy transfer through assembly-disassembly processes.[283] Utilizing a variety of structures, polymer sensors have been widely used for various analytes, such as pesticides, metals, and toxins (Table 11). In the following sections, we discuss the application of conjugated fluorescent polymers, organometallic polymers, and molecularly imprinted polymers for monitoring the above-mentioned analytes (Fig. 52).

5.1.1 Conjugated fluorescent polymers. Conjugated polymers are compounds that form high molecular weight compounds consisting of one or more π–π^* conjugated electronic structural unit linked by covalent bonds. The conjugated structure of conjugated fluorescent polymers allows the free flow of electrons/energy throughout their structure, and the light energy captured by each monomer can be delivered as a collection, producing a fluorescent signal multiplication effect. Some research groups have reported the use of conjugated fluorescent polymers for the detection of pesticides in water and the development of polymer test papers for the visual detection of pesticides in a recyclable manner. In one example, an article reported a carbazole-containing polymer (PAN-Cs, chemosensor **178**) that could incorporate six pesticides (isopropalin, trifluralin, fenitrothion, glyphosate, cyfluothrin, and imidacloprid) in its porous structure for detecting these pesticides. Among the pesticides, trifluralin was the best at quenching the fluorescence of **178**, with a pronounced fluorescence-quenching response could be seen for the determination of trifluralin both in water and on a test paper prepared from the polymer. Furthermore, the test paper could be recycled 12 times and still retained its original detection function (Fig. 53a).[284] The results indicated that **178** can recognize multiple pesticides and its specificity should be improved by adding specific recognition units or utilizing different reaction mechanisms. Another illustrious instance of the utilization of fluorescence for the identification of detrimental pesticides is fluorescent microporous polyamines (PAN-Ls, chemosensor **179**) with suspended dibromotriphenylamine and triphenylamine chromophore groups, which could also bind three pesticides (trifluralin, fenitrothion, and glyphosate) in their porous structure. The PAN-L-Br chemosensor exhibited higher sensitivity to the pesticide molecules and the chemosensing test papers prepared with the polymers to test for fenitrothion, possessed a quick and sensitive fluorescence quenching reaction, and could be recycled 10 times. The pore size of **179** showed a positive correlation with the sensitivity detection of pesticides, owing to the fact that the larger size can increase the interaction of pesticides with recognition groups (Fig. 53b).[285] However, although these studies demonstrated that paper coated with chemosensors is an efficient, rapid and promising method for the detection of pesticide residues, studies are still lacking on measuring the pesticide residues in real samples.

To realize the detection of pesticide residues in water resources, farmland and agricultural products, researchers have developed a variety of pesticide sensors. One paper reported a fluorescent sensor combining fluorescent conjugated polymer

This journal is © The Royal Society of Chemistry 2024

Chem. Soc. Rev., 2024, **53**, 6992–7090 | **7065**

Table 11 The applications of polymer system-based fluorescent sensors for monitoring the health and environment of plants

Classifications	Chemosensors	Name	$\lambda_{ex}/\lambda_{em}$ (nm)	Solvents	Limit of detection (LOD)	Target analytes	Applications	Ref.
Conjugated fluorescent polymers	178	PAN-Cs	365/467–500	Aqueous solutions	0.350 μM	Trifluralin, isopropalin, glyphosate, fenitrothion, imidacloprid, and cyfluothrin	Detecting six different pesticides in water	284
	179	PAN-Ls	365/479–490	Ethanol	0.100 mM	Fenitrothion, trifluralin and glyphosate	Detection for three pesticides in water	285
	180	FCPNPs–MnO$_2$ nanosheets	470/536	Phosphate buffer (PB, 10 mM, pH = 8.5)	1.12 pg mL^{-1}	Carbaryl	Detecting Carbaryl by fluorescence quenching	286
	181	Su-TPE/PrS	320/470	Tris-buffer (20 mM, pH = 8.2)	500 μM	Paraoxon methyl	Detection of paraoxon methyl in farmland or water	287
	182	UCNPs–GNPs	980/660	Acetone-phosphate buffer (0.3 mmol L^{-1}, pH = 6.5)	1.42 nM	Malathion	Detection of malathion in water and tea powder	288
	183	rGO-TPP	414/649, 717	$V_{DMF}:V_{methanol}$ = 1:1	27.7 fM	Cd^{2+}	Monitoring the concentration of Cd^{2+} in water	289
Organometallic polymers	184	—	293/617	Methanol	0.800 μM	Fipronil	Monitoring fipronil in water	290
	185	—	377/590, 615	Hexane	—	Triethyl phosphate	Detecting triethyl phosphate in solution and gas states	291
	186	CFP-Sm-CeO$_2$-	310/350, 615	Tris–HCl buffer solution (5 mmol L^{-1}, pH = 8.0)	1.00 μM	Methyl parathion	Detection of methyl paraoxon in Chinese herbal plants (Poria cocos and semen coicis)	292
	187	Cd-CBCD	390/467	Dimethylacetamide	145 ppb	2,6-Dichloro-4-nitroaniline (DCN)	Detecting DCN in water	293
	188	LCP 1	345/405	THF; Aqueous solution	1.15 μM; 3.83 μM for Fe^{2+}, 2.33 μM for Hg^{2+}, 1.97 μM for Fe^{3+}	DCN; Fe^{2+}; Hg^{2+}; Fe^{3+}	Detection of DCN in water; Detecting Fe^{3+} . Fe^{2+}, Hg^{2+}, and Fe^{3+} in river water	294
	189	—	324/462	Aqueous solution	0.360 μM; 0.590 μM	DCN; Fe^{3+}	Detection of the pesticide DCN in water; Detection of the Fe^{3+} in water	295
	190	—	365/484	Aqueous solution	1.02 ppm	Fe^{3+}	Detection of Fe^{3+} in river water samples	296
Molecularly/ion imprinted polymers	191	Microfluidic paper chip (paper@QDs@NBD@MIPs)	395/528, 640	NR	90.0 nM	2,4-Dichlorophenoxyacetic acid (2,4-D)	Detecting 2,4-D in soybean sprout and lake water	297
	192	Molecularly imprinted membrane chromatography strip	450–470/525	NR	20.0 μg mL^{-1}	Triazophos	Detecting the concentration of triazophos in water	298
	193	AgNPs-MIP films sensor	365/420	Na-phosphate buffer (20 mM, pH = 6.0, containing 10% acetonitrile)	0.300 ng mL^{-1}	Aflatoxin B1	Detecting the distribution and concentration of AFB1 in maize flour	299
	194	ARS-MIP	469/560	Phosphate buffer (20 mM, pH = 8.5)	0.100–100 μM	Cu^{2+}	Detecting Cu^{2+} in water.	300
	195	CQDs@Cu-IIP	343/448	Aqueous solution	0.0160 mg L^{-1}; 0.0280 mg L^{-1}	Cu^{2+}	Detecting Cu^{2+} in river water	301
Other special fluorescent polymers	196	Cu(II)-FIIS	438/493	Double-distilled water	0.140 μM	Cu^{2+}	Detecting Cu^{2+} in river water	302
	197	Pb(II)-IIP	395/430	Pure water	2.10 μg L^{-1}	Pb^{2+}	Detecting Pb^{2+} in different water samples	303
	198	FD@ALB	370/505, 575	PBS (1 mM, pH = 7.4)	0.570 μM	Chlorpyrifos	Detection the concentration of CPF in food, water, and soil	304
	199	HN-Chitosan-3	440/555	Deionized water containing 0.1 M hydrochloric acid	1.66 μM	HCHO	Detecting HCHO in water samples	305

7066 | Chem. Soc. Rev., 2024, 53, 6992–7090

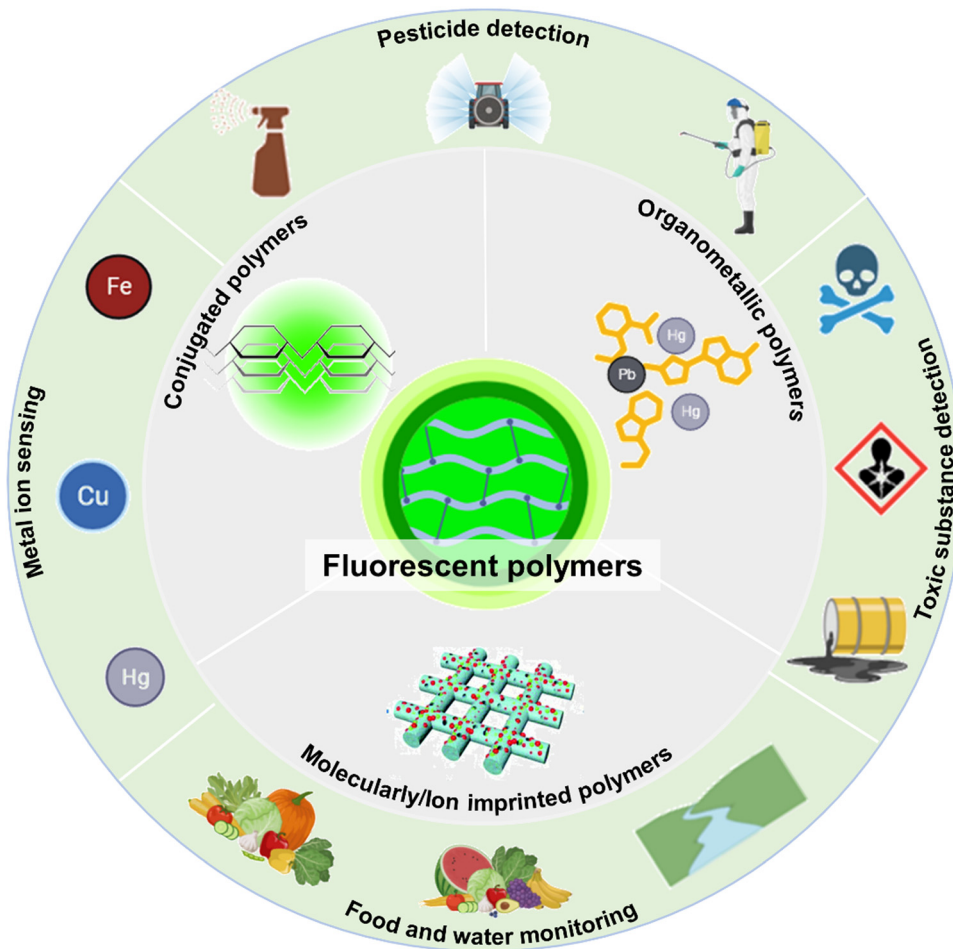This journal is © The Royal Society of Chemistry 2024

Fig. 52 Application of fluorescent polymers for monitoring the living environments of plants and food safety. Mainly divided into pesticide residue detection, soil environment heavy metal testing and fruit safety aspects of the test.

nanoparticles (FCPNPs) (chemosensor **180**) with manganese oxide (MnO_2) nanosheets, and then the fluorescence of **180** could be quenched by the MnO_2 nanosheets. AChE could induce the disruption of MnO_2 nanosheets, and then result in the recovery of the fluorescence of FCPNPs. To restrict the recovery of the fluorescence signals, we could limit the destruction of MnO_2 nanosheets through the inhibition of AChE activity *via* carbaryl (Fig. 53c). **180** showed good linear concentration responses in the range of 5–300 pg mL^{-1} with an LOD of 1.02 μU mL^{-1}. The "off–on" property increased the sensitivity and accuracy of **180** for monitoring the effect of pesticides on AchE activity.[286] Researchers also developed a polymerization-induced emission (AIE)-based sensor (**181**) assembled by electrostatic interaction between a cationic polyelectrolyte protamine (PrS) and tetra-anionic sulphonyl derivative of tetraphenylethylene (Su-TPE). The supramolecular complex disintegrated as a result of the enzyme degradation of PrS in the presence of trypsin, and the enzymatic activity of trypsin was significantly inhibited by the pesticide methyl paraoxon, thus restoring the fluorescent signals of the Su-TPE/PrS polymers (Fig. 53d). **181** showed a good linear concentration range of 0 nM to 16 nM with an LOD of 0.22 nM.[287] The results implied that the use of **181** was an effective method

for the quantitative detection of organophosphorus in agricultural fields or water resources by monitoring enzymatic activity. In another conjugated polymer (chemosensor **182**) for the detection of pesticides assembled by electrostatic interactions, to produce FRET, negatively charged upconversion fluorescent nanoparticles (UCNPs) were combined with cationic conjugated polymer-encapsulated gold nanoparticles (GNPs), and the fluorescence intensity decreased linearly with an increase in malathion concentration from 0.01 to 1 μM with an LOD of 1.42 nM (Fig. 53e). However, the fluorescence quenching of **182** may increase false positives in the detection of pesticides, which implies that the polymerization mechanism of **182** should be improved.[288] These studies have successfully designed fluorescent sensors for monitoring a variety of pesticides, and further studies should focus on developing novel detection kits for measuring enzymatic activity or pesticide concentration.

In addition to detecting pesticides, conjugated fluorescent polymer sensors were designed to detect heavy metal ions in water. One study employed noncovalent-coupled 5,10,15,20-tetraphenylporphyrin-reduced graphene oxide (rGO-TPP) to create a sensor (chemosensor **183**), which could detect Cd^{2+} with high sensitivity and without interference. The detection

This journal is © The Royal Society of Chemistry 2024

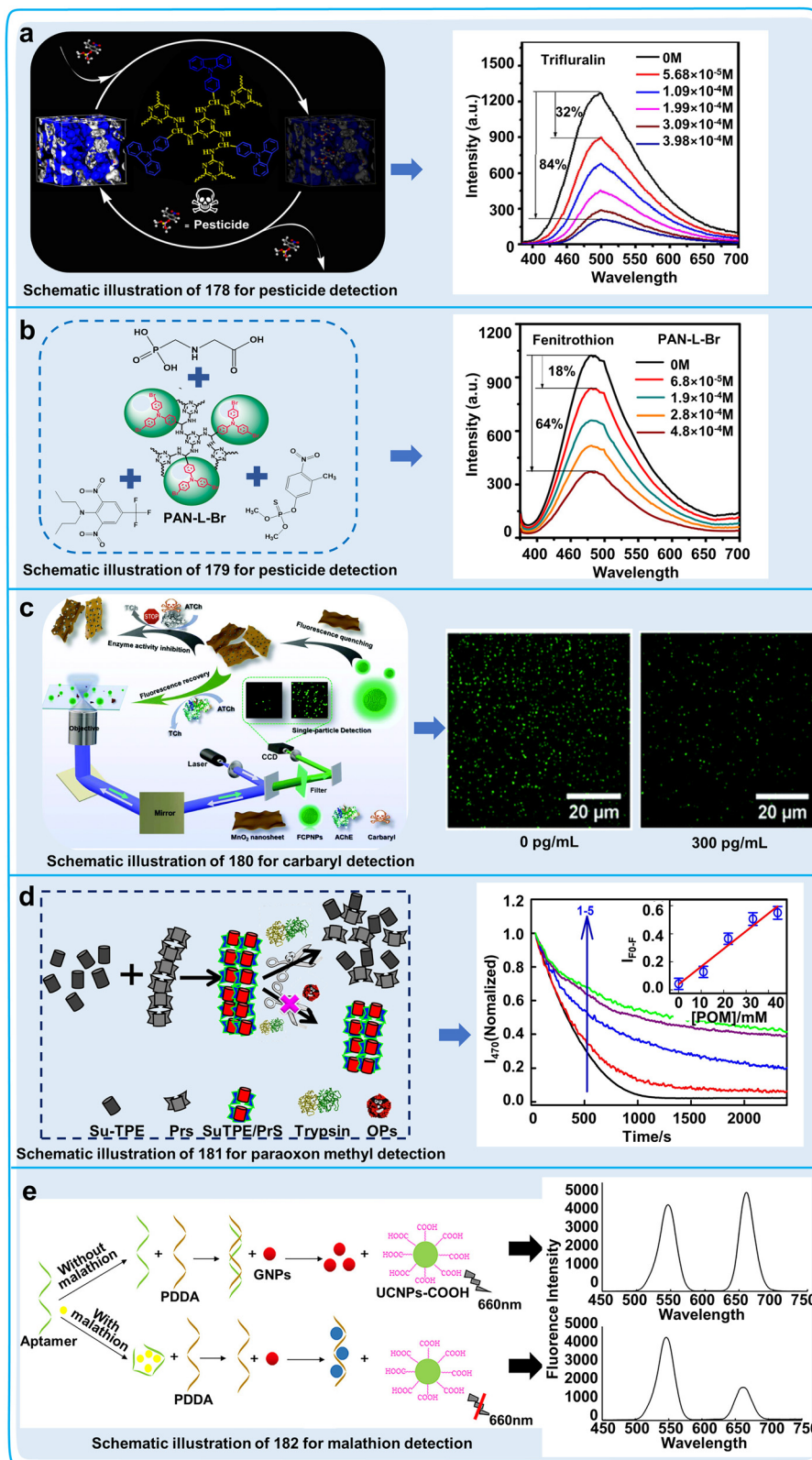*Chem. Soc. Rev.*, 2024, **53**, 6992–7090 | **7067**

Fig. 53 Detection process, data graphs and practical application diagrams of conjugated fluorescent polymers for the detection of pesticides. (a) Detection mechanism and spectra of different concentrations of pesticides (trifluralin as an example) in water by **178**.[284] Copyright © 2020, the American Chemical Society. (b) Schematic and spectra of **179** for the detection of different concentrations of pesticides (fenitrothion as an example).[285] Copyright © 2018, the American Chemical Society. (c) Schematic representation of the detection of the pesticide carbaryl by **180** and fluorescence images of FCPNPs detecting different concentrations of carbaryl. Reproduced from ref. 286 with permission from The Royal Society of Chemistry.[286] Copyright © 2019, The Royal Society of Chemistry. (d) Schematic representation of the **181** assay for methyl paraoxon and a plot of data on the inhibition of trypsin activity as measured by the fluorescence decay of the **181** complex at different concentrations of methyl paraoxon.[287] Copyright © 2021, Elsevier. (e) Schematic and fluorescence spectra of malathion detection by **182**.[288] Copyright © 2020, Elsevier.

7068 | *Chem. Soc. Rev.*, 2024, **53**, 6992–7090

This journal is © The Royal Society of Chemistry 2024

behavior of **183** was examined for 20 significant metal ions, and only Cd^{2+} was found to enhance the non-fluorescent rGO-TPP sensor to resume fluorescence. Cd^{2+}-induced fluorescence turn-on of the analyte was observed in the response range from micromolar to femtomolar, and the system was found to be the most sensitive Cd^{2+} sensor to date at the lowest experimentally detectable concentration of 3.86 fM (Fig. 54). Ultimately, rGO-TPP was also created as a solid-phase filter paper sensor that may be employed in on-site Cd^{2+} monitoring applications.[289] In terms of convenience and applicability, the rGO-TPP filter paper sensor is an effective tool for detecting metal ions in practice, but its application scope should be improved.

Currently, conjugated fluorescent polymers are commonly used to identify pesticides and ions in the living environment of plants. To improve the application scope of these sensors, some challenges should be solved. (i) We should focus on the development of ''off–on'' conjugated fluorescent polymers that can improve the detection accuracy and sensitivity. (ii) Further studies should focus on the detection of more stable conjugated fluorescent polymers or combined with a smartphone for increasing their application in a variety of practical environments. (iii) The complex synthesis process and difficult purification of conjugated fluorescent polymers limit their wide application.

5.1.2 Organometallic polymers. The family of crystalline organic–inorganic materials known as metal coordination polymers is made up of organic linkers and metal ions or clusters with well-defined structures, tunable pore sizes, and inherent crystallinity. Metal coordination polymers have been used to

trace pesticide residues in water and in Chinese herbs. One example was the first use of a europium metal coordination polymer (chemosensor **184**) for detecting fipronil (Fig. 55a), which had no impact on the luminescence of the fipronil-quenched polymers in the presence of other common pesticides. **184** showed a good linear concentration range of 10^{-6} to 10^{-4} M with an LOD of 0.8 μM. This is the first time that metal–organic coordination polymers were established for detecting pesticides and further studies should focus on developing a europium metal polymer test paper to facilitate the detection of fipronil in real samples.[290] Besides, another similar europium-containing metal supramolecular polymer was used to recognize pesticide mimics. 4-Oxy-2,6-bis-(1′-methylbenzimidazolyl)pyridine-containing amphiphilic end-capped poly(tetrahydrofuran) supramolecular polymeric films (chemosensor **185**), consisting of different ratios of Eu^{3+} and Zn^{2+}, exhibited a significant optical response in the presence of triethyl phosphate, a mimic of organophosphorus pesticides (Fig. 55b). With an increase in temperature, **185** showed greater sensitivity for detecting triethyl phosphate, implying that it has high potential for monitoring temperature and chemicals.[291] In another example of supramolecular polymers, fluorescent chemosensor **186** with cerium-based fluorescent polymers (CFP) and samarium-doped cerium oxide composites (Sm-CeO$_2$), depolymerization of the supramolecular structure and fluorescence quenching were induced by *para*-nitrophenol (*p*-NP) generated by hydrolysis of methyl parathion (MP) by Sm-CeO$_2$, which in turn was used for the detection of the pesticide methyl parathion in Chinese herbal plants (*Poria cocos* and *Semen coicis*) (Fig. 55c).[292] Although the use of metal coordination polymers
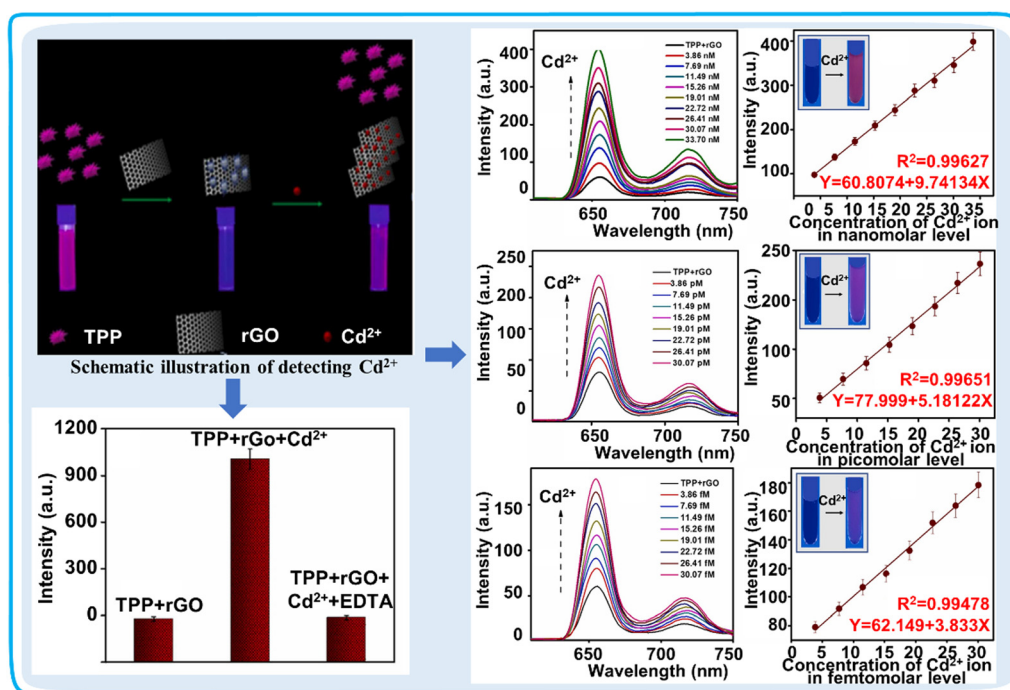

Fig. 54 Schematic of the detection of Cd^{2+} by the **183** sensor, statistical plot of the competitive interaction in the presence of different molecules and quantitative fluorescence detection spectra of Cd^{2+} concentration (nanomolar, picomolar and femtomolar concentrations) by **183**.[289] Copyright © 2023, Elsevier.
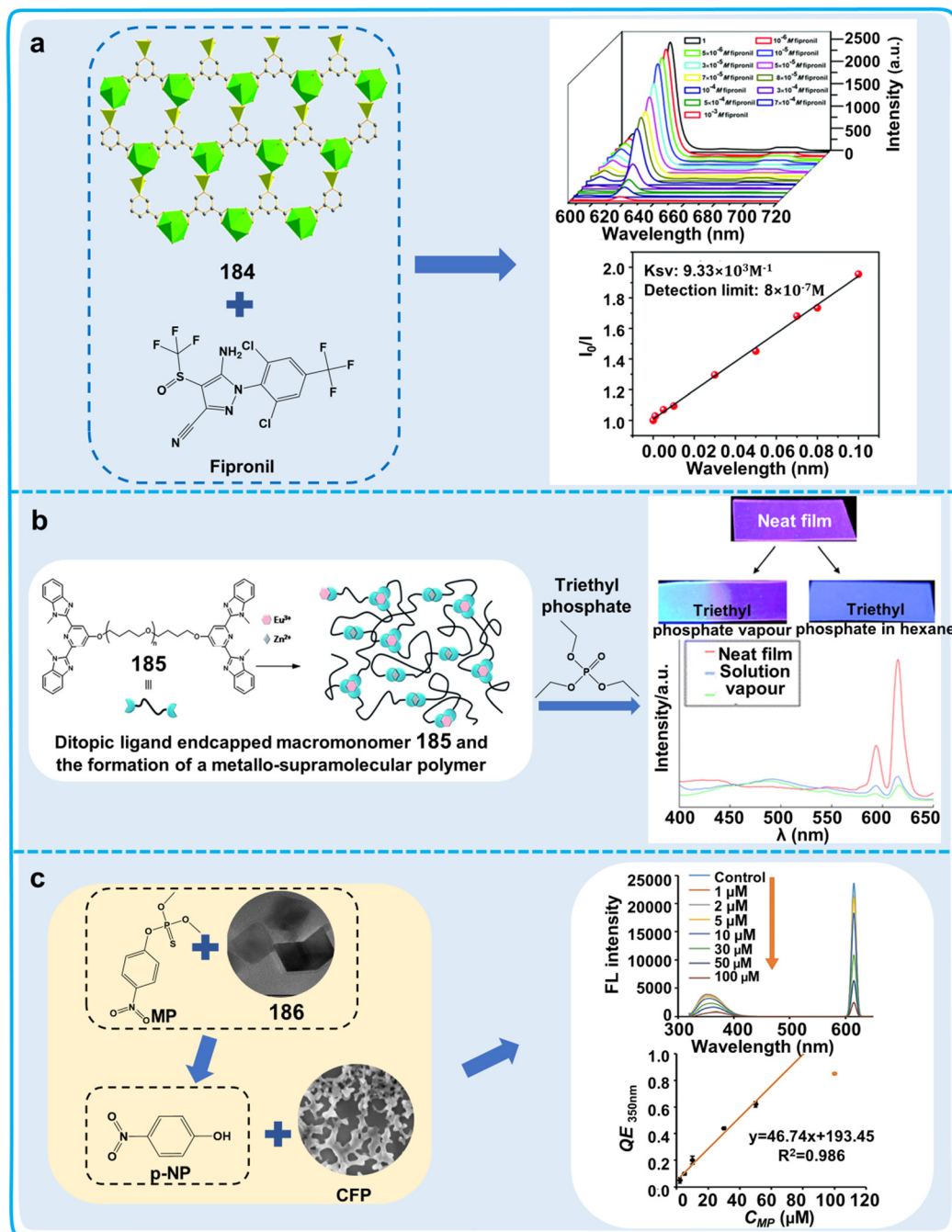
Fig. 55 Detection process, data graphs and practical application diagrams of organometallic fluorescent polymers for the detection of pesticides. (a) Spectrograms and Stern–Volmer plots of **184** for the detection of different concentrations of fipronil in methanol solutions. Reproduced from ref. 290 with permission from The Royal Society of Chemistry.[290] Copyright © 2018, The Royal Society of Chemistry. (b) Fluorescence images and spectrograms of **185** thin film test triethyl phosphate (solution and gas states).[291] Reproduced from ref. 291 with permission from The Royal Society of Chemistry. Copyright © 2010, The Royal Society of Chemistry. (c) Schematic diagram, fluorescence spectrogram and linear range plot of the fluorescence detection system **186** for the detection of methyl paraoxon (MP).[292] Copyright © 2023, BioMed Central Ltd.

has begun to address pesticide residue testing, most of these applications are still at the scientific research level, and thus it necessary to extend these testing tools to agriculture as a top priority.

In addition, studies have shown that metal coordination polymers can detect heavy metals and trace chemicals that

affect plant health. The carbazole-functionalized metal–organic polymer $[Cd_3(CBCD)_2(DMA)_4(H_2O)_2]$-10DMA (Cd-CBCD, chemo-sensor **187**) was developed as a highly efficient new fluorescent sensor for the detection of 2,6-dichloro-4-nitroaniline (DCN) by fluorescence quenching. **187** featured an LOD of 145 ppb together with a high quenching effect coefficient. **187** showed

7070 | *Chem. Soc. Rev.*, 2024, **53**, 6992–7090

This journal is © The Royal Society of Chemistry 2024

biofunction for the removal or detection of chemicals in water systems, implying it can be used as a scavenger of environmental pollutants (Fig. 56a).[293] In addition to carbazole-functionalized metal–organic polymers for the identification of DCN, other metal coordination polymers can also detect DCN. For example, a new Ag(I) luminescent coordination polymer, LCP1 (chemosensor 188), was developed with multi-substance recognition capability. It was found that 188 could specifically identify DCN, organosolvents and heavy metal ions by static quenching (Fig. 56b). The fluorescence quenching of 188 was ascribed to the FRET mechanism.[294] In another example, a novel cadmium-based metal organic fluorescent
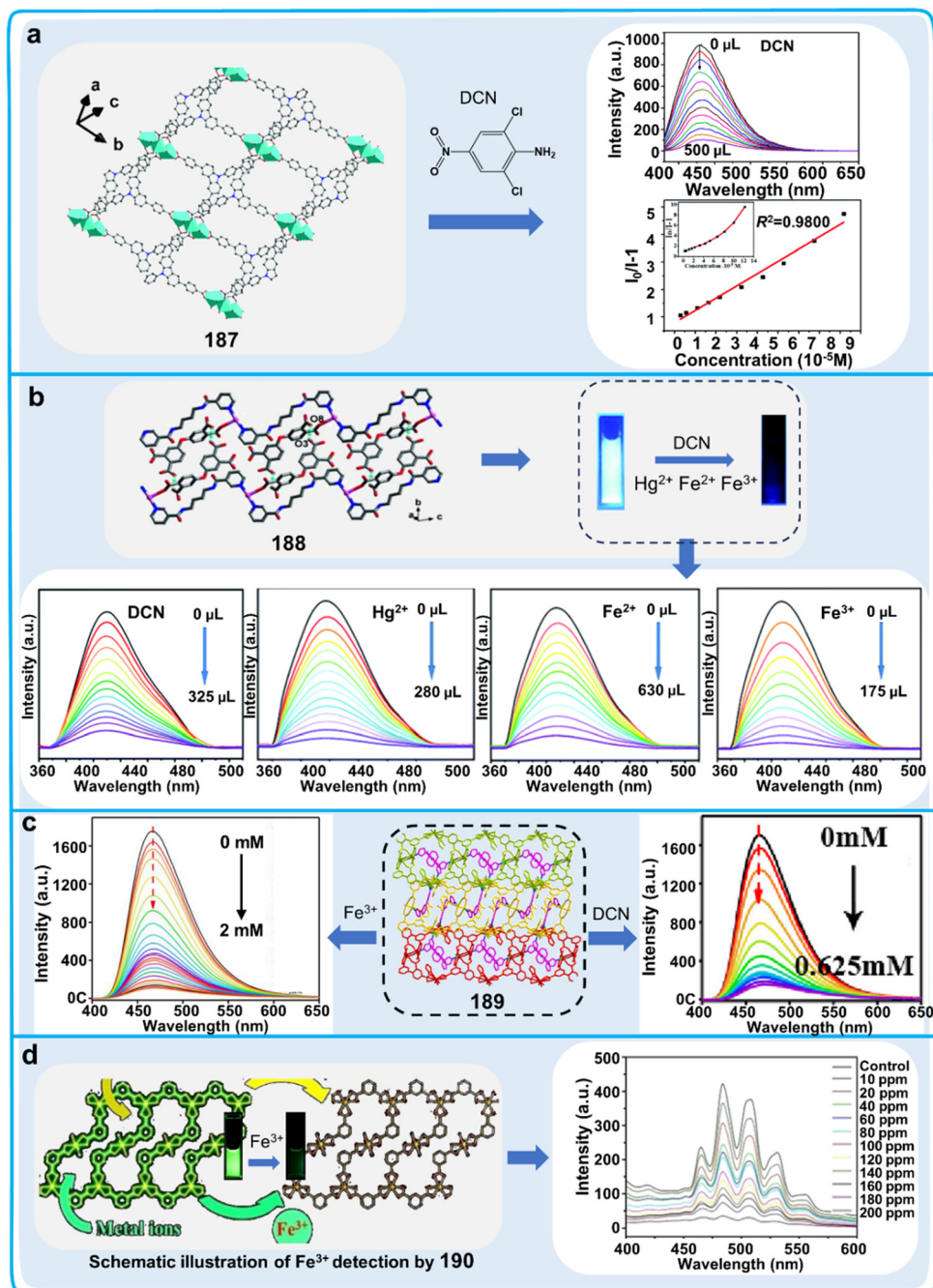

Fig. 56 Detection process and data graphs of organometallic fluorescent polymers for the detection of 2,6-dichloro-4-nitroaniline (DCN) or metal ions. (a) Fluorescence spectra and Stern−Volmer plots of different concentrations of DCN detected by 187. Reproduced from ref. 293 with permission from The Royal Society of Chemistry.[293] Copyright © 2019, The Royal Society of Chemistry. (b) Fluorescence images and titration spectra of 188 for the detection of different concentrations of DCN, Hg^{2+}, Fe^{2+}, and Fe^{3+}.[294] Reproduced from ref. 294 with permission from The Royal Society of Chemistry. Copyright © 2020, The Royal Society of Chemistry. (c) Titration spectra of 189 detecting different concentrations of Fe^{3+} and DCN.[295] Copyright © 2020, Elsevier. (d) Fluorescence images and titration spectra of different concentrations of Fe^{3+} detected by 190.[296] Copyright © 2019, Wiley-VCH Verlag GmbH & Co. KGaA, Weinheim.

This journal is © The Royal Society of Chemistry 2024

Chem. Soc. Rev., 2024, 53, 6992–7090 | 7071

polymer (chemosensor **189**) was developed, which showed fluorescence turn-off behavior in water towards the pesticide DCN (Fig. 56c), with quenching efficiencies of up to 94.45%.[295] Interestingly, chemosensor **189** was also designed as an optical signal quenching fluorescent sensor for monitoring metal ions. Among fifteen metal cations, only Fe^{3+} could induce the quenching of the fluorescence emission signal of **189** in water (Fig. 56c). The fluorescence of Fe^{3+}@**189** was recovered after the addition of ascorbic acid. This chemosensor showed an "on–off–on" mechanism for the recognition of DCN, Fe^{3+} and ascorbic acid, implying that the complex mechanism may reduce the detection accuracy of **189**.[295] The final example of metal ion recognition was a water-stable uranyl coordination polymer (chemosensor **190**), which enabled the feasible and effective detection of Fe^{3+} in real river water samples (Fig. 56d). **190** was a 3D supramolecular framework that was formed by π–π and hydrogen bond interactions. This chemosensor has bifunctions for identifying and detecting Fe^{3+} and pesticides.[296] If metal coordination polymers have dual detection function, that can be widely used to detect or remove pesticides and metal ions in water sources.

A well-known advantage of using organometallic polymers is their high sensitivity. However, their main disadvantage is that many metals and even heavy metals are toxic and can have a negative effect on plant health, and also there is radiation from radioactive metals. The raw materials for the preparation of organometallic polymers, the prepared organometallic polymers and the products after the use of organometallic polymers may all have a certain degree of toxicity.

Therefore, it is necessary to choose less toxic metals as the raw materials for the preparation of organometallic polymers, which is also a direction that needs to be the focus of research.

5.1.3 Molecularly/ion imprinted polymers. Molecularly imprinted polymers (MIPs) are polymers obtained by polymerization reactions between various functional monomers in the presence of a template molecule, which is covalently or noncovalently bonded to the polymer scaffold. When the template is removed after polymerization, a structure with sites designed to bind an analyte is produced, which is comparable to the template. Examples of constructing relevant molecularly imprinted polymers can be used to detect pesticides and plant toxins. Researchers constructed a novel microfluidic paper chip based on the FRET of nitrobenzoxadiazole (NBD) and CdTe QDs (chemosensor **191**), which showed visual changes in ratiometric fluorescence for monitoring the concentration of 2,4-D (Fig. 57a). **191** showed a good concentration linear range of 0.56–0.80 μM with an LOD of 90 nM. This chemosensor was combined with cellulose paper for separating and detecting 2,4-D in bean sprouts and water samples. Further studies should focus on the integration of **191** with more sensitive sensors for the on-site and quantitative detection of pesticides.[297] Another study established a molecularly imprinted membrane chromatography strip (chemosensor **192**) combining electrostatic spinning, molecularly imprinted polymers, and fluorescent lateral flow test strips (LFTS) for the detection of pesticides. Then, based on the synthesis of a triazophos hapten-murine IgG/fluorescein isothiocyanate conjugate (THBu-IgG-FITC) fluorescent

chemosensor with triazophos at the molecularly imprinted binding site on the membrane chromatography strip by competition to produce fluorescence changes as a method could realize the rapid detection of triazophos (Fig. 57b). This chemosensor showed a good linear concentration range of 20–500 μg mL^{-1} with an LOD of 20 μg mL^{-1}.[298] In the case for the detection of plant toxins, researchers demonstrated a new sensor system for detecting aflatoxin B1 (AFB1 a common grain toxin), preparing molecularly imprinted polymer films (chemosensor **193**) on the surface of glass slides to recognize aflatoxins and embedded spherical silver nanoparticles, which enhance the fluorescence signal of the analyte molecules, thereby increasing the QY and brightness (Fig. 57c).[299] **193** showed a good performance for the measurement of AFB1 in samples of grain extracts that were naturally infected as well as samples that were spiked. This chemosensor realized molecular imprinting reactions that allowed the researchers to study the dissociation and binding of the toxin in real time. The last type of MIP combining a template and functional monomers detects metal cations by competition. For example, Alizarin Red S (ARS) and 4-vinylphenylboronic acid (VPBA) were chosen as the functional monomers and structural template, respectively, and precipitation polymerization was used to create ARS imprinted polymer particles (chemosensor **194**). When Cu^{2+} and ARS formed a stable complex, it accomplished the purpose of detecting Cu^{2+} by separating ARS from **194** and causing fluorescence quenching (Fig. 57d), which was utilized for the detection of Cu^{2+} in water.[300] The fluorescent sensors constructed by selecting the corresponding analytes as templates in the above-mentioned studies have high detection specificity. There are also studies in which the molecularly imprinted polymers have been used to prepare test paper/membrane chromatography strip-type sensors, which can be easily used for analyzing and detecting samples in the field.

By imprinting and polymerizing template ions in the imprinting process, ion-imprinted polymers are unique polymers that have the ability to selectively adsorb the template ions. In the following research examples, a batch of ion-imprinted polymers for the selective detection of metal ions should be prepared based on various heavy metal ions as effective tool for the analysis and removal of contaminants in the living environment of plant. For instance, citric acid was used as a carbon source for the synthesis of CQDs via the hydrothermal method, and then an amidation procedure. The produced CQDs were attached as fluorescent groups on the surface of SBA-15 mesoporous molecular sieves. Then, the fluorescent sensor CQDs@Cu-IIP (chemosensor **195**) was prepared via the surface blotting method, and Cu^{2+} could effectively quench the fluorescence of CQDs@Cu-IIP. Thus, CQDs@Cu-IIP was used as an ion-imprinted polymer for the detection of Cu^{2+} in river water (Fig. 58a).[301] In addition to other IIPs for the detection of Cu^{2+}, a type of quick and easy fluorescent ion-imprinted sensor (FIIS) for Cu^{2+} detection was made by creating a fluorescent polymeric ligand. 4-(2-Aminomethyl)pyridinyl-*N*-allylnaphthalimide was employed as a fluorescent functional monomer, a layer of Cu(II) ion-imprinted polymer was coated on the surface of a PVDF membrane with a surface-functionalized
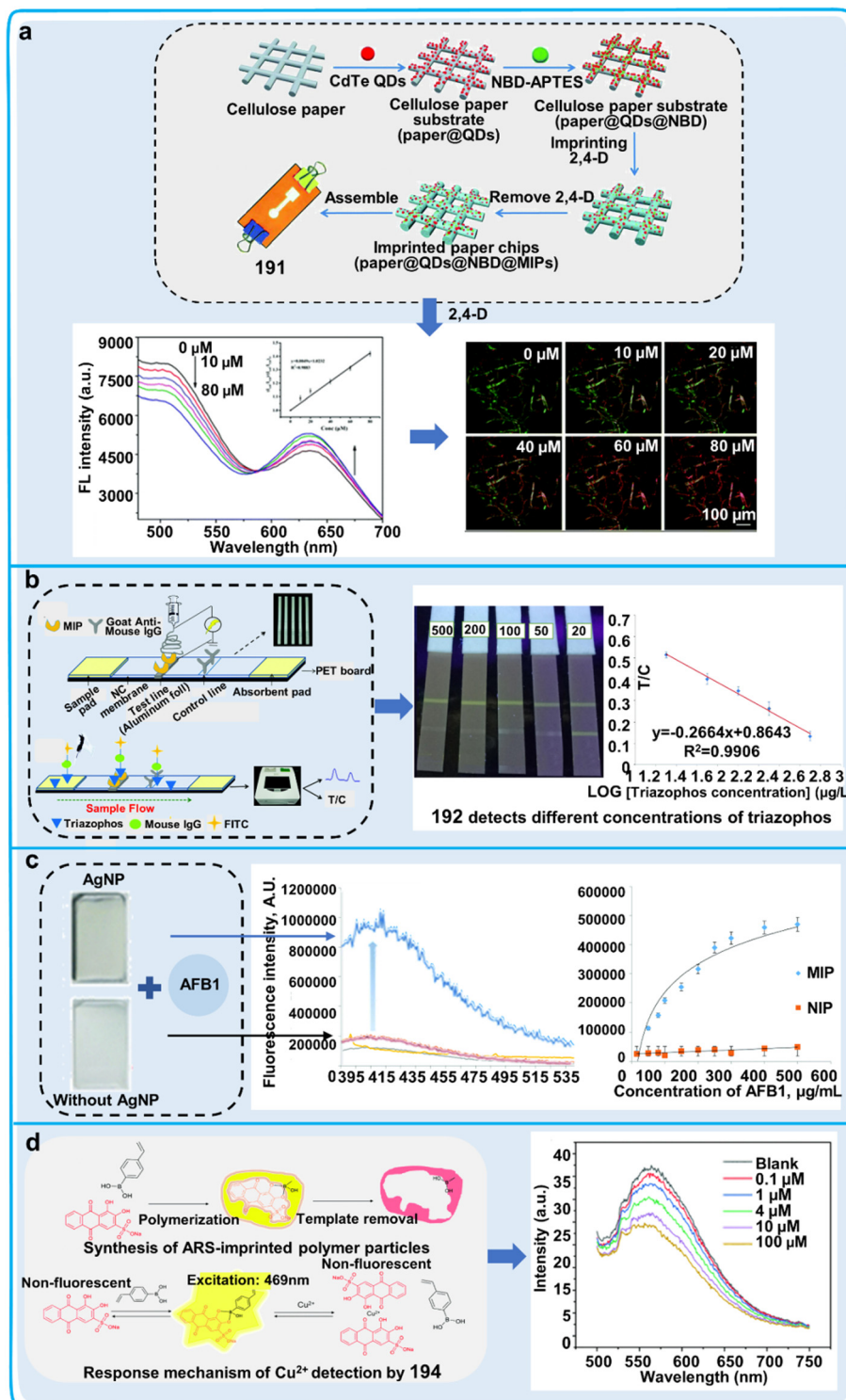
7072 | *Chem. Soc. Rev.*, 2024, **53**, 6992–7090

This journal is © The Royal Society of Chemistry 2024

Fig. 57 Extraction mechanism and data tracing of molecularly imprinted polymers employed in pesticides, metal ions and toxin detection. (a) Procedure for fabricating **191** and its fluorescence spectra and images for the detection of 2,4-D. Reproduced from ref. 297 with permission from The Royal Society of Chemistry.[297] Copyright © 2020, The Royal Society of Chemistry. (b) Structure of test strips of **192**, competitive fluorescence detection process for triazophos, images and calibration curves of test strips for the determination of distinct concentrations of triazophos.[298] Reproduced from ref. 298 with permission from The Royal Society of Chemistry. Copyright © 2020, The Royal Society of Chemistry. (c) Fluorescence spectra of AFB1 detected by silver-doped and non-silver-doped **193**. Reproduced from ref. 299 with permission from The Royal Society of Chemistry.[299] Copyright © 2022, The Royal Society of Chemistry. (d) Synthesis process of **194**-imprinted polymer particles and their principle and fluorescence spectra for the detection of Cu^{2+}.[300] Reproduced from ref. 300 with permission from The Royal Society of Chemistry. Copyright © 2022, The Royal Society of Chemistry.

This journal is © The Royal Society of Chemistry 2024

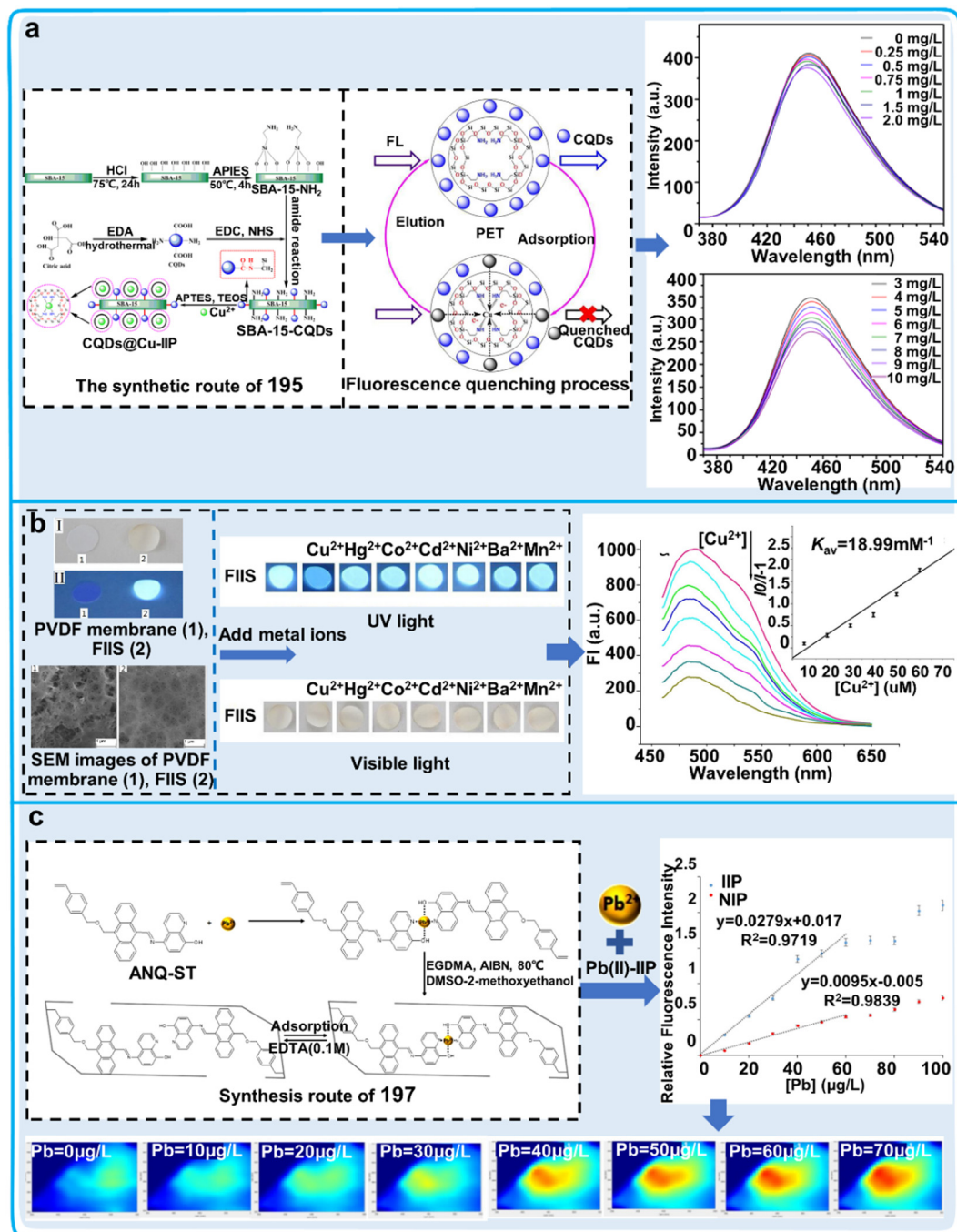*Chem. Soc. Rev.*, 2024, **53**, 6992–7090 | **7073**

Fig. 58 Detection process and data graphs of ion imprinted polymers for the detection of metal ions. (a) Synthesis route of **195** and its quenching process and fluorescence spectrum for detecting Cu^{2+}.[301] Copyright © 2021, Multidisciplinary Digital Publishing Institute. (b) Images of **196** testing different metal ions under visible and UV light, and fluorescence spectra of 196 detecting Cu^{2+}.[302] Copyright © 2021, Elsevier. (c) Synthesis route of **197**, and its fluorescence curves and images for the detection of Pb^{2+}.[303] Copyright © 2020, Elsevier.

FIIS (chemosensor **196**). The fluorescence emission intensity of **196** decreased with an increase in the incorporation of copper(II) ions (Fig. 58b).[302] The Cu^{2+} concentration in river water samples was effectively determined using **196**, which possessed a high degree of selectivity and sensitive recognition capacity for Cu^{2+}. This study indicated that 1,8-naphthalimide can serve as versatile building block, implying that other fluorophores such as

coumarin and rhodamine can also have the same function. In another ion-imprinted polymer, anthracene-coupled styrene motifs and 5-amino-8-hydroxyquinoline served as significant chemical units in a precipitation copolymerization process to create a novel Pb(II)-fluorescent IIP (chemosensor **197**). **197** demonstrated a remarkably selective fluorescence switching property for Pb^{2+} and high fluorescence enhancement upon the

7074 | *Chem. Soc. Rev.*, 2024, **53**, 6992–7090

This journal is © The Royal Society of Chemistry 2024

binding of Pb^{2+} (Fig. 58c), which proved its successful quantitative detection of Pb^{2+} in environmental water. Compared with normal fluorescent chemosensors, the imprinted polymer showed more selective properties for detecting ions in the environment.[303] Ion imprinted polymers are similar to molecularly imprinted polymers, which they have high specificity for the analytes used as templates.

Overall, MIPs/IIPs have become popular as pesticide sensors due to their extremely high selectivity for target analytes and their durability in a variety of environments. However, they still have certain drawbacks, as follows: (i) the preparation of MIPs/IIPs is still difficult and how to prepare these two types of imprinted polymers at lower cost and higher yields should be investigated. (ii) The specific recognition ability caused by the template may be lost after preparation and optimizing the preparation process of MIPs/IIPs will be an important condition to promote their application.

5.1.4 Other special fluorescent polymers. In addition to the above-mentioned three structural types of fluorescent polymers, combining fluorescent groups with proteins by means of hydrogen bonding to create supramolecular fluorescent polymers can effectively detect pesticide residues in agricultural products, soil, and water. In one example, FD@ALB (chemosensor **198**), a new supramolecular sensor based on albumin (ALB) with a dual-mode response to chlorpyrifos, was designed and prepared. **198** showed a good linear concentration range of 0–200 μM with an

LOD of 0.57 μM. It was combined with a smartphone, and then was used to perform the on-site detection of chlorpyrifos in a wide variety of environmental samples, including food, water, and soil samples, even at low concentrations (Fig. 59a).[304] Another article reported the synthesis of a hydrazino-naphthalimide-functionalized chitosan (NH-Chitosan) polymer (chemosensor **199**), which was conducted through a chemical transformation process. **199** exhibited a turn-on fluorescence response by means of the particular chemical interaction between the incorporated hydrazino-naphthalimide functionalities and HCHO. Compared to small molecule chemosensors, the NH-chitosan random helical polymer chains in **199**, which were derived from biopolymerized chitosan, had the ability to aggregate the marginally dilute concentration of HCHO surrounding the polymeric chains *via* minimal supramolecular affinities. The rapid chemical reaction between the hydrazino-naphthalimide groups and HCHO achieved an ultra-fast yellow fluorescent response to HCHO, and then realized the detection of HCHO in water (Fig. 59b).[305] The development of new fluorescent polymers that do not belong to the traditional classification can sometimes get unexpected new detection modes, fast detection capabilities and high applicability.

In summary, the advantages of using these combinatorial systems include a variety of detection response modes and adaptability to a wide range of field environments. Therefore, there is great potential for the progression of novel combinatorial patterns and superior-performing fluorescent polymers.
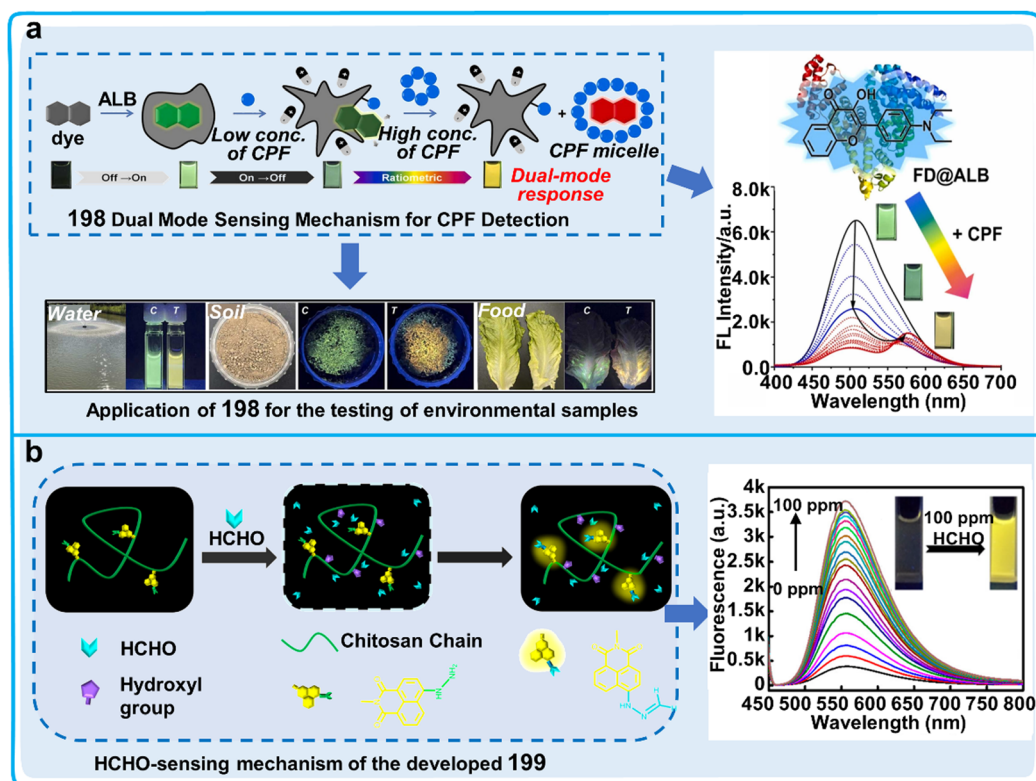

Fig. 59 Detection process, data graphs and practical application diagrams of other special fluorescent polymers for the detection of pesticides and toxins. (a) Dual-mode sensing mechanism of 198 for CPF and its titration spectrum for CPF and application to detect CPF in samples.[304] Copyright © 2023, Elsevier. (b) Sensing mechanism and titration spectra of HCHO by 199.[305] Copyright © 2018, the American Chemical Society.

This journal is © The Royal Society of Chemistry 2024

Chem. Soc. Rev., 2024, **53**, 6992–7090 | **7075**

5.2 Hydrogelator systems

The self-assembling network structures present in supramolecular hydrogels are developed by the non-covalent connections in hydrogelators.[306] Supramolecular fluorogenic hydrogels generate fluorescence with an autonomic assembly procedure to generate potent nanoscale architectures for visualization.[307] In comparison to other types of chemosensor imaging, fluorescent supramolecular hydrogels have the advantages of versatility, biocompatibility, accessibility, low damage and high stability, and have been used in the fields of bioimaging and environmental monitoring (Table 12).[307,308] In the following section we introduce the applications of supramolecular fluorescent hydrogels in monitoring the living environment of plants, including detecting hazardous heavy metals in their surrounding environment and pesticide residues in fruits (Fig. 60).

There are some examples of the preparation of fluorescent supramolecular hydrogels that have been instrumental for assessing heavy metals in environmental water samples. A novel bifunctional AIE hydrogel (NDG, chemosensor **200**) was established, which was ingeniously devised through a straightforward host–guest interaction. This involved a 1-naphthaleneacetic hydrazide amino-derivatized tripodal hydrazide, acting as the molecular host (NTS), and a tri-(pyridine-4-yl)-functionalized trimesoyl amide functioning as the guest (DTB) (Fig. 61a).[309] Researchers delved into the cation-responsive attributes by incorporating and disseminating various metal ions in water into **200** and only the presence of Fe^{3+} caused the quenching of the fluorescence of this sensor. Moreover, with an increase in the Fe^{3+} dosage (0–0.45 equiv.), the emission intensity corresponding to the fluorescent response of **200** showed an impressive degree of linearity along the titration curve, and the fluorescence emission band decreased at 470 nm with an LOD of 5.33×10^{-9} M. Meanwhile, **200** exhibited bifunction for the removal and detection of metal ions and this chemosensor could be applied to selectively identify Fe^{3+} in real water samples. Another example involved the development of an expedient gelator (chemosensor **201**), which was prepared using a phenylalanine derivative augmented with a quinoline ring harbouring a single N atom (3-phenyl-2-[(quinolin-2-ylmethyl)-amino]-propionic acid, namely, 2-QF) (Fig. 61b).[310] The impact of diverse metallic ions on the photoluminescence of **201** was assessed, which revealed that the visible fluorescence response to Zn^{2+} of **201** was perceivable to the naked eye under UV radiation with a wavelength of 365 nm. Notably, the fluorescence intensity of **201** was substantially augmented by approximately 230-fold upon incorporating Zn^{2+}, whereas the systems of **201**-Cd or **201**-Pb exhibited only a marginal increase in fluorescence intensity. These findings suggested that **201** exhibits potential as a superior sensor for the detection of Zn^{2+}. **201** showed favorable membrane permeability, indicating that it can be applied for detecting metal ions in the environment and plants. Meanwhile, supramolecular fluorescent hydrogels have been used to detect heavy metal contaminants in plants. It was reported that fluorescent hydrogel-coated sensing gloves were created for monitoring the Hg^{2+} content in plants based on chemosensor **202** coated with a flexible paper/textile film (Fig. 61c).[311]

Table 12 The applications of hydrogelator system-based fluorescent sensors for monitoring the health and environment of plants

Chemosensor	Name	$\lambda_{ex}/\lambda_{em}$ (nm)	Solvents	Target analytes	Limit of detection (LOD)	Applications	Ref.
200	NDG	300/470	$V_{DMSO}:V_{H_2O} = 3.3:6.7$	Fe^{3+}	5.33 nM	Detecting Fe^{3+} in water via the form of fluorescence quenching	309
201	2-QF	317/377	Aqueous solutions	Zn^{2+}	0.145 μM	Detecting Zn^{2+} in water via the form of fluorescence enhancement	310
202	FHCP	365/501	Aqueous solutions	Hg^{2+}	8.00 nM	Detecting Hg^{2+} in plants and water via the form of fluorescence color change	311
203	GQDs/Enz/Gels	360/465	Phosphate buffer solution (pH = 8)	Dichlorvos	26.1 nM	Detection the concentration of dichlorvos in plants via the form of fluorescence enhancement	312
204	Cyclo-WW+Zn(II)	450/550	Aqueous solution	Lambda cyhalothrin	2.90 μg L^{-1}	Detected Lambda cyhalothrin in plants via the form of fluorescence quenching	313

7076 | Chem. Soc. Rev., 2024, **53**, 6992–7090

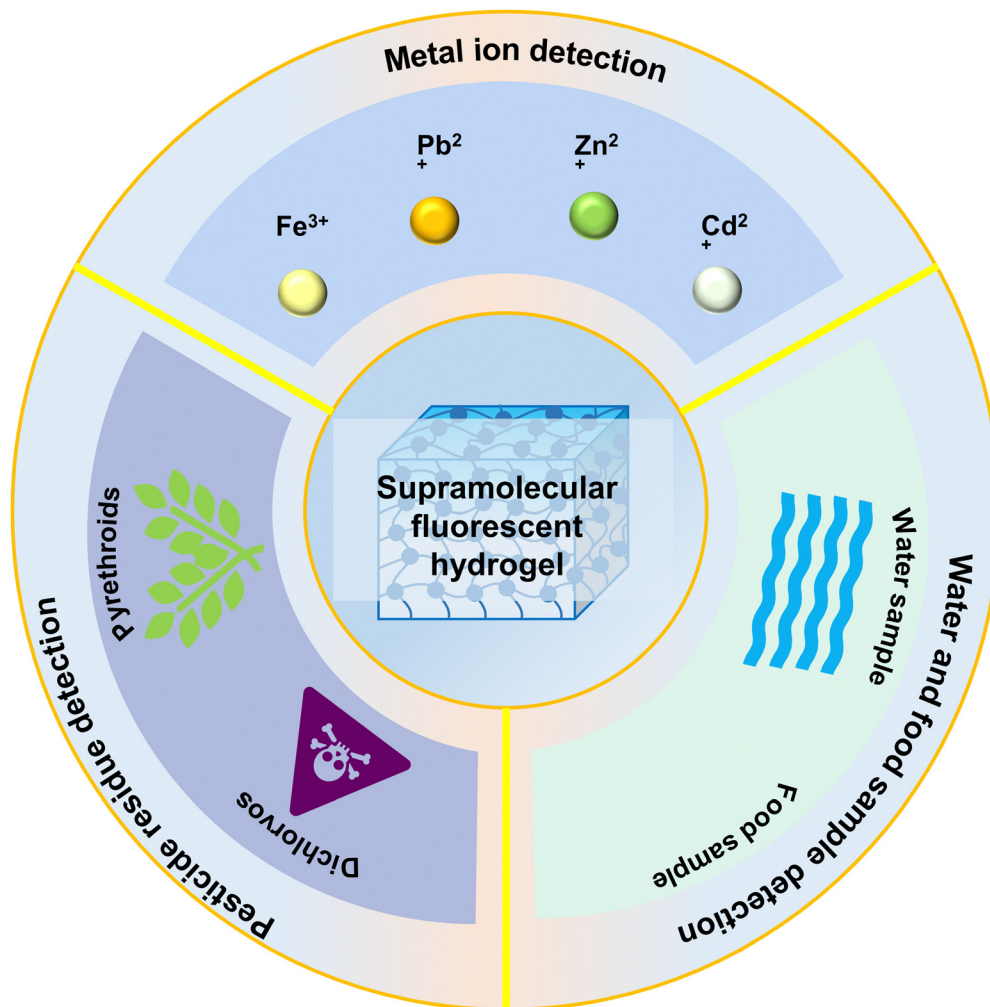This journal is © The Royal Society of Chemistry 2024

Fig. 60 Application of supramolecular fluorescent hydrogel in monitoring the living environment of plants and fruit safety. Supramolecular fluorescent hydrogel can be used to monitor plant health by detecting the heavy metals in the environment, pesticide residues in plants and pollution in water and fruit.

The results showed color changes from green to blue with an increase in the concentration of Hg^{2+}. **202** showed remarkable analytical selectivity for Hg^{2+} with an LOD of 2.61×10^{-8} M. **202** was used to test Hg^{2+} in potherb and *Canna* leaf, and the measured results showed good consistency. Supramolecular hydrogels are not the only potential candidates for the evolution of a new class of digital apparatus, but also aid in the synthesis of smart supramolecular polymer sensors with superior fluorescent attributes. If widely used, supramolecular hydrogels can discover and help remove heavy metal ions in water samples and foods.

In addition to detecting heavy metals, researchers have developed supramolecular fluorescent hydrogels for detecting trace amounts of pesticides in agricultural products and the environment. It was reported that researchers synthesized new fluorescent hybrid materials comprised of enzymatic entities affixed to an L-phenylalanine-derived bis(urea) supramolecular hydrogel platform coupled with graphene quantum dots (GQDs/Enz/Gels, chemosensor **203**) for the qualitative analysis of organophosphates (Fig. 62a).[312] AChE induces the degradation

of acetylcholine (ACh), yielding choline. Subsequently, choline is incessantly oxidized by choline oxidase (ChOx), leading to the production of H_2O_2 and culminating in photochemical suppression of the integrated gel assemblies. Upon exposure to UV radiation at 365 nm, a substantial enhancement in visible fluorescence image intensity was observed for **203** impregnated with dichlorvos as the analyte concentration increased from 1×10^{-6} to 1×10^{-3} M. The anti-cholinergic potency of dichlorvos against AChE demonstrated a linear response in the range of 1.25×10^{-8} to 1.25×10^{-4} M, indicating that the low molecular weight hybrid hydrogels can also have high sensitivity and stability for detecting pesticides. Considering that AChE and ChOx can be combined in **203** as a signaling unit, this chemosensor can be developed as an enzymatic activity detection kit. Another visual platform (chemosensor **204**) was constructed using a cyclo-ditryptophan (cyclo-WW) + Zn(II)-based photoluminescent hydrogel, which showed good ability to detect lambda cyhalothrin (LC) (Fig. 62b).[313] In the process of oxidative PET, post formation of a coordination complex between the surface group of **204** and LC, this complex triggered non-
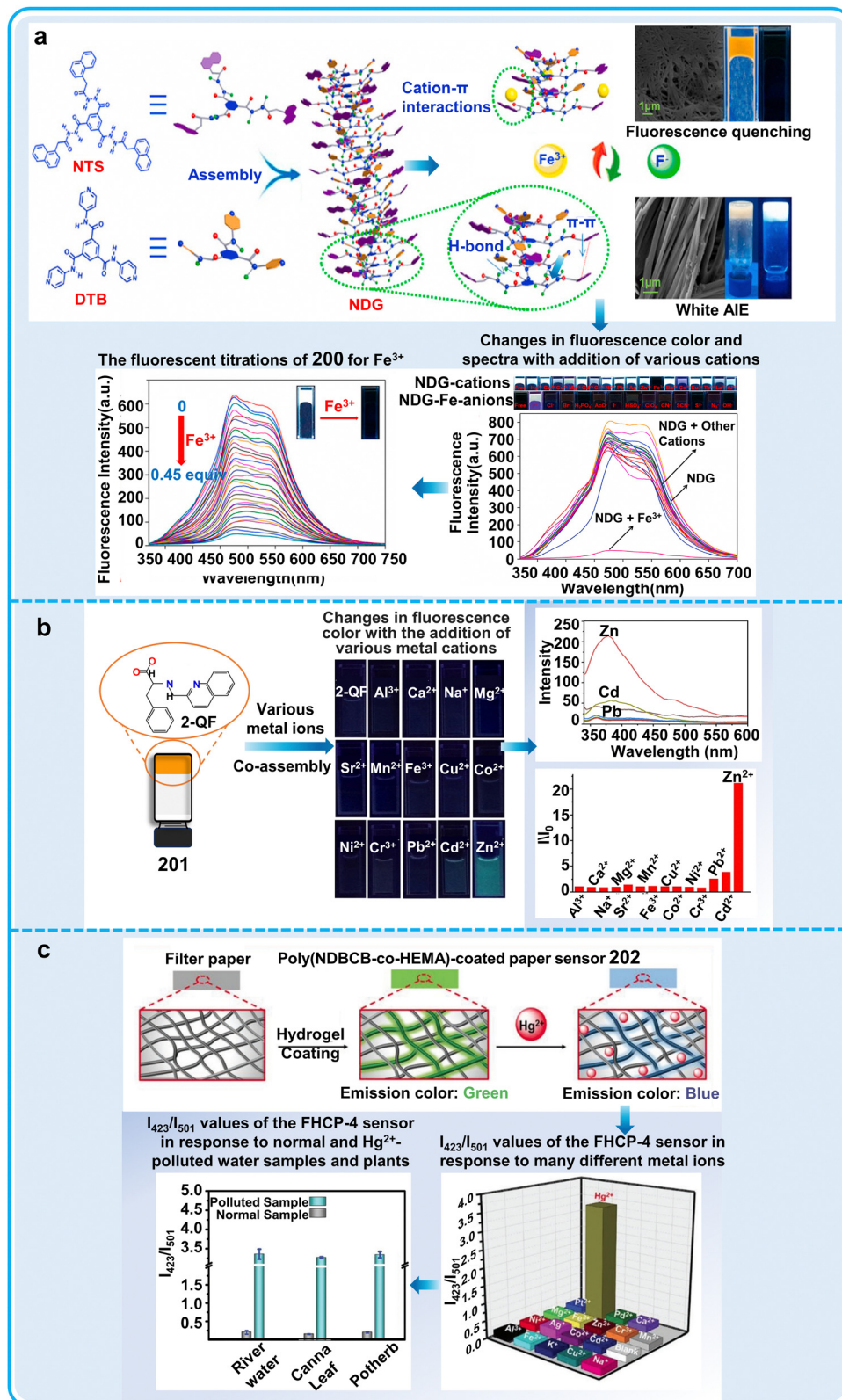
This journal is © The Royal Society of Chemistry 2024

Chem. Soc. Rev., 2024, **53**, 6992–7090 | **7077**

Fig. 61 Detection process, data graphs and practical application diagrams of supramolecular fluorescent hydrogels system for detecting ions in plant surroundings. (a) Construction of 200 and the possible mechanisms, as well as the fluorescence effect and data statistics about the sensing of Fe^{3+} and other cations.[309] Copyright © 2020, Elsevier. (b) Chemical structure of 201 and the fluorescence effect and data statistics of Zn^{2+} and other metal ions.[310] Copyright © 2020, Elsevier. (c) Preparation of the fluorescent hydrogel-coated paper (FHCP, 202) for Hg^{2+} detection in water and food samples.[311] Copyright © 2020, WILEY-VCH Verlag GmbH.

7078 | *Chem. Soc. Rev.*, 2024, **53**, 6992–7090

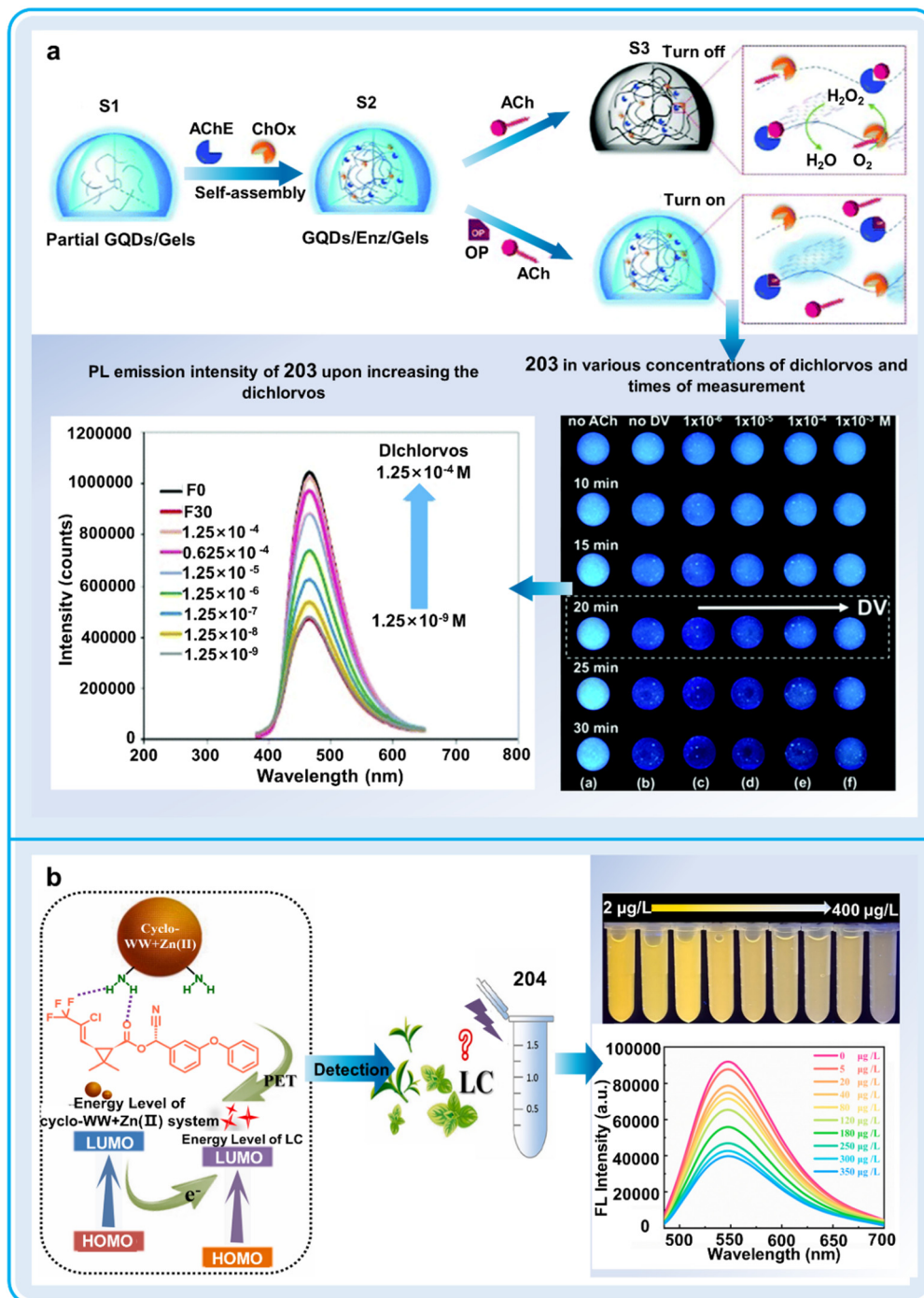This journal is © The Royal Society of Chemistry 2024

Fig. 62 Detection process, data graphs and practical application diagrams of supramolecular fluorescent hydrogel system for the detection of pesticides in the living environment of plants. (a) Proposed mechanism of hybrid 203 for organophosphate pesticide detection and the fluorescence effect and data statistics after adding dichlorvos.[312] Reproduced from ref. 312 with permission from The Royal Society of Chemistry. Copyright © 2021, The Royal Society of Chemistry. (b) Schematic illustration of the sensing mechanism and the fluorescence effect of 204 and data statistics after adding lambda cyhalothrin.[313] Copyright © 2022, Elsevier.

radiative emission upon relaxation from the excited electronic state into the ground state. Under these conditions, **204** acted as an electron donor, providing electrons to the electron acceptor LC. When subjected to LC, the intensity of the yellow luminescence emitted by **204** progressively diminished with an increase in the concentration of LC. **204** exhibited outstanding precision and

robust stability when assessing pesticides in actual samples, which can provide guidance for developing polypeptide-based biosensors. The above-mentioned studies developed a miniature hybrid hydrogel confined to a glass slide, or developed a smartphone-assisted sample-to-answer analyzer, which can be used as a rapid, convenient, and high-throughput sensor for the detection of pesticides.

This journal is © The Royal Society of Chemistry 2024

Chem. Soc. Rev., 2024, **53**, 6992–7090 | **7079**

In conclusion, the environmental friendliness and high sensitivity of supramolecular fluorescent hydrogels make these chemosensors suitable for detecting heavy metals in the environment and pesticide residues in plants and food. However, there are also some challenges that need to be considered, as follows: (i) modification of the backbone structure frequently perturbs the stability of the hydrogel networks and (ii) the leakage of fluorescent materials combined with the accumulation of chromophores may induce a reduction in optimum emission intensity and potential quenching of fluorescence. Therefore, improving the stability of supramolecular fluorescent hydrogels will be an important aspect to promote their practical application.

6. Analysis of fluorescent chemosensor data

6.1 Techniques for fluorescent chemosensor data analysis

The processes for dealing with the data obtained from fluorescent chemosensors mainly involve two steps, image capture and image processing. High-quality and resolution fluorescence images can maintain the integrity, accuracy and repeatability of the results from microscopy. High precision analytical techniques and statistically rigorous quantification methods are frequently required to gain enhanced comprehension of the

intricate biological mechanisms for governing plant health and monitoring the living environment of plants. In the following section, we describe these two steps in detail.

For image capture, fluorescence microscopy, including fluorescence microscopy, confocal laser scanning microscopy (CLSM), two-photon fluorescence microscopy, fluorescence lifetime imaging microscopy (FLIM), stimulated emission depletion (STED), single molecule localization microscopy (SMLM), structured illumination microscopy (SIM), and total internal reflection fluorescent microscope (TIRFM) are frequently used (Fig. 63a). (1) Fluorescence microscopy can only visualize pre-sliced specimens and does not have the potential of optical slicing. In the case of three-dimensional samples thicker than 2 μm, the whole sample fluoresces, causing defocused emissions, obscuring the focal plane detail and reducing the image contrast. However, it also has some advantages such as the utilization of a mercury arc lamp or xenon lamp to offer a comprehensive spectral range spanning the UV, visible and NIR bands.[314] (2) CLSM represents an alternative technique for recovering thin fluorescent sections through optical isolation of fluorescence emission within the imaged plane, facilitating the visualization of plant cells in thick sections at high resolution. However, despite point-scan imaging, the imaging speed of CLSM is slow due to the limited laser excitation, narrow frequency band, and high intensity laser radiation.[315] (3) Two-photon fluorescence microscopy allows non-destructive examination of biological
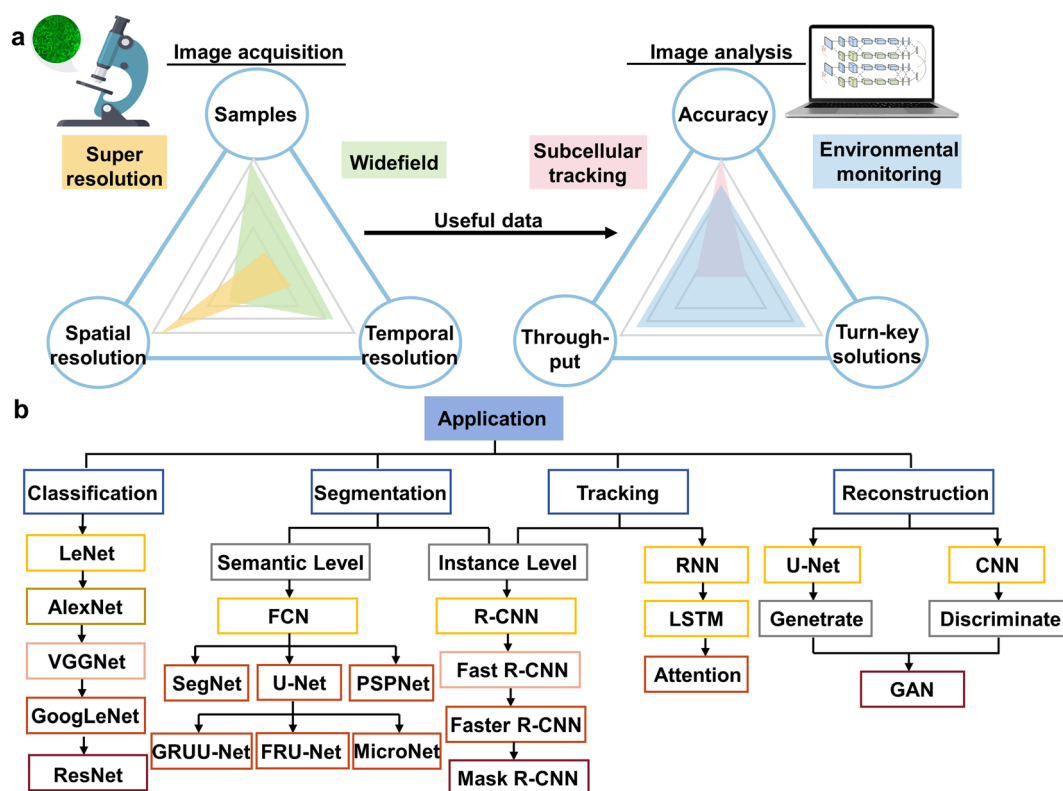

Fig. 63 Potential methods for the analysis of fluorescent chemosensor data from monitoring the health and living environment of plants. (a) Image acquisition and analysis approaches for the above-mentioned areas. (b) Various networks are constructed according to the specific processes in image analysis. © 2021, Elsevier Ltd.

7080 | Chem. Soc. Rev., 2024, 53, 6992–7090

This journal is © The Royal Society of Chemistry 2024

specimens in three-dimensions with submicron precision. Excitation of two-photon fluorophores originates from dual photon absorption simultaneously.

This distinctive emission mechanism possesses several advantages such as diminished sample photodegradation, reduced photoblinking, improved penetrative depth, and producing superior contrasting images.[316] (4) FLIM, a microscopy strategy dependent on the nanosecond fluorescence lifetime of molecules, has gained immense popularity due to its superior sensitivity to the environment and variations in the structure of molecules. This technology shows advantageous characteristics such as identifying spectrally overlapping fluorophores by the fluorescence lifetime, detecting fluctuations within fluorophore molecular environments, measuring quenching dynamics, and executing self-referenced assessment. However, FLIM analysis needs technical proficiency and has high computational costs, extensive photon usage for fluorescence lifetime determination, and susceptibility to multiple factors ranging from molecular interactions/binding activities to environmental conditions (temperature, viscosity and pH).[317] (5) In the case of SIM, a collection of complex patterns of intensity is utilized to illuminate the targeted object, thereby facilitating the reconstruction of an accurate image of the subject material. Its advantages include straightforward sample processing, swift imaging rate, expansive imaging field, and widespread adoption in biology. However, SIM displays low tissue penetration depth, restricting its application in single-cell imaging due to the substantial scattering caused by its low excitation power density.[318] (6) SMLM is an imaging technique capable of overcoming the diffraction obstacle to yield super-resolution images. The random switching between on and off states is followed by the collection of substantial photons to computationally simulate and merge the locations of all individually activated fluorophores to generate a super-resolution image. However, this technology is associated with some challenges such as complex sample processing procedures, fluorophore photobleaching, and substantial computational requirements.[319] (7) STED is a novel enhancement of confocal microscopy, which is regarded as the primary far-field super-resolution imaging technology applicable to cell observation. Its proficiency in cell imaging and three-dimensional chromatographic capacity have attracted considerable attention in biological research. Nevertheless, these advantages are counterbalanced considering its potential cellular phototoxicity, photobleaching, and advanced technical proficiency.[320] (8) TIRFM is complex optical technology, enabling the activation of fluorophores within an exceptionally thin axial zone, and then producing a satisfactory S/N ratio. By exploiting the inherent characteristics of an evanescent wave or field confined to a specific specimen vicinity immediately adjacent to the interface between two media possessing different refractive indices, it facilitates the comprehensive observation of the entire wide field rather than utilizing point-by-point scanning. The fundamental limitation of TIRFM as an innovative detection tool in biochemical and chemical research is its inability to utilize selective fluorescent chemosensors specifically.[321] In short, each of the above-mentioned eight primary techniques has

advantages and limitations, indicating that we should select the optimal equipment depending on the sample under investigation and the associated scientific requirements.

The traditional methodologies for processing microscopic images mainly include morphological differentiation, image fusion, edge detection, classification, region growing, and feature extraction. These techniques typically necessitate the expertise of computational experts, who are scarce within plant science and necessitate complex computational processes. Additionally, traditional fluorescence microscopy images consistently exhibit relatively diminished resolution and inferior S/N ratio owing to the restraints imposed by imaging systems and the restrictions of diffraction. Consequently, conventional image processing methodologies are often insufficient for efficient data interpretation.[322] Deep learning (DL), a novel approach representing data learning, is a significant segment of artificial intelligence (Fig. 63b).[323] For microscopic image analysis, scientists are progressively incorporating DL into various complex challenges such as cellular components, subcellular structures, tissue architectures, and the diversity of environment. Specially, DL in images processing involves four main steps including image classification, image segmentation, target tracking and super-resolution reconstruction.[324] (1) Classification. Establishing classification tools capable of distinguishing diverse pollutants within the living environment of plants, specific cell stages or subcellular structures can provide important insights into plant health. This may enable farmers or chemical engineers to adopt effective strategies for managing plant health. Presently, convolution neural network (CNN), including ResNet, AlexNet, and LeNet, are prevalent in classification procedures. Typically, initial DL-based classification exhibits higher accuracy and greater efficiency compared to its conventional counterparts. (2) Segmentation. Establishing boundaries around regions of interest is an indispensable phase in microscopic image analysis, facilitating focus on data-rich areas of significance. Intracellular compartment segmentation supplies quantifiable data regarding cell structure and functionality. Dl-Based segmentation methodologies are categorized into two types, instance-level segmentation and semantic-level segmentation, depending on the incorporation of a fully interconnected layer. Prioritized semantic-level and instance-level segmentation algorithms originate from the U-Net and R-CNN models, respectively. (3) Tracking. Assessing the viscosity of cells, infection of pathogens or distribution of pollutants within the living environment of plants is fundamental for discerning significant plant health signals. The networks employed for localization predominantly utilize the methodologies of recurrent neural networks (RNNs). With advancements in long short-term memory (LSTM), issues related to gradient explosions and gradient vanishing have been effectively managed. Consequently, data such as the prevalence of environmental pollutants, early plant health diagnosis, or the interaction between plant-environment interactions can be more accurately recorded. (4) Reconstruction. Image reconstruction involves generating a two-dimensional or three-dimensional visualization from fragmented or incomplete data. The discipline of microscopy image interpretation includes techniques such as super-resolution reconstruction, denoising, and three-dimensional reconstruction to generate high-quality and

This journal is © The Royal Society of Chemistry 2024

Chem. Soc. Rev., 2024, **53**, 6992–7090 | 7081

comprehensive images. DL-based image restoration techniques can facilitate the rapid capture of photosensitive specimens and promote high-quality and long-term dynamic observation of plants. Methods integrating GANs have been employed to facilitate super-resolution imaging across various microscope platforms, enabling the conversion of diffraction-limiting signals into super-resolution images. Furthermore, recent developments in augmented intelligent microscopy and proficiency in deep learning technologies are beneficial for managing plant-environment interactions in sustainable agriculture.

6.2 Networking of fluorescent chemosensor data

The spatial and temporal complexity of the health and surrounding ecosystems of plants pose substantial challenges to accurately enforce plant health management. Despite the extensive reliance on remote sensing techniques or sophisticated mass spectrometry chromatography tandem methods, they are limited by the spatial and temporal resolution, labor intensive and resource consuming. As illustrated in Fig. 64, fluorescent chemosensors can be effectively employed to monitor the soil environment, the quality of irrigation water and plant health in a timely manner and accurately. Firstly, fluorescent chemosensors can detect moisture, pesticides, nutrients, heavy metals, microorganism diversity and ions to evaluate the soil environment. Soil functioning as a living ecosystem can offer various services such as food and fibrous yield, water quality and supply, managing pest and disease, modulating the atmospheric composition, climate regulation and biodiversity conservation. Wholesome soil produces robust plants, significantly contributing to plant proliferation and maturity. Any pollution of the soil with detrimental substances such as inorganic pollutants and organic toxins can disrupt plant assimilation

and metabolic activities, resulting in impaired plant growth and developmental disorders. Meanwhile, soil organic matter functions as an indispensable nutrient source for plants, providing crucial materials for maintaining soil texture, regulating pH, and storing nutrients. Insufficient soil organic matter can hinder plant growth and potentially lead to nutritional deficiencies. Secondly, fluorescent chemosensors facilitate the continuous monitoring of irrigation water such as heavy metals, pesticides, and ions, which have a direct impact on plant growth. Irrigation is crucial in addressing food insecurity and water scarcity issues. High-quality irrigation water can provide sufficient water together with nutrients that can promote plant physiological metabolism, facilitate robust root systems evolution, and enhance crop vitality. In contrast, low-quality irrigation water can decrease plant nutrient assimilation capabilities, facilitating the transfer of damaging pathogens and pests, thereby increasing plant disease incidence. For example, heavy metals in irrigation water are found to be assimilated by plants, and subsequently accumulated across multiple plant tissues, which not only influence plant root growth and above-ground biomass production but also pose potential health risks to humans. Thirdly, fluorescent chemosensors offer an invaluable tool to evaluate plant health by evaluating the nutrient uptake dynamics, signaling molecule synthesis, cell components, metabolites, and food quality. For example, hormones serve as critical signaling molecules and are essential for governing numerous plant physiological processes, such as growth, metabolism, organogenesis, reproduction and stress resistance, which significantly affect plant growth and survival. A comprehensive array of metabolically diverse molecules with diverging structural and functional attributes, serving a myriad of roles in plant health, by modulating plant resilience amidst persistently
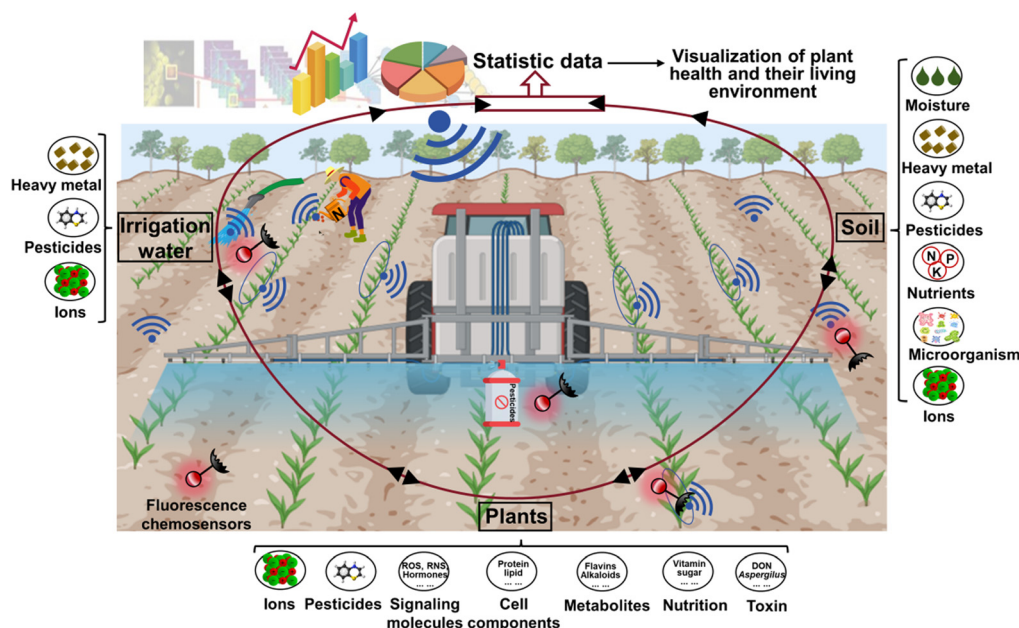

Fig. 64 Fluorescent chemosensor networks for monitoring the health and living environment of plants. Fluorescent chemosensors can monitor the health status and living environment of plants. Then the collected data will be analyzed and provide accurate suggestions for plant health regulation.

7082 | *Chem. Soc. Rev.*, 2024, **53**, 6992–7090

This journal is © The Royal Society of Chemistry 2024

fluctuating environmental variables together with both non-living stressors and biological aggressions. Therefore, the use of fluorescent chemosensors provides real-time data and a feasible solution to improve our capability to manage plant health.

7. Conclusions and outlook

This work provides a comparatively comprehensive summary and analysis of studies during the last decade towards the design of fluorescence chemosensors including small-molecule, nano- and supramolecular-chemosensors in regulating plant health. Chemosensors can provide a better understanding of the plant health status under abiotic and biotic stresses, and different nutrient utilization, as well as their living environments. We described the structural features of these chemosensors, their fluorescence characteristics, response mechanism and the intrinsic multi-function. This fluorescent technique will contribute to the enhanced comprehension of the complex interdependence among the environment, human behavior and plant health.

When initiating the detailed design processes for a state-of-the-art fluorescent chemosensor to monitor the health and surroundings of plants, it is vital to establish a connection between the fluorescence features of chemosensors and the requirements of plant health regulation. Therefore, future studies should focus on the following aspects: (1) increased emphasis must be placed on developing two-photon and NIR-II fluorescent probes. It is universally acknowledged plant imaging presents difficulties distinct from other model systems because of its robust endogenous auto-fluorescence attributed to chlorophyll in the wavelength range of 400–800 nm. The NIR laser utilized by two-photon and NIR-II fluorescent chemosensors could not only avoid the autofluorescence within plant tissues, but also achieve superior imaging resolution compared to traditional fluorophores. (2) To enhance comprehension of the distribution, translocation and metabolism of signaling molecules under biotic or abiotic stresses, fluorescent chemosensors should be endowed with sub-organelle targeting potential including mitochondria and plasma membrane.

By pinpointing their location at the subcellular level, the elucidation of signaling molecules involved in plant health can be enhanced. (3) Fluorescent nano-chemosensors constructed from QD, COF and MOF materials have made great progress in detecting agricultural pollutants with good recyclability. Future endeavors should concentrate on minimizing the nano dimensions of the aforementioned materials for improving the functionality within plant tissues such as molecular imaging, pesticide release, and labeling signaling molecules. (4) Presently, existing detection methods for plant health are primarily concentrated on individual plant tissues, and thus implementing comprehensive field testing utilizing portable smart devices poses a novel hurdle in future investigations. (5) Further studies should devise super-resolved fluorescent chemosensors to determine the subcellular distribution and transportation mechanism of HPPD in plants to monitor the plant health condition under abiotic stress. Meanwhile, it will serve as an useful tool for *in vivo* and *in vitro* inhibitor screening. The inhibitors can compete with the binding sites of proteins with fluorescent chemosensors. When the binding affinity of inhibitors with proteins surpasses their affinity towards fluorescent chemosensors, they may be regarded as highly effective inhibitors. (6) AI should be applied in processing fluorescence images by improving image quality, extracting relevant information and analyzing data. Compared with the vision of professionals, AI technologies have some advantages such as improving image quality with reducing noise, correcting illumination, enhancing contrast, precise analysis by segmentation images, identification of interesting objects, tracking dynamics of biological processes by analyzing temporal changes in images, and comprehensive data analysis by integrating fluorescence images data with other types of data including genomic or proteomic data.

Conflicts of interest

There are no conflicts to declare.

Acknowledgements

Notes and references

1 J. Pretty, *Science*, 2018, **362**, eaav0294.
2 Z. L. Cui, H. Y. Zhang, X. P. Chen, C. C. Zhang, W. Q. Ma, C. D. Huang, W. F. Zhang, G. H. Mi, Y. X. Miao, X. L. Li, Q. Gao, J. C. Yang, Z. H. Wang, Y. L. Ye, S. W. Guo, J. W. Lu, J. L. Huang, S. H. Lv, Y. X. Sun, Y. Y. Liu, X. L. Peng, J. Ren, S. Q. Li, X. P. Deng, X. J. Shi, Q. Zhang, Z. P. Yang, L. Tang, C. Z. Wei, L. L. Jia, J. W. Zhang, M. R. He, Y. A. Tong, Q. Y. Tang, X. H. Zhong, Z. H. Liu, N. Cao, C. L. Kou, H. Ying, Y. L. Yin, X. Q. Jiao, Q. S. Zhang, M. S. Fan, R. F. Jiang, F. S. Zhang and Z. X. Dou, *Nature*, 2018, **555**, 363–366.
3 A. Muñoz-Sáez and L. L. R. Renwick, *Nature*, 2022, **609**, 32.
4 P. K. Rai, S. S. Lee, M. Zhang, Y. F. Tsang and K. H. Kim, *Environ. Int.*, 2019, **125**, 365–385.
5 F. Martinelli, R. Scalenghe, S. Davino, S. Panno, G. Scuderi, P. Ruisi, P. Villa, D. Stroppiana, M. Boschetti, L. R. Goulart, C. E. Davis and A. M. Dandekar, *Agron. Sustainable Dev.*, 2015, **35**, 1–25.
6 Y. Fang and R. P. Ramasamy, *Biosensors*, 2015, **5**, 537–561.
7 P. Li, Y. Y. Chen, Q. R. Xie, Y. Z. Xu, Z. Li, Y. Li, Z. B. Yin, X. H. Zhu, H. H. Xu and X. Z. Wu, *Adv. Agrochem*, 2023, **2**, 340–348.
8 Y. L. Wu, L. J. Han, X. M. Wu, W. N. Jiang, H. Liao, Z. Xu and C. P. Pan, *Adv. Agrochem*, 2022, **1**, 113–124.

This journal is © The Royal Society of Chemistry 2024

Chem. Soc. Rev., 2024, **53**, 6992–7090 | **7083**

9 E. M. Hamilton, S. D. Young, E. H. Bailey, O. S. Humphrey and M. J. Watts, *Environ. Sci. Technol.*, 2021, **55**, 2422–2429.

10 A. M. Mustafa, S. Angeloni, D. Abouelenein, L. Acquaticci, J. B. Xiao, G. Sagratini, F. Maggi, S. Vittori and G. Caprioli, *Food Chem.*, 2022, **367**, 130743.

11 X. H. Li, X. H. Gao, W. Shi and H. M. Ma, *Chem. Rev.*, 2014, **114**, 590–659.

12 X. G. Liu, *Adv. Agrochem*, 2023, **2**, 1–2.

13 Y. B. Huang, J. Zhai, L. H. Liu, Z. Y. Shang, X. Zhang, H. Huang, B. X. Shen and G. X. Chen, *Anal. Chim. Acta*, 2022, **1215**, 339974.

14 S. Luo, R. C. Peng, Y. Wang, X. J. Liu, J. L. Ren, W. Li, Y. Xiong, S. L. Yi and Q. Wen, *Anal. Bioanal. Chem.*, 2023, **415**, 4849–4859.

15 M. Wang, K. Su, J. Cao, Y. X. She, A. M. Abd El-Aty, A. Hacımüftüoglu, J. Wang, M. M. Yan, S. H. Hong, S. B. Lao and Y. L. Wang, *Talanta*, 2019, **192**, 295–300.

16 X. B. Shi, W. Wei, Z. D. Fu, W. L. Gao, C. Y. Zhang, Q. Zhao, F. M. Dene and X. Y. Lu, *Talanta*, 2019, **194**, 809–821.

17 J. Wang, D. Q. Li, Y. X. Ye, Y. Qiu, J. W. Liu, L. Huang, B. Liang and B. L. Chen, *Adv. Mater.*, 2021, **33**, 2008020.

18 W. S. Zhang, H. D. Zhong, P. P. Zhao, A. G. Shen, H. B. Li and X. H. Liu, *Food Control*, 2022, **133**, 108591.

19 Z. Z. Gong, L. M. Xiong, H. Z. Shi, S. H. Yang, L. R. Herrera-Estrella, G. H. Xu, D. Y. Chao, J. R. Li, P. Y. Wang, F. Qin, J. J. Li, Y. L. Ding, Y. T. Shi, Y. Wang, Y. Q. Yang, Y. Guo and J. K. Zhu, *Sci. China: Life Sci.*, 2020, **63**, 635–674.

20 A. Anzano, G. Bonanomi, S. Mazzoleni and V. Lanzotti, *Phytochem. Rev.*, 2022, **21**, 503–524.

21 P. Coatsworth, L. Gonzalez-Macia, A. S. P. Collins, T. Bozkurt and F. Gueder, *Nat. Rev. Chem.*, 2023, **7**, 7–25.

22 H. Zhang, J. Zhu, Z. Gong and J. K. Zhu, *Nat. Rev. Genet.*, 2022, **23**, 104–119.

23 M. Weih, K. Hamnér and F. Pourazari, *Plant Soil*, 2018, **430**, 7–21.

24 A. Singh, S. Jones, B. Ganapathysubramanian, S. Sarkar, D. Mueller, K. Sandhu and K. Nagasubramanian, *Trends Plant Sci.*, 2021, **26**, 53–69.

25 M. Ray, A. Ray, S. Dash, A. Mishra, K. G. Achary, S. Nayak and S. Singh, *Biosens. Bioelectron.*, 2017, **87**, 708–723.

26 J. M. Roper, J. F. Garcia and H. Tsutsui, *ACS Omega*, 2021, **6**, 5101–5107.

27 L. Y. Wang, Y. L. Zou, H. Y. Kaw, G. Wang, H. Z. Sun, L. Cai, C. Y. Li, L. Y. Meng and D. H. Li, *Plant Methods*, 2020, **16**, 1–17.

28 L. Li, Q. Zhang and D. F. Huang, *Sensors*, 2014, **14**, 20078–20111.

29 B. A. Boughton, D. Thinagaran, D. Sarabia, A. Bacic and U. Roessner, *Phytochem. Rev.*, 2016, **15**, 445–488.

30 T. Wen, J. H. Li, Q. Wang, Y. Y. Gao, G. F. Hao and B. A. Song, *Sci. Total Environ.*, 2023, **899**, 165626.

31 S. Paulus, *Plant Methods*, 2019, **15**, 1–13.

32 D. Wu, A. C. Sedgwick, T. Gunnlaugsson, E. U. Akkaya, J. Yoon and T. D. James, *Chem. Soc. Rev.*, 2017, **46**, 7105–7123.

33 J. Krämer, R. Kang, L. M. Grimm, L. De Cola, P. Picchetti and F. Biedermann, *Chem. Rev.*, 2022, **122**, 3459–3636.

34 Y. Pang, M. Lu, H. Rha, W. Yang, A. Sharma, Y. Sun and J. S. Kim, *Sci. China: Chem.*, 2023, **66**, 1–14.

35 J. L. Yin, L. Huang, L. L. Wu, J. F. Li, T. D. James and W. Y. Lin, *Chem. Soc. Rev.*, 2021, **50**, 12098–12150.

36 J. Du, K. Chen, Z. Yu, Y. Qiao, J. Liu, Q. Zhai, Z. Hu, S. G. Yang, J. Li and H. Teng, *Adv. Agrochem.*, 2022, **1**, 162–173.

37 D. X. Cao, Z. Q. Liu, P. Verwilst, S. Koo, P. Jangjili, J. S. Kim and W. Y. Lin, *Chem. Rev.*, 2019, **119**, 10403–10519.

38 A. Dorlars, C. W. Schellhammer and J. Schroeder, *Angew. Chem., Int. Ed. Engl.*, 1975, **14**, 665–679.

39 D. Lancet and I. Pecht, *Biochemistry*, 1977, **16**, 5150–5157.

40 H. Zhan, Y. Wang, Z. Li, Z. Tang, J. Tian and X. Fei, *J. Phys. Chem. A*, 2021, **125**, 2866–2875.

41 Y. Y. Zhang, Y. L. Zhao, Y. N. Wu, A. Y. Zhou, Q. L. Qu, X. L. Zhang, B. Song, K. M. Liu, R. H. Xiong and C. B. Huang, *Mater. Chem. Front.*, 2021, **5**, 4981–4988.

42 Y. L. Chen, W. Yan, D. J. Guo, Y. Li, J. Li, H. Liu, L. R. Wei, N. Yu, B. Wang, Y. Zheng, M. F. Jing, J. Zhao and Y. H. Ye, *Angew. Chem., Int. Ed.*, 2021, **60**, 21934–21942.

43 Y. Tobimatsu, A. Wagner, L. Donaldson, P. Mitra, C. Niculaes, O. Dima, J. I. Kim, N. Anderson, D. Loque, W. Boerjan, C. Chapple and J. Ralph, *Plant J.*, 2013, **76**, 357–366.

44 K. Chen, M. Zhang, Y. Qi, J. Fan, X. Ma, H. L. Zhu and Y. Qian, *Analyst*, 2019, **144**, 2320–2326.

45 Y. L. Wang, F. Ding, X. S. Sun, S. J. Chen, H. R. Huang and H. Chen, *Talanta*, 2021, **234**, 122655.

46 W. Pan, L. L. Han, X. Q. Cao, S. L. Shen, X. H. Pang and Y. Zhu, *Food Chem.*, 2023, **407**, 135163.

47 H. Q. Dong, T. B. Wei, X. Q. Ma, Q. Y. Yang, Y. F. Zhang, Y. J. Sun, B. B. Shi, H. Yao, Y. M. Zhang and Q. Lin, *J. Mater. Chem. C*, 2020, **8**, 13501–13529.

48 P. Gopikrishna, N. Meher and P. K. Iyer, *ACS Appl. Mater. Interfaces*, 2018, **10**, 12081–12111.

49 G. Q. Yuan, H. Y. Ding, L. P. Peng, L. Y. Zhou and Q. L. Lin, *Food Chem.*, 2020, **331**, 127221.

50 S. Kusano, S. Nakamura, M. Izumi and S. Hagihara, *Chem. Commun.*, 2022, **58**, 1685–1688.

51 Y. K. Zhang, C. Xu, H. Sun, J. D. Ai, M. G. Ren and F. G. Kong, *Spectrochim. Acta, Part A*, 2024, **304**, 123345.

52 L. Wang, G. Wang, C. D. Shang, R. Kang and Y. Fang, *ACS Appl. Mater. Interfaces*, 2017, **9**, 35419–35426.

53 F. Liu, M. Y. Xu, X. J. Chen, Y. G. Yang, H. J. Wang and G. P. Sun, *Environ. Sci. Technol.*, 2015, **49**, 11356–11362.

54 L. Li, S. Gao, L. Yang, Y. L. Liu, P. Li, F. Ye and Y. Fu, *J. Hazard. Mater.*, 2021, **404**, 124015.

55 Y. P. Zhang, Y. Qu, Y. Q. Zhang, Y. Gao and L. Wang, *Chem. Eng. J.*, 2022, **448**, 137631.

56 X.-F. Wu, Q.-J. Ma, X.-J. Wei, Y.-M. Hou and X. Zhu, *Sens. Actuators, B*, 2013, **183**, 565–573.

57 Z. Y. Meng, J. Yin, F. Zhao, M. X. Li, Y. Zhang, Y. Y. Liang, Z. L. Wang and Y. Q. Yang, *Eur. Polym. J.*, 2021, **158**, 110705.

58 Z. Y. Meng, X. Y. Li, Y. Y. Liang, Y. X. Gu, X. Xu, Z. L. Wang, Y. Q. Yang and S. F. Wang, *Int. J. Biol. Macromol.*, 2023, **247**, 125807.

59 J. B. Grimm, A. N. Tkachuk, L. Q. Xie, H. Choi, B. Mohar, N. Falco, K. Schaefer, R. Patel, Q. S. Zheng, Z. Liu,

7084 | *Chem. Soc. Rev.*, 2024, **53**, 6992–7090

This journal is © The Royal Society of Chemistry 2024

J. Lippincott-Schwartz, T. A. Brown and L. D. Lavis, *Nat. Methods*, 2020, **17**, 815–821.

60 C. J. Liu and C. N. Scott, *Dyes Pigm.*, 2021, **196**, 109792.

61 Z. X. Han, X. B. Zhang, L. Zhuo, Y. J. Gong, X. Y. Wu, J. Zhen, C. M. He, L. X. Jian, Z. Jing, G. L. Shen and R. Q. Yu, *Anal. Chem.*, 2010, **82**, 3108–3113.

62 F. T. Suo, X. W. Chen, H. X. Fang, Q. Y. Gong, C. M. Yu, N. D. Yang, S. Li, Q. Wu, L. Li and W. Huang, *Dyes Pigm.*, 2019, **170**, 107639.

63 F. Deng and Z. C. Xu, *Chin. Chem. Lett.*, 2019, **30**, 1667–1681.

64 L. L. Yang, S. Y. Zou, Y. H. Fu, W. Li, X. P. Wen, P. Y. Wang, Z. C. Wang, G. P. Ouyang, Z. Li and S. Yang, *J. Agric. Food Chem.*, 2020, **68**, 4285–4291.

65 L. Y. Wu, X. Wang, J. Huang, H. Y. Wei and C. Kan, *J. Photochem. Photobiol., A*, 2022, **429**, 113936.

66 C. Kan, X. T. Shao, L. Y. Wu, Y. Zhang, X. F. Bao and J. Zhu, *J. Photochem. Photobiol., A*, 2020, **398**, 112618.

67 C. Kan, F. Song, X. T. Shao, L. Y. Wu and J. Zhu, *J. Photochem. Photobiol., A*, 2020, **390**, 112306.

68 B. Biswal, D. Mallick, M. Thirunavoukkarasu, R. Mohanty and B. Bag, *Sens. Actuators, B*, 2016, **232**, 410–419.

69 W. J. Ma, S. Tan, P. Yang, A. L. Tang, L. L. Yang, J. Y. Chen, S. T. Liu, M. H. Ge, X. Zhou and S. Yang, *Sens. Actuators, B*, 2023, **390**, 133948.

70 F. Song, C. Yang, X. T. Shao, L. Du, J. Zhu and C. Kan, *Dyes Pigm.*, 2019, **165**, 444–450.

71 S. Paul, S. Bhuyan, S. K. Mukhopadhyay, N. C. Murmu and P. Banerjee, *ACS Sustainable Chem. Eng.*, 2019, **7**, 13687–13697.

72 S. Erdemir, M. Oguz and S. Malkondu, *J. Hazard. Mater.*, 2023, **452**, 131278.

73 J. Y. Zhao, K. Liu, R. T. Wang, T. H. Liu, Z. F. Wu, L. P. Ding and Y. Fang, *ACS Appl. Mater. Interfaces*, 2022, **14**, 53323–53330.

74 X. Wang, S. Y. Cheng, C. Y. Liu, Y. Zhang, M. J. Su, X. D. Rong, H. C. Zhu, M. H. Yu, W. L. Sheng and B. C. Zhu, *Sci. Total Environ.*, 2022, **840**, 156445.

75 F. Y. Yan, K. Q. Fan, Z. J. Bai, R. Q. Zhang, F. L. Zu, J. X. Xu and X. Li, *TrAC, Trends Anal. Chem.*, 2017, **97**, 15–35.

76 S. Keerthana, B. Sam, L. George, Y. N. Sudhakar and A. Varghese, *J. Fluoresc.*, 2021, **31**, 1251–1276.

77 T. S. Wang, N. Zhang, W. Bar and Y. Y. Bao, *Polym. Chem.*, 2020, **11**, 3095–3114.

78 M. N. Potter, J. R. Green and B. Mutus, *Talanta*, 2022, **237**, 122981.

79 Y. Takaoka, S. Miyagawa, A. Nakamura, S. Egoshi, S. Tsukiji and M. Ueda, *Sci. Rep.*, 2020, **10**, 5333.

80 M. A. Assiri, M. T. Waseem, A. Hamad, M. Imran, U. Farooq and S. A. Shahzad, *Spectrochim. Acta, Part A*, 2023, **290**, 122298.

81 B. Parízkova, A. Zukauskaite, T. Vain, P. Grones, S. Raggi, M. F. Kubes, M. Kieffer, S. M. Doyle, M. Strnad, S. Kepinski, R. Napier, K. Dolezal, S. Robert and O. Novák, *New Phytol.*, 2021, **230**, 535–549.

82 J. H. Wang, Y. M. Liu, Z. M. Dong, J. B. Chao, H. Wang, Y. Wang and S. M. Shuang, *J. Hazard. Mater.*, 2020, **382**, 121056.

83 Q. H. Yu, F. Ding, J. L. Shen and X. J. He, *Talanta*, 2021, **228**, 122218.

84 Y. F. Huang, Y. B. Zhang, F. G. Huo, Y. M. Liu and C. X. Yin, *Sens. Actuators, B*, 2019, **301**, 127123.

85 C. Y. Jiang, H. J. Huang, X. Y. Kang, L. Yang, Z. Xi, H. Y. Sun, M. D. Pluth and L. Yi, *Chem. Soc. Rev.*, 2021, **50**, 7436–7495.

86 Q. Li, L. J. Chai, G. P. Dong, X. M. Zhang and L. P. Du, *Front. Mol. Biosci.*, 2021, **8**, 666605.

87 S. Lee, M. Jen, T. Jang, G. Lee and Y. Pang, *Sci. Rep.*, 2022, **12**, 6557.

88 T. Ueno and T. Nagano, *Nat. Methods*, 2011, **8**, 642–645.

89 M. Benstead, G. H. Mehl and R. W. Boyle, *Tetrahedron*, 2011, **67**, 3573–3601.

90 H. Wen, Q. H. Wu, C. N. Li, T. T. Sun and Z. G. Xie, *ACS Appl. Nano Mater.*, 2022, **5**, 1500–1507.

91 H. Lu and Z. Shen, *Front. Chem.*, 2020, **8**, 290.

92 A. Kamkaew, S. H. Lim, H. B. Lee, L. V. Kiew, L. Y. Chung and K. Burgess, *Chem. Soc. Rev.*, 2013, **42**, 77–88.

93 M. Poddar and R. Misra, *Coord. Chem. Rev.*, 2020, **421**, 213462.

94 Y. Zhang, H. Li, L. Y. Niu, Q. Z. Yang, Y. F. Guan and L. Feng, *Analyst*, 2014, **139**, 3146–3153.

95 L. Michels, V. Gorelova, Y. Harnvanichvech, J. W. Borst, B. Albada, D. Weijers and J. Sprakel, *Proc. Natl. Acad. Sci. U. S. A.*, 2020, **117**, 18110–18118.

96 W. J. Chen, Y. H. Guan, Q. Chen, J. Ren, Y. Xie and J. Yin, *Dyes Pigm.*, 2022, **200**, 110134.

97 A. Starodubtseva, T. Kalachova, O. Iakovenko, V. Stoudková, V. Zhabinskii, V. Khripach, E. Ruelland, J. Martinec, L. Burketová and V. Kravets, *Int. J. Mol. Sci.*, 2021, **22**, 3599.

98 X. K. Yang, J. M. Wang, Z. L. Zhang, B. Zhang, X. L. Du, J. Zhang and J. H. Wang, *Food Chem.*, 2023, **416**, 135730.

99 Y. X. Fu, Z. Y. Zhang, W. Y. Z. Guo, Y. J. Dai, Z. Y. Wang, W. C. Yang and G. F. Yang, *Pest Manage. Sci.*, 2022, **78**, 4947–4955.

100 J. J. Wu, D. D. Su, C. Q. Qin, W. Li, J. Rodrigues, R. L. Sheng and L. T. Zeng, *Talanta*, 2019, **201**, 111–118.

101 Y. D. Guo, Y. Luo, N. Wang, M. G. Tang, J. C. Xiao, S. W. Chen and J. Y. Wang, *Talanta*, 2020, **212**, 120583.

102 X. X. Ma, Y. R. Huang, W. J. Chen, J. Liu, S. H. Liu, J. Yin and G. F. Yang, *Angew. Chem., Int. Ed.*, 2023, **62**, e202216109.

103 A. Promchat, P. Rashatasakhon and M. Sukwattanasinitt, *J. Hazard. Mater.*, 2017, **329**, 255–261.

104 N. Vijay, S. P. Wu and S. Velmathi, *Sens. Actuators, B*, 2022, **371**, 132567.

105 W. Yuan, C. Y. Wan, J. J. Zhang, Q. S. Li, P. Zhang, K. Zheng, Q. Zhang and C. F. Ding, *Spectrochim. Acta, Part A*, 2023, **297**, 122719.

106 A. Nicol, K. Wang, R. T. K. Kwok, Z. G. Song, N. Li and B. Z. Tang, *ACS Appl. Mater. Interfaces*, 2019, **11**, 22028.

107 J. Q. Zuo, E. A. Zhu, W. J. Yin, C. Y. Yao, J. J. Liao, X. N. Ping, Y. Q. Zhu, X. T. Cai, Y. C. Rao, H. Feng, K. W. Zhang and Z. S. Qian, *Chem. Sci.*, 2023, **14**, 2139–2148.

108 V. Martinez and M. Henary, *Chem. – Eur. J.*, 2016, **22**, 13764–13782.

109 H. Tajalli, A. G. Gilani, M. S. Zakerhamidi and P. Tajalli, *Dyes Pigm.*, 2008, **78**, 15–24.

110 G. S. Alemán-Nava, S. P. Cuellar-Bermudez, M. Cuaresma, R. Bosma, K. Muylaert, B. E. Ritmann and R. Parra, *J. Microbiol. Methods*, 2016, **128**, 74–79.

This journal is © The Royal Society of Chemistry 2024

Chem. Soc. Rev., 2024, **53**, 6992–7090 | **7085**

111 X. Y. Zeng, X. X. Ma, J. Dong, B. Li, S. H. Liu, J. Yin and G. F. Yang, *Angew. Chem., Int. Ed.*, 2023, **135**, e202312618.

112 X. Zeng, Y. Huang, J. Dong, X. Ma, J.-X. Nan, W. Chen, H.-Y. Lin, W.-C. Yang, X. Liu, J. Yin and G.-F. Yang, *Adv. Agrochem.*, 2022, **1**, 73–84.

113 H. A. Shindy, *Dyes Pigm.*, 2017, **145**, 505–513.

114 L. Li, X. G. Dong, J. R. Li and J. Wei, *Dyes Pigm.*, 2020, **183**, 108756.

115 Y. N. Hong, J. W. Y. Lam and B. Z. Tang, *Chem. Commun.*, 2009, 4332–4353.

116 Q. Peng, Y. Yi, Z. Shuai and J. Shao, *J. Am. Chem. Soc.*, 2007, **129**, 9333–9339.

117 M. Wang, G. X. Zhang, D. Q. Zhang, D. B. Zhu and B. Tang, *J. Mater. Chem.*, 2010, **20**, 1858–1867.

118 D. Ding, K. Li, B. Liu and B. Z. Tang, *Acc. Chem. Res.*, 2013, **46**, 2441–2453.

119 L. Burratti, E. Ciotta, F. De Matteis and P. Prosposito, *Nanomaterials*, 2021, **11**, 276.

120 J. M. Wang, J. Z. Jiang, F. Y. Li, J. Zou, K. Xiang, H. T. Wang, Y. J. Li and X. Li, *Green Chem.*, 2023, **25**, 32–58.

121 G. Gao, Y. W. Jiang, W. Sun and F. G. Wu, *Chin. Chem. Lett.*, 2018, **29**, 1475–1485.

122 G. Yu, J. Liang, Z. He and M. Sun, *Chem. Biol.*, 2006, **13**, 723–731.

123 A. Singh, A. Guleria, S. Neogy and M. C. Rath, *Arabian J. Chem.*, 2020, **13**, 3149–3158.

124 A. Kumar and K. Gupta, *J. Mater. Chem. A*, 2017, **5**, 6146–6163.

125 J. M. Li, H. H. Wu, I. Santana, M. Fahlgren and J. P. Giraldo, *ACS Appl. Mater. Interfaces*, 2018, **10**, 28279–28289.

126 Z. K. Hu, W. J. Long, T. K. Liu, Y. T. Guan, G. H. Lei, Y. X. Suo, M. G. Jia, J. L. He, H. Y. Chen, Y. B. She and H. Y. Fu, *Spectrochim. Acta, Part A*, 2023, **294**, 122517.

127 D. Saika, P. Dutta, N. Sen Sarma and N. C. Adhikary, *Sens. Actuators, B*, 2016, **230**, 149–156.

128 L. Zhang, C. Xu and B. Li, *Microchim. Acta*, 2009, **166**, 61–68.

129 J. Wang, D. Q. Li, Y. Qiu, X. Y. Liu, X. Zhang, L. Huang, H. M. Wen and J. Hu, *Sens. Actuators, B*, 2019, **301**, 126984.

130 K. Zhang, Q. Mei, G. Guan, B. Liu, S. Wang and Z. Zhang, *Anal. Chem.*, 2010, **82**, 9579–9586.

131 F. Qu, X. Zhou, J. Xu, H. Li and G. Xie, *Talanta*, 2009, **78**, 1359–1363.

132 X. W. Meng, J. F. Wei, X. L. Ren, J. Ren and F. Q. Tang, *Biosens. Bioelectron.*, 2013, **47**, 402–407.

133 K. He, X. Yu, L. Qin and Y. Wu, *Food Chem.*, 2022, **390**, 133116.

134 H. Wang, C. Chen, Y. Liu, Y. Wu, Y. Yuan and Q. Zhou, *Talanta*, 2019, **198**, 242–248.

135 S. Y. Chen, S. N. Yun, Y. J. Liu, R. J. Yu, Q. Tu, J. Y. Wang and M. S. Yuan, *Analyst*, 2022, **147**, 3258–3265.

136 I. A. Mir, S. Kumar, M. A. Bhat, Y. L. Xie, A. A. Wani and L. Zhu, *Colloids Surf., A*, 2021, **626**, 127090.

137 F. Zhang, Y. Liu, P. Ma, S. Tao, Y. Sun, X. Wang and D. Song, *Talanta*, 2019, **204**, 13–19.

138 C. Zhang, K. Zhang, T. T. Zhao, B. H. Liu, Z. Y. Wang and Z. P. Zhang, *Sens. Actuators, B*, 2017, **252**, 1083–1088.

139 N. Ding, D. L. Zhou, G. C. Pan, W. Xu, X. Chen, D. Y. Li, X. H. Zhang, J. Y. Zhu, Y. A. Ji and H. W. Song, *ACS Sustainable Chem. Eng.*, 2019, **7**, 8397–8404.

140 N. V. Ghinaiya, T. J. Park and S. K. Kailasa, *J. Photochem. Photobiol., A*, 2023, **444**, 114980.

141 S. Huang, M. Guo, J. Tan, Y. Geng, J. Wu, Y. Tang, C. Su, C. C. Lin and Y. Liang, *ACS Appl. Mater. Interfaces*, 2018, **10**, 39056–39063.

142 X. Z. Jin, X. B. Sun, G. Chen, L. X. Ding, Y. H. Li, Z. K. Liu, Z. J. Wang, W. Pan, C. H. Hu and J. P. Wang, *Carbon*, 2015, **81**, 388–395.

143 J. Lin, X. Huang, E. Kou, W. Cai, H. Zhang, X. Zhang, Y. Liu, W. Li, Y. Zheng and B. Lei, *Biosens. Bioelectron.*, 2023, **219**, 114848.

144 S. S. Wee, Y. H. Ng and S. M. Ng, *Talanta*, 2013, **116**, 71–76.

145 R. Y. Xie, Y. Y. Qu, M. Y. Tang, J. Q. Zhao, S. Chua, T. T. Li, F. Zhang, A. E. H. Wheatley and F. Chai, *Food Chem.*, 2021, **364**, 130366.

146 J. Plácido, S. Bustamante-López, K. E. Meissner, D. E. Kelly and S. L. Kelly, *Sci. Total Environ.*, 2019, **656**, 531–539.

147 P. Keerthana, A. K. Das, M. Bharath, M. Ghosh and A. Varghese, *J. Environ. Chem. Eng.*, 2023, **11**, 109325.

148 D. Pooja, S. Saini, A. Thakur, B. Kumar, S. Tyagi and M. K. Nayak, *J. Hazard. Mater.*, 2017, **328**, 117–126.

149 B. X. Lin, Y. Yan, M. L. Guo, Y. J. Cao, Y. Yu, T. Y. Zhang, Y. Huang and D. Wu, *Food Chem.*, 2018, **245**, 1176–1182.

150 M. M. F. Chang, I. R. Ginjom and S. M. Ng, *Sens. Actuators, B*, 2017, **242**, 1050–1056.

151 J. Hou, J. Dong, H. Zhu, X. Teng, S. Ai and M. Mang, *Biosens. Bioelectron.*, 2015, **68**, 20–26.

152 F. A. Tafreshi, Z. Fatahi, S. F. Ghasemi, A. Taherian and N. Esfandiari, *PLoS One*, 2020, **15**, e0230646.

153 B. B. Chen, M. L. Liu, L. Zhan, C. M. Li and C. Z. Huang, *Anal. Chem.*, 2018, **90**, 4003–4009.

154 L. Behera, D. Pati, B. B. Sahu and S. Mohapatra, *Colloids Surf., A*, 2022, **653**, 130002.

155 G. J. Ren, Q. Zhang, S. Li, S. S. Fu, F. Chai, C. G. Wang and F. Y. Qu, *Sens. Actuators, B*, 2017, **243**, 244–253.

156 G. Yang, X. Wan, Y.-K. Su, X. Zeng and J. Tang, *J. Mater. Chem. A*, 2016, **4**, 12841–12849.

157 L. Li, D. Liu, A. P. Shi and T. Y. You, *Sens. Actuators, B*, 2018, **255**, 1762–1770.

158 H. Li, C. Sun, R. Vijayaraghavan, F. Zhou, X. Zhang and D. R. MacFarlane, *Carbon*, 2016, **104**, 33–39.

159 M. Yang, M. Liu, Z. Wu, Y. He, Y. Ge, G. Song and J. Zhou, *Microchim. Acta*, 2019, **186**, 585.

160 W. K. Li, J. T. Feng and Z. Q. Ma, *Carbon*, 2020, **161**, 685–693.

161 S. Mohapatra, M. K. Bera and R. K. Das, *Sens. Actuators, B*, 2018, **263**, 459–468.

162 S. Patel, K. Shrivas, D. Sinha, I. Karbhal, T. K. Patle, Monisha and Tikeshwari, *Spectrochim. Acta, Part A*, 2023, **299**, 122824.

163 H. Yuan, D. Li, Y. Liu, X. Xu and C. Xiong, *Analyst*, 2015, **140**, 1428–1431.

7086 | *Chem. Soc. Rev.*, 2024, **53**, 6992–7090

This journal is © The Royal Society of Chemistry 2024

164 Y. Q. Shi, D. D. Kong, W. T. Li, Y. Z. Wei, X. Wei, F. F. Qu, Y. H. Zhang, P. C. Nie, X. P. Feng and Y. He, *Anal. Chim. Acta*, 2023, **1244**, 340844.

165 T. Anusuya, V. Kumar and V. Kumar, *Chemosphere*, 2021, **282**, 131019.

166 L. Wang, W. Li, B. Wu, Z. Li, S. Wang, Y. Liu, D. Pan and M. Wu, *Chem. Eng. J.*, 2016, **300**, 75–82.

167 Z. S. Qian, X. Y. Shan, L. J. Chai, J. R. Chen and H. Peng, *Biosens. Bioelectron.*, 2015, **68**, 225–231.

168 L. L. Wang, J. Zheng, S. Yang, C. C. Wu, C. H. Liu, Y. Xiao, Y. H. Li, Z. H. Qing and R. H. Yang, *ACS Appl. Mater. Interfaces*, 2015, **7**, 19509–19515.

169 C.-T. Hsieh, P.-Y. Sung, Y. A. Gandomi, K. S. Khoo and J.-K. Chang, *Chemosphere*, 2023, **318**, 137926.

170 C. P. Zhang, B. X. Lin, Y. J. Cao, M. L. Guo and Y. Yu, *J. Agric. Food Chem.*, 2017, **65**, 3065–3073.

171 J. Jiménez-López, E. J. Llorent-Martínez, P. Ortega-Barrales and A. Ruiz-Medina, *Talanta*, 2020, **207**, 120344.

172 C. Sahub, T. Tuntulani, T. Nhujak and B. Tomapatanaget, *Sens. Actuators, B*, 2018, **258**, 88–97.

173 Y. Liu, L. Cao, M. Zan, J. Peng, P. Wang, X. Pang, Y. Zhang, L. Li, W.-F. Dong and Q. Mei, *Talanta*, 2021, **233**, 122465.

174 X. Zhang, C. Li, S. Zhao, H. Pang, Y. Han, X. Luo, W. Tang and Z. Li, *Opt. Mater.*, 2020, **110**, 110461.

175 S. Shen, B. Huang, X. Guo and H. Wang, *J. Mater. Chem. B*, 2019, **7**, 7033–7041.

176 Z. Zhang, Q. R. Zhang, L. F. Li, D. Lin and C. L. Jiang, *ACS Sustainable Chem. Eng.*, 2023, **11**, 4998–5006.

177 M. C. Rong, J. C. Ye, B. Y. Chen, Y. Z. Wen, X. Z. Deng and Z. Q. Liu, *Sens. Actuators, B*, 2020, **309**, 127807.

178 Y. L. Xu, X. Y. Niu, H. L. Chen, S. G. Zhao and X. G. Chen, *Chin. Chem. Lett.*, 2017, **28**, 338–344.

179 P. Sharma and M. S. Mehata, *Mater. Res. Bull.*, 2020, **131**, 110978.

180 L. Zhang, Z.-W. Wang, S.-J. Xiao, D. Peng, J.-Q. Chen, R.-P. Liang, J. Jiang and J.-D. Qiu, *ACS Appl. Nano Mater.*, 2018, **1**, 1484–1491.

181 Y. E. Shi, P. Zhang, D. Q. Yang and Z. G. Wang, *Chem. Commun.*, 2020, **56**, 10982–10988.

182 X. Wang, W. Guo, X. Wang, Q. Hua, F. Tang, X. Li, F. Luan, Z. Zhang, C. Tian, X. Zhuang and L. Zhao, *Arabian J. Chem.*, 2022, **15**, 104080.

183 H. Q. Zhang, Y. F. Li and F. Gan, *Sens. Actuators, B*, 2023, **374**, 132817.

184 X. Y. Li, C. Chen, F. F. Xu, Z. G. Liang, G. H. Xu, F. D. Wei, J. Yang, Q. Hu, J. J. Zou and Y. Cen, *Talanta*, 2023, **260**, 124639.

185 J. Sun, B. S. Shengping Zhang, M. Alomar, A. S. Alqarni, M. S. Najla Alotaibi, M. S. Badriah Alshahrani, A. A. Alghamdi, Z. Kou, W. Shen, Y. Chen and J. Zhang, *Chem. Rec.*, 2023, **23**, e202200268.

186 J. Gu, X. Lu, G. Li, B. Shan, J. Liu, Y. Qu, H. Ye, K. Xi and H. Wu, *Chem. Eng. J.*, 2023, **467**, 143445.

187 S. Zhang, Z. J. Qi and Y. Li, *Ceram. Int.*, 2022, **48**, 21118–21124.

188 Y. Feng, F. Zhou, Q. Deng and C. Peng, *Ceram. Int.*, 2020, **46**, 8320–8327.

189 X. Wang, X. Zhang, C. Haiyan and Y. Huang, *J. Mater. Chem. B*, 2020, **8**, 10837–10844.

190 F. P. G. de Arquer, D. V. Talapin, V. I. Klimov, Y. Arakawa, M. Bayer and E. H. Sargent, *Science*, 2021, **373**, eaaz8541.

191 R. Chen and D. J. Lockwood, *J. Electrochem. Soc.*, 2002, **149**, S69.

192 M. Zulfajri, H. N. Abdelhamid, S. Sudewi, S. Dayalan, A. Rasool, A. Habib and G. G. Huang, *Biosensors*, 2020, **10**, 68.

193 D. Xu, Q. Lin and H.-T. Chang, *Small Methods*, 2020, **4**, 1900387.

194 X. R. Li, H. Ma, M. Deng, A. Iqbal, X. Y. Liu, B. Li, W. S. Liu, J. P. Li and W. W. Qin, *J. Mater. Chem. C*, 2017, **5**, 2149–2152.

195 I. Song, C. Park and H. C. Choi, *RSC Adv.*, 2015, **5**, 7495–7514.

196 Z. Li, X. Yang, Y. Zhou, A. Huang, Y. Sun, Z. Duan, S. Yang, C. Liao, Y. Liu and X. Wen, *Microchem. J.*, 2023, **193**, 109135.

197 J. Gu, X. Lu, G. Li, B. Shan, J. Liu, Y. Qu, H. Ye, K. Xi and H. Wu, *Chem. Eng. J.*, 2023, **467**, 143445.

198 F. Yan, J. Sun, Y. Zang, Z. Sun, H. Zhang, J. Xu and X. Wang, *Dyes Pigm.*, 2021, **195**, 109720.

199 C. Guan, X. Yue, J. Fan and Q. Xiang, *Chin. J. Catal.*, 2022, **43**, 2484–2499.

200 R. Li, T. T. Chen and X. L. Pan, *ACS Nano*, 2021, **15**, 3808–3848.

201 S. Y. Wu, H. Min, W. Shi and P. Cheng, *Adv. Mater.*, 2020, **32**, 1805871.

202 X. Xu, M. Ma, T. Sun, X. Zhao and L. Zhang, *Biosensors*, 2023, **13**, 435.

203 D. Zhao, S. Yu, W. J. Jiang, Z. H. Cai, D. L. Li, Y. L. Liu and Z. Z. Chen, *Molecules*, 2022, **27**, 2226.

204 Y. Shu, Q. Y. Ye, T. Dai, Q. Xu and X. Y. Hu, *ACS Sens.*, 2021, **6**, 641–658.

205 Q. Li, J. H. Wu, Q. T. Yang, H. Y. Li and F. Li, *Anal. Chem.*, 2021, **93**, 7362–7368.

206 W. X. Chen, J. S. Fang, Y. W. Zhang, G. L. Chen, S. Zhao, C. Zhang, R. Xu, J. H. Bao, Y. M. Zhou and X. Xiang, *Nanoscale*, 2018, **10**, 4463–4474.

207 J. Yang, C. J. Ren, M. Liu, W. W. Li, D. J. Gao, H. D. Li and Z. L. Ning, *Molecules*, 2023, **28**, 4919.

208 X. Y. Xu and B. Yan, *ACS Appl. Mater. Interfaces*, 2015, **7**, 721–729.

209 Y. F. Xia, G. M. Bao, X. X. Peng, X. Y. Wu, H. F. Lu, Y. F. Zhong, W. Li, J. X. He, S. Y. Liu, Q. Fan, S. H. Li, W. Xiao and H. Q. Yuan, *Anal. Chim. Acta*, 2022, **1221**, 340115.

210 N. W. H. Guo, L. P. Peng, Y. Chen, Y. S. Liu, C. L. Li, H. Zhang and W. Yang, *Talanta*, 2022, **250**, 123710.

211 H. Xu, C. S. Cao and B. Zhao, *Chem. Commun.*, 2015, **51**, 10280–10283.

212 G. X. Qin, Y. Q. Kong, T. J. Gan and Y. H. Ni, *Inorg. Chem.*, 2022, **61**, 8966–8975.

213 T. Wang, L. Zhang, J. Y. Zhang, G. X. Guo, X. H. Jiang, Z. W. Zhang and S. Q. Li, *Food Chem.*, 2023, **416**, 135853.

214 H. Eskandari, M. Amirzehni, J. Hassanzadeh and B. Vahid, *Microchim. Acta*, 2020, **187**, 673.

215 K. P. Yin, S. Q. Wu, H. Zheng, L. Gao, J. F. Liu, C. L. Yang, L. W. Qi and J. J. Peng, *Langmuir*, 2021, **37**, 5321–5328.

This journal is © The Royal Society of Chemistry 2024

Chem. Soc. Rev., 2024, **53**, 6992–7090 | **7087**

216 S. L. Zhao, J. N. Xiao, T. X. Zheng, M. Y. Liu, H. N. Wu and Z. L. Liu, *ACS Omega*, 2019, **4**, 16378–16384.

217 G. F. Ji, X. C. Gao, T. X. Zheng, W. H. Guan, H. T. Liu and Z. L. Liu, *Inorg. Chem.*, 2018, **57**, 10525–10532.

218 Y. Qiang, W. X. Yang, X. S. Zhang, X. L. Luo, W. Z. Tang, T. L. Yue and Z. H. Li, *Microchim. Acta*, 2022, **189**, 130.

219 P. Chakraborty, A. Rana, S. Mukherjee and S. Biswas, *Inorg. Chem.*, 2023, **62**, 802–809.

220 Q. Wu, H. Tao, Y. Wu, X. Wang, Q. Shi and D. Xiang, *Foods*, 2022, **11**, 2405.

221 P. Janjani, U. Bhardwaj, R. Gupta and H. S. Kushwaha, *Anal. Chim. Acta*, 2022, **1202**, 339676.

222 Y. Q. Zhang, J. X. Liu, X. H. Wu, W. Q. Tao and Z. Li, *Anal. Chim. Acta*, 2020, **1131**, 68–79.

223 Y. Yu, G. L. Huang, X. L. Luo, W. M. Lin, Y. Han, J. H. Huang and Z. H. Li, *Microchim. Acta*, 2022, **189**, 325.

224 D. W. Zhang, Y. Xu, Q. L. Liu and Z. G. Xia, *Inorg. Chem.*, 2018, **57**, 4613–4619.

225 T. Yan, H. L. Ding, R. Feng, R. F. Yuan, Y. X. Zhao, M. Sun, L. G. Yan and Q. Wei, *ACS Appl. Mater. Interfaces*, 2022, **14**, 25308–25316.

226 M. X. Fan, T. T. Gan, G. F. Yin, F. B. B. Cheng and N. J. Zhao, *RSC Adv.*, 2021, **11**, 27845–27854.

227 F. Asadi, S. N. Azizi and M. J. Chaichi, *Mater. Sci. Eng., C*, 2019, **105**, 110058.

228 L. Yang, Y. L. Liu, C. G. Liu, Y. Fu and F. Ye, *RSC Adv.*, 2020, **10**, 19149–19156.

229 M. L. Li, Y. Gao, W. T. Yang, C. W. Zhang, Y. Fang, C. Wang, S. Y. Song and Q. H. Pan, *Inorg. Chem.*, 2022, **61**, 9801–9807.

230 Q. Li, D. Li, Z. Q. Wu, K. Shi, T. H. Liu, H. Y. Yin, X. B. Cai, Z. L. Fan, W. Zhu and D. X. Xue, *Inorg. Chem.*, 2022, **61**, 15213–15224.

231 J. T. Liu, L. Y. Ye, Y. Y. Mo and H. Yang, *Food Chem.*, 2022, **370**, 131034.

232 T. Y. Zhong, D. L. Li, C. Li, Z. Zhang and G. Wang, *Anal. Methods*, 2022, **14**, 2714–2722.

233 M. L. Guo, J. T. Chi, Y. J. Li, G. I. N. Waterhouse, S. Y. Ai, J. Y. Hou and X. Y. Li, *Microchim. Acta*, 2020, **187**, 534.

234 S. Govindaraju, P. Puthiaraj, M. H. Lee and K. Yun, *ACS Omega*, 2018, **3**, 12052–12059.

235 Y. Cai, H. S. Zhu, W. C. Zhou, Z. Y. Qiu, C. C. Chen, A. R. Qileng, K. S. Li and Y. J. Liu, *Anal. Chem.*, 2021, **93**, 7275–7282.

236 W. T. Li, X. A. Zhang, X. T. Hu, Y. Q. Shi, W. Xin, N. N. Liang, T. T. Shen, J. B. Xiao, M. Daglia, X. B. Zou and J. Y. Shi, *Anal. Chim. Acta*, 2022, **1226**, 340153.

237 P. T. Liu, R. S. Hao, W. L. Sun, Z. Y. Lin and T. F. Jing, *Luminescence*, 2022, **37**, 1793–1799.

238 H. N. Abdelhamid, A. Bermejo-Gómez, B. Martín-Matute and X. D. Zou, *Microchim. Acta*, 2017, **184**, 3363–3371.

239 Y. Shu, Q. Y. Ye, T. Dai, J. Guan, Z. P. Ji, Q. Xu and X. Y. Hu, *J. Hazard. Mater.*, 2022, **430**, 128360.

240 Y. Q. Sun, Y. Cheng and X. B. Yin, *Anal. Chem.*, 2021, **93**, 3559–3566.

241 M. Gutiérrez, Y. Zhang and J. C. Tan, *Chem. Rev.*, 2022, **122**, 10438–10483.

242 Z. K. Zhang, L. Zhang, P. Han and Q. J. Liu, *Microchim. Acta*, 2022, **189**, 438.

243 A. Biranje, N. Azmi, A. Tiwari and A. Chaskar, *J. Fluoresc.*, 2021, **31**, 1241–1250.

244 B. K. John, T. Abraham and B. Mathew, *J. Fluoresc.*, 2022, **32**, 449–471.

245 R. Yousefi, S. Asgari, A. B. Dehkordi, G. M. Ziarani, A. Badiei, F. Mohajer, R. S. Varma and S. Iravani, *Environ. Res.*, 2023, **226**, 115664.

246 R. Xue, Y. S. Liu, S. L. Huang and G. Y. Yang, *ACS Sens.*, 2023, **8**, 2124–2148.

247 J. X. Fan, J. Li, W. F. Zhou, H. X. Gao, R. H. Lu and H. C. Guo, *Luminescence*, 2023, **38**, 1729–1737.

248 R. Paz, H. Viltres, N. K. Gupta, V. Phung, S. Srinivasan, A. R. Rajabzadeh and C. Leyva, *Chemosphere*, 2023, **342**, 140145.

249 M. Afshari, M. Dinari, H. Farrokhpour and F. Zamora, *ACS Appl. Mater. Interfaces*, 2022, **14**, 22398–22406.

250 L. L. Song, Q. Zhang, L. Min, X. Y. Guo, W. Q. Gao, L. Cui and C. Y. Zhang, *Talanta*, 2024, **266**, 124964.

251 S. Knežević, N. T. Jovanović, F. Vlahović, V. Ajdačić, V. Costache, J. Vidić, I. Opsenica and D. Stanković, *Chemosphere*, 2023, **341**, 139930.

252 G. Chen, H. H. Lan, S. L. Cai, B. Sun, X. L. Li, Z. H. He, S. R. Zheng, J. Fan, Y. Liu and W. G. Zhang, *ACS Appl. Mater. Interfaces*, 2019, **11**, 12830–12837.

253 Z. F. Yan, L. Fang, Z. G. He, H. Xie, B. B. Liu, B. Guo and Y. W. Yao, *Small*, 2022, **18**, 2200388.

254 B. Zhu, L. Zhu, S. Deng, Y. Wan, F. Qin, H. Han and J. Luo, *J. Hazard. Mater.*, 2023, **459**, 132081.

255 J. W. Li, M. C. Gao, X. Y. Xia, Y. Cen, F. D. Wei, J. Yang, L. Wang, Q. Hu and G. H. Xu, *ACS Appl. Mater. Interfaces*, 2023, **15**, 6473–6485.

256 S. H. Wen, H. Y. Zhang, S. Yu, J. P. Ma, J. J. Zhu and Y. Z. Zhou, *Anal. Chem.*, 2023, **95**, 14914–14924.

257 Y. Zhang, X. C. Zhu, M. J. Li, H. L. Liu and B. G. Sun, *J. Agric. Food Chem.*, 2022, **70**, 6059–6071.

258 S. L. Qin, X. D. He, F. L. Jin, Y. Wang, H. T. Chu, S. Han, Y. Y. Sun and L. D. Gao, *RSC Adv.*, 2022, **12**, 18784–18793.

259 X. Wang, Y. X. Wang, H. Qi, Y. Chen, W. Guo, H. Y. Yu, H. Y. Chen and Y. B. Ying, *ACS Nano*, 2022, **16**, 14297–14307.

260 X. L. Zhang, G. L. Li, D. Wu, B. Zhang, N. Hu, H. L. Wang, J. H. Liu and Y. N. Wu, *Biosens. Bioelectron.*, 2019, **145**, 111699.

261 Z. Meng and K. A. Mirica, *Chem. Soc. Rev.*, 2021, **50**, 13498–13558.

262 A. Aparna, H. Sreehari, A. Chandran, K. P. Anjali, A. M. Alex, P. Anuvinda, G. B. Gouthami, N. P. Pillai, N. Parvathy, S. Sadanandan and A. Saritha, *Talanta*, 2022, **239**, 123134.

263 G. Panthi and M. Park, *J. Hazard. Mater.*, 2022, **424**, 127565.

264 X. Y. Wang, H. J. Yu, Q. H. Li, Y. H. Tian, X. L. Gao, W. Q. Zhang, Z. C. Sun, Y. T. Mou, X. Sun, Y. M. Guo and F. L. Li, *Food Chem.*, 2024, **431**, 137067.

265 X. P. Zhang, K. Y. Huang, S. B. He, H. P. Peng, X. H. Xia, W. Chen and H. H. Deng, *J. Hazard. Mater.*, 2021, **405**, 124259.

266 A. M. Hada, M. Zetes, M. Focsan, S. Astilean and A. M. Craciun, *Int. J. Mol. Sci.*, 2022, **23**, 12410.

7088 | *Chem. Soc. Rev.*, 2024, **53**, 6992–7090

This journal is © The Royal Society of Chemistry 2024

267 J. M. Xu, H. M. Zhou, Y. X. Zhang, Y. Zhao, H. Yuan, X. X. He, Y. Wu and S. Zhang, *J. Hazard. Mater.*, 2022, **428**, 128158.

268 M. Chen, W. Ao, J. N. Bai, P. J. Li, W. Wei, S. J. Pang and X. D. Yang, *Nanotechnology*, 2022, **33**, 345501.

269 L. Chen, J. Lu, M. Luo, H. Yu, X. J. Chen, J. G. Deng, X. T. Hou, E. W. Hao, J. C. Wei and P. Li, *Food Chem.*, 2022, **379**, 132139.

270 F. R. Nie, L. Ga, J. Ai and Y. Wang, *RSC Adv.*, 2018, **8**, 13708–13713.

271 Z. Shojaeifard, N. Heidari and B. Hemmateenejad, *Spectrochim. Acta, Part A*, 2019, **209**, 202–208.

272 H. B. Wu, R. Y. Xie, Y. Q. Hao, J. Y. Pang, H. Gao, F. Y. Qu, M. M. Tian, C. H. Guo, B. D. Mao and F. Chai, *Food Chem.*, 2023, **418**, 135961.

273 X. Gao, Z. Y. Ma, M. J. Sun, X. Y. Liu, K. L. Zhong, L. J. Tang, X. P. Li and J. R. Li, *Food Chem.*, 2022, **369**, 130964.

274 E. Babaee, A. Barati, M. B. Gholivand, A. Taherpour, N. Zolfaghar and M. Shamsipur, *J. Hazard. Mater.*, 2019, **367**, 437–446.

275 Z. Y. Wang, R. Liu, Z. F. Fu, X. Yi, Y. J. Hu, C. H. Liu, D. Pan and Z. Y. Wu, *Anal. Methods*, 2023, **15**, 2505–2511.

276 T. H. Wang, L. N. Zhang and H. Xin, *Front. Chem.*, 2022, **10**, 855281.

277 J. Zou, Q. Yu, Y. S. Gao, S. X. Chen, X. G. Huang, D. N. Hu, S. W. Liu and L. M. Lu, *ACS Omega*, 2022, **7**, 1132–1138.

278 I. M. Khan, S. Niazi, L. Yue, Y. Zhang, I. Pasha, M. K. I. Khan, W. Akhtar, A. Mohsin, M. F. J. Chughati and Z. P. Wang, *Talanta*, 2022, **241**, 123228.

279 J. Tang, H. H. Shi, G. Y. Ma, L. P. Luo and Z. H. Tang, *Front. Bioeng. Biotechnol.*, 2020, **8**, 1019.

280 G. Z. Ou, J. Zhao, P. Chen, C. J. Xiong, F. Dong, B. Li and X. J. Feng, *Anal. Bioanal. Chem.*, 2018, **410**, 2485–2498.

281 T. L. Mako, J. M. Racicot and M. Levine, *Chem. Rev.*, 2019, **119**, 322–477.

282 A. Alvarez, J. M. Costa-Fernández, R. Pereiro, A. Sanz-Medel and A. Salinas-Castillo, *TrAC, Trends Anal. Chem.*, 2011, **30**, 1513–1525.

283 Y. Deng, M. Wang, Y. Zhuang, S. Liu, W. Huang and Q. Zhao, *Light: Sci. Appl.*, 2021, **10**, 76.

284 B. Zhang, B. Li and Z. G. Wang, *ACS Sens.*, 2020, **5**, 162–170.

285 B. Zhang, J. Yan, Y. Q. Shang and Z. G. Wang, *Macromolecules*, 2018, **51**, 1769–1776.

286 Y. M. Han, Z. J. Ye, F. Y. Wang, T. Y. Chen, L. Wei, L. X. Chen and L. H. Xiao, *Nanoscale*, 2019, **11**, 14793–14801.

287 J. Kaur, J. N. Malegaonkar, S. V. Bhosale and P. K. Singh, *J. Mol. Liq.*, 2021, **333**, 115980.

288 Q. S. Chen, R. Sheng, P. Y. Wang, Q. Ouyang, A. C. Wang, S. Ali, M. Zareef and M. M. Hassan, *Spectrochim. Acta, Part A*, 2020, **241**, 118654.

289 A. A. Kumaran, R. Gopal, C. P. Jijil, D. Joshy, N. K. Hijas, S. B. A. Rajukrishnan and R. N. Kizhakayil, *J. Environ. Chem. Eng.*, 2023, **11**, 109918.

290 S. L. Yang, J. N. Lu, S. J. Zhang, C. X. Zhang and Q. L. Wang, *Analyst*, 2018, **143**, 4901–4906.

291 J. Kumpfer, J. Jin and S. Rowan, *J. Mater. Chem.*, 2010, **20**, 145–151.

292 J. C. Wei, Y. Xue, J. Y. Dong, S. P. Wang, H. Hu, H. Gao, P. Li and Y. T. Wang, *Chin. Med.*, 2020, **15**, 22.

293 N. Xu, Q. H. Zhang and G. A. Zhang, *Dalton Trans.*, 2019, **48**, 2683–2691.

294 J. X. Ma, Y. Wang, G. C. Liu, N. Xu and X. L. Wang, *RSC Adv.*, 2020, **10**, 44712–44718.

295 D. D. Feng, J. Tang, J. Yang, X. H. Ma, C. Z. Fan and X. Q. Wang, *J. Mol. Struct.*, 2020, **1221**, 128841.

296 L. Wang, W. Xu, W. Y. Li, M. Xie and Y. Q. Zheng, *Chem. – Asian J.*, 2019, **14**, 4246–4254.

297 Z. Zhang, X. Ma, B. W. Li, J. Zhao, J. Qi, G. Y. Hao, J. H. Rong and X. B. Yang, *Analyst*, 2020, **145**, 963–974.

298 Y. H. He, S. H. Hong, M. Wang, J. Wang, A. M. Abd El-Aty, J. Wang, A. Hacimuftuoglu, M. Khan and Y. X. She, *New J. Chem.*, 2020, **44**, 6026–6036.

299 T. Sergeyeva, D. Yarynka, V. Lytvyn, P. Demydov, A. Lopatynskyi, Y. Stepanenko, O. Brovko, A. Pinchuk and V. Chegel, *Analyst*, 2022, **147**, 1135–1143.

300 X. T. Xue, M. Zhang, H. Y. Gong and L. Ye, *J. Mater. Chem. B*, 2022, **10**, 6698–6706.

301 Z. M. Wang, C. Zhou, S. W. Wu and C. Y. Sun, *Polymers*, 2021, **13**, 1376.

302 Z. F. Xu, P. H. Deng, J. H. Li and S. P. Tang, *Sens. Actuators, B*, 2018, **255**, 2095–2104.

303 W. René, V. Lenoble, M. Chioukh and C. Branger, *Sens. Actuators, B*, 2020, **319**, 128252.

304 M. Y. Zhang, Z. H. Chen, X. H. Liu, C. Song, C. H. Zeng, T. Y. Z. Lv, Z. Y. Xu, X. Q. Chen, L. Wang, B. Liu and X. J. Peng, *J. Hazard. Mater.*, 2023, **452**, 131177.

305 P. Li, D. Zhang, Y. C. Zhang, W. Lu, W. Q. Wang and T. Chen, *ACS Sens.*, 2018, **3**, 2394–2401.

306 J. Hoque, N. Sangaj and S. Varghese, *Macromol. Biosci.*, 2019, **19**, 1800259.

307 N. Mehwish, X. Q. Dou, Y. Zhao and C. L. Feng, *Mater. Horiz.*, 2019, **6**, 14–44.

308 R. J. Dong, Y. Pang, Y. Su and X. Y. Zhu, *Biomater. Sci.*, 2015, **3**, 937–954.

309 Q. Zhao, X. Y. Dai, H. Yao, Y. M. Zhang, W. J. Qu, Q. Lin and T. B. Wei, *Dyes Pigm.*, 2021, **184**, 108875.

310 H. X. Wang, C. W. Wei, X. J. Wang, H. F. Xiang, X. Z. Yang, G. L. Wu and Y. W. Lin, *Spectrochim. Acta, Part A*, 2021, **250**, 119378.

311 D. Zhang, Y. C. Zhang, W. Lu, X. X. Le, P. Li, L. Huang, J. W. Zhang, J. T. Yang, M. J. Serpe, D. D. Chen and T. Chen, *Adv. Mater. Technol.*, 2019, **4**, 1800201.

312 C. Sahub, J. L. Andrews, J. P. Smith, M. A. M. Arif, B. Tomapatanaget and J. W. Steed, *Mater. Chem. Front.*, 2021, **5**, 6850–6859.

313 X. C. Zhu, Y. Zhang, L. X. Han, H. L. Liu and B. G. Sun, *Biosens. Bioelectron.*, 2022, **210**, 114265.

314 J. W. Lichtman and J.-A. Conchello, *Nat. Methods*, 2005, **2**, 910–919.

315 N. Sharif, S. Khoshnoudi-Nia and S. M. Jafari, in *Characterization of Nanoencapsulated Food Ingredients*, ed. S. M. Jafari, Academic Press, 2020, vol. 4, pp. 131–158.

316 P. T. C. So, C. Y. Dong, B. R. Masters and K. M. Berland, *Annu. Rev. Biomed. Eng.*, 2000, **2**, 399–429.

This journal is © The Royal Society of Chemistry 2024

Chem. Soc. Rev., 2024, **53**, 6992–7090 | **7089**

317 R. Datta, T. M. Heaster, J. T. Sharick, A. A. Gillette and M. C. Skala, *J. Biomed. Opt.*, 2020, **25**, 1–43.

318 X. Chen, S. Zhong, Y. Hou, R. Cao, W. Wang, D. Li, Q. Dai, D. Kim and P. Xi, *Light: Sci. Appl.*, 2023, **12**, 172.

319 I. M. Khater, I. R. Nabi and G. Hamarneh, *Patterns*, 2020, **1**, 100038.

320 G. Vicidomini, P. Bianchini and A. Diaspro, *Nat. Methods*, 2018, **15**, 173–182.

321 K. N. Fish, *Curr. Protoc. Cytom.*, 2009, **50**, 12–18.

322 R. B. Hegde, K. Prasad, H. Hebbar and B. M. K. Singh, *Probl. Biocybern. Biomed. Eng.*, 2019, **39**, 382–392.

323 E. Moen, D. Bannon, T. Kudo, W. Graf, M. Covert and D. Van Valen, *Nat. Methods*, 2019, **16**, 1233–1246.

324 Z. C. Liu, L. H. Jin, J. C. Chen, Q. Y. Fang, S. Ablameyko, Z. Z. Yin and Y. K. Xu, *Comput. Biol. Med.*, 2021, **134**, 104523.

7090 | *Chem. Soc. Rev.*, 2024, **53**, 6992–7090

This journal is © The Royal Society of Chemistry 2024